

IN VIVO ASTROCYTE CALCIUM ACTIVITY IN THE
SOMATOSENSORY CORTEX DURING LOCOMOTION AND NON-
CONVULSIVE SEIZURES

FRANCIS DELICATA

Doctor of Philosophy

ASTON UNIVERSITY

September 2021

©Francis Delicata, 2021

Francis Delicata asserts his moral right to be identified as the author of this thesis.

This copy of the thesis has been supplied on condition that anyone who consults it is understood to recognise that its copyright belongs to its author and that no quotation from the thesis and no information derived from it may be published without appropriate permission or acknowledgement.

Thesis Summary

Francis Delicata - Year of submission 2021

In vivo astrocyte calcium activity in the somatosensory cortex during locomotion and non-convulsive seizures

Key words: astrocyte, calcium imaging, somatosensory cortex, locomotion, absence seizures

Astrocytes make up a significant portion of the total cells in the brain. Intracellular Ca^{2+} changes in astrocytes have been attributed to various physiological processes that directly influence neuronal activity and brain network synchrony. Moreover, altered Ca^{2+} patterns are indicative of astrocyte dysfunction and of diseased states.

Astrocytes are active following sensory stimulation, such as visual cues and tactile whisker stimuli. Astrocytes participate in the cortical response to sensory input and synchronously respond to locomotion with an intracellular Ca^{2+} increase, predominantly modulated by widespread neuromodulator release and direct activation of astrocyte α 1-adrenergic receptors. However, an in-depth study focussed on astrocyte activity in the primary somatosensory cortex (S1) during locomotion is lacking. To address this gap in the field, we recorded astrocyte Ca^{2+} changes in head-restrained, awake mice that were free to run on a wheel. Animals were chronically implanted with ECoG electrodes and a cranial window above S1. Ca^{2+} changes were visualised using a virally delivered genetically encoded Ca^{2+} indicator, GCaMP6f, driven by a GFAP promoter for selective expression in astrocytes. Semi-automated Ca^{2+} analysis protocols were used to measure Ca^{2+} fluorescence within the different sub-cellular compartments. We show that layer 2/3 astrocytes rapidly respond to locomotion onset, within a sub-second timescale. This was most evident in the cell periphery that activated most consistently to locomotion, even when soma activation was weak or absent. The Stargazer mouse, a model of ataxia, maintained a strong astrocyte response to locomotion, which was enhanced in view of its quicker astrocyte response time, especially in the cell periphery.

Astrocytes regulate neuronal network excitability and modulate cortical state switching and network synchrony. Astrocytes are capable of modifying neuronal activity through gliotransmitter release and have been consequently shown to elicit epileptic discharges in slice models, as well as precede epileptic events in in vivo epilepsy models. During absence seizures (AS), an increased rhythmicity and synchrony among thalamic and cortical neurons is evidenced by generalised spike and wave discharges (SWD) throughout this network. fMRI studies have revealed potential astrocyte recruitment preceding seizure onset and astrocyte GABA dysfunction is known to contribute to SWD occurrence. However, astrocyte calcium activity during AS is not known. We imaged astrocyte Ca^{2+} changes to determine if astrocytes were indeed active prior to seizure onset and potentially drove the neuronal paroxysmal activity of AS. We showed for the first time, astrocyte Ca^{2+} activity in two genetic animal models of AS. Stargazer mice exhibited enhanced microdomain and endfoot activation during periods of prolonged ictal ECoG activity, but no clear widespread astrocyte activation preceded seizure onset. Astrocytes within the cortical initiation site of AS were imaged in the Genetic Absence Epilepsy Rat from Strasbourg, using the Inscopix miniature head-mounted microscope. Astrocytes within the cortical initiation site engaged in a synchronous Ca^{2+} pattern during a state of prolonged seizure activity. Moreover, astrocyte-specific chemogenetic activation or IP3 receptor type 2 knockout, did not influence seizure occurrence.

In conclusion, we show a diverse and complex astrocyte response to locomotion which is driven by microdomain activation with potential summation of inputs that leads to widespread soma and endfoot activation. Furthermore, evidence we obtained from two well-established models of AS further strengthens past findings of dysfunctional astrocytes within the cortico-thalamic network involved in AS initiation, and we reveal novel astrocyte Ca^{2+} patterns associated with spontaneous generalised seizures.

To my wife for her constant love and support

Acknowledgements

I would like to express my gratitude to all those who contributed to the successful completion of my PhD project.

First and foremost, my supervisor Prof Rhein Parri for welcoming me to his team, for his support, expertise and the invaluable knowledge he has shared with me, and for his patience and encouragement during the tough times of the project.

Prof Vincenzo Crunelli for hosting me in his lab, for his time and support, and for always keeping his door open (literally!) when I needed advice, and his expert guidance throughout the project.

My colleagues and friends, Zoe, Tatiana and Alberto for the company during the long hours spent in the lab, Dr Stephanie Bagstaff and Ms Fangli Chen for their patience and assistance in the lab, and Dr Adam Ranson for his help with the two-photon imaging setup.

Aston University and Cardiff University animal facility staff, with special thanks to Mrs Veronica Walker, for their assistance and training, and for always taking excellent care of the animals.

The EU Horizon 2020 funding programme (Marie Skłodowska-Curie grant 722053) for the financial support and the EU-GliaPhD network for the opportunity to participate in a unique neuroscience training network and work with such inspirational scientists.

My parents for encouraging me to further my studies and teaching me the virtues of hard work and dedication. For their love and support, despite the distance.

Finally, Dorianne, the one constant in my life these past years, who never doubted my abilities and encouraged me to keep going even in the face of overwhelming emotions and setbacks. I emerge from this journey not only with a doctorate, but also with a lifelong partner.

List of Contents

Chapter 1: Introduction	14
1.1 An overview of basic astrocyte structure and functions	14
1.2 Astrocyte morphology	15
1.3 Significance of astrocyte calcium signalling and mechanisms	16
1.3.1 Calcium signalling mechanisms	16
1.3.2 Astrocyte-neuron communication at synapses	18
1.3.3 Astrocytes modulate cortical and thalamic rhythmicity	19
1.4 Calcium detection and analysis	20
1.4.1 Genetically encoded calcium indicators	20
1.4.2 Calcium imaging analysis	22
1.4.3 Astrocyte calcium imaging software packages	22
1.4.4 Application of 3-D two-photon laser scanning microscopy with event-based calcium detection	25
1.4.5 Overview of calcium detection and analysis	26
1.5 Astrocyte response to sensory input	27
1.5.1 The somatosensory system	27
1.5.2 Astrocyte response in the barrel field cortex	28
1.5.3 Astrocyte response to sensory input and locomotion	28
1.6 Epilepsy	30
1.6.1 Classification of seizures and epilepsies	30
1.6.2 Astrocytes in epilepsy	31
1.6.3 Astrocyte calcium activity in epilepsy	32
1.7 Childhood absence epilepsy and animal models of absence seizures	33
1.7.1 Classification and features of childhood absence epilepsy	33
1.7.2 Current treatment strategies	35
1.7.3 Animal models of absence seizures	35
1.7.4 Cortico-thalamic circuitry involved in absence seizure initiation and generalisation	38
1.7.5 Evidence of astrocyte dysfunction in animal models of absence seizure... ..	41
1.8 Aims	43
Chapter 2: Methodology	45
2.1 Animal use and ethics	45
2.2 Surgical procedures and sterility	46
2.3 Bilateral Electrocorticogram Recordings for absence seizure detection	46
2.3.1 Electrode preparation	47
2.3.2 Electrode implantation	47

2.3.3	ECoG recording setup and protocol for seizure detection	50
2.4	Chemogenetics.....	50
2.4.1	DREADD injection preparation.....	51
2.4.2	Surgical procedure.....	51
2.4.3	ECoG recording setup and protocol with DREADD activation	52
2.5	Seizure detection and quantification	52
2.6	Two-photon calcium imaging experiments and ECoG recording in head-restrained, awake mice	54
2.6.1	ECoG electrode and headplate preparation	54
2.6.2	ECoG implantation, AAV injection and chronic window implantation.....	55
2.6.3	Calcium imaging and ECoG recording	57
2.6.4	Imaging protocol and analysis.....	58
2.7	Calcium imaging and ECoG recording in freely moving GAERS during different behaviours	60
2.7.1	Step 1: AAV injection	61
2.7.2	Step 2: ECoG electrodes and lens implantation	62
2.7.3	Step 3: Baseplate attachment.....	63
2.7.4	Step 4: One-photon astrocyte calcium imaging, with video monitoring and ECoG recording	64
2.7.5	Calcium Analysis	65
2.8	Immunohistochemistry	67
2.8.1	Brain Extraction	67
2.8.2	Brain Slicing.....	67
2.8.3	Immunostaining	67
2.8.4	Antibody preparations.....	68
2.9	Statistical Analysis	69
2.10	Resources used.....	69
Chapter 3:	Cortical astrocyte calcium response to locomotion	72
3.1	GCaMP6f expression in S1 cortical astrocytes.....	72
3.2	Astrocyte calcium activity in S1 cortex during locomotion	74
3.2.1	Astrocyte population recruitment during periods of locomotion	74
3.2.2	Single astrocyte response to locomotion.....	81
3.3	Astrocyte calcium activity in an animal model of ataxia: the Stargazer mouse model	84
3.4	Astrocyte calcium activity following PMCA pump expression in S1 cortical astrocytes	89
3.5	Discussion and further work.....	92
3.5.1	Synchronous full-cell astrocyte activation with sub-cellular independence	92
3.5.2	Microdomains initiate the astrocytic response to locomotory input and may engage in summation of input	93

3.5.3	Further work	94
3.6	Conclusions	95
Chapter 4: Cortical astrocyte calcium activity in rodent models of absence seizures		97
4.1	S1 layers 2/3 astrocyte calcium activity in Stargazer mice	97
4.2	S1 layers 2/3 cortical astrocyte calcium activity in GHB-injected wild-type mice	104
4.2.1	Suitability of the GHB-model in rats and mice	104
4.2.2	Calcium imaging from S1 cortical astrocytes during GHB-induced absence-like seizures.....	107
4.3	Quantification of astrocyte calcium events during ictal periods.....	108
4.4	IP3R2 KO mice show similar susceptibility to GHB-induced absence-like seizures	111
4.5	Effect of Gq-DREADD cortical astrocyte activation on absence seizure properties.....	112
4.5.1	Gq-DREADD activation does not alter absence seizures in Stargazer mice and GAERS rats.....	112
4.5.2	Immunohistochemical confirmation of DREADD expression in cortical astrocytes.....	116
4.6	Discussion and further work.....	120
4.6.1	Astrocytes are moderately active during periods of ictal activity.....	120
4.6.2	Stargazers show enhanced microdomain and endfoot activation during ictal periods.....	121
4.6.3	GHB-induced absence-like activity induces a general dampening of astrocyte calcium activity.....	122
4.6.4	Concerted intracellular calcium transients do not precede or follow seizure onset in Stargazer mice.....	124
4.6.5	Manipulating astrocyte calcium activity does not alter seizure occurrence	125
4.6.6	Conclusions	126
Chapter 5: Cortical astrocyte calcium imaging in freely moving rodent models of absence seizures		128
5.1	Immunohistochemical confirmation of GCamP6f-expressing astrocytes	128
5.2	Pilot lens implantations in GAERS	131
5.3	Astrocyte calcium imaging and SWD detection in a freely moving GAERS	132
5.4	Astrocyte calcium imaging in a freely moving mouse	142
5.5	Discussion and further work.....	145
5.5.1	Astrocyte calcium activity patterns are modified during SWDs.....	145
5.5.2	Comparison with established in vivo astrocyte calcium activity in mouse models	147
5.5.3	Considerations and further work	149
5.6	Conclusion.....	150
Chapter 6: Concluding discussion.....		152

6.1	Summary of main findings	152
6.2	The astrocyte calcium response to locomotion vs SWDs	154
6.3	The contribution of S1 astrocyte calcium signalling to seizure initiation.....	157
6.4	Conclusion.....	158
Chapter 7: References.....		160

List of Abbreviations

4-AP - 4-aminopyradine
AAV - Adeno associated virus
ADK - Adenosine kinase
AP - Antero-posterior
AQP4 - Aquaporin-4 water
AS - Absence seizure
ATP - Adenosine triphosphate
AUC - Area under curve
C - Central
CED - Cambridge Electronic Design
CHIPS - Cellular and hemodynamic image processing suite
CNO - Clozapine N-oxide
CT - Cortico-thalamic
Cx43 - Connexin channel 43
DREADD - Designer receptors exclusively activated by designer drug
DV - Dorso-ventral
EAAT1 - Excitatory amino acid transporter 1
EAAT2 - Excitatory amino acid transporter 2
ECoG - Electrocorticogram
EEG - Electroencephalogram
EMG - Electromyography
EN - Endonucleotidases
F - Frontal
FOV - Field of view
Fp - Frontal pole
FRET - Förster resonance energy transfer
GAERS - Genetic absence epilepsy rat from Strasbourg
GBL - Gamma butyrolactone
GECI - Genetically encoded calcium indicator
GFP - Green fluorescent protein
GHB - Gamma-hydroxybutyrate
GPCR - G-protein-coupled receptor
GS - Glutamine synthetase
hM3D - Human M3 muscarinic receptor DREADD
ICA - Independent component analysis
IP3R2 - Inositol 1,4,5-trisphosphate type-two receptor

IP3R2 KO - IP3R2 knock-out
Kir4.1 - Inwardly rectifying potassium channel 4.1
ML - Medio-lateral
NEC - Non-epileptic control
NETCAL - Network and population dynamics analysis of calcium imaging recordings
NMDA - N-methyl-D-aspartate
NRT - Nucleus reticularis thalami
O - Occipital
P - Parietal
PCA - Principal components analysis
PLC - Phospholipase C
PMCA - Plasma membrane Ca²⁺ ATPase
PSD - Power spectral density
PTZ - Pentylentetrazole
ROA - Regions of activity
ROI - Regions of interest
RyR - Ryanodine receptor
S1 - Primary somatosensory cortex
S1BF - Barrel field cortex
SERCA - Sarcoendoplasmic reticulum Ca²⁺ ATPases
SNpr - Substantia nigra pars reticulata
Stg - Stargazer
Str - Striatum
SWD - Spike and Wave Discharge
TC - Thalamo-cortical
VB - Ventrobasal thalamus
WAG/Rij - Wistar Albino Glaxo/Rij rat
WT - Wild-type

List of Figures

Figure 1-1: Cytoplasmic calcium signalling and control.	17
Figure 1-2: Gliotransmitter release as a feedback mechanism at the tripartite synapse.	19
Figure 1-3: The vibrissal sensorimotor system in rodents.....	27
Figure 1-4: Astroglial mechanisms involved in epilepsy.....	32
Figure 1-5: Typical electroencephalogram traces of a child suffering from childhood absence epilepsy.	34
Figure 1-6: Typical human and rodent spike and wave discharges.	36
Figure 1-7: Brain networks involved in spike and wave discharges.	40
Figure 2-1: A typical stereotaxic surgery setup used in our lab.....	46
Figure 2-2: ECoG electrode design.....	47
Figure 2-3: Electrode and craniotomy placement.	49
Figure 2-4: Chemogenetic activation of astrocytes.....	51
Figure 2-5: Ictal event detection with Spike2 SeizureDetect script.	53
Figure 2-6: Two-photon calcium imaging mouse setup at Cardiff University.....	54
Figure 2-7: Custom ECoG electrodes and laser-cut head-plate design.	55
Figure 2-8: Electrode and chronic window craniotomy placement for two-photon imaging experiments.	56
Figure 2-9: Mouse implantation for awake, head-restrained two-photon imaging.	58
Figure 2-10: Calcium analysis workflow	60
Figure 2-11: Sites of AAV GCaMP6f injection for Inscopix experiments.	61
Figure 2-12: Prism lens and ECoG electrode placement for Inscopix experiments.....	63
Figure 2-13: Miniscope system layout.....	64
Figure 2-14: GAERS calcium analysis workflow.....	66
Figure 3-1: GCaMP6f expression in mouse cortical astrocytes.	73
Figure 3-2: Global astrocyte response to locomotion.	75
Figure 3-3: Different patterns of astrocyte calcium activity in response to locomotion.	76
Figure 3-4: Correlation between locomotion and astrocyte calcium changes in wild-type mice.	78
Figure 3-5: Locomotion-induced calcium transients restricted to the cell periphery. ...	79
Figure 3-6: Multi-peak and single-peak calcium events.	80
Figure 3-7: Changes in ECoG power spectra during locomotion-induced calcium events.	80
Figure 3-8: Locomotion-induced calcium activity in single astrocytes.....	81
Figure 3-9: Sub-cellular activation with respect to locomotion onset.....	82
Figure 3-10: Cumulative distribution curves of the calcium events with respect to locomotion onset.....	82
Figure 3-11: Activity in processes and microdomains preceded locomotion onset.	83
Figure 3-12: Correlation between locomotion and astrocyte calcium increase in Stargazer mice.....	85
Figure 3-13: Calcium event properties of astrocyte sub-compartments in wild-types and Stargazers during locomotion.....	86
Figure 3-14: Differences in locomotion-induced averaged calcium transients between Stargazers and wild-types.....	88
Figure 3-15: Individual compartment timing with respect to locomotion onset in Stargazer mice.	88
Figure 3-16: hPMCA2w/b pump expression in mouse S1BF.....	89
Figure 3-17: Astrocyte expression of hPMCA2w/b pump in mouse S1BF.	90
Figure 3-18: Astrocyte-selective expression of hPMCA2w/b pump in mouse S1BF. ...	90
Figure 3-19. Calcium activity following hPMCA2w/b expression in S1 astrocytes.....	91
Figure 4-1: Stargazer ECoG ictal activity.	99
Figure 4-2: Cortical astrocyte calcium activity during ictal states.	101
Figure 4-3: Ictal onset trigger average of calcium transients.	102

Figure 4-4: Changes in calcium fluorescence during seizure-related increase in theta and alpha activity, in comparison with changes in calcium fluorescence during locomotion.	103
Figure 4-5: Distinct ECoG stages following GBL (150 mg/kg, i.p.) administration in Wistar rats.	105
Figure 4-6: GBL-induced (75 mg/kg, i.p.) ECoG changes in C57Bl6/J mice.	106
Figure 4-7: Cortical astrocyte calcium activity during GBL-induced ictal states.	108
Figure 4-8: Calcium changes in astrocyte sub-compartments during spontaneous and GHB-induced absence seizures.	110
Figure 4-9: GHB-induced ECoG changes in IP3R2 knockout mice and wild-type littermates.	112
Figure 4-10: Effect of S1 cortical astrocyte DREADD activation on absence seizure properties in Stargazer mice.	114
Figure 4-11: Effect of S1 cortical astrocyte DREADD activation on absence seizure properties in GAERS.	115
Figure 4-12: DREADD expression in Stargazer S1 astrocytes.	117
Figure 4-13: Astrocyte-specific DREADD expression in S1BF of Stargazer mice.	118
Figure 4-14. DREADD expression in S1BF of GAERS.	119
Figure 5-1: GCaMP6f expression in GAERS S1BF astrocytes.	129
Figure 5-2: GCaMP6f expression in GAERS cortical neurons.	130
Figure 5-3: Detecting calcium fluorescence with the Inscopix Data Processing Suite.	131
Figure 5-4: Cylindrical and prism lens placement with respect to AAV spread in S1.	132
Figure 5-5. Astrocyte calcium activity in a freely moving GAERS during various behaviours.	136
Figure 5-6: Calcium event properties associated with different behavioural events.	139
Figure 5-7: Electrophysiological confirmation of SWDs, transition states and sleep.	141
Figure 5-8: Prism lens placement with respect to AAV spread in S1BF.	142
Figure 5-9: Astrocyte calcium imaging in a freely moving mouse with the Inscopix system.	144

List of Tables

Table 2-1: Resource Table.....	69
Table 5-1: Calcium event properties during different behaviours, stimuli or ECoG state.	138

Chapter 1: Introduction

1.1 An overview of basic astrocyte structure and functions

The central nervous system (CNS) is composed of numerous cell types that vary in structure, function, number and anatomical location (Hodge et al. 2019), and can be broadly subdivided into neurons, glia, pericytes and endothelial cells (Keller et al. 2018). Astrocytes are a type of glial cell found throughout the CNS, comprising about 20% of cells found in the brain (Pelvig et al. 2008). Astrocytes exist as a heterogeneous population of cells, adapted to the brain region or species they are located in, such as grey matter protoplasmic astrocytes, white matter fibrous astrocytes, and interlaminar astrocytes in higher primates (Nimmerjahn 2009).

Astrocytes were first described early in the 19th century and assigned a purely structural, supportive role (Verkhatsky and Toescu 2006). They were believed to be inactive and incapable of interacting with neuronal cells (Dennis and Gerschenfeld 1969). Their basic 'house-keeping' role was restricted to structural support, scar formation and tissue repair, nutrient supply, vasodilation and maintenance of the blood brain barrier (Sofroniew and Vinters 2010). However, by the end of the 19th century it was well established that astrocytes play a role in CNS signalling. In contrast to neurons, astrocytes form a continuous syncytium that allows the intercellular movement of molecules, including secondary messengers (Dermietzel and Spray 1993; Dani et al. 1992) and the propagation of calcium waves in response to neuronal activity and revealed a potential role in long-range information processing (Dermietzel and Spray 1993; Dani et al. 1992). It was shown that astrocyte-neuron communication occurred, at least partly, through glutamate mediated mechanisms. Astrocytes respond to glutamate with an increase in intracellular calcium and propagating calcium waves (Cornell-Bell et al. 1990), astrocytes stimulate neuronal activity following astrocyte intracellular calcium increases (Nedergaard 1994), astrocytes respond to synaptically released glutamate (Porter and McCarthy 1996), astrocytes signal neurons via glutamate release (Pasti et al. 1997), and astrocyte calcium mediated glutamate release modifies synaptic function (Araque, Parpura, et al. 1998; Araque, Sanzgiri, et al. 1998). This work culminated in the description of the tripartite synapse in which astrocytes form a functional component of the synapse and are able to respond to synaptic activity and release their own neurotransmitters to provide a feedback mechanism (Araque et al. 1999; Carmignoto 2000).

Accumulating evidence now shows that astrocytes, partly via their intracellular calcium transients and release of gliotransmitters (glutamate, ATP, GABA and D-serine), are key players in neuronal excitability, synaptic plasticity and complex behaviours (Oliveira et al. 2015; Araque et al. 2014; Pirttimaki and Parri 2013; Guerra-Gomes et al. 2017; Park and Lee 2020; Ransom et al. 2003; Parri et al. 2001). The close association between astrocytes and neurons is further evidenced by their number and distribution in the CNS. In humans, glia are about as abundant as neurons and their abundance is dependent on the density of neurons. Indeed, the proportion of glia to neurons increases with decreasing neuronal density and with increasing neuronal size, reflecting the intimate physiological relationship between the two cell types (Herculano-Houzel 2014).

1.2 Astrocyte morphology

Astrocytes possess a complex three-dimensional morphology (Bindocci et al. 2017) and are described as star-shaped cells, with five to ten branches extending from a central core/soma (Kettenmann and Verkhratsky 2011). Each branch (or proximal process) subdivides into finer processes (distal processes), which contact blood vessels through endfeet and interact with synapses forming the tripartite synapse (Araque et al. 1999). A single astrocyte may interact with hundreds of thousands of synapses (Bushong et al. 2002), and astrocytes vary in size, spreading up to a few hundred μm from the central core/soma (Kettenmann and Verkhratsky 2011).

Early imaging studies on astrocytes focussed on activity within the somata and proximal processes, leading to an inaccurate conclusion of astrocytes having a limited role in brain physiology (Petravicz et al. 2008; Agulhon et al. 2010; Agulhon et al. 2013). It has now been unequivocally shown that astrocytes' finer processes and their unresolved microdomains (areas of restricted size within the finer branches) are highly active and modulate synaptic activity and neurovascular coupling (Bazargani and Attwell 2016), mediating their influence through their vast surface area of tens of thousands of μm^2 (Kettenmann and Verkhratsky 2011).

Astrocytes show extensive morphological and functional diversity, depending on the brain region (Ben Haim and Rowitch 2017; Matyash and Kettenmann 2010). Astrocytes occupy their own territory and do not overlap with one another, except at their very tips through which they communicate by gap junctions via connexin hemichannels, Cx43 and Cx30 (Khakh and Sofroniew 2015). In the neocortex, astrocytes form a continuous syncytium spanning 600 μm in diameter (Haas et al. 2006) and show region-specific variability in connectivity. In the somatosensory cortex, Cx43 expression varies between

layers and the number of gap junction-coupled cells diminishes with increasing cortical layer depth. Moreover, cells form a distinct oval arrangement restricted to single barrels in layer IV and a transversely connected arrangement in the top layers (Houades et al. 2008; Houades et al. 2006). Brain region-specific peculiarities are also observed in the ventrobasal thalamus, which receives sensory input from the whiskers and projects to the barrel field cortex (Bourassa et al. 1995). Here, the majority of astrocytes lack Cx43 and gap junctions are predominantly formed by Cx30 (Griemsmann et al. 2015). Moreover, astrocytes form panglial gap junctions with oligodendrocytes (Griemsmann et al. 2015), creating an astroglial network contained within barreloid borders that are lined by uncoupled or weakly coupled oligodendrocytes (Claus et al. 2018).

1.3 Significance of astrocyte calcium signalling and mechanisms

1.3.1 Calcium signalling mechanisms

Calcium signalling in astrocytes has been intensely studied since the remarkable observation that astrocytes in cultured hippocampal slices respond to synaptic activity by means of an increase in intracellular calcium (Dani et al. 1992), and boosted by in situ observations in the ventrobasal thalamus that spontaneous astrocyte calcium signalling triggers slowly decaying NMDA receptor-mediated inward currents in neurons (Parri et al. 2001) and shows pacemaker-like oscillations (Parri and Crunelli 2001). Since then, numerous studies have revealed a plethora of physiological processes associated with intracellular calcium fluxes in astrocytes (Guerra-Gomes et al. 2017) arising from different intra-cellular sources as well as from trans-membrane entry (Shigetomi et al. 2016). Calcium transients arise due to fluxes from various intracellular organelles (e.g. mitochondria and the endoplasmic reticulum), pumps, receptors and channels (Kettenmann and Verkhratsky 2011). Inositol 1,4,5-trisphosphate type-two receptor (IP3R2) mediated calcium changes are considered to be a major source of calcium activity in astrocytes, but it is not the only mechanism relevant to astrocytic physiology (Haustein et al. 2014; Srinivasan et al. 2015). For instance, calcium waves propagate through astrocyte syncytia by an IP3-dependent process through gap junctions (Finkbeiner 1992) and by astrocyte ATP release that activates purinergic receptors on nearby astrocytes (Guthrie et al. 1999).

IP3R2 receptors are highly expressed in astrocytes (Cahoy et al. 2008) and through G-protein-coupled receptor (GPCR) activation, it has been shown that IP3R2-mediated calcium release from the endoplasmic reticulum is a key process of intracellular calcium release in astrocytes. In fact, an IP3R2 knock-out (IP3R2 KO) mouse model has

severely reduced intracellular calcium transients, initially thought to be totally abolished (Petraovic et al. 2008; Agulhon et al. 2010), but later shown to still be present in the finer processes and microdomains of astrocyte territories (Srinivasan et al. 2015). This suggested that while IP3R2-mediated calcium release is a dominant calcium releasing mechanism, other processes are involved, such as ryanodine receptor-mediated calcium release (Shigetomi et al. 2016) and trans-membrane calcium influx (Figure 1-1). The latter is mostly observed in the finer processes where it is thought to contribute to 50% of calcium signalling in the hippocampus (Srinivasan et al. 2015). Recent studies have revealed the importance of investigating calcium fluctuations within the entire astrocyte territory, which have been shown to occur independently within the different sub-compartments and highlighted the physiological relevance of ongoing calcium changes in the finer processes and microdomains (Bindocci et al. 2017).

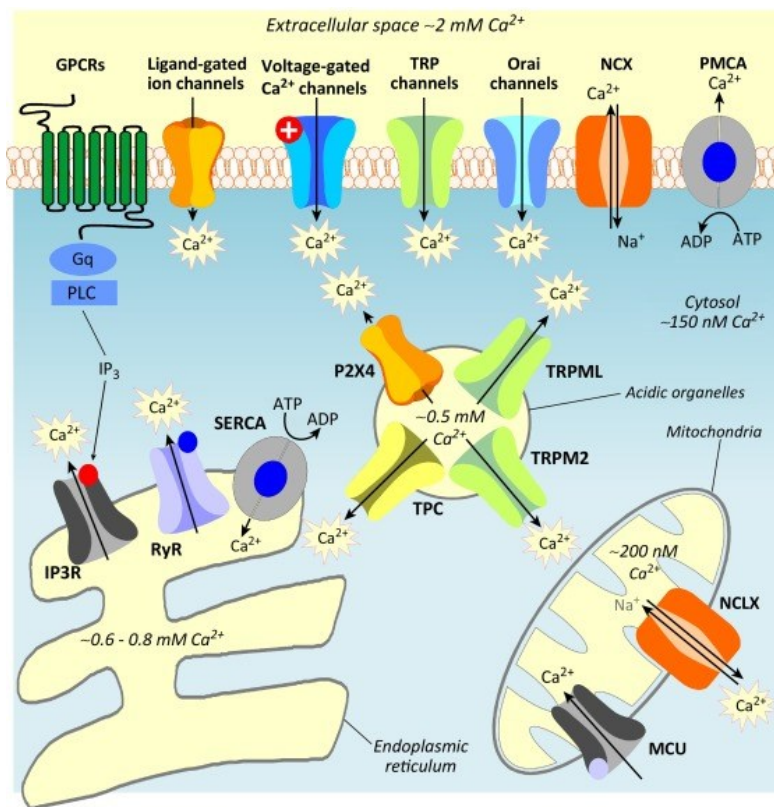


Figure 1-1: Cytoplasmic calcium signalling and control. Various calcium transporters, pumps and channels are involved in maintaining cytosolic calcium levels. Intracellular organelles serve as a calcium store. The endoplasmic reticulum releases calcium through ryanodine receptor- (RyR) and IP3R2-mediated mechanisms, and its calcium is replenished by sarcoendoplasmic reticulum Ca^{2+} ATPases (SERCA). Acidic organelles and mitochondria also contribute to intracellular calcium levels. Various trans-membrane channels and receptors are expressed in astrocytes, including TRP ion channels, plasma membrane Ca^{2+} ATPase (PMCA) channels and G protein-coupled receptors (GPCR), but lack others, such as voltage-gated Ca^{2+} channels. Reproduced from (Shigetomi et al. 2016)

1.3.2 Astrocyte-neuron communication at synapses

Tripartite synapses form the essence of bidirectional astrocyte-neuron communication, in which astrocytes respond to synaptic activity and exert an influence on neuronal excitability. Neurotransmitters released from pre-synaptic terminals activate astrocyte metabotropic and ionotropic receptors (Perea and Araque 2005; Porter and McCarthy 1996). This induces intracellular calcium fluxes and subsequent gliotransmitter release: glutamate, GABA, ATP and D-serine, among others (Bezzi and Volterra 2001). Figure 1-2 summarizes the calcium-mediated feedback mechanism involved. Gliotransmitter-release mechanisms are still widely debated, however, they undoubtedly influence neuronal synaptic transmission and plasticity (see Araque et al. 2014, Table 1, for a list of studies in this area, including glutamate release in the ventrobasal thalamus (Parri et al. 2001; Pirttimaki et al. 2011) and cortex (Min and Nevian 2012; Gómez-Gonzalo et al. 2010), ATP and D-serine release in the cortex (Halassa, et al. 2009a; Fellin et al. 2009; Takata et al. 2011). Four important consequences of gliotransmitter release have been highlighted: (i) single astrocytes release numerous gliotransmitters, (ii) gliotransmitters may act on different targets; (iii) gliotransmitters can coordinate whole neuronal networks; and (iv) diverse modulation is possible due to the variety of gliotransmitters and their targets (Araque et al. 2014).

The astrocyte response to synaptic activity by intracellular calcium increase depends on a number of factors and varies depending on brain region and the frequency and pattern of afferent input (Perea et al. 2009; Pasti et al. 1997). An individual cortical astrocyte makes contact with 300 to 600 neuronal dendrites (Halassa et al. 2007) and is able to perform spatial and temporal integration of received inputs, with implied synaptic information processing (Perea and Araque 2005). A summation of smaller astrocyte calcium events into a synchronous full cell and population-wide excitation has been hypothesised, but not yet fully evidenced (Araque et al. 2014).

High-affinity, slowly desensitizing receptors are the most common receptors involved in the response to neurotransmitter release at synapses, which has been described in depth and confirmed in various studies, including mGluR5 receptor activation by glutamate (Panatier et al. 2011), muscarinic receptor activation by acetylcholine (Araque et al. 2002), P2Y receptor activation by ATP (Bowser and Khakh 2004), GABA_B receptor activation by GABA (Perea et al. 2016), and CB1 receptor activation by endocannabinoids (Gómez-Gonzalo et al. 2015). Similar high affinity, slowly desensitizing receptors in neurons are also involved in the detection and response to gliotransmitters outside the synaptic cleft, such as extrasynaptic NMDA receptors in response to glutamate release from astrocytes (Fellin et al. 2004).

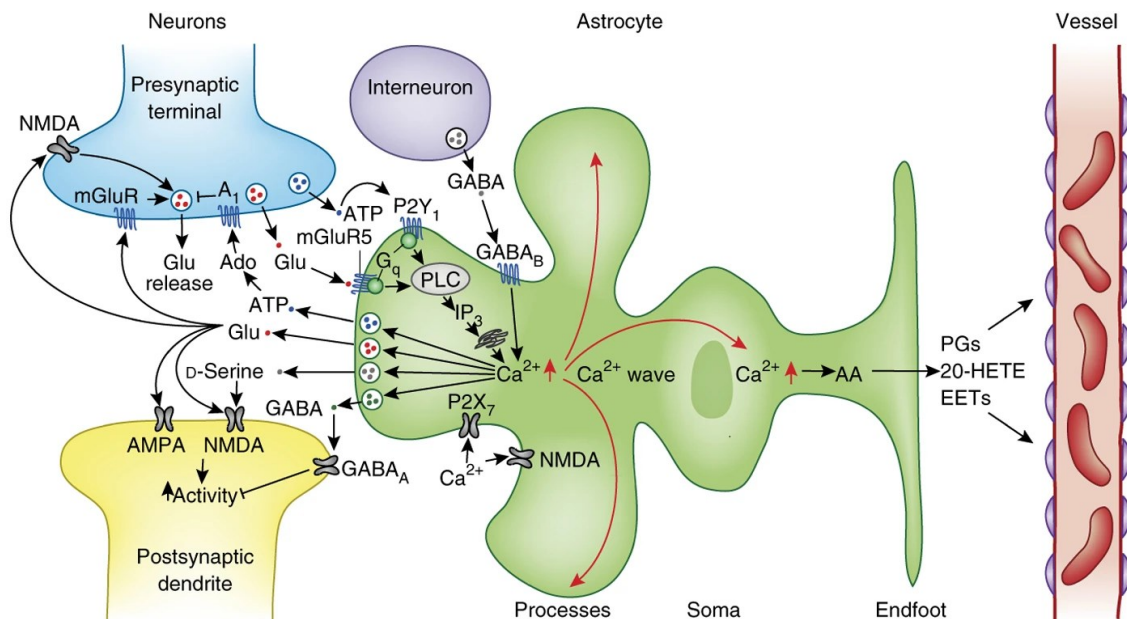


Figure 1-2: Gliotransmitter release as a feedback mechanism at the tripartite synapse. Neurotransmitter release activates G protein-coupled receptors expressed on astrocytes and leads to intracellular calcium release. A major signalling pathway involves inositol 1,4,5-trisphosphate type-two receptors (IP3R2) on the endoplasmic reticulum which are activated following IP3 release after hydrolysis from phospholipase C (PLC). This in turn induces gliotransmitter release from astrocytes which can act on neurons pre- or post-synaptically and modulate neuronal excitability. Intracellular calcium release also mediates the release of vasoactive messengers that act on blood vessels to modify blood flow. AA, arachidonic acid; PGs, prostaglandins; 20-HETE, 20-hydroxyeicosatetraenoic acid; EETs, epoxyeicosatrienoic acids; PLC, phospholipase C; Ado, adenosine; A1, adenosine's A1 receptor; P2Y1, ATP's P2Y1 receptor. Reproduced from (Bazargani and Attwell 2016)

1.3.3 Astrocytes modulate cortical and thalamic rhythmicity

The brain shows several electroencephalographic oscillatory bands ranging from 0.05 Hz to 500 Hz, different frequencies being associated with different brain states, behaviours or physiological functions, in rodent models as well as in humans (Buzsáki and Draguhn 2004). Synaptic neurotransmitter release is known to be a major modulator of brain rhythms (Buzsáki and Draguhn 2004), however non-synaptic and non-neuronal mechanisms have been identified to contribute, such as gap junction electrical coupling in the thalamus (Hughes et al. 2011). Cortical rhythmicity has been associated with important physiological processes, such as consciousness, sleep/wake cycles, attention, memory consolidation, movement execution and spatial navigation, aversion and nociception (Steriade et al. 1993; Hughes et al. 2002; Babiloni et al. 2002; Uhlhaas et al. 2008; Cebolla and Cheron 2019; Tan et al. 2019). Recently, astrocyte calcium elevations have been associated with neuronal rhythmicity, cortical and thalamic synchronisation.

On a local level, astrocytes are known to spontaneously induce slow inward currents in cortical pyramidal neurons, for instance following astrocyte GABA_B receptor activation and IP3-mediated calcium release (Mariotti et al. 2016). Astrocyte-mediated slow inward currents have been observed in human epileptic cortical tissue mediated by NMDA-receptor activation (Navarrete et al. 2013), as well as in the thalamus following astrocyte glutamate release and NMDA receptor activation (Pirttimaki et al. 2011; Parri et al. 2001). Moreover, astrocytes in the ventrobasal thalamus selectively respond to corticothalamic or sensory synaptic stimulation and signal to surrounding neurons potentially creating a delayed feedforward excitation to thalamocortical neurons (Parri et al. 2010).

On a wider-scale, astrocytes are known to cause increased neuronal synchrony in the somatosensory cortex and thalamus, through increased gliotransmitter release, influencing neurons more than 200 μm away (Pirttimaki et al. 2017). On a network level, disruption of intracellular calcium release results in reduced neuronal synchrony in cortical slices, due to the disruption of astrocyte purinergic signalling, which triggers highly synchronous up-state depolarization shifts in neurons (Poskanzer and Yuste, 2011). Moreover, astrocyte calcium-mediated regulation of extracellular glutamate modulates a slow neuronal cortical rhythm, induced by intracellular calcium increase in astrocytes followed by a glutamate spike and a shift to a neuronal cortical down-state (Poskanzer and Yuste, 2016). Reduced astrocyte function has been linked to various oscillatory anomalies, such as decreased gamma power and recognition memory performance (Lee et al. 2014). Cortical astrocytes have been shown to play a significant role in thalamocortical network function and synchrony, such as in the modulation of slow wave activity during NREM sleep (Vaidyanathan et al. 2021), wakefulness, sleep spindles, sleep pressure and sleep deprivation (Bojarskaite et al. 2019; Ingiosi et al. 2020; Halassa, et al. 2009b).

1.4 Calcium detection and analysis

1.4.1 Genetically encoded calcium indicators

The relevance of astrocytes to brain function, together with their complex morphology, has led to the development of astrocyte-specific genetically encoded calcium indicators (GECIs), a ground-breaking technological advancement that allows chronic/long-term imaging in awake animals with negligible modification to brain function (Broussard et al. 2014; Russell 2011). These preceded the earlier approaches of membrane-permeable dye bulk loading or intracellular dialysis using patch pipettes of calcium-sensitive dyes,

which while useful, do not offer the chronic and subcellular resolution imaging advantages of GECIs (Shigetomi et al. 2016).

Astrocyte calcium imaging was first carried out using bulk loading of organic calcium indicators such as Fluo-3 and Fura 2, in cultures (Cornell-Bell et al. 1990) and brain slices (Yuste and Katz 1991). However, this technique has two major limitations: (i) the dye does not penetrate the finer processes, which limits imaging to the astrocyte soma and processes wider than 25 μm (Reeves et al. 2011), and (ii) it is not effective in adult tissue (Khakh and McCarthy 2015) due to neuropil development which interferes with membrane penetration of the dye (Mauleon et al. 2013). Alternatively, astrocytes may also be loaded with a dye using an intracellular electrode to deliver the dye directly inside the cell and load more of the astrocyte structure (Nett et al. 2002). However, this technique also comes with various limitations, including the need of high concentrations of the dye, which still does not provide adequate penetration in the finer processes, and potentially washing out intracellular components (Khakh and McCarthy 2015). GECIs thus provide a solution to overcome these limitations and have since been specifically delivered to astrocytes using various techniques, such as viral transfection with adeno-associated viruses (AAVs) (Shigetomi et al. 2013a), in utero electroporation (Gee et al. 2015) and genetic manipulation of mouse models, transgenic or knock-in (Atkin et al. 2009; Paukert et al. 2014).

GECIs are made up of a single polypeptide of fluorescent protein and a calcium binding site. The two most widely used sensors are the FRET (Förster Resonance Energy Transfer) based ratiometric sensors and the GCaMP sensors. While FRET sensors, for example the yellow cameleon-Nano (Horikawa et al. 2010), have their advantages, such as the possibility to quantify the resting calcium level, the GCaMP sensors remain more widely-available and currently the best option for single-wavelength calcium monitoring in astrocytes: GCaMP sensors have better dynamic ranges and are simpler to adapt to an imaging setup since they require a single detector channel, unlike FRET sensors which require two different excitation wavelengths and two detector channels (Shigetomi et al. 2016; Akerboom et al. 2012; Lohr et al. 2021).

The GCaMP sensors are mutant green fluorescent protein (GFP) variants, which produce large increases in GFP baseline green fluorescence in response to increased calcium concentration, with unrivalled brightness and excellent signal-to-noise that can be applied for high speed imaging of cellular activity (Shigetomi et al. 2016; Russell 2011). The GCaMP6 series developed by the Janelia GENIE Project, has been adapted to chronic imaging with minimal deleterious cellular effects (Srinivasan et al. 2015) and allows the visualisation of entire astrocytes (Bindocci et al. 2017; Shigetomi et al.

2013a). Viral transfection with adeno-associated viruses (AAVs) and Cre-driven genetic expression of GCaMP indicators have widened the availability of animal models for studying astrocytic involvement in physiological functions and in disease states. The fast kinetics of GCaMP6f (Chen et al. 2013) offers high spatial and temporal resolution that allows the detection of rapid calcium changes within processes and microdomains, at a similar timescale to neuronal firing (Stobart et al. 2018a). A membrane-tagged variant, Ick-GCaMP6f offers the possibility to visualise astrocytic activity relevant to synaptic modulation and neurovascular coupling (Shigetomi et al. 2013a; Shigetomi et al. 2013b; Stobart et al. 2018a). All these technical developments have unlocked the possibility of investigating previously undetectable mechanisms. However, one must keep in mind that calcium indicators do have their drawbacks. They buffer calcium and in so doing may modify astrocyte function, may induce astrogliosis (Ortinski et al. 2010) and may decrease overall neuronal health (Zariwala et al. 2012).

1.4.2 Calcium imaging analysis

The application of GECIs to astrocyte calcium imaging, in combination with two-photon laser scanning microscopy, has revealed complex calcium signalling spanning the entire astrocyte territory. This added critical information about physiologically-relevant astrocyte sub compartments that were previously inaccessible, such as activity within the finer processes/microdomains related to synaptic activity. GECIs crucially revealed the true nature and abundance of astrocyte activity. This brought with it a parallel development of calcium analysis protocols to address the increased complexity that now necessitates a certain degree of automated analysis due to the large data sets and user-bias (Venugopal et al. 2019). A major inconsistency is now shrouding astrocyte calcium imaging analysis, since a standardised protocol has yet to be established.

1.4.3 Astrocyte calcium imaging software packages

A number of calcium analysis packages have been developed to tackle population, single cell, and sub-cellular imaging, especially in the past decade, most based on the definition of static regions of interest (ROIs). Static ROIs vary greatly between neurons and astrocyte due to the cells' entirely different morphology and the overall slower calcium kinetics in astrocytes. A number of static ROI analysis packages are available for neuronal calcium analysis, including SIMA (Kaifosh, Zaremba, Danielson, & Losonczy, 2014), Suite2p (Pachitariu et al. 2016), NETCAL (Orlandi et al. 2017), CalmAn (Giovannucci et al. 2019) and EZcalcium (Cantu et al. 2020), as well as static ROIs for astrocyte calcium analysis, GECIquant (Venugopal et al. 2019; Srinivasan et al. 2015), and CaSCaDe (Agarwal et al. 2017). The latest crucial advancements came with the advent of dynamic, event based astrocyte calcium detection, namely

CalciumCV (Kustikova et al. 2018), AQuA (Wang et al. 2019), and Begonia (Bjørnstad et al. 2021). AQuA and Begonia were specifically designed for the analysis of complex astrocyte calcium dynamics detected with GECIs, however are proving to be extremely versatile and applicable to most cell types, not just astrocytes. Previously applied algorithms were unable to appreciate the full complexity of astrocyte calcium fluctuations, since static ROIs couldn't be accurately applied to activity that varied in location, size and duration, with possible overlap with neighbouring activity. A common theme in most packages is the need of a certain degree of programming knowledge to apply them to one's datasets.

The detection of calcium activity and events involves four common steps, irrespective of the application or algorithms employed: (i) denoising to improve the signal to noise ratio, since calcium imaging tends to be noisy, and generally includes a smoothing filter such as the Gaussian smoothing filter; (ii) motion correction to make up for shifts in x and y directions, or more complex shifts in and out of the z plane - several algorithms have been successfully applied, such as the subpixel image registration, a form of two-dimensional rigid transformation based on discrete Fourier transform (Guizar-Sicairos et al. 2008); (iii) classification of active regions: pixel or object based segmentation is commonly used – object-based segmentation uses spectral and spatial information to define objects made up of a group of similar pixels, such as in CalmAn and EZcalcium, which are however not suitable for activity within complex structures; pixel-based methods consider only spectral similarities but map out each pixel, such as the Otsu thresholding method that distinguishes light or dark clustered pixels (Otsu 1979), used in SIMA; (iv) quantification: the previous steps serve to define independent regions of fluorescence activity within the field of view, which is then most commonly quantified by calculating the relative change in fluorescence, defined as the change in fluorescence relative to baseline fluorescence levels ($\Delta F/F_0$). (Robbins et al. 2021). Raw or normalised data is then commonly exported to widely used programming platforms, such as MATLAB (The MathWorks, Inc., USA) for further analysis that may be lab or experiment specific.

1.4.3.1 GECIQuant: an astrocyte calcium analysis package based on static ROIs

GECIQuant software, an ImageJ plugin, uses an ROI-based approach for the semi-automated detection and quantification of astrocyte calcium changes (Venugopal et al. 2019). It is particularly useful since it was developed with the intention of analysing in vivo astrocyte calcium imaging acquired with GECIs and two-photon laser scanning microscopy (Shigetomi, et al. 2013a), a technique responsible for numerous critical advances in the field of astrocyte research (Bazargani and Attwell 2016). GECIQuant

was the first available package that effectively picked up calcium changes within the finer astrocyte structures. The defined ROIs have a unique spatial location with a defined static area. The package defines ROIs within the different sub-cellular compartments based on a user-defined size (i.e., the central soma, proximal and distal processes and microdomains). The user also defines a pixel intensity threshold calculated from a maximum intensity projection of the whole image stack, and which also includes a background subtraction step to improve the signal-to-noise ratio. The magnitude and duration of calcium transients within each ROI is extracted, together with ROI intensity kymographs to reveal spatio-temporal calcium patterns.

1.4.3.2 NETCAL and CHIPS: automated cell sorting algorithms for neuronal or astrocyte calcium analysis

Various calcium analysis packages are based on automated cell-sorting algorithms which have gained popularity, some modelled on the successful combination of (i) Principal Components Analysis (PCA) to detect active regions and reduce the spatial dimensionality, and (ii) Independent Component Analysis (ICA), which combines the spatial components with the changes observed over time to determine independent signals, and in doing so defining static ROIs. This algorithm was first developed by Mukamel (Mukamel et al. 2009) and later incorporated into calcium analysis software packages for the network analysis of neuronal calcium signals (NETCAL©: NETwork and population dynamics analysis of CALcium imaging recordings) and also for the analysis of neuronal and astrocyte calcium dynamics in subcellular compartments (CHIPS, Cellular and Hemodynamic Image Processing Suite (Barrett et al. 2018)). Each software package has its own combination of denoising, filtering and other parameters that better suit their specific aims. CHIPS has the added feature of detecting the velocity of red blood cells passing through blood vessels, while NETCAL is able to pick up coordinated network activity in neuronal populations while also offering various spike inference algorithms. Both packages are based on MATLAB programming language and make use of the 'findpeaks' MATLAB (The MathWorks, Inc., USA) function to detect peaks in calcium fluctuations to define calcium events. User input is however still essential since IPA and ICA parameters need to be adapted to the imaging quality and type of ongoing activity.

1.4.3.3 AQuA and Begonia: event-based automated algorithms for astrocyte calcium signalling

Begonia is the latest example of an automated, event-based algorithm (Bjørnstad et al. 2021), that improved on an earlier, but also very recent, analysis package: AQuA, Astrocyte Quantitative Analysis (Wang et al. 2019). AQUA revolutionised calcium signalling detection by defining a calcium 'event as a cycle of a signal increase and

decrease that coherently occurs in a spatially connected region defined by the fluorescence dynamics' (Wang et al. 2019), irrespective of cell structure. Both packages were specifically designed for the analysis of astrocyte calcium signals acquired with the use of GECIs, but which are highly versatile and can be applied to one or two-photon imaging and any cell type. Begonia requires less computational power, handles noisy data, can easily manage higher acquisition rates of >30 Hz, and requires less user-defined parameters, all-in-all creating a 'precise and unbiased' (Bjørnstad et al. 2021) toolbox that also combines extracted calcium data with other typically acquired in-vivo signals, such as electroencephalogram (EEG), electromyogram (EMG), locomotion and whisking. Begonia's output is however less extensive than AQuA, since the former only outputs the frequency of events, density of events per time unit, duration and spatial spread. AQuA on the other hand, gives the spatiotemporal dynamics of each single event, describing such parameters as area, direction and speed of propagation. The common limitation of both algorithms is that they once again fail to provide automated detection of the different subcellular compartments.

AQuA and Begonia proved to be a huge advancement in the field of astrocyte calcium signalling, since earlier approaches of static ROIs failed to fully appreciate the complex dynamics of intracellular calcium changes in astrocytes. Begonia is based on independent regions of activity (ROA) that replace the traditional ROIs. ROAs are based on a method that analyses the spectral qualities of the images in a pixel-by-pixel fashion, creating a highly precise algorithm that pick up the slightest significant changes in pixel intensity. It employs event detection based on a pixel-specific threshold: it combines information on spatially linked active voxels with active voxels linked also in time, to define single calcium events that are dynamic, i.e. the shape and area of a single event changes with time. This is highly useful since intracellular calcium fluctuations in astrocytes are not restricted to specific locations within the cell and calcium does not originate within the same subcellular region in the different events. This gives a complex picture of calcium activity which varies not only in location and size, but also in the way it spreads to neighbouring regions, and whether it occurs independently or in coordinated fashion with other subcellular regions or on a population level.

1.4.4 Application of 3-D two-photon laser scanning microscopy with event-based calcium detection

Bindocci et al. (2017) combined the latest two-photon imaging technology and GECIs with dynamic ROI and voxel-based fluorescence detection to observe and quantify complex intracellular calcium changes in the entire territory of single astrocytes. They capture the full three-dimensional shape of a single astrocyte and monitor full-single cell

calcium fluctuations by acquiring z-stacks of a volume of interest. They show that calcium signalling within the astrocyte entire territory is highly heterogenous and compartmentalised, with the major activity occurring in its periphery, termed 'glialpil', which makes up about 75% of the astrocyte volume. This highlights the failings of previous studies that focussed solely, or mostly, on activity within the soma, which Bindocci et al. (2017) show are mostly inactive. Bindocci et al. (2017) were able to make several observations, including: (i) calcium tends to initiate around the periphery and spreads to the core/soma; (ii) endfeet activity is heterogenous and not synchronous and may or may not spread to the soma; (iii) synaptic activity induces time-correlated calcium changes in less than 1% of the astrocyte volume, which highlights the importance of picking up minor calcium fluctuations in the cell peripheries that are most likely to be relevant to ongoing synaptic activity and network excitability. This study was critical in reinforcing the idea that astrocyte calcium activity within the finer processes reflects physiologically significant events, and previous studies that ignored this activity by focussing only on the somata, while still relevant and useful, may have missed crucial information and require re-evaluation.

1.4.5 Overview of calcium detection and analysis

While standard, static ROIs, are becoming less popular, they are still valid semi-automated methods of astrocyte calcium detection, partly due to their simpler and less power-intensive algorithms that are able to pick up crucial differences in the different astrocyte sub-compartments. Capturing the full complexity of astrocyte calcium signalling with automated algorithms, while being an impressive feat, might in the end not reveal more than the simpler ROI approaches that 'ignore' the full complexity of the ongoing activity. This is because the physiological relevance of the additional activity is unknown. So while the latest advances in calcium analysis are providing a more complete observational picture of astrocyte calcium activity, the physiological relevance of the complexity of the ongoing activity will remain a mystery until we gain a better understanding of basic calcium signalling mechanisms in astrocytes, and until specific calcium patterns can be linked to certain behaviours or physiological events or diseased states. Moreover, fully automated algorithms do have a vital limitation, which is the exclusion of experimenter input, who can judge what is relevant for hypothesis testing based on his/her expertise and experience.

1.5 Astrocyte response to sensory input

1.5.1 The somatosensory system

The somatosensory system involves coordinated activity in several body/brain regions, to facilitate spatial awareness and feedback for motor control and coordination. Sensory ganglion cells in the body's periphery, i.e. neurons of the trigeminal ganglia and dorsal root ganglia, propagate information to the central nervous system and transduce the sensory information into a change in membrane potential (see Figure 1-3 for an example from the vibrissae of rats). This ability enables them to depolarise in response to a stimulus, such as a change in temperature, pH or mechanical input, and in turn generate action potentials by means of voltage-gated Na⁺ channels, which are propagated along their axons to the central nervous system. Needless to say, several receptor types with different properties and sensory function are involved in somatic sensation. (Coggeshall 1986; Rosenfalck 1969; Darian-Smith 1969)

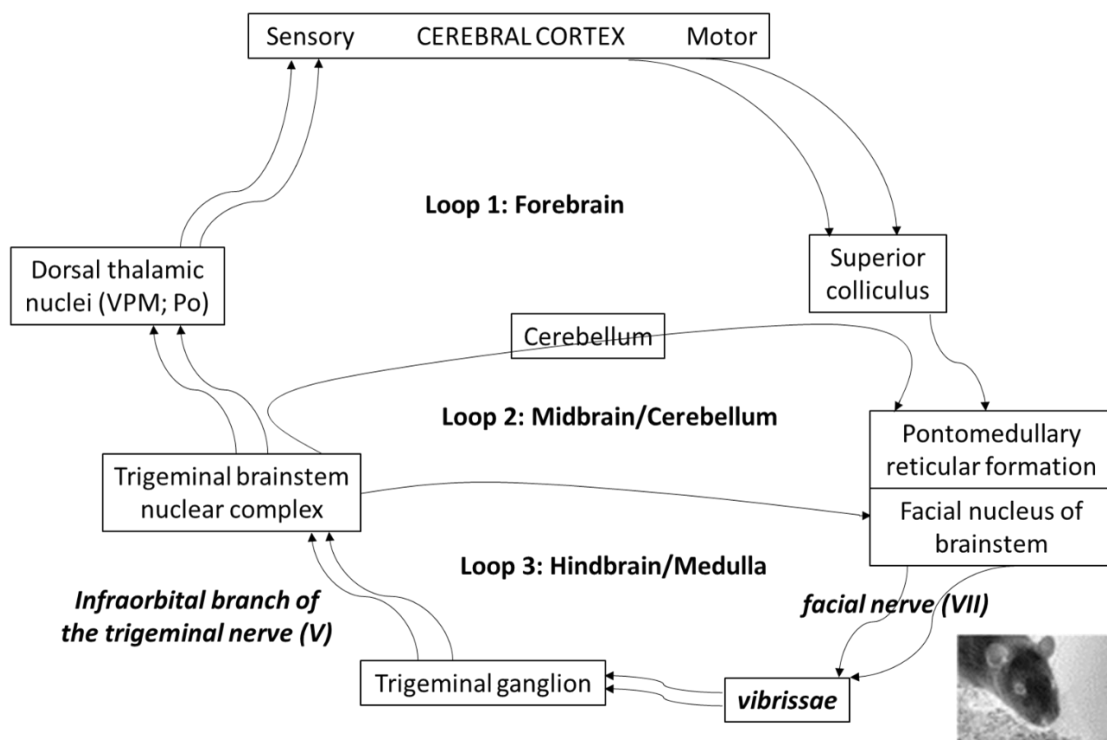


Figure 1-3: The vibrissal sensorimotor system in rodents.

The vibrissal (or trigeminal) system in rodents involves several brain regions, including the hindbrain, cerebellum, and the thalamo-cortical network. Adapted from van Lujtelaar & Sitnikova (2006)

Several brain regions are involved in the processing of sensory information for touch, most crucially, the thalamus and somatosensory cortex. Afferent sensory fibres originating in the sensory ganglion cells pass through the spinal column to the ventrobasal complex (VB) of the thalamus. The thalamus then sends separate afferents (from the ventral posterior medial and lateral thalamic nuclei) to the primary and

secondary somatosensory cortex, which in turn relay the information intra-cortically. Thalamic neurons exhibit so called lemniscal properties, reinforced by the anatomical presence of thalamic rods. Such rods receive axons from the same part of the body and only carry that specific information. This creates an effective system that distinguishes place- and modality- specific responses. (Van Der Loos 1976; Bourassa et al. 1995; Koralek et al. 1990; Jones and Friedman 1982)

Moreover, the primary somatosensory cortex (S1) exhibits somatic body mapping (Sanchez Panchuelo et al. 2018). For instance, the barrel field cortex (S1BF) in layer IV of S1 in rodent models, shows barrel-specific activation to single whisker stimulation (Petersen and Sakmann 2001). Each whisker is contralaterally mapped in the different anatomically defined barrels in S1BF. Vibrissae stimulation and whisker deflections send signals to specific barrels depending on which whisker is activated, making this an ideal model to study information processing (Lübke et al. 2003). Barreloids in the VB receive this information and project it to layer IV S1BF neurons, which in turn project to cortical layers II/III or layers V/VI (Petersen 2007).

1.5.2 Astrocyte response in the barrel field cortex

Similar to neurons, astrocytes in S1BF exhibit somatotopic selectivity. Neural stimulation of individual barrels induces an mGluR-receptor-dependent response in astrocytes, in the form of intracellular calcium increase. The calcium increase is restricted to single barrels, independent of gap-junctions coupling, but also spreads to layers II/III where it spreads horizontally across the barrel borders, following the same pathway of activation as neuronal responses (Schipke et al. 2008). This implies that astrocytes within the barrels have a peculiar property that restricts their calcium response to within the barrel. In fact, (i) astrocytes in layer IV do not respond to spontaneous neuronal activity in layers II/III, and (ii) disruption of purinergic and GABA signalling inhibition results in a wider layer IV astrocyte activation, no longer restricted to within the barrels (Schipke et al. 2008). This evidence indicates that astrocytes selectively respond to excitatory neuronal input emerging from layer IV, and that the localised response to barrel stimulation is not an anatomical one, but rather depends on a delicate balance of excitatory/inhibitory signalling, which astrocytes may, in turn, modulate through excitatory or inhibitory gliotransmitter release.

1.5.3 Astrocyte response to sensory input and locomotion

Various *in vivo* studies have established that astrocytes respond to various forms of sensory input in different brain areas by intracellular calcium elevation. Astrocytes respond to locomotion with global, synchronous intracellular calcium increase, observed

in the visual cortex (Slezak et al. 2019; Srinivasan et al. 2015; Paukert et al. 2014) and S1 (Dombeck et al. 2007; Bojarskaite et al. 2020; Bindocci et al. 2017), mediated by noradrenaline release and α -1 noradrenergic receptor activation (Slezak et al. 2019). Similarly, specialised astrocytes in the cerebellum (Bergmann glia) respond with global synchronous intracellular calcium increase during voluntary or forced locomotion (Paukert et al. 2014; Dombeck et al. 2007), mediated by noradrenergic and glutamatergic signalling which act synergistically (Paukert et al. 2014). A similar global, widespread response has been reported to startle stimuli in the visual cortex, mediated by α -1 noradrenergic receptors and IP3R2-mediated signalling, with a longer-lasting calcium increase that is independent of these signalling pathways (Srinivasan et al. 2015), as well as in the somatosensory cortex, also mediated by α -1 noradrenergic receptors (Ding et al. 2013).

Astrocytes in the visual cortex respond to visual stimuli in a reliable but more subtle way (Slezak et al. 2019; Asada et al. 2015; Paukert et al. 2014; Sonoda et al. 2018), depending on the behavioural state and state of arousal; a heightened state of vigilance induces a stronger and more synchronous astrocyte calcium response (Slezak et al. 2019; Paukert et al. 2014), which is TTX-dependent (Asada et al. 2015), but contradicting results indicate that the astrocyte response might or might not be mediated by α -1 noradrenergic receptor activation (Slezak et al. 2019; Paukert et al. 2014). The influence of noradrenaline release on astrocyte calcium activation was confirmed in the somatosensory cortex following hindlimb stimulation (Bekar et al. 2008; Lines et al. 2020), shown to be mediated by α -1 noradrenergic receptor activation, with no influence from glutamatergic signalling (Bekar et al. 2008), while occurring in a summative manner and modulating the increased levels of cortical gamma activity that accompany sensory stimulation (Lines et al. 2020).

Further studies in the somatosensory cortex show that astrocytes respond to whisker stimulation sporadically, with an intracellular calcium increase, mediated by α -1 noradrenergic receptors with no influence from glutamatergic signalling (Ding et al. 2013). Astrocytes respond accordingly to an increased whisker stimulus frequency, following a similar pattern of neuronal response (Zhao et al. 2012). A further study performed in S1 under anaesthesia, confirms that astrocytes respond differently depending on the frequency of whisker stimulation, however, in contrast, they show that the astrocyte response is partly mediated by mGluR1 and mGluR5 receptors (Wang et al. 2006). The latter observation was reinforced by more recent *in vivo* studies which investigated the astrocyte response in S1BF layers II/III, also in response to whisker stimulation. The bulk of the astrocyte calcium response was shown to be strongly

mediated by noradrenergic or cholinergic input, but fast astrocyte signalling, occurring on a time scale similar to neurons and possibly linked to synaptic activity, was potentially mediated by glutamatergic signalling (Stobart et al. 2018a). The direct involvement of mGluR mediated signalling pathway has been confirmed (Lind et al. 2013; Lind et al. 2018). Moreover, astrocytes also show an increase in coordinated, synchronous activity during whisker deflection (Stobart et al. 2018b) as well as during hind paw stimulation (Stobart et al. 2018b).

These studies unequivocally show that astrocytes selectively respond to sensory stimulation in a summative manner, with two separate mechanisms, one dependent on widespread neuromodulator release and a second dependent on glutamatergic transmission. The latter is accompanied by fast calcium activity in the astrocyte periphery that outlasts the initial response to sensory input (Srinivasan et al. 2015; Stobart et al. 2018a), possibly contributing to the maintenance of ongoing network changes. Widespread neuromodulator release clearly has a strong effect on the sensory response, by strengthening local interactions between astrocytes and neurons and synchronised activity (Paukert et al. 2014; Wahis and Holt 2021), also supported by more recent evidence that high vigilance states increase noradrenaline release as well as astrocyte recruitment, which in turn release cAMP (to boost energy metabolism mediated by glycogenolysis), but only after sustained noradrenergic activation, this time modulated by β -1 noradrenergic receptor activation (Oe et al. 2020).

1.6 Epilepsy

1.6.1 Classification of seizures and epilepsies

Epilepsy has been classified as one of the most common neurological diseases that affects people of all ages. Approximately 46 million people worldwide suffer from some form of epilepsy, 10-20% of which do not respond to approved anti-epileptic drugs (Beghi 2020). Epilepsy is characterised by the manifestation of recurrent, unprovoked seizures, defined by the International League Against Epilepsy and International Bureau for Epilepsy as “a transient occurrence of signs and/or symptoms due to abnormal excessive or synchronous neuronal activity in the brain” (Fisher et al. 2005). Four stages of classification need to be considered, based on the type of (i) seizure, (ii) epilepsy, (iii) syndrome and (iv) etiology. Briefly, seizures are classified in terms of type of onset, as (i) focal onset seizures accompanied by loss of consciousness or impaired awareness and with (motor) or without (non-motor) motor paroxysms; (ii) generalized onset seizures accompanied by impaired awareness, motor or non-motor, (iii) unknown onset, motor or

non-motor or (iv) unclassifiable. Focal to bilateral onset seizures have also been introduced to define secondarily generalised seizures. Epilepsies are classified by considering all the types of seizures that a patient experienced, and are classified as (i) focal (ii) generalized (iii) combined generalized and focal, or (iv) unknown. Epilepsy syndromes are then classified depending on a number of combined features that occur together, such as different types of seizures, triggers and age-related features, such as remission, while also considering the underlying causes and mechanisms, including structural, genetic, infectious, metabolic or immune etiologies. (Falco-Walter et al. 2018)

1.6.2 Astrocytes in epilepsy

Decades of research has revealed that various forms of epilepsy are accompanied by some form of astrocyte dysfunction, for instance, childhood absence epilepsy, temporal lobe epilepsy, tumor-associated epilepsy and post-traumatic epilepsy (Binder and Steinhäuser 2021; Carmignoto and Haydon 2012; Crunelli and Carmignoto 2013). A large body of evidence now points to epilepsy as being an ‘astrocytopathy’, arising from astrocyte morphological alterations, changes in astrocyte channels, receptors, transporters and enzymes, activation of inflammatory pathways, modified gap junctions, and dysregulated secretion of neuroactive molecules (Figure 1-4) (Binder and Steinhäuser 2021). Overwhelming evidence shows that astrocytes influence neuronal excitability and signalling, through GABA and glutamate uptake and release (Malarkey and Parpura 2008; Parpura et al. 1994; Araque et al. 1999), regulation of extracellular K^+ levels (Kofuji and Newman 2004), including Kir- and aquaporin-4-mediated K^+ clearance and release (Nagelhus and Ottersen 2013), and by the modulation of synaptic transmission and plasticity (Pannasch et al. 2011) and neuronal oscillations and synchrony (Carmignoto and Fellin 2006; Poskanzer and Yuste 2016). Binder & Steinhäuser (2021) argue, backed by decades of evidence, that colocalization of AQP-4, Kir4.1 and GLT1 on astrocyte membranes at synapses, provide crucial water, potassium, and glutamate homeostasis, which when disrupted, lead to hyperexcitability and seizures. Steinhäuser summarizes very well the several astroglial sources of an epileptic phenotype (Figure 1-4) (Boison and Steinhäuser 2018), and astrocytes have rightly been suggested as potential therapeutic targets to control or treat convulsive and non-convulsive epilepsies (Crunelli and Carmignoto 2013; Binder and Carson 2013).

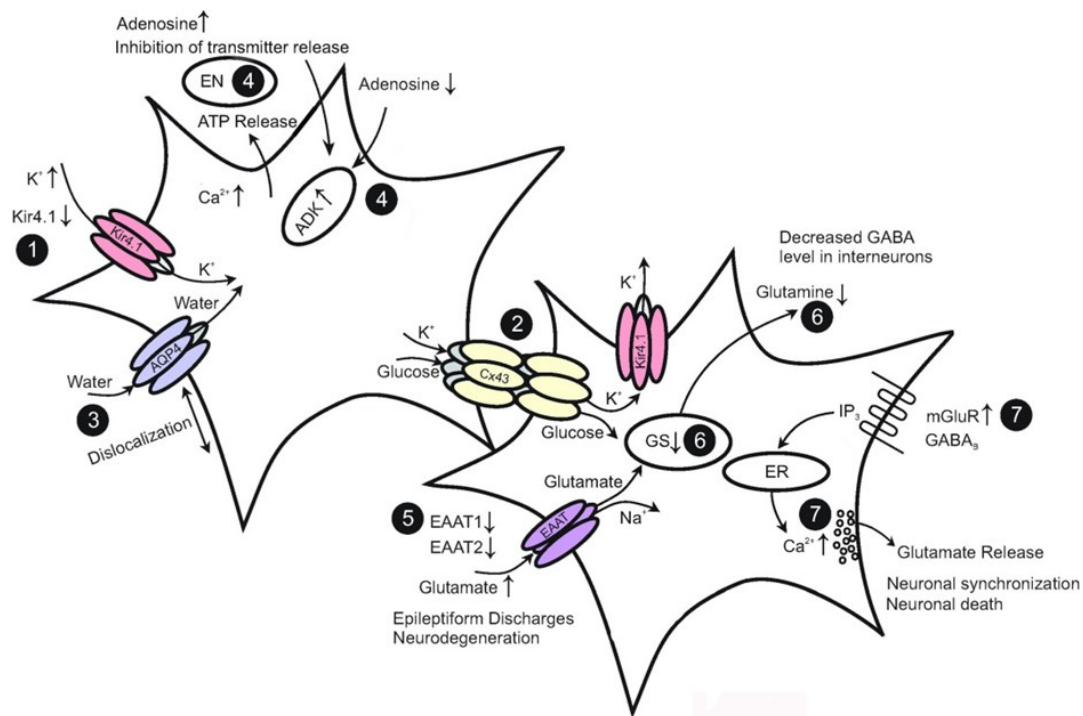


Figure 1-4 Astroglial mechanisms involved in epilepsy.

(1) Decreased Kir currents due to dysfunctional inwardly rectifying potassium channels (Kir4.1) are accompanied by increased extracellular K^+ and an epileptic phenotype in humans and animal models; (2) Loss of gap junction permeability due to connexin channel (Cx43) impairment causes impaired K^+ buffering and hyperexcitability; (3) Impaired K^+ buffering follows dislocation of aquaporin-4 water (AQP4) channels; (4) Upregulation of adenosine kinase (ADK) results in decreased adenosine levels and coincides with seizure manifestation. EN: endonucleotidases, ATP: adenosine triphosphate; (5) Impaired glutamate uptake results in a lower threshold for seizure induction, a result of reduced EAAT1 and EAAT2 channels (excitatory amino acid transporter 1 and 2); (6) Glutamine synthetase (GS) impairment leads to elevated glutamate levels and impaired inhibition due to reduced interneuron GABA release; (7) Glutamate release from astrocytes induces neuronal excitability, which is amplified by increased mGluR levels. Reproduced from (Boison and Steinhäuser 2018).

1.6.3 Astrocyte calcium activity in epilepsy

Intracellular calcium changes in astrocytes have long been linked to neuronal excitability and epileptiform activity. Calcium-dependent glutamate release excites nearby neurons (Parpura et al. 1994), promotes synchronised neuronal events by activating extrasynaptic N-methyl-D-aspartate (NMDA) receptors (Fellin et al. 2004), co-occurs with epileptiform activity (Fellin et al. 2006; Tian et al. 2005; Tashiro et al. 2002; Gould et al. 2014; Szokol et al. 2015; Ding et al. 2007; Gould et al. 2014), precedes kainate-induced seizures (Heuser et al. 2018), and is reduced after the application of anti-convulsant drugs (Tian et al. 2005). Moreover, receptors involved in intracellular calcium changes are increased in models of epilepsy (Aronica et al. 2000). Interestingly, in a slice model of focal epilepsy in which ictal discharge is induced by NMDA stimulation, ictal onset is dependent on astrocyte calcium-dependent release of glutamate or D-

serine, that induces a wider population of neurons to engage in a synchronous epileptic event, not possible without the calcium-release feedback by astrocytes that follows the initial NMDA-induced neuronal activation (Gómez-Gonzalo et al. 2010). This evidence shows that astrocytes may play a role in lowering seizure threshold and may easily tilt the network balance to a hyperexcitable one by feedback in the form of excitable gliotransmitter release.

Some studies however shed doubt on the role of astrocytes in seizure onset. Astrocyte glutamate release is not needed to induce epileptiform activity in two in vitro models using hippocampal slices, either low Mg^{2+} plus the addition of picrotoxin, or high K^+ (Fellin et al. 2006). Moreover, epileptiform events induced in somatosensory cortical slices by the application of 4-aminopyridine (4-AP) are immediately followed by gap-junction-mediated calcium waves in astrocytes, which are however shown to be independent of neuronal activity and insignificant to ictal onset (Baird-Daniel et al. 2017). However, the studies do not doubt the role that astrocytes play in prolonging seizure events or in reducing seizure threshold, which are still very important ictal-generating properties that may be exploited in the development of novel anticonvulsants. In fact, astrocytes are a source of extracellular adenosine, a known anticonvulsant (Boison 2005), and astrocyte calcium-mediated ATP release induces an inhibitory effect by activating P2Y₁-receptors on inhibitory interneurons and a subsequent increase in inhibitory post synaptic currents and inhibitory transmission in the surrounding area, thus showing anticonvulsant properties (Torres et al. 2012).

1.7 Childhood absence epilepsy and animal models of absence seizures

1.7.1 Classification and features of childhood absence epilepsy

Childhood absence epilepsy is classified as an idiopathic generalized epilepsy, also commonly defined as a genetic generalised epilepsy (Scheffer et al. 2017). It is diagnosed mostly in children between 3 and 8 years of age, and makes up 10-17% of all childhood epilepsy cases (Crunelli and Leresche 2002). The most evident clinical manifestation comes in the form of absence seizures, which consist of a sudden, relatively brief impairment of consciousness, accompanied by lack of voluntary movements and generalized, bilateral, 2.5-4 Hz synchronous (poly)Spike and slow Wave Discharges (SWDs) detected in the electroencephalograph and generated in the cortico-thalamic network (Figure 1-5) (Crunelli et al. 2020). Absence seizures are genetically determined and may represent a complex channelopathy arising from a variable genetic background, as indicated by the presence of abnormalities/mutations in

various voltage- and transmitter-gated channels in affected patients (Crunelli and Leresche 2002), such as the P/Q-type voltage-gated Ca^{2+} channel $\alpha 1\text{A}$ subunit (Jouvenneau et al. 2001) and the $\text{GABA}_{\text{A}}\gamma 2$ receptor subunit (Wallace et al. 2001). Several linkage and genome-scan studies have identified a number of other receptors and channels associated with patients suffering from childhood absence epilepsy, including GABA, glutamate and acetylcholine receptors, and voltage gated Na^{+} , K^{+} and Ca^{2+} channels (Crunelli and Leresche 2002), a variety of which were also identified in animal models (Maheshwari and Noebels 2014). A further two recent studies identified two novel loci associated with patients suffering from childhood absence epilepsy (International League Against Epilepsy Consortium on Complex Epilepsies 2018; EPICURE Consortium et al. 2012).

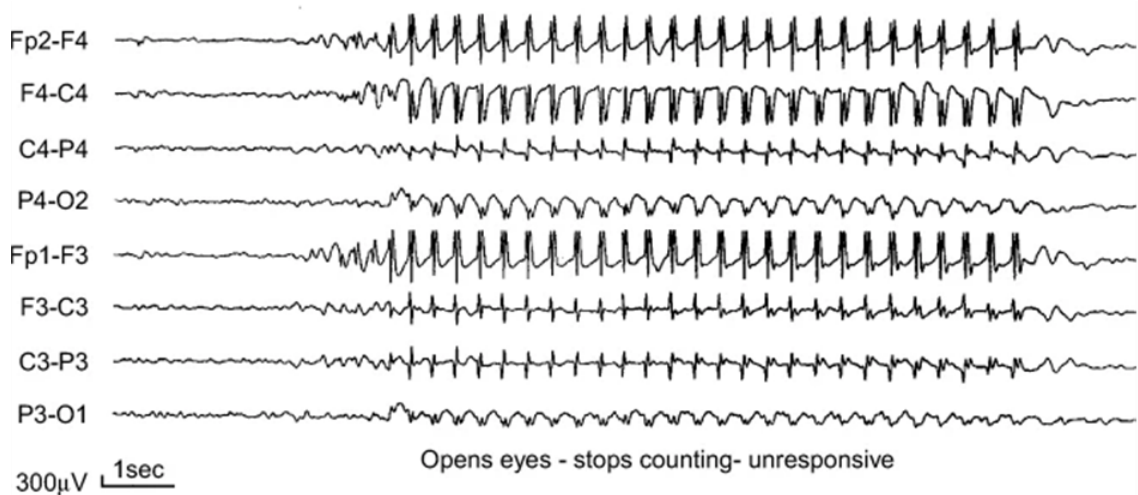


Figure 1-5: Typical electroencephalogram traces of a child suffering from childhood absence epilepsy.

Characteristic 3Hz spike and slow wave discharges in an eight-year-old boy suffering from childhood absence epilepsy. Fp2, F4, C4, P4, O2, Fp1, F3, C3, P3 and O1 refer to the location of the EEG electrodes, positioned on the frontal pole (Fp), frontal (F), central (C), parietal (P) and occipital (O) cortex. Reproduced from (Panayiotopoulos 2001)

Despite the vast clinical and EEG evidence obtained from different patient cohorts, it is still difficult to link specific genetic abnormalities to a pure absence seizure phenotype. In fact, absence seizures and other clinical observations vary greatly between patients, such as seizure occurrence, which can vary from only a few per day to up to a hundred per day, and motor symptoms which may or may not include hyperventilation, facial ticks, and loss of muscle tone. Seizures typically occur during passive wakefulness when the child is involved in a non-engaging task, but in some patients may be induced by exercise. (Crunelli et al. 2020; Crunelli and Leresche 2002)

Childhood absence seizures were, until recently, considered relatively benign, partly due to the 70% remission rate by the time children enter adolescent age. However, the failure

of monotherapy with gold-standard anti-absence drugs in more than 50% of patients (Glauser et al. 2013), the persistence of cognitive impairments even after successful seizure treatment or remission (Caplan et al. 2008; Glauser et al. 2017; Masur et al. 2013) and the possibility of developing generalized tonic-clonic seizures (Matricardi et al. 2014), suggest otherwise. Moreover, it is now known that about 60% of children suffer from various learning and behavioural comorbidities, such as increased anxiety, depression and attention deficits, possibly due to abnormal basal ganglia-limbic-monoamine networks (Crunelli et al. 2020). Further research into the understanding of basic mechanisms of absence seizure onset and termination are still required in order to identify novel therapeutic targets to overcome the current pharmaco-resistance and long-term physiological and behavioural ill-effects.

1.7.2 Current treatment strategies

Two gold-standard monotherapies have been used for decades in the treatment of childhood absence epilepsy, ethosuximide or valproic acid, together with a less successful alternative, lamotrigine. 44-45% of children treated with ethosuximide or valproic acid are seizure-free within one year of the start of treatment, which is vastly superior to the 21% achieved after lamotrigine treatment (Brigo et al. 2021). Moreover, ethosuximide achieves complete remission in 76% of patients, even in the long term (Berg et al. 2014), and with less cognitive and behavioural effects compared to valproic acid (Shinnar et al. 2017; Brigo et al. 2021), making it the current treatment of choice. Ethosuximide is a weak and non-selective blocker of T-type Ca^{2+} channels, which are key to the absence seizure pathology since blockade of these channels results in absence seizure suppression (McCafferty et al. 2018). Ethosuximide reduces hypersynchronous thalamic network activity and effectively blocks SWDs by the suppression of low-threshold calcium currents that are produced by these T-type Ca^{2+} channels in thalamic neurons (Coulter et al. 1989). The mechanisms of absence seizure suppression by valproate and lamotrigine, both broad spectrum antiepileptic drugs, are largely unknown (Kessler, Sudha Kilaru and McGinnis 2019).

1.7.3 Animal models of absence seizures

Various animal models of absence seizures have been established, the most commonly used and extensively studied being the Genetic Absence Epilepsy Rat from Strasbourg (GAERS), the Wistar Albino Glaxo/Rij (WAG/Rij) rat and the Stargazer mouse (Jafarian et al. 2020). In line with expectations from clinical epileptologists, these models are a good representation of childhood absence epilepsy in humans since they replicate four main aspects of the disease: all three models (i) suffer from spontaneous spike and wave discharges (SWD) (Figure 1-6) (ii) that occur with concomitant behavioural arrest

and minor motor paroxysms; (iii) demonstrate pharmacological specificity to anti-absence drugs, namely ethosuximide; (iv) and have underlying cortico-thalamo-cortical network dysfunction (Depaulis et al. 2016). This being said, some basic differences remain, highlighting the importance of including multiple animal models when studying a complex human disease. Absence seizures occur at 2-4 Hz in humans, but at a higher frequency in these models: 7-10 Hz in GAERS (Depaulis et al. 2016), 7-11 Hz in WAG/Rij (Sarkisova and van Luijtelaaar 2011), and 5-7 Hz in Stargazer (Felix 2002). Also, childhood absence epilepsy is a developmental disease since, as already described, it emerges early on in childhood and has a tendency to remit by adulthood, whereas in animal models absence seizures fully develop once the animals enter adulthood and persist till death.

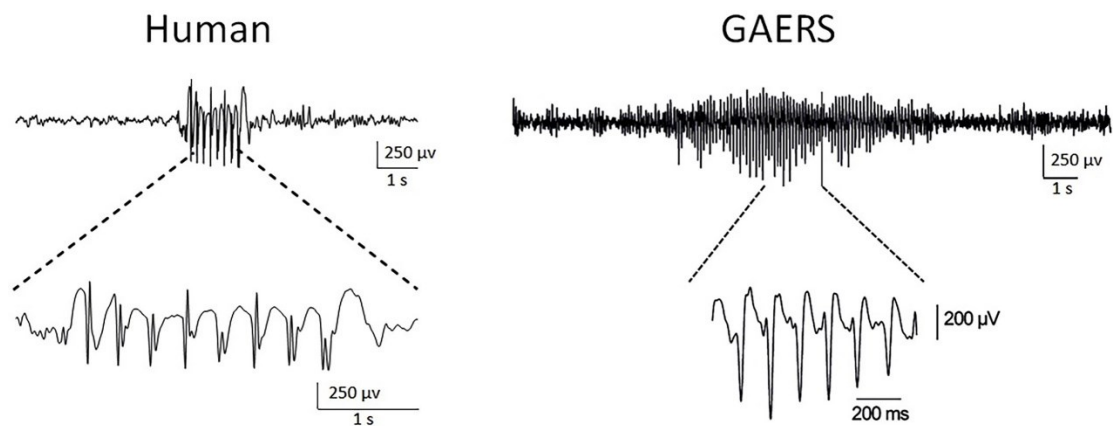


Figure 1-6: Typical human and rodent spike and wave discharges. Absences seizures can be detected with electroencephalographic (EEG) recordings and are characterised by spike and wave discharges (SWDs), detected in human patients and in animal models of absence seizures, such as the genetic absence epilepsy rat from Strasbourg (GAERS). Left: EEG from a human patient with typical 3 Hz SWDs. Right: EEG from a rat model with typical 5-9 Hz SWDs. Reproduced from (Depaulis and Charpier 2018).

GAERS and Stargazers are the two models of most interest to my study due to their altered GABA signalling. Their GABA dysfunction strengthens their suitability as a model of childhood absence epilepsy, since GAERS and Stargazers show enhanced thalamic tonic GABA_A inhibition (Cope et al. 2009), which concurs with evidence in humans that also show higher thalamic GABA levels (Leal et al. 2016). Stargazers and GAERS have an important similarity, they both have compromised T-type calcium channels. The Stargazer, a monogenetic model, has a single nucleotide mutation in the Cacng2 protein, also referred to as stargazin. The stargazin protein is critical in the trafficking of AMPA receptors to the plasma membrane. This mutation is also accompanied by a number of other dysfunctions, including altered voltage-dependent calcium channels and T-type channels activity, and a subsequent increase in their activity. These channels

are crucial in thalamo-cortical rhythmicity and contribute to absence seizure generation in this model (Letts 2005). Moreover, GABA signalling in Stargazers is severely compromised (e.g. through reduced GABA synapses) satisfying the essential basis of absence seizure ictogenesis (Letts 2005). GAERS, a polygenic model, has a single nucleotide mutation in the Cav3.2 T-type Ca^{2+} channel gene, *Cacna1h*. This mutation was similarly observed in the human counterpart, the *CACNA1H* gene, in children suffering from childhood absence epilepsy (Chen et al. 2003; Liang et al. 2006). Given the importance of low voltage T-type channels in the burst firing and oscillatory activity of the thalamo-cortical network, this mutation is a significant contributor to absence seizure generation in this model (Perez-Reyes 2003). The critical contribution of GABA dysfunction in absence seizures is discussed in more detail in section 1.7.5.

The gamma-hydroxybutyrate (GHB) pharmacological model of absence seizures is another popular model used to investigate childhood absence epilepsy (Crunelli et al. 2006; Venzi et al. 2015; Velazquez et al. 2007). This model has been especially useful for application in transgenic mice, to investigate the influence of particular genes on absence seizures (Venzi et al. 2015). GHB is a commonly used recreational drug (Wong et al. 2004; Degenhardt et al. 2005) and consumption in humans induces a series of behavioural effects, namely sedation, euphoria, sleep, amnesia and coma (Miotto et al. 2001; Carter et al. 2006). GHB is a weak GABA_B agonist (Pistis et al. 2005; Mathivet et al. 1997; Lingenhoehl et al. 1999) and is thought to act directly on astrocytes by binding putative GHB receptors (Gould et al. 2014). In fact (i) a GABA_B agonist, baclofen, reproduces the GHB pro-epileptic effects (Crunelli et al. 2006), (ii) GABA_B antagonists block the pro-absence action of GHB (Crunelli et al. 2006), (iii) which is also blocked by NCS382, a putative GHB receptor antagonist (Maitre 1997; Danober et al. 1998).

While GHB has been extensively used in rodent models, it is now strongly believed that its suitability for use in mouse models is questionable, since most of the observed EEG and behavioural effects observed in mice are those of sedation/hypnosis (Venzi et al. 2015). Notably, valproate was ineffective at blocking GHB-induced SWDs (Ishige et al. 1996), and following GHB administration, the EEG shows a clear increase in power of lower frequency bands but with unclear or only occasional SWDs (Venzi et al. 2015). Nonetheless, it has been shown that GHB mediates its pro-absence effect by acting directly on the thalamus and increasing the tonic GABA_A current (Cope et al. 2009), in agreement with the genetic animal models and human data discussed above. The GHB pharmacological model thus remains an attractive means of investigating absence seizures in mouse models with specific abnormalities, such as the IP3R2 KO mouse

which shows highly reduced intracellular calcium release in astrocytes (refer to section 1.3.1).

1.7.4 Cortico-thalamic circuitry involved in absence seizure initiation and generalisation

1.7.4.1 Cortical initiation site

A series of high density EEG studies, fMRI and PET studies in humans have confirmed the cortico-thalamo-cortical circuitry involved in the initiation and generalisation of absence seizures (Blumenfeld 2005; Matricardi et al. 2014). Paroxysmal activity initiates in a frontal cortical region, termed the cortical initiation site, and rapidly spreads to the rest of the cortical areas and the thalamic nuclei (Holmes et al. 2004; Bai et al. 2010; Tenney et al. 2013). fMRI studies have shown that cortical activity increases significantly in the fourteen seconds before seizure onset, i.e. prior to SWD detection in the EEG (Bai et al. 2010), and that cortical regions enter a pro-ictal state one minute prior to SWD onset, characterised by increased central sensorimotor synchrony and decreased posterior synchrony, and a pre-ictal state in the 6-10 seconds prior to SWD onset, characterised by extensive synchronization of cortical hubs (Tangwiriyasakul et al. 2018). The initiation site does however vary between patients, but is consistently located in the frontal cortex and does not vary within the same patient (Bai et al. 2010).

The cortical initiation site has also been well described in polygenic rat models of absence seizures, first shown in the WAG/Rij rat (Meeren et al. 2002) and subsequently in the GAERS (Polack et al. 2007). The initiation site in the latter model has since been extensively investigated by the same Depaulis group (Depaulis et al. 2016; Studer et al. 2019; Polack et al. 2007) who investigated neuronal behaviour during the phases leading to and during SWD initiation and spread. They report several important observations related to network activity in the initiation site: (i) SWDs are first observed within the barrel field cortex, which is the cortical initiation site of absence seizures in this model; (ii) identify ictogenic properties of these cells, defined as 'short periods of suprathreshold oscillations during interictal and preictal epochs' restricted to the initiation site neurons; (iii) identify brief paroxysms restricted to the initiation site that are not accompanied by SWD generalization to other areas or behavioural/motor symptoms; (iv) cortical initiation site neurons have a more depolarized membrane potential, making them more excitable; (v) layer 5 neurons have a higher ictal firing rate and precede the EEG spike by a fast depolarization and a rapid burst of action potentials; (vi) layer 5 neurons undergo a slow, brief depolarizing phase during the wave component of the EEG; (vii) whisker-related sensory processing in the barrel field remains functional, however a less synchronised and selective response is evident. The critical role of the

cortical initiation site is clearly shown in three studies: (i) local application of tetrodotoxin (a neurotoxin) within the initiation site eliminated absence seizures (Polack et al. 2009); (ii) ethosuximide reverses the altered electrophysiological characteristics of these ictogenic cortical neurons (Polack and Champier 2009); (iii) local application of ethosuximide or a GABA_B antagonist in the cortical initiation site immediately blocks absence seizures (Manning et al. 2004). The S1BF was also confirmed as the cortical initiation site in the GHB model, using high resolution EEG and topographic mapping (Choi et al. 2010). This further strengthens the overwhelming evidence in favour of the cortical initiation hypothesis.

1.7.4.2 Thalamic-driven oscillatory behaviour

Direct evidence from neuronal recordings in various animal models has served as confirmation of the cortico-thalamo-cortical network involvement in absence seizures and to understand the cellular mechanisms of what drives SWDs within this network (Avoli 2012). However, the precise mechanism and network behaviour is still disputed, despite the numerous studies carried out in the past decades involving state-of-the-art techniques (Huguenard 2019). Recent evidence has strengthened the notion of the thalamus as a pillar in absence seizure ictogenesis, while not disputing the ictogenic role of the cortical initiation site (McCafferty et al. 2018).

An intra-thalamic excitatory-inhibitory loop has been established, composed of reciprocally connected ventrobasal (VB) thalamo-cortical (TC) neurons and nucleus reticularis thalami (NRT) neurons (Figure 1-7). Low-voltage-activated Ca²⁺ channels, T-type CaV3.1, are highly expressed in TC neurons, giving them a unique feature of producing burst firing responses following membrane hyperpolarisation due to synaptic inhibition. Moreover, TC neurons are reciprocally connected to NRT GABA-containing inhibitory neurons that also express CaV3-family channels, but which generate burst firing even in the absence of hyperpolarization. NRT cells activate during bouts of SWDs and in doing so induce a strong inhibition in TC cells causing a decrease in overall firing and forcing them to enter a slow oscillatory state. In fact, blocking NRT-induced TC inhibition causes an effective seizure block.

The interplay between these two cell types, i.e. TC excitation of NRT cells and NRT inhibition of TC cells, is the basis of the highly coordinated firing in the thalamus during absence seizures. Nonetheless, cortical pyramidal cortico-thalamic (CT) neurons add an extra and very important dimension. CT and TC neurons are bidirectionally connected through excitatory glutamatergic connections. Moreover, the cortex projects glutamatergic terminals to NRT, but does not receive NRT input. Thus cortical hyperexcitability is conveyed to the NRT-TC internal loop, and the cortex receives

feedback from the TC neurons, that are highly influenced from NRT burst firing. This creates an intimate and delicate balance of network synchrony in the distinct, but highly interconnected brain regions. The feedforward CT → NRT → TC and feedback TC → NRT → TC circuits form the basis of SWD network generalisation. (Huguenard 2019; McCafferty et al. 2018; Shepherd and Yamawaki 2021)

Accumulating evidence has also implicated the basal ganglia in absence seizure network dysfunction (Deransart et al. 2000; Depaulis et al. 1989; Paz et al. 2005; Deransart et al. 2003; Miyamoto et al. 2019; Li et al. 2009; Luo et al. 2011). The striatum (Str) and substantia nigra pars reticulata (SNpr) act as a source of inhibitory input to TC neurons, whereby suppression of Str interneurons is translated into an increase in GABAergic interneuron firing in the SNpr projecting to TC neurons, strengthening inhibitory input to the VB. This acts as an additional source of inhibition to TC neurons that adds to the strong NRT-induced TC suppression (Crunelli et al. 2020).

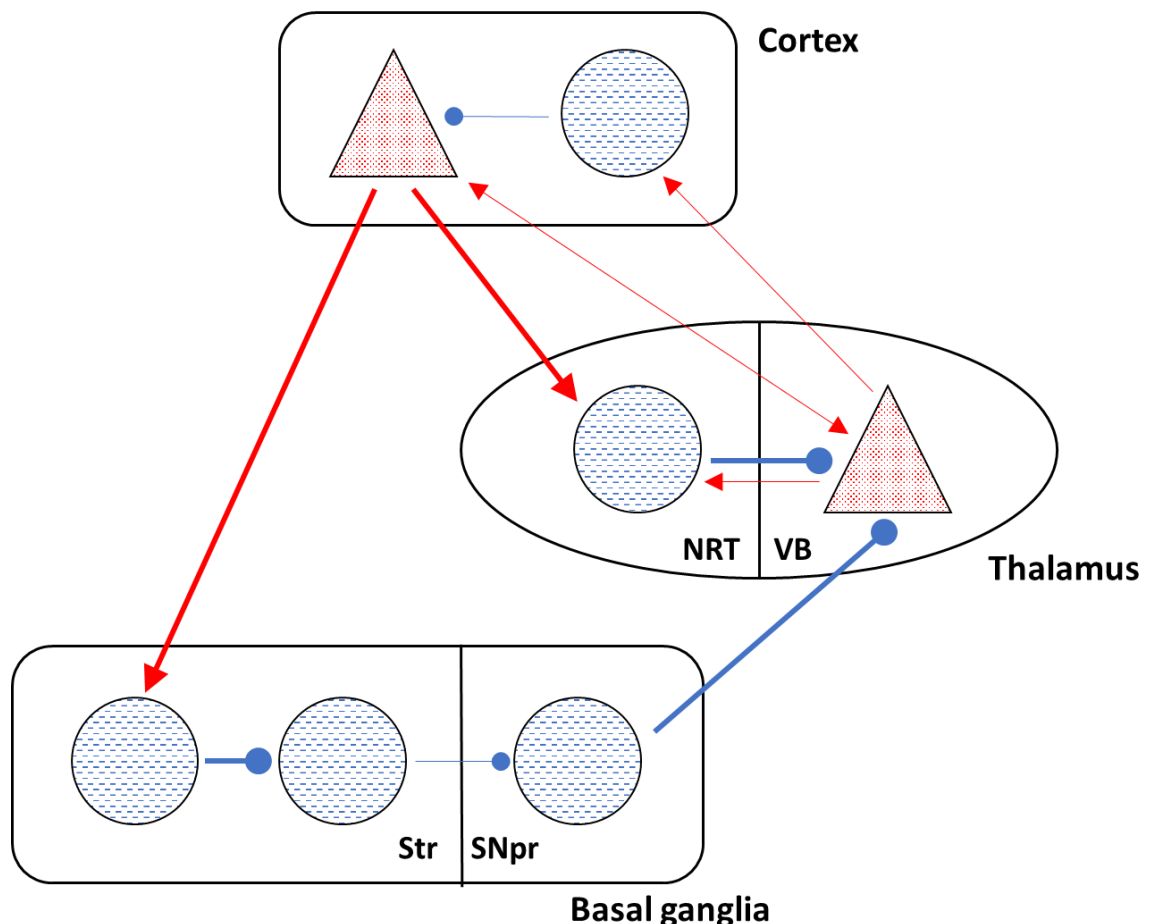


Figure 1-7: Brain networks involved in spike and wave discharges. Excitatory glutamatergic projections arise from cortico-thalamic (CT) cells and project to the ventrobasal thalamus (VB) and nucleus reticularis thalami (NRT). Thalamo-cortical (TC) cells in the VB reciprocate this connection with excitatory glutamatergic projections to cortical pyramidal neurons and inhibitory inter-neurons. The VB also sends excitatory

projections to the NRT which in turn sends inhibitory GABAergic projections to TC cells. This creates a delicate web of interconnections between the cortex and thalamus, which, through increased cortical excitability and increased GABAergic tone to TC cells, creates the typical oscillatory patterns observed in Childhood Absence Epilepsy. This system is reinforced with inhibitory projections arising from the basal ganglia and related nuclei (Striatum, Str; Substantia nigra pars reticulata, SNpr). (The thickness of the red excitatory projections (arrows) or blue inhibitory projections (circles) represents the strength of the connections)

1.7.5 Evidence of astrocyte dysfunction in animal models of absence seizure

1.7.5.1 Abnormal GABA and glutamate signalling

The all important increase in tonic GABA_A current in GAERS and Stargazers has been shown to arise from a loss-of-function of the GAT-1, GABA transporter and not from increased neuronal GABA release or GABA_A receptor expression (Cope et al. 2009). Crucially, in the thalamus of humans and rodents, the GAT-1 transporter is exclusively expressed in astrocytes (Borden 1996; De Biasi et al. 1998; Pow et al. 2005). Patch clamp data has shown that the GABA transporter current in thalamic slices is abolished by SNAP5114, a selective GAT-3 blocker, and not by NO-711, a GAT-1 selective blocker, unlike non-epileptic control (NEC) rats which require a GAT-1 and GAT-3 block co-antagonism for a complete block (Pirttimaki et al. 2010; Pirttimaki et al. 2013). GAT-1 is located near GABAergic synapses (Beenhakker and Huguenard 2010) placing it at a prime location to modulate GABA levels and network excitability. It has been posited that reduced GAT-1 thalamic activity is the cause of increased GABAergic inhibition in the area, arising from impaired astrocytic GABA uptake (Crunelli and Carmignoto 2013). In contrast, glutamatergic astrocyte-neuron communication, based on slow inward currents, is intact in GAERS thalamic nuclei (Pirttimaki et al. 2010; Pirttimaki et al. 2013). This might however not be the case in GAERS cortical networks, as evidenced by reduced glutamate uptake (Touret et al. 2007) and reduced levels of GLT-1 and GLAST glutamate transporters (Dutuit et al. 2002).

All-in-all, it is clear that GABAergic and glutamatergic signalling in the cortico-thalamo-cortical network is severely altered in animal models of absence seizures due to abnormal astrocyte function. Therefore, astrocytes lie at the heart of the cortico-thalamo-cortical network imbalance responsible for absence seizure generation.

1.7.5.2 Other astrocytic abnormalities

Abnormal IL-1 β signalling, which forms part of a pro-inflammatory pathway, has been linked to limbic seizures (Vezzani et al. 2000), febrile seizures (Dube et al. 2005) and temporal lobe epilepsy (Ravizza et al. 2008), and more recently also to absence seizure ictogenesis. Indeed, impairing IL-1 β signalling in GAERS by blocking IL-1 β synthesis, reduces the duration and number of absence seizures by half (Akin et al. 2011). Akin et

al. (2011) hypothesise that IL-1 β -mediated inhibition of astroglial glutamate uptake leads to increased glutamate extracellular levels and cortical hyperexcitability, and reversing this imbalance partly recovers the cortico-thalamic network balance. This theory was prompted from the observation that GAERS show increased IL-1 β levels specifically in the cortical initiation site and more generally in the entire somatosensory cortex (Akin et al. 2011). An earlier study suggests that GAERS cortical and thalamic astrocytes are compromised as a result of enhanced GFAP levels detected in young animals before seizure occurrence and in epileptic adults, indicative of activated astrocytes throughout their lifetime (Dutuit et al. 2000).

Connexins are protein channels that make up gap-junctions in astrocytes (Nagy et al. 2004), which are involved in: (i) intercellular ion exchange (Nedergaard et al. 2003), (ii) uptake of neurotransmitters and release of gliotransmitters, and synchronisation of astrocyte networks that may influence neuronal synchronous firing and epileptiform activity (Fellin and Carmignoto 2004), (iii) potassium and glutamate buffering, and calcium wave propagation (Lapato and Tiwari-Woodruff 2018), and (iv) synaptic plasticity (Halassa et al. 2009a; Pannasch et al. 2011), all of which may have serious implications in neuronal excitability. Studies have presented a clear link between gap junctions and epileptiform activity, but unfortunately a conflicting picture is currently available for their role in epileptiform activity. Steinhäuser and Bedner (2012) argue that while reduced gap junction coupling in astrocytes would lead to decreased K⁺ and glutamate clearance, and subsequent neuronal hyperexcitability, it would also result in an inadequate energy supply to sustain this neuronal hyperactivity and dampen neuronal synchronisation due to an impaired spread of calcium waves between astrocytes. In contrast, increased gap junction coupling would have an opposing effect, i.e. support neuronal hyperexcitability by maintaining adequate energy supplies and calcium wave propagation, while keeping efficient K⁺ and glutamate clearance to control neuronal hyperexcitability. Nonetheless, it is clear that astrocyte gap junction dysfunction is present in various forms of epilepsy, such as human mesial temporal lobe epilepsy, in which increased gap junction coupling (Lee et al. 1995), upregulated Cx43 levels (Fonseca et al. 2002) and complete uncoupling (Bedner et al. 2015) has been determined. It has recently been shown that absence seizures are also modulated by astrocyte gap junctions, since blocking gap junctions worsens absence seizures while gap-junction opening alleviates absence seizures in the WAG/Rij model (Vincze et al. 2019), and levels of Cx30 and Cx43 are elevated in the somatosensory cortex and thalamic nuclei of GAERS and WAG/Rij animals (Cavdar et al. 2021). Vincze et al. (2019) propose that increased gap junction coupling in WAG/Rij astrocytes is beneficial

for two reasons: (i) it maintains K^+ and glutamate clearance; (ii) since NMDA and AMPA receptors, including the extrasynaptic NR2B subunits, are downregulated in the thalamus of this model, enhanced glutamate and d-serine release due to increased gap junction coupling, does not result in an increased excitatory drive.

1.8 Aims

This study investigates two physiological processes: (i) synchronous and predictable cortical astrocyte calcium signalling following onset of locomotion, a process shown to be predominantly due to widespread noradrenaline release and direct binding to astrocyte $\alpha 1$ -noradrenergic receptors; and (ii) previously unexplored cortical astrocyte calcium signalling during aberrant generalisation of absence seizures, characterised by SWDs.

The study has two main aims:

1. To set up two-photon calcium imaging in awake, head-restrained mice, that are free to move on a rotating wheel, and validate our recording and analysis protocols by investigating the astrocyte response to locomotion. Furthermore we will look for calcium signalling patterns in the somatosensory cortex that might be reflective of different locomotion patterns. We hypothesise that astrocytes typically and efficiently respond to locomotion with an increase in intracellular calcium following a short delay, and that the calcium changes will be reflective of different locomotion patterns and/or intensity.
2. To investigate if patterns of astrocyte calcium activity in the cortical initiation site of animal models of absence seizures are reflective or predictive of ongoing SWDs. In addition to two-photon calcium imaging with concurrent ECoG monitoring, in head-restrained epileptic mice, LED-based calcium imaging in freely moving rodents will be set up using the Inscopix implantable miniscope. We hypothesise that astrocytes in the cortical initiation site are active prior to seizure onset, indicative of a potential role in seizure initiation, and that calcium signalling patterns are altered during periods of SWDs.

To address these goals, in vivo astrocyte calcium imaging, locomotion detection and ECoG monitoring will be performed concurrently in awake rodents. GECIs, chronic cranial windows, intra-cranial electrodes and head-restrained two-photon laser scanning microscopy techniques in mice will be set up, as well as single-photon miniature implantable microscopy for calcium imaging and seizure detection in freely-moving rats. We will look for different calcium activity patterns during periods of voluntary locomotion while focussing on sub-cellular events. A model of ataxia, the Stargazer mouse, will

reveal if astrocyte calcium changes are impaired during locomotor activity in this model. Moreover, using well-established animal models of absence seizures, the Stargazer mouse and GAERS rat, we will investigate whether astrocytes in the cortical initiation site are active prior to seizure onset and if they mirror neuronal spike and wave synchrony during absence seizures with similar calcium patterns. Astrocyte manipulation tools will also be applied to determine if altered astrocyte function influences seizure initiation and occurrence, namely the IP3R2 KO mouse that exhibits highly reduced IP3-mediated intracellular calcium release, and chemogenetic Gq-DREADD activation of cortical astrocytes that induces intracellular calcium release.

Chapter 2: Methodology

2.1 Animal use and ethics

All animal procedures were performed in accordance with the UK Home Office Animals (Scientific Procedures) Act 1986. The number of animals used and any suffering were kept to a minimum and within the limits stipulated in the Home Office Project license. Excess animal stock or animals at the end of experimentation were culled using an approved Schedule 1 method of humane killing: by exposure to carbon dioxide in a CO₂ chamber followed by cervical dislocation, or overdose of pentobarbital followed by transcatheterial perfusion.

All animals were housed in a 12:12 hour light cycle (lights on at 8 a.m., lights off at 8 p.m.) and provided with food and water ad libitum. All experiments were performed on adult animals, p90 to p180.

The following animal models were used: (i) C57BL6/J mice (purchased from The Jackson Laboratory, USA) to investigate the astrocyte response during locomotion; (ii) Stargazer mice and wild-type (WT) litter mates (bred and maintained at the Cardiff University animal facility) to investigate astrocyte activity during seizure events; (iii) Genetic Absence Epilepsy Rats from Strasbourg (GAERS; bred and maintained at the Cardiff University animal facility) to investigate astrocyte activity in the cortical initiation site during seizure events; (iv) IP3R2 knock-out (KO) mice and WT littermates (bred and maintained at the Aston University animal facility) to investigate the role of astrocyte activation in pharmacologically-induced absence seizures.

In vivo techniques were the best option to investigate astrocyte calcium activity during natural behaviours and during absence seizures, since SWDs require an anatomically and functionally intact cortico-thalamo-cortical network to be generated (Avoli and Gloor 1981; Crunelli et al. 2020; Danober, et al. 1998; Sitnikova et al. 2008; van Luijtelaar and Sitnikova 2006). Rodents were chosen for all experimental procedures since two-photon calcium imaging techniques and ECoG recordings of absence seizures have already been perfected in such species, and the readily-available and well-established genetic rat and mouse models of absence seizures offered the possibility to instantly detect ictal activity and concurrently image astrocyte calcium activity using GECIs in awake, behaving animals.

2.2 Surgical procedures and sterility

Surgical procedures were performed with utmost care for the animals. Anti-inflammatories and pain killers were administered prior to each surgery, and additional doses and/or antibiotics were given when needed, in consultation with the animal facility NACWO and veterinary. Aseptic technique was respected as outlined in the Laboratory Animal Science Association Guiding Principles for Preparing for and Undertaking Aseptic Surgery (Jennings & Berdoy, 2016). All surfaces, equipment and instruments used were sterilised before use. The surgery area and non-electrical equipment was sprayed down and wiped with 70% ethanol before each surgery. Instruments were autoclaved, drugs were prepared fresh and diluted with sterile physiological saline. Sterile surgical gowns, hair coverings, face masks and sterile gloves were worn and changed when contaminated. Separate preparation, surgery and recovery areas were used for ease of cleaning between procedures and to maintain sterility during surgery. Hands were scrubbed with HiBiScrub® before wearing any sterile clothing or gloves.

Surgical procedures that involved the use of Adeno Associated Viruses (AAVs) were carried out in special procedure rooms designated for viral work and equipped with autoclaves. Surfaces and equipment were decontaminated with Virkon™ after each procedure, and contaminated consumables were soaked in Virkon™ overnight and disposed of through the University Waste Disposal System.

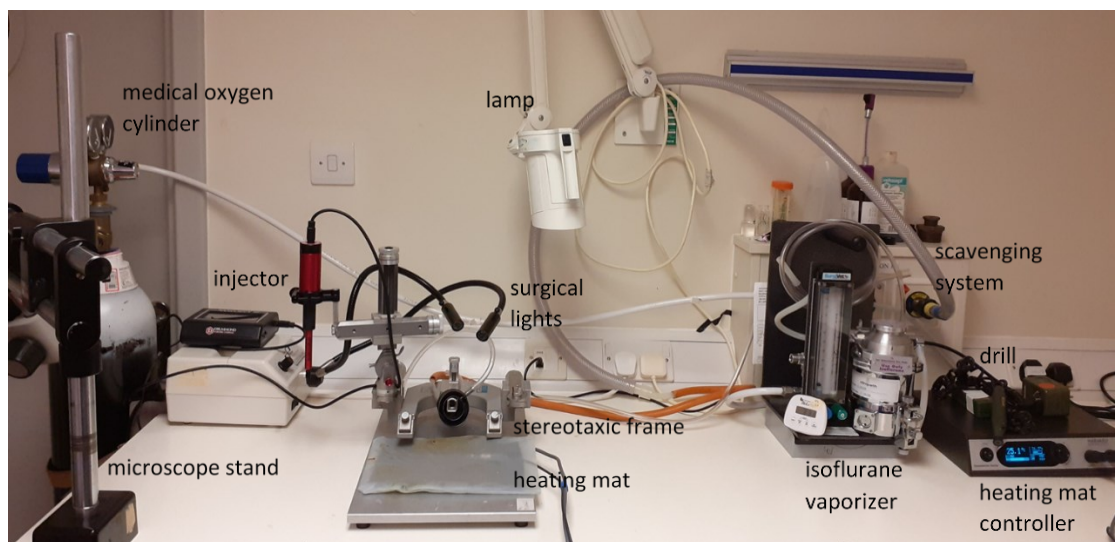


Figure 2-1: A typical stereotaxic surgery setup used in our lab.

2.3 Bilateral Electrocorticogram Recordings for absence seizure detection

GAERS rats, Stargazer mice, or IP3R2 mice were implanted with bilateral chronic electrocorticogram (ECoG) electrodes, based on a previously published protocol (Cope

et al. 2009). An ECoG signal was acquired in the freely moving animals by recording the voltage difference between two electrodes embedded in the skull, one placed in the frontal bone and one in the parietal bone, with a grounding screw placed just above the cerebellum. An amplification and digitising system converted the brain activity detected by the electrodes into a continuous quantifiable voltage change over time. Cortical activity and seizure events were thus picked up. (Further detail is given in the sections below)

2.3.1 Electrode preparation

ECoG electrodes were custom-made and prepared in the lab, and consisted of a gold-plated screw attached to a copper wire (Figure 2-2). A 1 cm section of insulated, 0.22 mm diameter, copper wire was de-insulated at either end. The tips of the wire were looped with fine tweezers, and one end was soldered to a gold-plated screw (for rat implants) or a stainless steel screw (for mouse implants) (see Table 2-1). Electrodes were rinsed with water, soaked in 70% ethanol, and dried with compressed air before implantation.

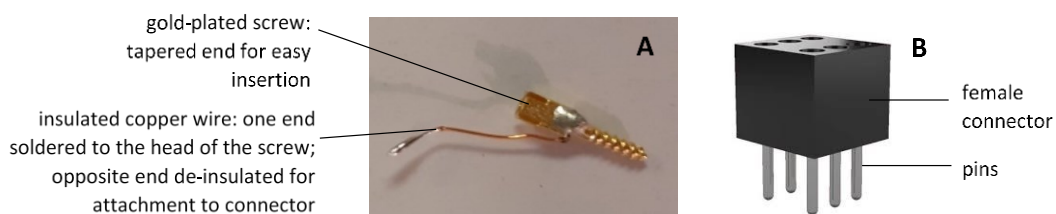


Figure 2-2: ECoG electrode design.

(A) Rat ECoG electrodes consisted of gold-plated dental screws soldered to copper wires. (B) During electrode implantation surgery, the exposed copper wire was soldered to the pins leading to a female connector, that would, in turn, be connected to the ECoG recording cable during recording sessions.

2.3.2 Electrode implantation

The animal was initially anaesthetised in an induction chamber with 5% isoflurane and 2% medical oxygen. Once the animal lost its righting reflex, it was transferred to a preparation area where it was placed on a heating pad. A nose piece was positioned over its face and anaesthesia was maintained with 3% isoflurane and 2% oxygen. An electric shaver was used to trim the portion of fur on the animal's head covering the skull. The head of the animal was cleaned from stray hairs and it was transferred to the surgery area, onto a heating pad and a stereotaxic frame. The animal was fixed to a mouth bar and a nose piece was pushed over the animal's nose to maintain anaesthesia with 2-3% isoflurane and 2% oxygen. The depth of anaesthesia was monitored throughout surgery by checking the respiration rate, pinch reflexes and vibrissae movements. Non-piercing ear bars were used to stabilise the head while avoiding

damage to the animal's skull or ear canals. Sterile eye lubricant was placed over the animal's eyes, and the scalp was cleaned with 70% ethanol and Iodine solution, alternating, each applied three times. 1 ml of physiological saline (kept at 37°C) was injected intraperitoneally, and this was supplemented with hourly subcutaneous injections of 5% glucose, dissolved in physiological saline. An incision was made with a scalpel, from between the eyes, down to between the ears. Bulldog clips were used to splay open the skin and expose the underlying tissue. Excess connective tissue was trimmed or pushed away to expose the skull. A few drops of Lidocaine/Bupivacaine mix were added on the skull surface and surrounding tissue, as a local anaesthetic to aid in the animal's recovery post-surgery. The skull was cleaned well with sterile, ice-cold physiological saline to minimise bleeding. Micro bleeds were stopped with a cauterizer. The skull was roughed up with a scalpel, by making shallow marks across its surface. This ensured a high surface area for the dental cement to attach to. In the case of rats, 5% hydrogen peroxide was applied for a few seconds on the skull surface, to further improve the grip of the dental cement and minimise bleeding.

To ensure replicability of the ECoG signal, coordinates for electrode placement were accurately determined using a micro-manipulator arm attached to a sterile stainless steel 25G needle tip. Bilateral coordinates were calculated with respect to bregma, and scuff marks to indicate the drilling site were done as follows: (1) +2 mm antero-posterior (AP) to bregma, and ± 1 mm medio-lateral (ML) to the sagittal suture, or midline, for two frontal electrodes; (2) -1 mm AP and ± 2 mm ML for two parietal electrodes; (3) 1 mm posterior to lambda and ± 2 mm ML (avoiding the third ventricle) for two ground screws (Figure 2-3). A burr drill and an 0.7 mm carbon steel tip, were used to drill a hole at the marked coordinates. Care was taken to avoid complete penetration of the skull, and to keep the dura mater intact. Electrodes were screwed in until they rested on the dura. A thin layer of Super-Bond C&B dental cement (Sun Medical, Japan) was applied on the skull and around the electrodes. While the cement hardened, the copper wires (pre-attached to the electrodes) were soldered to a female six-pin connector.

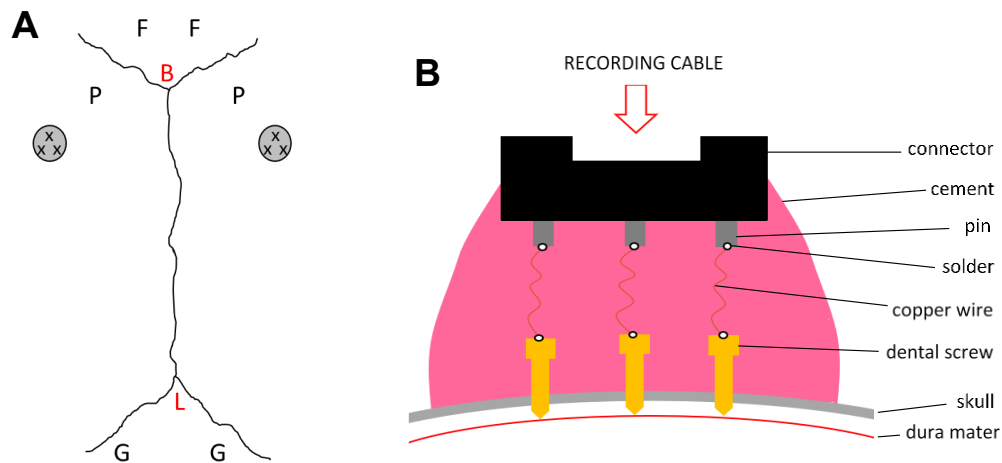


Figure 2-3: Electrode and craniotomy placement.

(A) ECoG electrode placement for bilateral ECoG recordings in freely moving animals, with sites of DREADD AAV injection, when applicable. F: frontal electrode; P: parietal electrode; G: ground electrode; X: site of injection; ○ : craniotomy; B: bregma (the point at which the coronal and sagittal sutures coincide, where the frontal and two parietal bones meet); L: lambda (the point at which the lambdoid sutures and sagittal suture coincide, where the occipital and two parietal bones meet). (B) Screws were inserted in the skull, just above the dura mater, and soldered onto a connector. The implant was cemented in place to ensure long-term recording, viable for months.

Optional step: If required, two electromyography (EMG) electrodes were implanted in the nuchal muscle of the animal to detect neck muscle activity during freely-moving recordings. An EMG electrode consisted of a stainless-steel wire embedded in the muscle and sutured in place. The other end was soldered to the same female connector used for the ECoG electrodes (modified to an eight-pin connector to accommodate the extra 2 EMG electrodes).

Super-Bond cement was brushed over the copper wires, the electrodes, and the underside of the connector. Once the Super-Bond cement set (10 – 15 minutes), Unifast Trad™ acrylic cement was used to fill in any gaps and create a crown to protect and secure the electrodes. Sterile, non-absorbable silk sutures (4-0 Mersilk™, Ethicon, USA) were used to close up the incision around the implant. The wound was rinsed with sterile physiological saline, and Iodine solution was applied. The isoflurane level was taken down to 0%, and the animal was given oxygen for 1-2 minutes to clear its airways from any anaesthetic. The animal was then taken to a heated, recovery chamber and monitored closely over the next few hours, and days. Animals were given at least 5 days of recovery before any training or recording sessions were started.

2.3.3 ECoG recording setup and protocol for seizure detection

To record the ECoG signal, the female connector on the animal's implant was attached to a cable with a male, gold-plated connector, leading to a pre-amplifier (0.08 Hz high-pass filter, 10 M Ω impedance) and an analogue ECoG amplifier (4-channel BioAmp, SuperTech Inc., Hungary; x1000 gain, 500 Hz low-pass filter). The signal was digitized with a Micro3 Cambridge Electronic Design (CED) digitizer at 1000 Hz, using CED Spike2 v7.4 (CED, UK).

One week after surgery, the animal was handled in its home cage for a few minutes per day to get accustomed to the experimenter. Two weeks after surgery, the animal was habituated to the recording room and recording cage (open-topped plexiglass cage, 40 cm x 40 cm), as follows:

- Day 1: animal placed in the recording room for 1 hour in home cage
- Day 2: animal placed in the recording room for 30 min in recording cage
- Day 3: repetition of day 2 with a dummy recording cable attached to the animal
- Day 4: repetition of day 3 with occasional handling
- Day 5: repetition of day 4
- Day 8: first day of recording

On the day of recording, the animal was transferred to the recording cage at 8 a.m. (at lights on) and attached to the recording setup. To detect spontaneous absence seizures, GAERS or Stargazer animals were recorded for a period of 2 hours. To detect pharmacologically induced absence seizures in a model of astrocyte dysfunction, IP3R2 KO or WT mice were recorded for a baseline period of 30 minutes and injected with 75 mg/kg (i.p.) of gamma butyrolactone (GBL) (or an equal volume of vehicle - sterile physiological saline). Seizure properties were quantified before and after seizure induction (see section 2.5).

Recording cages were cleaned with 30 % ethanol at the end of each recording session and replenished with fresh bedding to maintain an identical recording environment between recording sessions.

2.4 Chemogenetics

To determine the role of astrocytes in SWD initiation and/or generation, ECoG recording in freely moving animals was supplemented with chemogenetic activation of astrocyte activity. A Designer Receptors Exclusively Activated by Designer Drug (DREADD), AAV5 GFAP-HA-hM3D(Gq)-IRES-mCitrine (Duke viral vector core, USA), was injected bilaterally into the somatosensory cortex to specifically target astrocytes within the

cortical initiation site of absence seizures (*Figure 2-4*). Activation of the DREADD was achieved by injecting Clozapine N-oxide (CNO, 1 mg/kg i.p., HelloBio, UK) or DREADD agonist 21 (1 mg/kg i.p., HelloBio, UK), both previously shown to specifically activate DREADDs (Thompson et al. 2018; Armbruster et al. 2007; Chen et al. 2015). DREADD agonist 21 was used as an alternative to CNO since it has been shown to have better brain penetration and less off-target binding (Thompson et al. 2018).

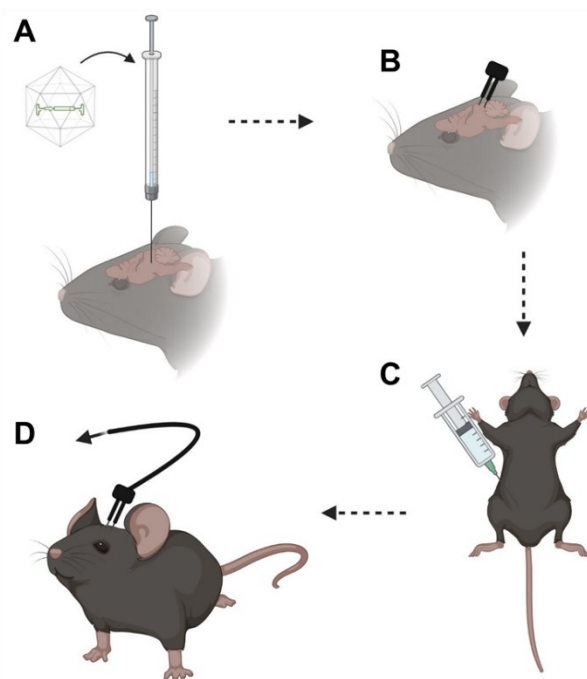


Figure 2-4: Chemogenetic activation of astrocytes.

(A) Step 1: An AAV carrying the DREADD is injected in the S1BF of the animal using a Hamilton™ syringe and an injection pump. (B) Step 2: Chronic ECoG electrodes are implanted to detect ictal activity. (C) Step 3: Three weeks are allowed for astrocytes to express the DREADD, and on the day of recording a DREADD activator is administered intraperitoneally to stimulate astrocyte activity. (D) Step 4: ECoG recordings are performed in awake, freely-moving animals to determine the effect of DREADD astrocyte activation on ECoG activity, in this case on SWD generation.

2.4.1 DREADD injection preparation

Single barrel borosilicate capillaries (WPI, USA) were pulled using a horizontal micropipette puller (Sutter Instruments Co., Model P-80 / PC, Heat: 789, Pull: 50, Velocity: 70, Time: 80). The tips were broken to a diameter of 10-30 μm and bevelled using a rotating disk, while attached to a vacuum pump that ejected air to expel any glass fragments. The pipette was then dipped in ethanol to remove any dust on its surface and placed in a petri dish under UV light for sterilization.

Prior to injection, the glass capillary was backfilled with mineral oil (Fisher Scientific, UK) and attached to a 5 μl Gastight Microliter™ Hamilton™ syringe by means of a Hamilton™ Compression Fitting (see Table 2-1).

2.4.2 Surgical procedure

Following the procedure described in section 2.3.2 above, the skull was prepared for drilling. To ensure precise coordinates for S1BF targeting, the skull was levelled, as follows. The dorso-ventral (DV) coordinates of bregma and lambda were checked, and the skull was adjusted if these varied by more than $\pm 50 \mu\text{m}$ (Resendez et al. 2016).

Similarly, the DV coordinates at 3 mm ML of either hemisphere were compared, and the skull was adjusted if these points varied by more than $\pm 50 \mu\text{m}$. Using an 0.5 mm carbon steel drill tip, a 1 mm craniotomy was performed above the barrel field cortex of both hemispheres: adult mouse coordinates, -1.5 mm AP and ± 3 mm ML; adult rat coordinates, -2.5 mm AP and ± 5 ML mm.

The DREADD was stored at -20°C until this point and defrosted on ice just before injection. 5 μl of the AAV were placed on a section of parafilm, and the injector (UMP3 injector, World Precision Instruments, WPI, USA) was loaded with approximately 3 μl of the AAV. The tip of the pipette was centered on the craniotomy and lowered to the brain surface. The injector was started (initial injection rate of 10 nl per minute) before penetrating the brain, to create positive pressure and avoid potential blockage of the pipette tip. The pipette was lowered to -2 mm DV in mice or -3.5 mm DV in rats. 750 nl of DREADD (titre $>10^{13}$ GC/ml) was then injected at 3 sites, 0.5 mm apart (Figure 2-3A), using an injection rate of 50 nl per minute. Once the injection was complete, the injection site was sealed with sterile bone wax (Harvard Apparatus, USA). The ECoG electrodes were then implanted as outlined in section 2.3.2 above, and the animal was allowed to recover. ECoG recording sessions were commenced after 3 weeks to allow the DREADD to be expressed in astrocytes.

2.4.3 ECoG recording setup and protocol with DREADD activation

The habituation protocol described in section 2.3.3 was carried out before the recording sessions were started. On the day of recording, the animal was transferred to the recording cage at lights on and connected to the recording setup. The animal was recorded for a 1-hour baseline period, injected intraperitoneally with CNO or DREADD agonist 21, and recorded for an additional 2 hours. Since SWDs rarely occur during sleep (Marescaux et al. 1992; Lannes et al. 1988), the animal was kept in a state of vigilance by occasional, gentle physical stimulation, which is most favourable for SWD occurrence (Lannes et al. 1988). Seizure properties were quantified before and after DREADD activation (see section 2.5).

2.5 Seizure detection and quantification

SWDs and ictal periods were detected and quantified using a semi-automated method, as previously described (Venzi et al. 2016), using the 'Sleep spindle/seizure' script in Spike2 v7.4, prepared by CED for the Crunelli group at Cardiff University (an updated version is available directly from the CED website, <http://ced.co.uk/downloads/scripts/spkanal>) (Figure 2-5). The acquired data was pre-

processed (high pass-filtered with DC remove, 0.1 s time constant) and an interictal period of control was manually selected, i.e., a period of awake desynchronized brain activity before any drug interventions were administered. The control period was used to define a suitable voltage threshold to detect spikes. The script used the detected spikes to define putative ictal periods containing SWDs using the following parameters: (i) the initiation of a SWD was detected when two spikes were separated by less than the maximum onset interval (set at 0.2 s); (ii) an ictal period remained ongoing as long as successive spikes were not separated by a value lower than the maximum continuation interval (set at 0.4 s); (iii) consecutive ictal periods with a separation of less than 0.5 s were defined as a single ictal event; (iv) ictal periods were no less than 1 s duration. Instantaneous frequencies were calculated for each putative ictal period, and only those within a 5 to 12 Hz range were accepted as true ictal periods with SWDs. The output of the script was visually inspected for any errors and the timings were exported as '.mat' files for further processing in Matlab (Matlab R2018b, The Mathworks Inc., USA). Using a custom-made Matlab script, the total number of seizures, the average duration of seizures and the total time spent in seizure (as described in (Marescaux et al. 1992)) were calculated and plotted in 20 minute blocks. Each block was normalized to the average of the 60-minute baseline period before drug administration and presented as a percentage change.

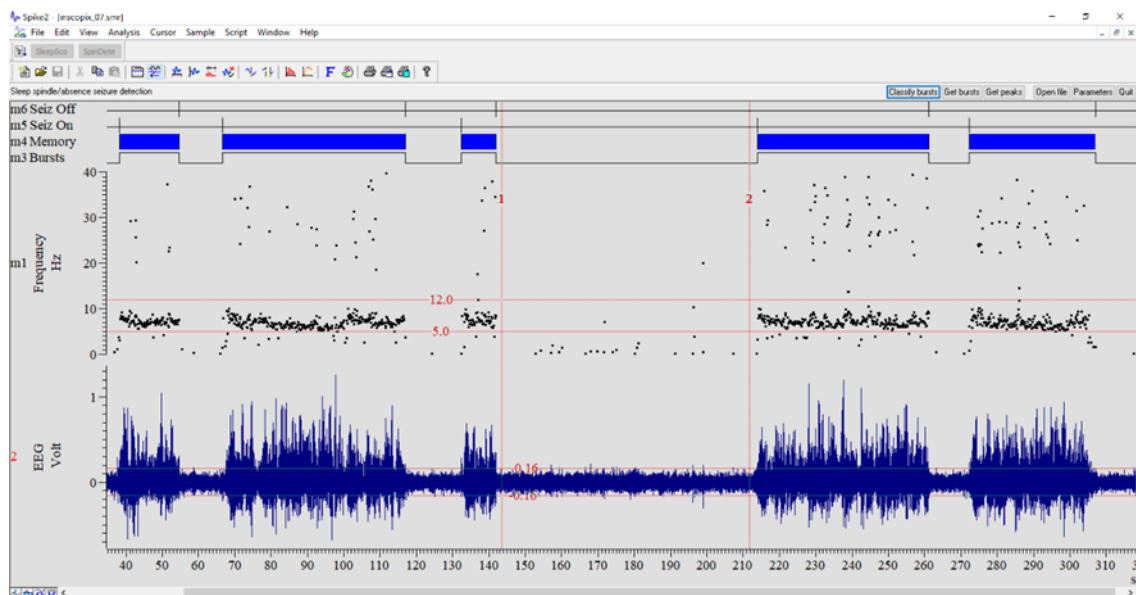


Figure 2-5: Ictal event detection with Spike2 SeizureDetect script.

A screenshot of Spike2 v7.4 workspace showing the output of the SeizureDetect script. The bottom channel, '2-EEG', shows the acquired ECoG data after pre-processing (DC remove, 0.1 s time constant). The SWDs are easily visible by eye, with a clear amplitude change. The vertical cursors show the control period chosen to calculate the voltage threshold, which is indicated by the two horizontal cursors. 'm1-Frequency' channel shows the individually detected points that exceed the threshold, and the selected

frequency range of 5 – 12 Hz indicated by the horizontal cursors. Channels 'm3-Bursts' and 'm4-Memory' show the detected and accepted ictal periods, respectively. Channels 'm5-Seiz On' and 'm6-Seiz Off' indicate seizure onset and termination, respectively.

2.6 Two-photon calcium imaging experiments and ECoG recording in head-restrained, awake mice

To measure and correlate astrocyte activity with neuronal ictal events, I made use of two-photon calcium imaging of GCaMP6f-expressing cortical astrocytes, with simultaneous ECoG recording in awake, head-restrained mice. Due to practical limitations only mouse models could be used, which is why the GAERS model was, unfortunately, not used in this set of experiments. The Stargazer genetic model and the GHB pharmacological model in WT mice were used as models of absence seizures. The setup is illustrated in Figure 2-6.

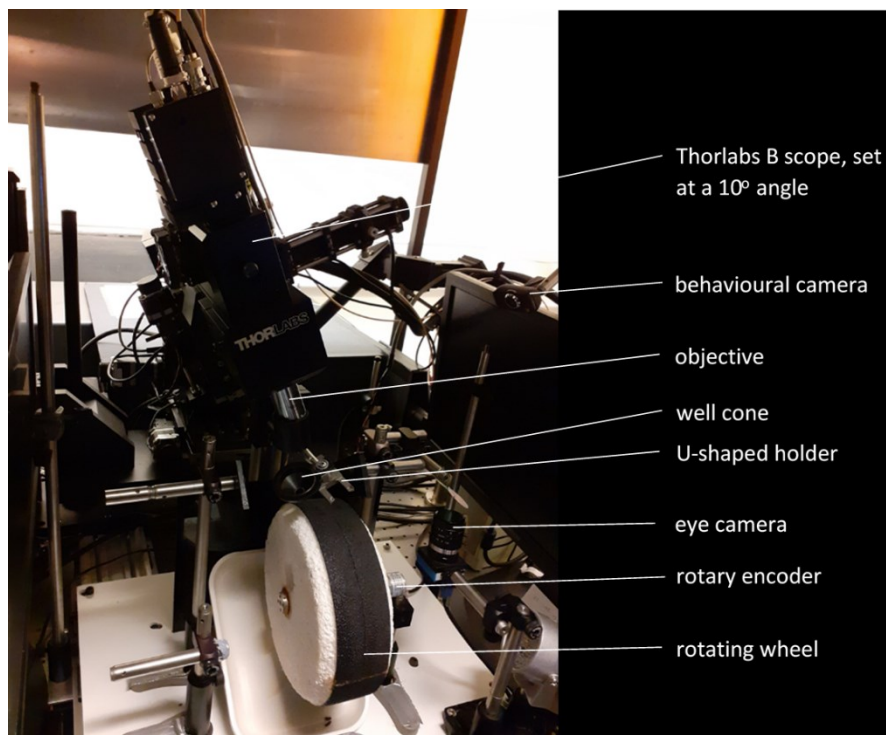


Figure 2-6: Two-photon calcium imaging mouse setup at Cardiff University.

2.6.1 ECoG electrode and headplate preparation

The implantation of a headplate for head-fixation and the proximity of the microscope objective to the cranial window, created space restrictions, which meant that the ECoG screw design described in section 2.3.1 above had to be revised and the headplate itself had to be slimmed down to make space for the electrodes (Figure 2-7). The stainless steel, 1 mm thick, headplates were designed to fit the already-established two-photon setup at Cardiff University (Crunelli and Sengpiel groups), specifically assembled for head-fixed calcium imaging in mice (refer to Figure 2-6). The new custom-made

electrodes consisted of three single strands of insulated, 0.125 mm diameter, silver wire (de-insulated at either end), each individually soldered to a pin leading to a female connector. The connector chosen was a slim, three-pin connector, that offered little stability, but which was suitable for head-fixed recordings.

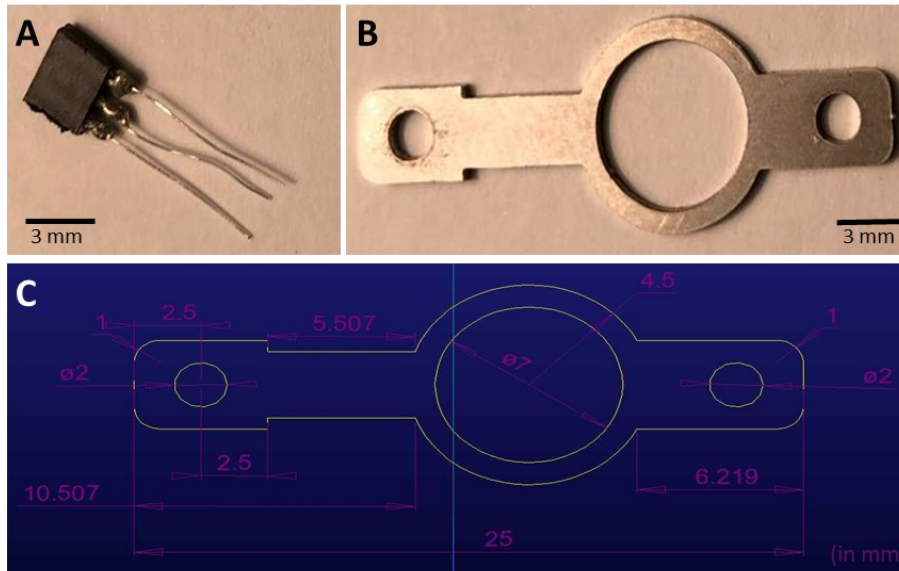


Figure 2-7: Custom ECoG electrodes and laser-cut head-plate design. (A) An ECoG electrode consisted of a slim 3-pin female connector (pins trimmed to 1 mm in length) soldered to three insulated silver wires. (B) The head-plate was designed to fit the imaging setup already established in the Cardiff lab. The circular frame of the head-plate was flanked with two vertical arms that were secured to a U-shaped frame with bolts for head-fixed imaging. The stainless-steel head-plate had a slim, 1 mm thick, frame that allowed room for the ECoG electrode to fit alongside it, while offering enough support to keep the animal's head still during calcium imaging experiments. (C) Head-plate AutoCAD® design (measurements shown in mm; Ø: diameter).

2.6.2 ECoG implantation, AAV injection and chronic window implantation

The protocol for chronic window implantation was based on Goldey et al. (2014). Dexamethasone (7.5 mg/kg) was administered intramuscularly in the thigh muscle at the start of surgery, to minimise brain swelling during the craniotomy. The mouse skull was prepared for electrode implantation, as explained in section 2.3.2 above. Three craniotomies (~ 0.5 mm diameter) were performed for electrode placement, as follows: over the frontal cortex (+1 mm AP, -2 mm ML), over the somatosensory cortex (-1.5 mm AP, -3.5 mm ML), and over the cerebellum (just posterior to lambda) (Figure 2-8). The electrode was secured to a custom-made gripper, in turn attached to a manipulator arm. The arm was held in place and the silver wires were moved in place over the craniotomies. The wires were trimmed to the desired length, and the ends were bent at 90° to create a hook shape. The 'hook' was gently inserted, using fine tweezers, into the craniotomy on the underside of the skull, touching, but not penetrating, the dura mater. A drop of 3M™ Vetbond™ (3M, USA), non-toxic tissue adhesive, was used to seal the

craniotomies and keep the wires in place while the female connector was positioned perpendicular to the skull, just above the left eye. Superbond C&B cement was then used to secure the connector and wires in place.

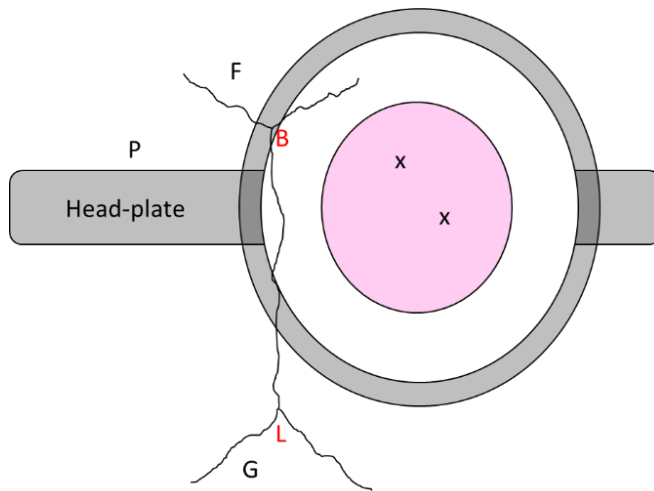



Figure 2-8: Electrode and chronic window craniotomy placement for two-photon imaging experiments. ECoG electrodes were implanted on the left hemisphere, and the craniotomy for AAV injection and chronic window placement was performed on the right hemisphere. The head bar was positioned across the skull to allow head-fixation during the recordings. F: frontal electrode; P: parietal electrode; G: ground electrode; X: site of AAV injection; : craniotomy; B: bregma; L: lambda.

The coordinates for the right hemisphere barrel field cortex (-1.5 mm AP, +3.5 mm ML) were marked-out on the surface of the skull with a blade. A headplate was attached to a manipulator arm with a custom-made gripper and was cemented in place parallel to the skull's curvature, using opaque SuperBond C&B cement. A 3.5 mm tissue punch was then used to score a circle around the marked coordinate, and an 0.5 mm carbon steel drill tip was used to open a 3 mm craniotomy. This was done slowly, with drilling frequently stopped, and the tip cooled in sterile ice-cold physiological saline to prevent over-heating and cortical inflammation/damage. When the skull was visibly thinned, and just about to start cracking, fine tweezers were used to gently pierce the skull and lift the flap of bone to one side, which was gently peeled off. The brain surface was kept moist at all times with sterile physiological saline. 1 μ l of AAV (AAV5 gfaABC1D-cyto-GCaMP6f, titre 1.4×10^{13} GC/ml, with/without AAV5 gfaABC1D-mCherry-hPMCA2w/b, titre $>10^{13}$ GC/ml) was injected at two sites (rate of 50 nl per minute) centered in the middle of the craniotomy, at a depth of 200 μ m. The pipette tip was kept in place for 10 minutes after each injection, to prevent the virus from seeping out as the pipette was pulled out.

A glass window (made from three layers of glass: one 5 mm window with two 3 mm windows beneath (Harvard Apparatus, UK), glued together with UV-curing adhesive) was snugly inserted inside the craniotomy and kept in place with a custom-made wooden holder. Vetbond™ was applied around the window, excess glue was removed with sterile absorbent sponges (Sugi®, QuestAlpha, USA), and allowed to set to create a water-tight seal. The window was permanently secured in place with opaque

Superbond C&B cement. The cement was given 15 minutes to set and harden, and the animal was brought out of anaesthesia and allowed to recover.

A high dose of Rimadyl (30 mg/l) was given to the mice in drinking water for 7 days post-surgery to minimise bone re-growth and avoid occlusion of the craniotomy.

2.6.3 Calcium imaging and ECoG recording

One week after surgery, the animal was handled in its home cage for a few minutes per day, to familiarise the animal with human contact. Two weeks after surgery, the animal was habituated to the recording setup and wheel, as follows:

- Day 1: the animal was handled in the recording room for a few minutes, and the animal's movement was periodically restricted by holding onto its headplate
- Day 2: additional handling, which included briefly setting the mouse on the wheel, with some head-movement restriction
- Day 3: the animal was head-fixed on the wheel for 5 minutes
- Day 4: the animal was head-fixed on the wheel for 15 minutes with ECoG cable attached and laser microscope occasionally powered up
- Day 5: the animal was head-fixed on the wheel for 30 minutes with ECoG cable attached and laser microscope occasionally powered up
- Day 8: first day of recording

Calcium imaging was started after at least three weeks following AAV injection to allow for AAV expression in astrocytes. Habituation of the animal to the recording setup was important for two reasons: (1) to ensure that the animal was not stressed during recording sessions, and (2) for the animals to get accustomed to running on the wheel.

On the day of recording, the animal was placed on the wheel and head-restrained by securing the headplate to a U-shaped holder (Figure 2-9). The microscope objective was lowered into a water-filled well that formed a tight seal with the headplate, and the ECoG cable was attached to the connector. Fluorescence imaging was performed using a resonant scanning microscope (B Scope, Thorlabs) with a 16x 0.8NA objective (Nikon). GCaMP6f was excited at 980 nm with a Ti:sapphire laser (Coherent, Chameleon) and the laser power set to a maximum of 60 mW. Data acquisition was at 30 Hz and averaged to 5 Hz for storage. A fixed axis cylindrical treadmill monitored the animal's rate of movement with a rotary encoder (Kübler, 05.2400.1122.0100). An infra-red eye camera and an infra-red behavioural camera were used to monitor the animal's movement/behaviour and pupil size. Data acquisition was controlled through a pre-written MATLAB (MathWorks, Massachusetts) code based on ScanImage 4.0 (custom written by the Cardiff lab) and multifunctional DAQ cards (NI PCIe-6323, National

Instruments). The fluorescence and ECoG outputs were coordinated by sending an alternating 5 V signal from a DAQ card to the micro1401 CED, which allowed sub-millisecond synchronisation.

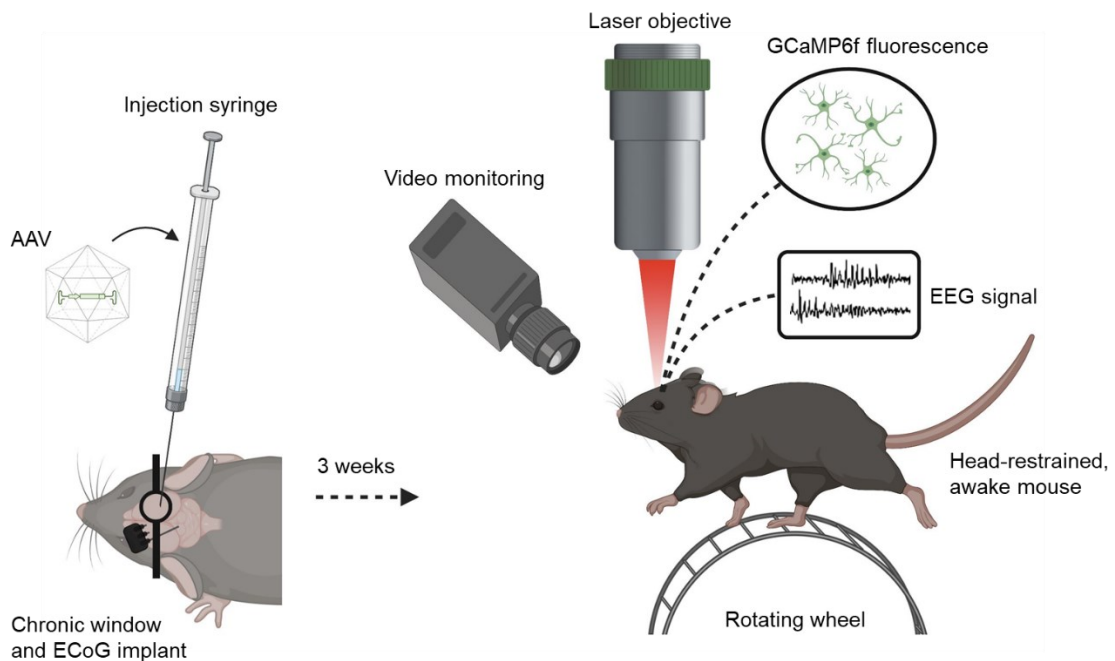


Figure 2-9: Mouse implantation for awake, head-restrained two-photon imaging. (A) Electrode placement, craniotomy, AAV injection, and headplate implantation in anaesthetised mouse. (B) Head-restrained, astrocyte calcium imaging in a mouse free to run on a treadmill, with simultaneous ECoG recording and video monitoring.

2.6.4 Imaging protocol and analysis

A number of raw data files were stored at the end of each imaging session: (1) .tiff stack of the acquired two-photon images, (2) .avi files of the body camera and the eye camera, (3) .mat file with the rotary encoder data, time, frame numbers and synchronization pulses, (4) ECoG channels and synchronization pulse. (Figure 2-10)

The .tiff stack was processed to extract astrocyte calcium changes, as follows. (1) DFT subpixel transformation (Guizar-Sicairos et al. 2008) was used to correct any movements of the field of view (FOV) in the x and y coordinates. This aligned all the images within the .tiff sequence and trimmed the edges of the FOV to produce a complete FOV throughout the recording. (2) The corrected .tiff file was imported into ImageJ for ROI selection and trace extraction. The ImageJ GECIQuant plugin enabled ROI selection in a semi-automated manner. Background subtraction was performed to deduct background fluorescence from each image. ROIs that contained calcium elevations were then selected using the GECIQuant ROI selection tool, with visual confirmation and manual modification if required. Four ROI types were selected: soma ($>30 \mu\text{m}^2$), proximal process ($>20 \mu\text{m}^2$), endfoot ($1\text{-}20 \mu\text{m}^2$) and microdomain ($1\text{-}20 \mu\text{m}^2$).

(3) Using ImageJ's Multi Measure tool, the pixel intensity within each ROI was averaged for each frame to give the mean ROI intensity for that frame, and extracted for the full time course to give the fluorescence changes over time for each ROI, $F(t)$. (4) The fluorescence traces were then imported into the MATLAB workspace and a custom script developed by the Carmignoto lab (Mariotti et al. 2018) was used to further process the fluorescence traces. The fluorescence changes were normalized to allow comparisons between different recordings and animals. The calcium changes for each ROI were expressed as $dF/F_0 = (F(t) - F_0)/F_0$, where F_0 was defined as the 15th percentile of that trace. A baseline trace was calculated from the points that fell between ± 2 SD of the entire trace. A new standard deviation was calculated for the baseline trace, and calcium peaks were detected (using the findpeaks function on MATLAB) if they exceeded a threshold set at 2 SD. Peaks were then accepted, using a supervised algorithm, when they exceeded 4 SD and any noisy ROIs were excluded manually. The number of accepted peaks (or events) were quantified, and their amplitude, duration, AUC, and frequency was extracted.

The ECoG data was synchronised to the imaging data by aligning the common pulse that was sent to the ECoG CED Spike 2v7 setup from the two-photon DAQ card. Similarly, the speed data from the rotary encoder was aligned with the imaging data and ECoG data.

The average calcium trace of each compartment (soma, proximal process, microdomain, endfoot), the calcium events, the detected ictal periods and the speed data were plotted. The plot was used to manually define calcium events belonging to periods of movement, stillness, or ictal activity. Three behavioural states were defined, as follows: (1) Awake Still, in which no wheel movement was detected and the animal had an awake ECoG signature; (2) Awake Active, in which the animal recorded movements with speeds of ≥ 5 cm/s. Multiple active periods separated by less than 5 seconds were defined as a single Awake Active period. (3) Ictal, in which epileptic mice underwent a period of at least 30 seconds of 'on and off' ictal activity detected in the ECoG, with wheel rotations of less than 2 cm/s and less than 2 seconds duration. The number of peaks per ROI per minute was then calculated for each behavioural state, using a custom written script on MATLAB.

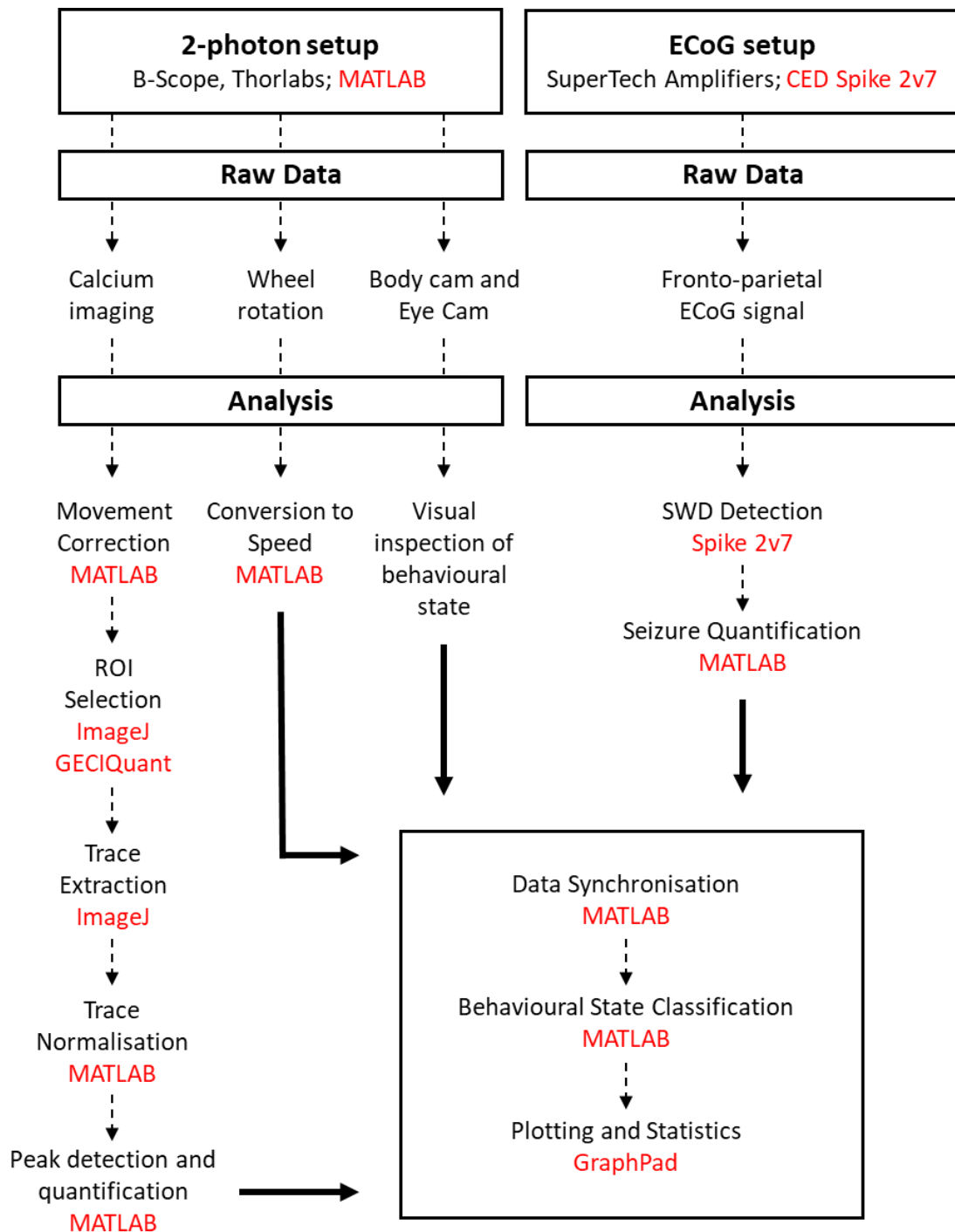


Figure 2-10: Calcium analysis workflow

2.7 Calcium imaging and ECoG recording in freely moving GAERS during different behaviours

A miniature head-mounted microscope (Inscopix, USA) was used to detect astrocyte calcium activity in the cortical initiation site of freely moving GAERS, while detecting ongoing seizure activity with ECoG electrodes. The surgical procedure involved a number of steps, each weeks apart: Step 1 – an AAV carrying GCaMP6f with an

astrocyte promoter was injected into the left S1BF; Step 2 - a grin lens was inserted in S1BF layer 5 within the area of GCaMP6f-expressing astrocytes, and ECoG electrodes were inserted in the skull on the opposite hemisphere; Step 3 – a baseplate was attached to the skull above the lens, to serve as a platform to which the miniscope would be attached; Step 4 – on the day of recording, the portable, miniature miniscope was secured to the baseplate for live imaging, the ECoG cable was attached and video monitoring was set up. (Further detail in the sections below.)

2.7.1 Step 1: AAV injection

The rat's skull was prepared for AAV injection in S1BF layer V, as outlined in 2.4.2 above. 1 μ l of AAV5 gfaABC1D-cyto-GCaMP6f (titre 1.4×10^{13} GC/ml) was injected at 2 sites in the left hemisphere (-2.25 and -2.75 mm AP, -5.0 mm ML) (Figure 2-11): 0.5 μ l were injected at -3.5 mm DV, and the remaining 0.5 μ l were injected at -3.0 mm DV. The injection site was sealed with bone wax, the skin was sutured back together, and the animal was allowed to recover. Three weeks were given for astrocytes to express GCaMP6f.

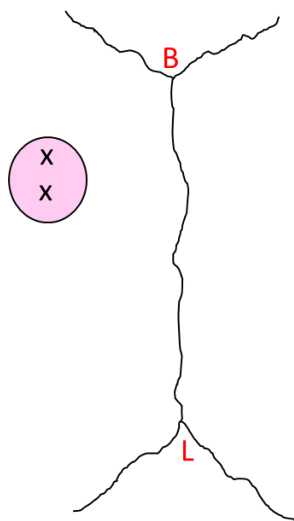


Figure 2-11: Sites of AAV GCaMP6f injection for Inscopix experiments. GCaMP6f was injected in the left S1BF, in preparation for grin lens and ECoG electrode implantation in subsequent steps. B: bregma; L: lambda; X: site of injection; \odot : craniotomy.

2.7.2 Step 2: ECoG electrodes and lens implantation

The rat's skull was prepared for electrode and lens implantation (refer to sections 2.3.2 and 2.4.2 above). Coordinates were marked out for the ECoG electrodes and lens placement (-2.5 mm AP and -4.5 mm ML). Due to the lateral positioning of the lens and the importance of placing cement all around the implant for a stable structure, the muscle attached to the left lateral skull ridge was gently detached using sterile wooden applicators to provide more skull surface to work with. Fronto-parietal ECoG screws were then inserted in the right hemisphere, together with a ground electrode above the cerebellum. An extra parietal screw was inserted to serve as a back-up reference screw. Four support stainless steel screws (0.5 mm diameter) were inserted around the site of lens implantation, and a 1 – 1.5 mm craniotomy was performed at the site of lens implantation (Figure 2-12A). Care was taken to keep the craniotomy as close to 1 mm in diameter as possible, to ensure a tight-fitting lens. The craniotomy was kept moist at all times. Bleeding was controlled using irrigation with ice-cold saline, and in case of stubborn bleeds, sterile cellulose hemostat (SURGICEL® FIBRILLAR™) was used.

The difference in the DV coordinates of the skull at -2.5 mm AP, -3 mm ML and at the brain surface at -2.5 mm AP, -5.0 mm ML was noted for future reference. The dura was carefully peeled off using a sterile, bent 25G needle tip. Care was taken to clear the craniotomy from any bone fragments, and to control bleeding and avoid the formation of large clots that would impair lens insertion. A dissecting knife (Fine Science Tools, UK) was attached to the manipulator arm and lowered to the brain surface at -2.5 mm AP, -5.0 mm ML. The knife was then lowered down to -1.6 mm DV at a rate of 0.2 mm per minute. The knife was moved medially, also at a rate of 0.2 mm per minute, to -4.0 mm ML. After 5 minutes the knife was gently removed from the brain. Once again, great care was taken to keep the brain surface moist, and clear from bleeds. The grin lens (ProView™ Prism Probe, Inscopix, USA) was attached to the ProView™ implant kit (Inscopix, USA) that secured the lens to the manipulator arm, and which allowed the miniscope to be attached to the cuff of the lens for live monitoring of calcium changes during surgery. Next, using the DV difference between the skull and brain surface noted above, the lens was lowered to the brain surface and centred at -2.5 mm AP, with the flat prism surface facing laterally at -5.0 mm ML. The prism was then slowly lowered to -4.0 mm DV, at a rate of 0.2 mm per minute, while keeping the brain surface moist and monitoring the site for bleeding. At this stage no bleeding should have been triggered. At the latter stages of lens lowering, the miniscope was powered on (attached to the nVista 3 Inscopix system and set to live imaging) to check for any increases in

fluorescence which should have occurred when the lens was positioned to within 150 – 200 μm of GCaMP6f-expressing cells (Figure 2-12B).

Once the prism was in position, opaque SuperBond C&B cement was used to cover the exposed sides of the lens, support screws, and electrodes to create a stable base. A platform was formed around the prism lens using PCB connector pins, which created a frame for extra stability. Cement was added in batches to allow for adequate drying, until the lens was completely encased with cement, apart from the lens cuff, which was left exposed. At this point, the ECoG electrodes were soldered to the pins of the female connector, which was positioned laterally, keeping in mind that space would be required for baseplate attachment and miniscope placement in the following steps. Cementing and suturing was completed, as described in 2.3.2 above. Five weeks were allowed for the tissue to heal before proceeding to the next stage.

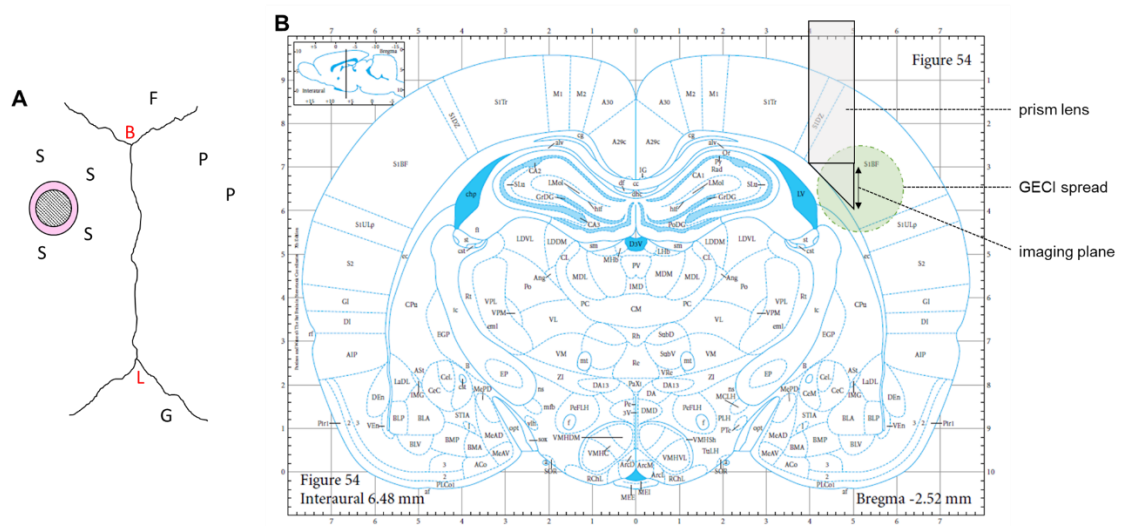


Figure 2-12: Prism lens and ECoG electrode placement for Inscopix experiments
 (A) Electrodes were placed on the right hemisphere, and included one ground electrode, one frontal electrode and two parietal electrodes, one serving as a backup. GCaMP6f was injected in the left S1BF, and a grin lens was inserted through a 1 mm craniotomy. Support screws and support rods were used to create a strong supportive structure for the miniscope. F: frontal electrode; P: parietal electrode; G: ground electrode; S: support screw; \circ : craniotomy; \bullet : grin lens; B: bregma; L: lambda. (B) Coronal brain section, showing sites of GCaMP6f GECI expression and prism lens implantation (image modified from Paxinos & Watson (2006)).

2.7.3 Step 3: Baseplate attachment

The baseplate was attached to the miniscope that was held in place with an Inscopix gripper attached to a stereotaxic arm (Figure 2-13). The animal was anaesthetised and its head fixed to the stereotaxic frame. The miniscope was powered up for live imaging, and the baseplate was positioned above the lens cuff. By moving the miniscope up and down in DV (while adjusting ML and AP coordinates to centre the lens in the field of

view), the acquired image was focussed at approximately 175 μm in front of the prism (prism working range is 150 – 200 μm). At this point, fluorescent cells should have been visible. When the desired baseplate position was achieved, the baseplate was cemented down with opaque SuperBond C&B cement, making sure that a thick layer covered all sides to prevent light entry while imaging.



Figure 2-13: Miniscope system layout.

The lens was inserted into the barrel field cortex and embedded in cement, leaving the surface of the cuff exposed. The baseplate was aligned with the lens and cemented in place. The miniscope was then attached to the baseplate prior to imaging and detached at the end of the recording session. (Graphics taken from the Inscopix online catalogue, Inscopix, USA)

2.7.4 Step 4: One-photon astrocyte calcium imaging, with video monitoring and ECoG recording

At this point, the animal was well habituated to the user and the recording room, due to regular handling over the past weeks. The animal was habituated for additional few days to the recording cage, while attached to a dummy miniscope and ECoG cable. At the end of each session, the animal was given a chocolate reward (Supreme Chocolate Mini Treats, Datesand group, UK) to improve its behaviour in subsequent sessions. Habituation was stopped when the animal was calm enough to sleep within an hour of being placed in the recording room, and recording sessions were started the next day.

On the day of recording, the animal was transferred to the recording cage, the miniscope was secured to the animal's baseplate and powered up. The ECoG cable was attached to the animal, and the 'Synch' port on the nVista DAQ system was used to send a common pulse to the CED system (used for ECoG acquisition as described in section

2.3.3 above), that was later used to synchronise the ECoG data (acquired through CED Spike7) and video recording data (acquired with a webcam connected to Spike7 Video Recorder) to the imaging data. Imaging was acquired in five to ten minutes periods, to keep the imaging files at a reasonable storage size. Recordings were done with the Inscopix DAQ software, and a recording session lasted for a maximum of 2 hours (on and off) to avoid bleaching and frustrating the animal. Animals were given at least 48 hours of rest between recording sessions.

2.7.5 Calcium Analysis

A number of raw data files were stored at the end of each imaging session: (1) .avi file of the acquired images, (2) accelerometer and rotational data of the miniscope movement; (3) .avi file from the behavioural camera, (4) ECoG channels and (5) synchronization pulse. (Figure 2-14)

The workflow used was similar to that adopted for the two-photon calcium imaging analysis (2.7.5), however, the process was greatly simplified due to the lack of subcellular or cellular resolution obtained with the miniscope. Calcium fluorescence was extracted from a single ROI that was manually drawn in the middle of the FOV, and only a single calcium trace was obtained per recording. The different signals were aligned and analysed using custom-written MATLAB scripts. Calcium event parameters were extracted: area under curve ($\Delta F/F \cdot s$), max slope rise ($\Delta F/F/s$), amplitude ($\Delta F/F$) and duration (s). The accelerometer data in the x, y and z planes were combined into a single movement index, using $movement = \sqrt{(x^2 + y^2 + z^2)}$. SWDs were detected as explained previously (2.5). Different behavioural states were defined, based on an altered ECoG signature and movement (explained in detail in Chapter 5). ECoG power spectra were prepared using the Welch method using a MATLAB custom-script (Welch's power spectral density estimate using L-Chebyshev window of 4 seconds, with 50% overlap). ECoG power spectrograms were prepared using the Chronux suite on MATLAB (ECoG multitaper spectrogram with 1 second windows spaced at 50 ms intervals).

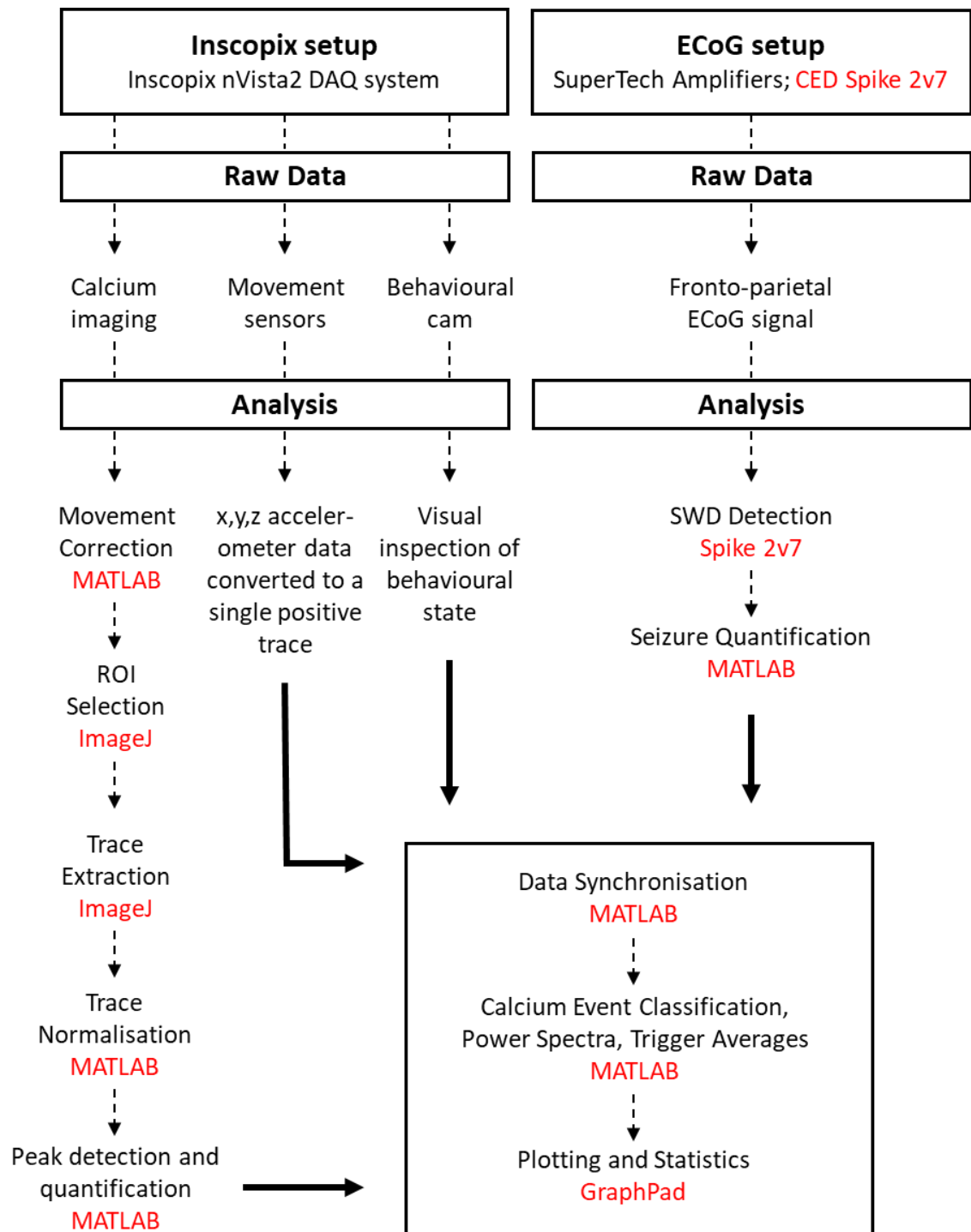


Figure 2-14: GAERS calcium analysis workflow

2.8 Immunohistochemistry

Immunohistochemical analysis was performed to confirm GCaMP6f, DREADD or calcium pump expression in astrocytes and the area of AAV spread. Inscopix lens placement was also confirmed with respect to GCaMP6f expression in GAERS.

2.8.1 Brain Extraction

The animal was given an overdose of pentobarbital, and when it lost the toe-pinch and corneal blink reflexes, transcardial perfusion was performed as follows. 10 mM PBS (at room temperature) was pumped into the animal's circulatory system until the liver and fluid leaking from the heart incision were clear. This was followed by perfusion with 4% PFA (at 4°C) dissolved in 0.1 M PBS, pH 7.4, for five minutes (approximately 75 ml) or until the animal's body stiffened. The animal was then decapitated using a guillotine, and the brain was carefully extracted using small sharp scissors, flat tweezers and a spatula. The brain was post-fixed for three hours in 4% PFA. It was then transferred to 0.9% NaCl in 0.1 M PBS and stored in the fridge for 12 hours. Finally, it was placed in 10 mM PBS with 0.1% sodium azide and 30% sucrose for cryoprotection and long-term storage.

(Unless otherwise specified, all reagents were purchased from MilliporeSigma, Inc., Germany)

2.8.2 Brain Slicing

Whole, free-floating coronal sections were prepared using a Leica vibratome (Leica Microsystems Inc., USA). The brain was rinsed in 10 mM PBS, and using a brain matrix, it was sliced coronally, anterior to the cerebellum. The posterior end was glued to the slicing block, which was attached to the slicing chamber and immersed in cold 10 mM PBS. The slicing chamber was kept cool using ice, which was replenished every few minutes. A razor blade was rinsed with ethanol, followed by PBS, and attached to the blade holder. 30 µm slices were prepared using a horizontal setting of 8.5 Hz, and a speed setting of 4. Slices within the desired coordinates were temporarily stored in sterile 10 mM PBS prior to immunostaining.

2.8.3 Immunostaining

The brain slices were transferred to well-plates and washed three times for 10 minutes with 500 µl PBS-T (0.1% Triton™ X-100 in sterile 10 mM PBS) on a circular rocker. To prevent non-specific binding, the slices were incubated for 1 hour in 250 µl of freshly prepared blocking solution (4% bovine serum albumin, 3% donkey serum and 0.1% Triton™ X-100 in sterile 10 mM PBS) per well. Primary antibodies were prepared using

a 1:1 solution of blocking solution and PBS-T. 250 µl of the antibody solution was added to each well and the slices were incubated overnight, at 4°C.

The next day, the samples were washed two times with 500 µl 10 mM PBS for 10 minutes, once with 500 µl 10 mM PBS for 20 minutes and finally twice with 500 µl PBS-T for 10 minutes. Secondary antibodies were prepared using a freshly prepared 1:1 solution of blocking solution and PBS-T. 250 µl of the antibody solution was added to each well and the samples were incubated for 1 hour at room temperature on a circular rocker, in dark conditions. Next, the samples were immersed in 250 µl of DAPI (5 µg/ml, in 10 mM PBS) for 10 minutes, and washed twice with 500 µl PBS-T and once with 500 µl 10 mM PBS for 5 minutes.

The slices were finally mounted on glass microscope slides using Molecular Probes™ SlowFade™ mountant and allowed to dry overnight at room temperature. Imaging was performed with an Olympus BX61 microscope using a Hamamatsu ORCA Spark digital camera, or a Zeiss LSM 880 upright confocal microscope.

(Unless otherwise specified, all reagents were purchased from MilliporeSigma, Inc., Germany)

2.8.4 Antibody preparations

To confirm the specificity of GCaMP6f expression in astrocytes, the following combinations of primary and secondary antibodies were used: Chicken anti-GFP (diluted 1:1000) with Chicken Alexa Fluor 488 (diluted 1:500), Mouse anti-NeuN (diluted 1:500) with Mouse Alexa Fluor 660 (diluted 1:500), and Rabbit anti-GFAP (diluted 1:500) with Rabbit Alexa Fluor 568 (diluted 1:500). GCaMP6f fluorescence was enhanced using a GFP label, and its expression on astrocytes was checked using a GFAP label. Neuronal expression of GCaMP6f was ruled out using the NeuN neuronal marker.

To confirm the specificity of DREADD (AAV5 GFAP-HA-hM3D(Gq)-IRES-mCitrine) expression in astrocytes, the following combinations of primary and secondary antibodies were used: Chicken anti-GFP (diluted 1:1000) with Chicken Alexa Fluor 488 (diluted 1:500), Mouse anti-NeuN (diluted 1:500) with Mouse Alexa Fluor 660 (diluted 1:500), and Rabbit anti-GFAP (diluted 1:500) with Rabbit Alexa Fluor 568 (diluted 1:500) (see Table 2-1). DREADD expression on astrocytes was confirmed using the GFAP label, and neuronal expression was ruled out using the NeuN label.

To confirm the specificity of calcium pump (AAV5 gfaABC1D-mCherry-hPMCA2w/b) expression in astrocytes, the following combinations of primary and secondary antibodies were used: Mouse anti-mCherry (diluted 1:500) with Mouse Alexa Fluor 488 (diluted 1:500), and Rabbit anti-GFAP (diluted 1:500) with Rabbit Alexa Fluor 568

(diluted 1:500) (see Table 2-1). The anti-mCherry antibody was used to reveal DREADD expression and overlap with GFAP confirmed its expression on astrocytes. NeuN was not included here since the antibody combinations already available did not allow this and was instead included in the antibody combinations described below.

To confirm the co-expression of the calcium pump and GCaMP6f in astrocytes, and rule out neuronal expression, the following combinations of primary and secondary antibodies were used: Chicken anti-GFP (diluted 1:1000) with Chicken Alexa Fluor 488 (diluted 1:500), Mouse anti-NeuN (diluted 1:500) with Mouse Alexa Fluor 660 (diluted 1:500) and Rabbit anti-mCherry (diluted 1:500) with Rabbit Alexa Fluor 568 (diluted 1:500). GFP enhanced GCaMP6f labelling and overlap with mCherry antibody was used to determine pump and GCaMP6f co-expression. Neuronal expression was ruled out using the NeuN label.

DAPI was used in all antibody preparations, to locate the cell body of astrocytes or neurons.

2.9 Statistical Analysis

Statistical analysis was performed with GraphPad Prism v9 (GraphPad Software, CA, USA). A Kolmogorov-Smirnov test was carried out on each data set to test for the normal distribution of data and appropriate parametric or non-parametric tests were carried out. More detail about which test was carried out is given in the relevant Results section. Where appropriate, data was represented as mean \pm SEM. Significance was taken as * $p < .05$, ** $p < .01$, *** $p < .001$, **** $p < .0001$.

2.10 Resources used

Table 2-1: Resource Table

Reagent or Resource	Source	Identifier
ECoG Electrode preparation		
Preci-Dip 853 Series female connector	RS Components	RS Components Cat# 702-3085
Preci-Dip 852 Series male connector	Precision	Precision Cat# 7227
Gold-plated screws	Svenska Dentorama	Dentorama Cat# POS-330
Stainless steel screw	Accu Limited	Accu Cat# SFK-M1-2-A2
Insulated copper wire	RS Components	RS Components Cat# 779-0690
Insulated silver wire	WPI	WPI Cat# AGT0525

AAVs		
AAV5 gfaABC1D-cyto-GCaMP6f	Addgene	Addgene Cat# 52925-AAV5
AAV5 gfaABC1D-mCherry-hPMCA2w/b	VectorBuilder	Custom-ordered
AAV5 GFAP-HA-hM3D(Gq)-IRES-mCitrine	Duke viral vector core	Plasmid #50470
AAV injection equipment		
Micro4: Microsyringe pump controller with UMP3 - Ultra Micro Pump	WPI	WPI Cat# UMP3-1
Single Barrel Borosilicate Capillaries	WPI	WPI Cat# 1B100-3
Hamilton™ Gastight Microliter™ Syringe	Fisher Scientific	Fisher UK Cat# 10444805
Hamilton™ Compression Fitting	Fisher Scientific	Fisher UK Cat# 11305942
Chronic window implantation		
3 mm cover glass	Harvard Apparatus	Harvard App Cat# 64-0720
5 mm cover glass	Harvard Apparatus	Harvard App Cat# 64-0700
NOA 71 UV curing optical adhesive	Norland Optical	Tech Optics Cat# 7106
Custom-ordered headplates	Laser Master ltd	N/A (Stainless steel)
Inscopix implantation		
nVista miniature microscope system	Inscopix	Inscopix nVista 3
ProView™ Prism Probe: 9.1 mm x 1mm	Inscopix	Inscopix Cat# 1050-002213
ProView™ implant kit	Inscopix	Inscopix Cat# 1000-004238
Gripper	Inscopix	Inscopix Cat# 1050-002199
Baseplate	Inscopix	Inscopix Cat# 1050-004638
Dissecting knife	Fine Science Tools	FST Cat# 10055-12
Immunohistochemistry		
Chicken anti-GFP	Abcam	Abcam Cat# ab13970
Mouse anti-NeuN	Merck Millipore	Merck Cat# MAB377
Rabbit anti-GFAP	Dako Agilent	Agilent Cat# Z0334
Mouse anti-mCherry	Abcam	Abcam Cat# ab125096
Rabbit anti-mCherry	Abcam	Abcam Cat# ab183628
Chicken Alexa Fluor 488	Thermofisher	Molecular Probes Cat# A-11039
Mouse Alexa Fluor 488	Abcam	Abcam Cat# ab150113

Rabbit Alexa Fluor 568	Thermofisher	Molecular Probes Cat# A-11011
Mouse Alexa Fluor 660	Thermofisher	Molecular Probes Cat# A-21055
Drugs		
Clozapine N-oxide (CNO) dihydrochloride	Hello Bio	Hello Bio Cat# HB6149
DREADD agonist 21 dihydrochloride	Hello Bio	Hello Bio Cat# HB6124
Gamma butyrolactone (GBL)	Sigma-Aldrich	Merck Cat# B103608
Ethosuximide	Sigma-Aldrich	Merck Cat# E7138

Chapter 3: Cortical astrocyte calcium response to locomotion

It is well-established that astrocytes participate in the cortical response to locomotion, which has been investigated in several brain regions, including the somatosensory cortex, visual cortex and cerebellum. Here we investigate the astrocyte calcium response in S1BF during head-restrained, voluntary, locomotion. We do this as a prelude to the investigation of astrocyte calcium activity during seizure events (Chapters 4 and 5) to establish the suitability of our setup to detect global and subtle spontaneous changes in calcium activity in the different astrocyte sub-compartments. We investigate the astrocyte response in WT animals and in a model of ataxia, to determine if impaired locomotor activity influences astrocyte calcium signalling. To visualise calcium changes, we make use of two-photon calcium imaging of GCaMP6f-expressing astrocytes in adult mice and monitor cortical neuronal activity in the contralateral hemisphere with ECoG electrodes.

3.1 GCaMP6f expression in S1 cortical astrocytes

Adult, male wild-type mice were injected intra-cortically with AAV-GFAP-cyto-GCaMP6f to selectively express GCaMP6f in S1BF astrocytes. 4 to 6 weeks after AAV injection, the mice were sacrificed and immunohistochemical staining was performed to confirm GCaMP6f expression in astrocytes. Overlap of GFP and GFAP staining and not of GFP and NeuN, confirmed specific GCaMP6f expression in mouse astrocytes that was absent in neurons (N = 5 animals, 5 slices per animal, 200 μm x 200 μm ROI per slice); *Figure 3-1B*) as previously described (Shigetomi et al. 2013a; Stobart et al. 2018a). GCaMP6f expression spanned across the cortex, into the deeper layers and laterally to fully cover the majority of a 3 mm cranial window (*Figure 3-1A*). Reference to a mouse brain atlas (Paxinos and Franklin 2001) confirmed that astrocyte expression was within the S1BF. Control experiments confirmed that GCaMP6f expression was limited to the intracranial delivery of the viral construct (*Figure 3-1C*).

It is worth noting that GFAP is not considered a universal astrocyte marker, since a proportion of astrocytes is not immunoreactive for GFAP (see Verkhratsky and Nedergaard 2018, pp. 249-252 for an in-depth review). GFAP was however suitable as an astrocyte marker for the current study since GFAP is astrocyte-specific in the CNS (Ludwin et al. 1976; Bignami et al. 1972) and since the AAV used in this study was based on a GFAP-promoter. Colocalization of GFAP and GFP staining therefore indicated that

the AAV correctly targeted GFAP-positive cells, and that GCaMP6f was successfully expressed in astrocytes.

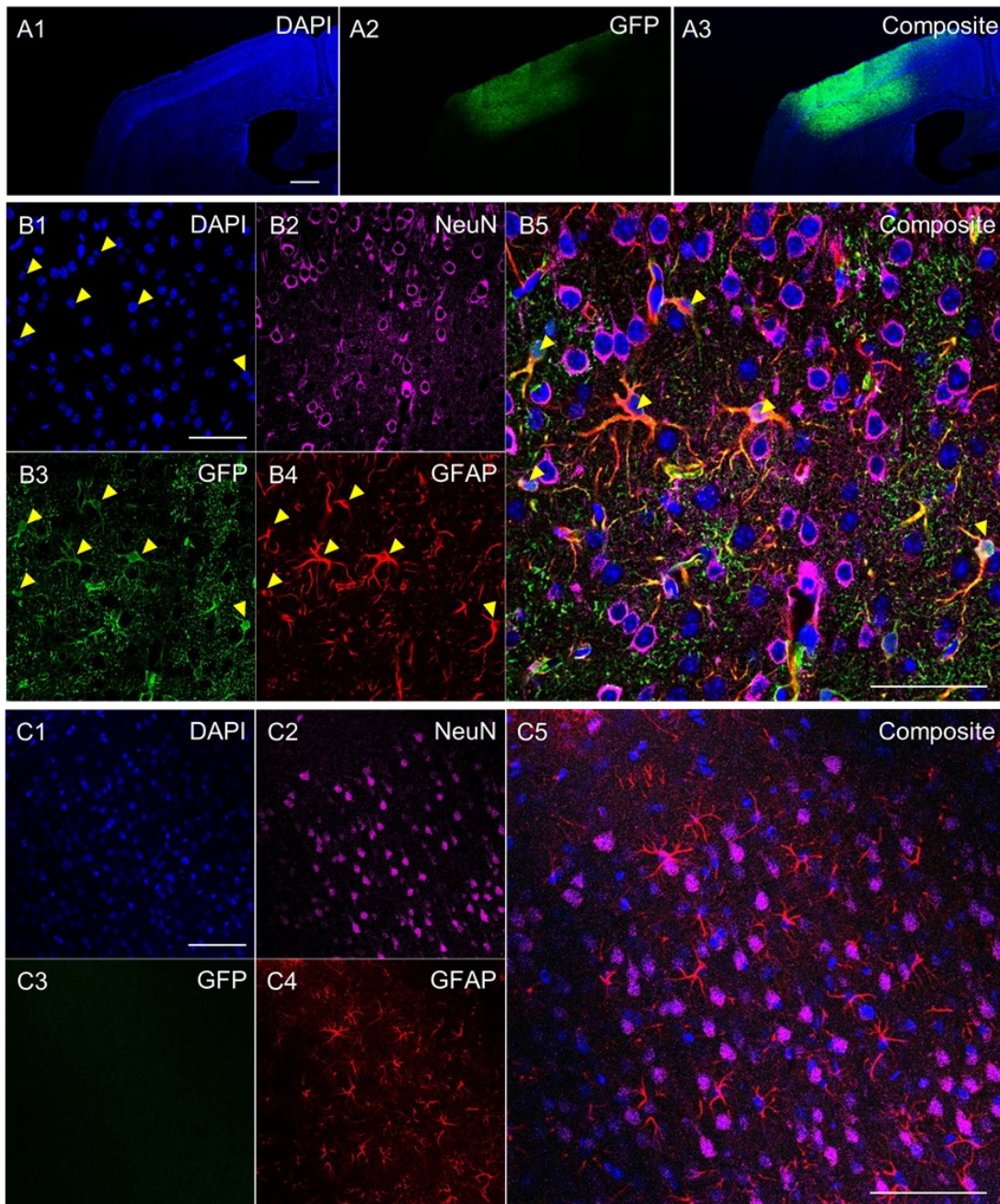


Figure 3-1: GCaMP6f expression in mouse cortical astrocytes.

(A) Cortical injection of AAV5 gfaABC1D-cyto-GCaMP6f in S1BF layers 2/3, resulted in significant spread and expression of GCaMP6f, which extended into the deeper cortical layers, and covered most of the 3 mm cortical window. Scale bar in A1 for A1-A3: 500 μ m. (B1- B4) Immunohistochemistry with DAPI, anti-NeuN, anti-GFP and anti-GFAP. Scale bar in B1 for B1-B4: 50 μ m. (B5) Overlap of the four channels revealed that expression of GCaMP6f was selective to astrocytes, revealed by the clear overlap of the GFP and GFAP channels, and no overlap with NeuN. Arrows indicate astrocyte somata with overlap of DAPI, GFP and GFAP. Other areas of clear overlap between GFAP and GFP were also evident. Scale bar in B5: 50 μ m. (C1-C5) Contralateral control lacked GFP fluorescence. Scale bar in C1 for C1-C4: 100 μ m; scale bar in C5: 100 μ m.

3.2 Astrocyte calcium activity in S1 cortex during locomotion

To determine astrocyte behaviour during periods of voluntary locomotion, adult, male mice were injected intra-cortically with AAV-GFAP-cyto-GCaMP6f to express GCaMP6f selectively in the cytosol of S1 astrocytes. Fronto-parietal electrodes were implanted contralaterally to the AAV injection site, to monitor cortical neuronal activity, and a cranial window and headplate were implanted to enable long-term imaging of the animal. Two-photon calcium imaging using a BScope Thorlabs resonance scanner (wavelength 980 nm, acquisition rate 30 Hz averaged to 5 Hz) was performed 4 to 12 weeks after chronic window implantation, to detect calcium changes while the mouse was head-restrained on a circular treadmill. Video monitoring was also set up to assess the animal's behaviour.

3.2.1 Astrocyte population recruitment during periods of locomotion

Global astrocyte recruitment in S1 was clear following periods of voluntary running on the treadmill, characterised by synchronous astrocyte activation of the vast majority of the field of view (100 – 400 μm), as previously described in other brain regions (Slezak et al. 2019; Paukert et al. 2014; Nimmerjahn et al. 2009) and in S1 (Bojarskaite et al. 2020). The mice comfortably moved on the treadmill and easily reached speeds of over 30 cm/s. Calcium changes at times originated from a focal point, while on other occasions calcium activity initiated at various points within the field. Astrocytes showed a strong, reliable population calcium response to locomotion which greatly overshadowed spontaneous calcium activity during periods of no locomotory input (duration: 37.0 ± 2.9 s vs 11.2 ± 4.3 s, Mann Whitney, unpaired test, $U = 526$, $p < 0.0001$; event frequency: 2.2 ± 0.1 events/ROI/min vs 0.1 ± 0.02 events/ROI/min, Mann Whitney, unpaired test, $U = 323$, $p < 0.0001$; amplitude: 5.8 ± 0.2 $\Delta F/F$ vs 3.5 ± 0.2 $\Delta F/F$, Mann Whitney, unpaired test, $U = 2625$, $p < 0.0001$; all data reported as mean \pm SEM; $N = 6$ WT mice, $n = 86$ locomotion events, spontaneous events taken from 58 minutes of Awake Still data). Prolonged periods of running reliably evoked calcium increase in the majority of the astrocyte population in the field of view, that outlasted locomotor activity (Figure 3-2). Periods of locomotion were defined as periods of at least 5 seconds with speeds greater than 5 cm/s, which were not preceded by other periods of movement for at least 30 seconds. Activation of the full field of view involving all astrocyte sub-compartments was observed 82% of the time ($N = 6$ WT mice, $n = 203$ locomotion events), similar to what was previously reported (Paukert et al. 2014; Nimmerjahn et al. 2009).

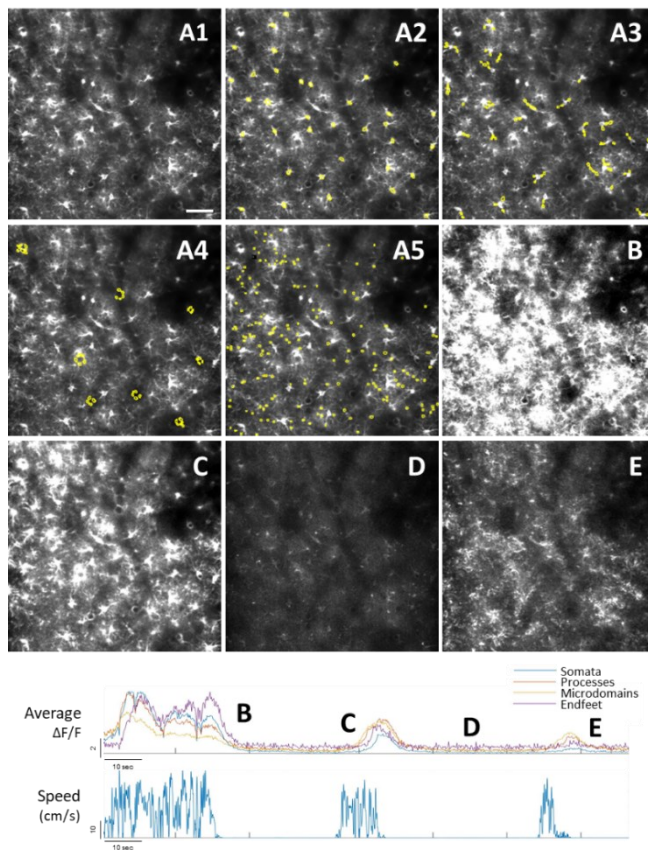


Figure 3-2: Global astrocyte response to locomotion.

(A1) Averaged image used for ROI selection: ROIs indicating (A2) somata, (A3) processes, (A4) endfeet, (A5) microdomains. (B) Activated astrocytes during a prolonged locomotion event involving all sub-compartments. (C) Activated astrocytes within all sub-compartments during a briefer movement. (D) Baseline fluorescence during a period of quiescence. (E) Activation of microdomains and processes, with little activity in the somata and endfeet. Traces beneath correspond to the images (B-E). Scale bar in A1 for A1-E: 60 μm .

Calcium activity patterns varied depending on the pattern of movement (Figure 3-3). Longer duration movements were accompanied by prolonged calcium increase, and breaks in movement were picked up as dips in the calcium peaks, creating multi-peak events, which contrasted with single-peak events induced by single uninterrupted locomotion periods (Figure 3-3 A). At times, locomotion failed to induce widespread or even local astrocyte activation, likely due to depleted intracellular calcium stores from preceding events (Figure 3-3C) (Nimmerjahn et al. 2009) and potentially consistent with a more depressed state of arousal, since a heightened state of arousal has been strongly correlated to increased astrocyte calcium activation during sensory input (Slezak et al. 2019; Ding et al. 2013; Zuend et al. 2020; Bazargani and Attwell 2017; Oe et al. 2020) (Figure 3-3 B,E). Astrocytes were able to respond to repeated input, as indicated by their calcium response to short bursts of repeated locomotion (Figure 3-3 F), as previously observed in response to sensory stimulation (Zhao et al. 2012; Lind et al. 2013). Successive calcium transients progressively weakened, indicative of astrocyte habituation to successive inputs, and possibly due to gradual calcium store depletion (Figure 3-3 F), as previously mentioned, or due to receptor desensitization (Shao and McCarthy 1995).

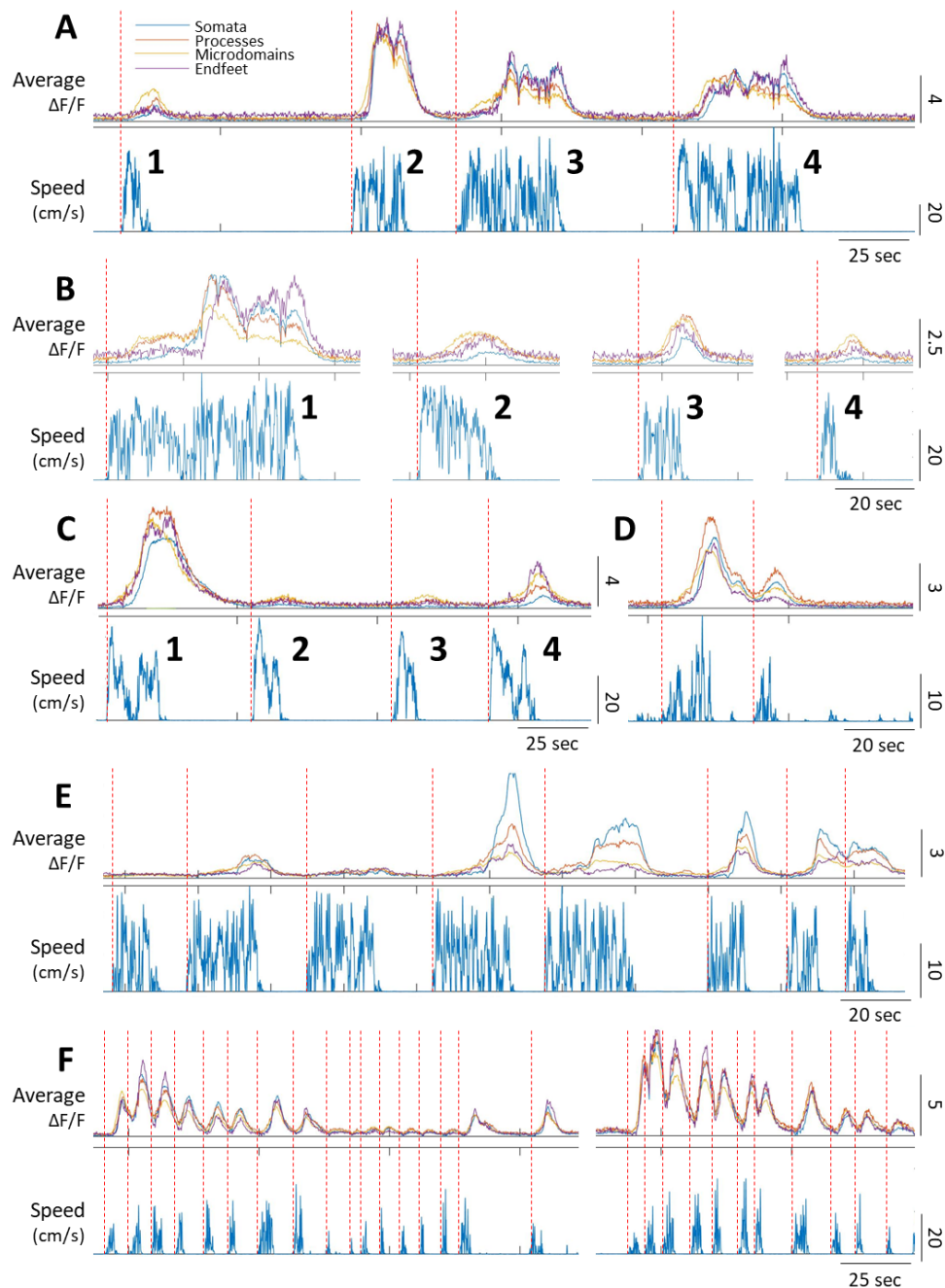


Figure 3-3: Different patterns of astrocyte calcium activity in response to locomotion. (A-F) Top: Averaged normalised calcium fluorescence from the different sub-compartments: somata, processes, microdomains, endfeet. Bottom: animal's speed of movement. Vertical, dashed red lines indicate locomotion onset. (A) Periods of locomotion, A2-4, reliably induce a calcium response, but the first brief period of locomotion, A1, induces only a weak calcium response. (B) Strong movements do not always elicit a strong increase in calcium activity. B1, the astrocyte response is weak for the first 20 seconds following locomotion onset; B2, the astrocyte response is weak despite the strong movement. (C) C1 elicits a strong astrocyte response, whereas subsequent movements, C2-4, are accompanied by weak calcium increases. (D) Two closely timed-movements induce a double calcium peak. (E) A number of closely-timed movements may or may not be accompanied by astrocyte activation. (F) Brief, closely-timed movements elicit a reliable calcium response that decays with each subsequent movement.

Astrocytes exhibited a graded response to locomotory input and overall the intensity of movement was correlated to the strength of astrocyte response (Figure 3-4). Taking the AUC as a measure of calcium fluorescence and as a measure of locomotion, a strong correlation was obtained between the two. Moreover, the duration of locomotion was strongly correlated with the AUC, duration, and amplitude of calcium fluorescence, however, the speed of locomotion was only weakly correlated (Figure 3-4). This indicated that a change in astrocyte calcium was dependent on the duration of the locomotion period but not the speed, as was previously shown in Bergmann glia (Paukert et al. 2014) and visual responses in the visual cortex (Slezak et al. 2019).

It has been well-established that astrocyte activity occurs independently in the different sub-compartments and may not involve the whole cell, as shown in several slice and in vivo studies (Srinivasan et al. 2015; Bindocci et al. 2017; Nett et al. 2002; Parri and Crunelli 2003). In fact, microdomain-specific activation was observed following periods of movement, in the absence of soma, process, or endfoot activation (N = 3 animals, n = 12 locomotion events; locomotion speed: 24 ± 10 cm/s; locomotion duration: 17 ± 3 s; mean \pm SEM; Figure 3-5). In such cases, astrocyte calcium increase in the cell periphery was possibly in response to synaptic input due to ongoing neuronal activity (Parri et al. 2010). It has been previously shown that astrocytes integrate and summate sensory input (Lines et al. 2020; Perea and Araque 2005; Araque 2008; Parri et al. 2010), which is expected to occur during locomotion, and would explain instances of microdomain-specific activation without the recruitment of other cellular compartments. An alternate explanation would be a temporary lack of neuromodulator release, which is what typically drives synchronous astrocyte calcium increase during locomotion and sensory input (Paukert et al. 2014; Ding et al. 2013; Stobart et al. 2018a; Bekar et al. 2008).

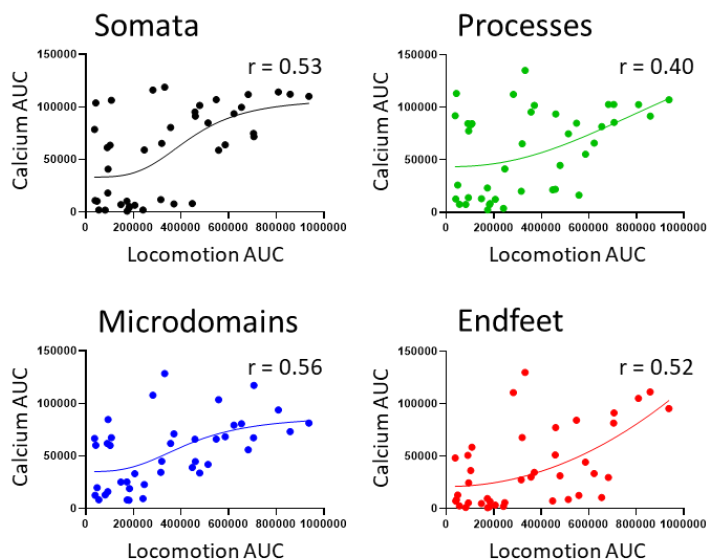
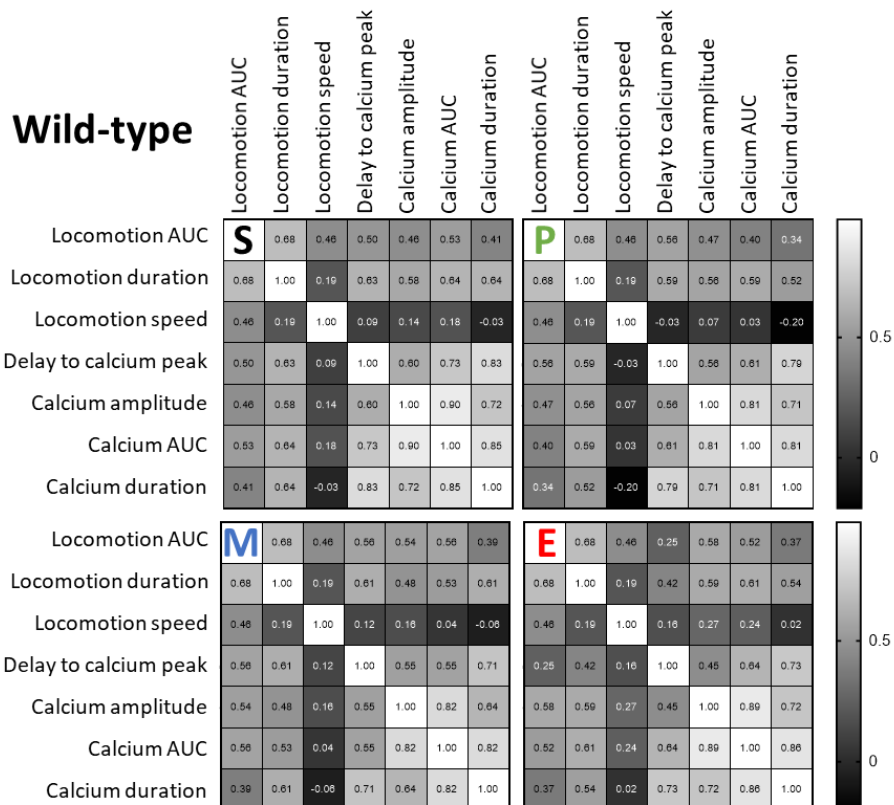


Figure 3-4: Correlation between locomotion and astrocyte calcium changes in wild-type mice.

Top: Nonparametric spearman correlation 'r' values obtained from comparisons made between locomotion (AUC/area under the curve, duration and speed of movement) and calcium events (delay of calcium peak from locomotion onset, calcium event amplitude, AUC/area under curve and duration) in the somata (S), processes (P), microdomains (M), and endfeet (E). Locomotion AUC and duration had a strong positive correlation with calcium event amplitude, AUC and duration, unlike locomotion speed. Bottom: Scatter plots of the calcium AUC and locomotion AUC with a nonlinear least squares fit, suggesting a positive correlation between the two in all astrocyte sub-compartments. (N = 6 animals, n = 40 locomotion events per sub-compartment)

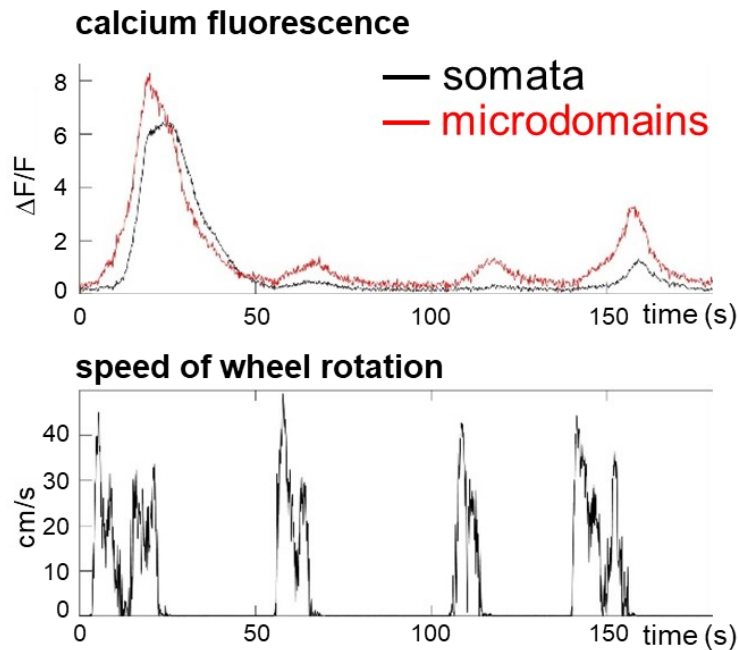


Figure 3-5: Locomotion-induced calcium transients restricted to the cell periphery. Top: calcium fluorescence; Bottom: the associated animal locomotion. Note the second and third events with minimal or no activity in the somata and a contrasting clear increase in overall microdomain activation.

As mentioned in the sections above, different patterns of calcium activity were observed, such as single-peak or multi-peak events (Figure 3-6). Short-lasting movements (<15 s) induced single-peak events, which contrasted with prolonged movements that resulted in longer lasting multi-peak events, with larger amplitudes and slower rise and fall times (34.2 ± 2.5 s vs 17.4 ± 1.1 s duration, Mann Whitney test, $U = 563$, $p < 0.0001$; 4.3 ± 0.3 $\Delta F/F$ vs 2.0 ± 0.2 $\Delta F/F$ amplitude, Mann Whitney test, $U = 1118$, $p < 0.0001$; 29.5 ± 8.3 s vs 13.3 ± 2.3 s rise tau, Mann Whitney test, $U = 1150$, $p < 0.05$; 20.5 ± 5.4 s vs 12.3 ± 2.8 s, decay tau, Mann Whitney test, $U = 1581$, $p < 0.005$; all data reported as mean \pm SEM; $N = 6$ animals, $n = 24$ multipeak events, $n = 21$ single peak events). In this way, astrocytes sustained calcium signalling that outlasted the entire movement.

ECoG changes were associated with different stages of global astrocyte calcium changes. The initial calcium rise was followed by an increase in power of the lower frequency bands, which dropped sharply following the end of the calcium event (Figure 3-7). Global cortical changes as acquired through ECoG were thus accompanied by the activation of astrocyte populations, indicating that changes in neuronal network activity is accompanied by changes in astrocyte population activation. This is backed up by an increase in the lower band frequencies, 1 – 10 Hz, of the sensorimotor and occipital cortex of cats observed during running, which has been associated with running fatigue (Angyán and Czopf 1998).

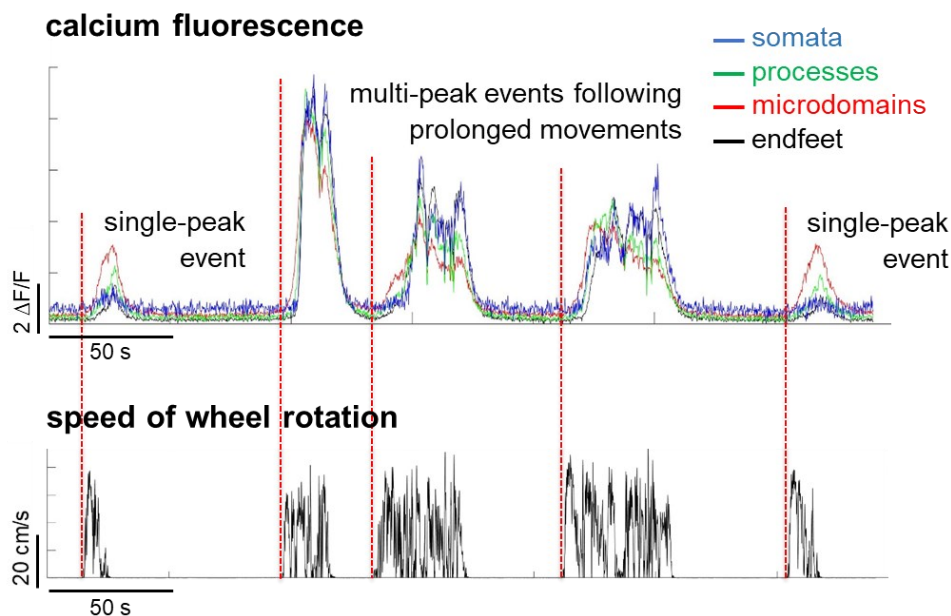


Figure 3-6: Multi-peak and single-peak calcium events. Multi-peak events were associated with prolonged movements, whereas single-peak events were associated with shorter, single uninterrupted locomotion periods.

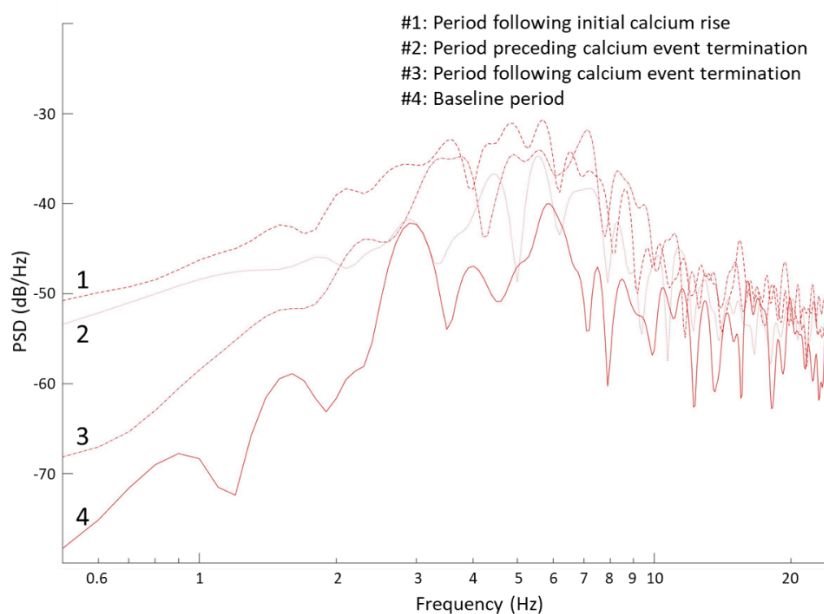


Figure 3-7: Changes in ECoG power spectra during locomotion-induced calcium events. Welch's power spectral density estimate (L-Chebyshev window of 4 seconds, with 50% overlap) shown in a logarithmic scale. Changes in the power of lower frequency bands (<10 Hz) were associated with changes in calcium fluorescence. Each period consisted of a 5 second sampling period, averaged from $n = 6$ locomotion events ($N = 3$ animals). The initial rise in calcium fluorescence was accompanied by an increase in the power of lower frequency bands (Trace #1) compared to the ECoG power during baseline calcium fluorescence (Trace #4). During the last portion of the calcium event, the power reduces (Trace #2), and even further following the termination of the calcium event (Trace #3), however still elevated from baseline levels (Trace #4).

3.2.2 Single astrocyte response to locomotion

Having determined that astrocytes respond to locomotion on a population level, we wanted to look at the astrocyte response at a sub-cellular level. Focussing on a field of view with one or two astrocytes, the timing of the response to locomotion of the different astrocyte sub-compartments was investigated (Figure 3-8).

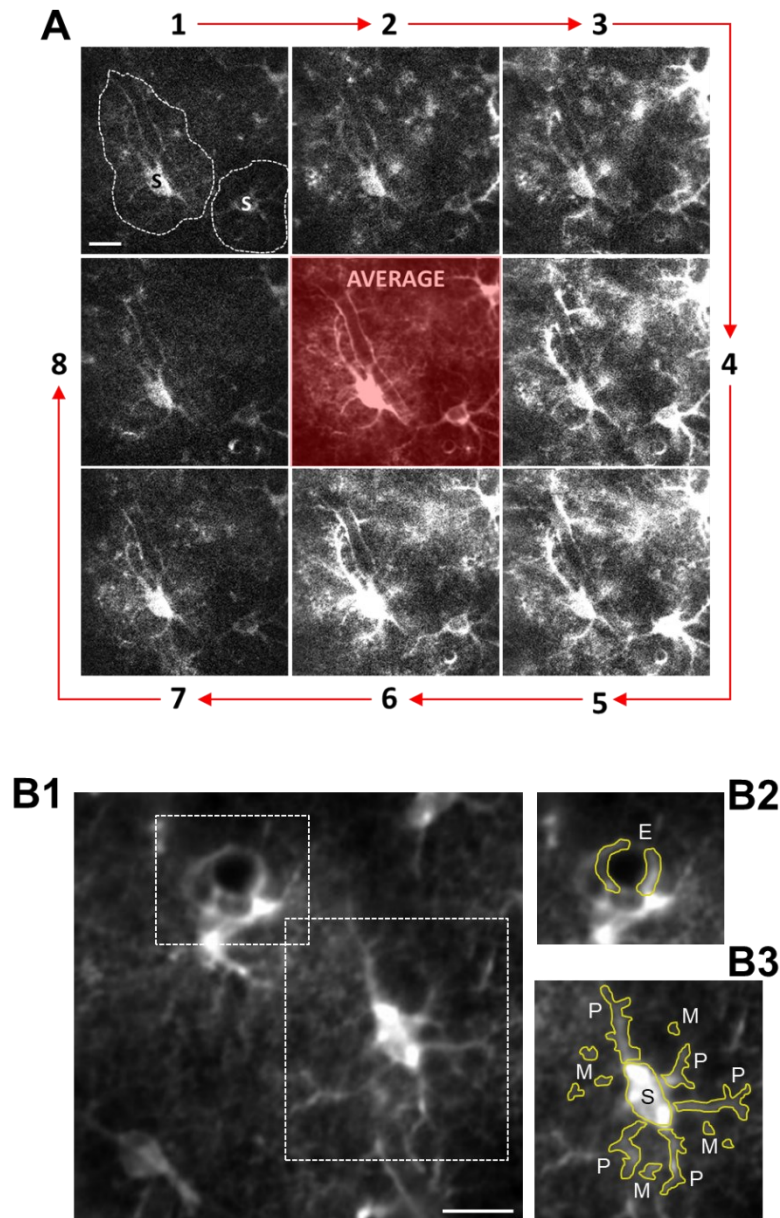
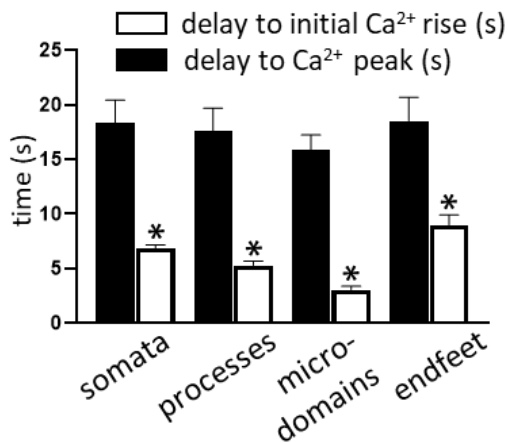


Figure 3-8: Locomotion-induced calcium activity in single astrocytes. (A) Central image shows the morphology of single astrocytes, represented by an averaged image of the full recording. Approximate single astrocyte territories are shown by the outlines in image #1. Images #1 to #8 show the progression of astrocyte calcium activation induced by locomotion. Scale bar in A1 for A1-A8: 20 μm . (B1-B3) Typical manually drawn ROIs used for calcium event detection: S: soma, P: process, M: microdomain, E: endfoot. Scale bar in B1 for B1-B3: 20 μm .

A wave of calcium typically initiated in the microdomains, spread to the soma and finally the endfeet (Figure 3-9). This supports the flow of information through astrocytes, that follows the progression of a response to neuronal activity in the astrocyte periphery, followed by soma activation and subsequent calcium-induced activation of endfeet that modulate blood flow according to increased metabolic demand (Lind et al. 2018; Lind et al. 2013).



*Figure 3-9: Sub-cellular activation with respect to locomotion onset. The delay from onset of locomotion to the initial calcium rise was shortest in microdomains and longest in endfeet. The delay to the calcium peak following locomotion onset was similar in all sub-compartments. (*one-way ANOVA comparing the delay to initial calcium rise in the four sub-compartments: $F(3, 88) = 20.66$, $p < 0.0001$; $N = 4$ animals, $n = 22$ locomotion events)*

Calcium events were also detected in the cell periphery before the onset of locomotion (Figure 3-10, Figure 3-11), possibly in response to muscle tensing not picked up by the rotation of the wheel (Paukert et al. 2014). Alternatively, astrocytes might in fact be truly active in anticipation of locomotion, potentially responding to the well-documented activation of the somatosensory system in anticipation of voluntary movement, known as the efference copy (Sun et al. 2015).

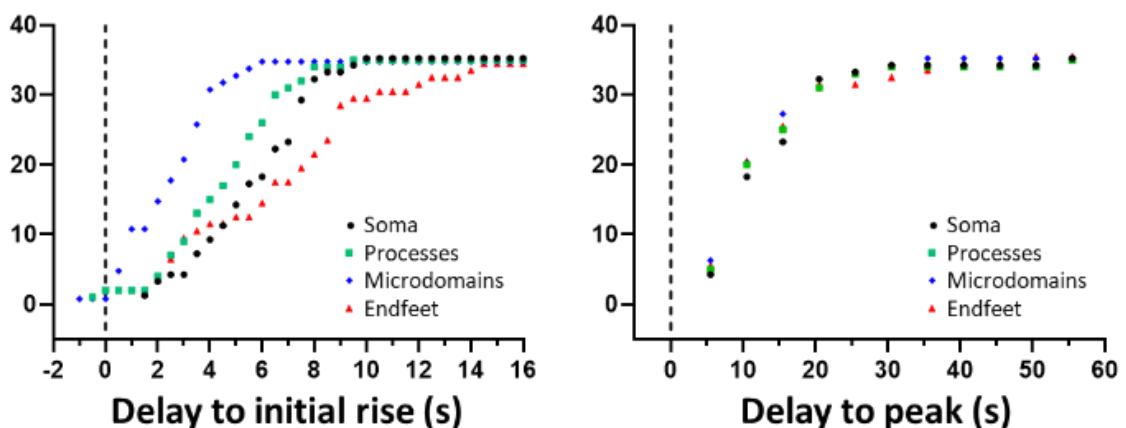


Figure 3-10: Cumulative distribution curves of the calcium events with respect to locomotion onset. (Left) Cumulative plot showing calcium event onset with respect to locomotion onset (set at zero and indicated by the dashed line) from the different cellular compartments. Note

the quicker response in the cell periphery to the initial input, especially in the microdomains ($N = 5$ animals, $n = 20$ locomotion events, plots binned at 0.5 s). (Right) Cumulative plot showing the timing of the calcium event peak with respect to locomotion onset (set at zero and indicated by the dashed line). Calcium events peak at a similar time in all sub-compartments since this coincides with the peak in the global astrocyte response. ($N = 5$ animals, $n = 20$ locomotion events, plots binned at 5 s).

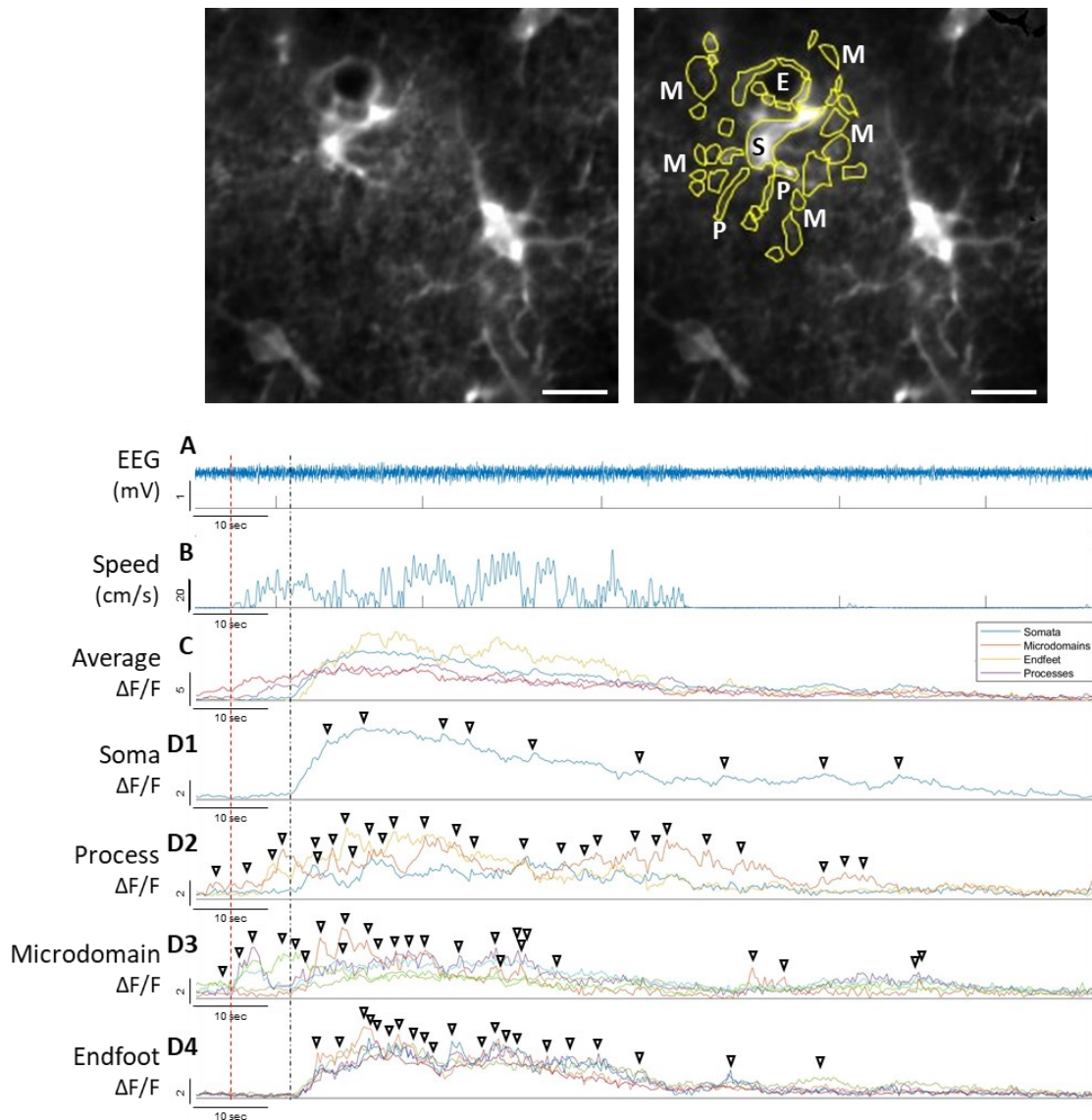


Figure 3-11: Activity in processes and microdomains preceded locomotion onset. (Top) Averaged image (left) showing the morphology of single astrocytes and (right) ROIs used for calcium detection. Scale bars: 20 μm . (A) Raw ECoG trace, (B) speed of wheel rotation, (C) average calcium changes in the four sub-compartments, (D1-4) calcium transients from individual ROIs in the soma, processes, microdomains and endfeet. Locomotion onset, shown in (B) and indicated by the dashed red line, preceded calcium rise in the soma (D1) by about 6 seconds, indicated by the black dashed line. Calcium events in the processes (D2) and microdomains (D3) precede events detected in soma and endfeet, and also precede the onset of locomotion.

3.3 Astrocyte calcium activity in an animal model of ataxia: the Stargazer mouse model

Stargazer mice display an ataxic phenotype, arising from cerebellar defects, including dysfunctional AMPA receptors in the granule cell layer that are responsible for a quick synaptic response to glutamate. AMPA deficiencies arise due a defect in the stargazin protein that is not able to bind and traffic AMPA receptors to the plasma membrane (Letts 2005). To determine if astrocyte signalling deficiencies accompany an ataxic phenotype, the astrocyte response to locomotion in Stargazers was investigated.

Stargazer mice astrocytes showed a robust synchronous response to locomotion, with similarly positive correlations between the duration of locomotion and calcium event properties, similar to what was observed in wild-type littermates (Figure 3-12). Stargazers reported more single-peak events compared to wild-type littermates (67% vs 45%, N = 4 Stargazer mice, n = 22 Stargazer locomotion events; N = 3 wild-type mice, n = 25 WT locomotion events), which reflected their shorter locomotion periods. In fact wild-types ran faster and for longer periods of time (speed: 33.7 ± 2.5 cm/s vs 13.1 ± 3.2 cm/s, mean \pm SEM, unpaired t-test, $t(45) = 7.689$, $p < 0.0001$; duration: 21.4 ± 2.7 s vs 13.1 ± 1.5 s mean \pm SEM, unpaired t-test, $t(45) = 2.735$, $p < 0.005$; N = 4 Stargazer mice, n = 22 Stargazer locomotion events; N = 3 wild-type mice, n = 25 WT locomotion events). Active states in wild-types and Stargazers, defined as locomotion events that exceeded a speed of at least 2.5 cm/s and lasted at least 5 seconds, had similar calcium event properties with similar AUCs, event frequencies and amplitudes (Figure 3-13).

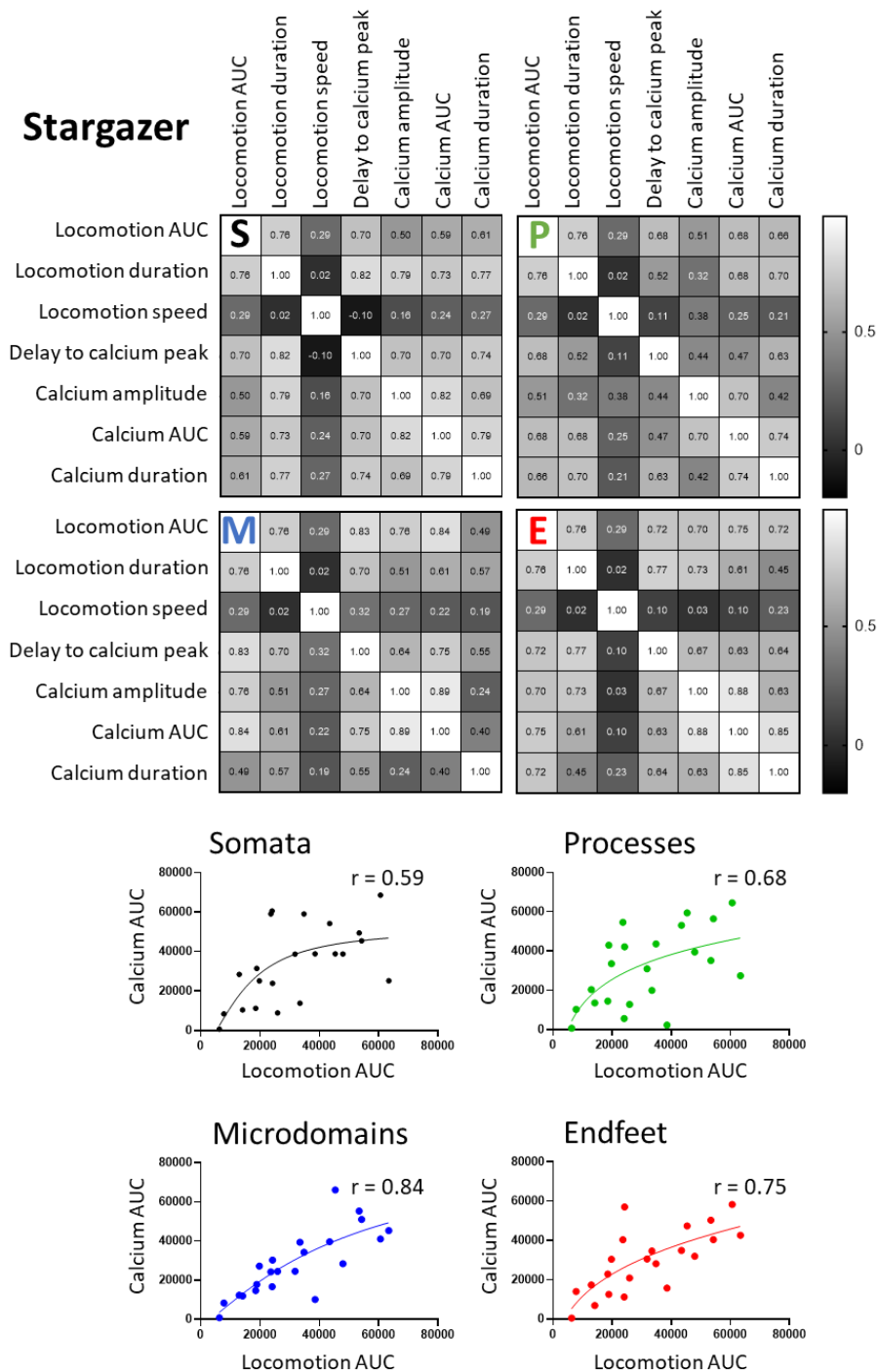


Figure 3-12: Correlation between locomotion and astrocyte calcium increase in Stargazer mice.

Top: Nonparametric spearman correlation 'r' values obtained from comparisons made between locomotion (AUC/area under the curve, duration and speed of movement) and calcium events (delay of calcium peak from locomotion onset, calcium event amplitude, AUC/area under curve and duration) in the soma (S), processes (P), microdomains (M), and endfeet (E). Locomotion AUC and duration had a strong positive correlation with calcium event amplitude, AUC and duration, unlike locomotion speed. Bottom: Scatter plots of the calcium AUC and locomotion AUC with a nonlinear least squares fit, suggesting a positive correlation between the two in all astrocyte sub-compartments. (N = 3 animals, n = 22 locomotion events per sub-compartment)

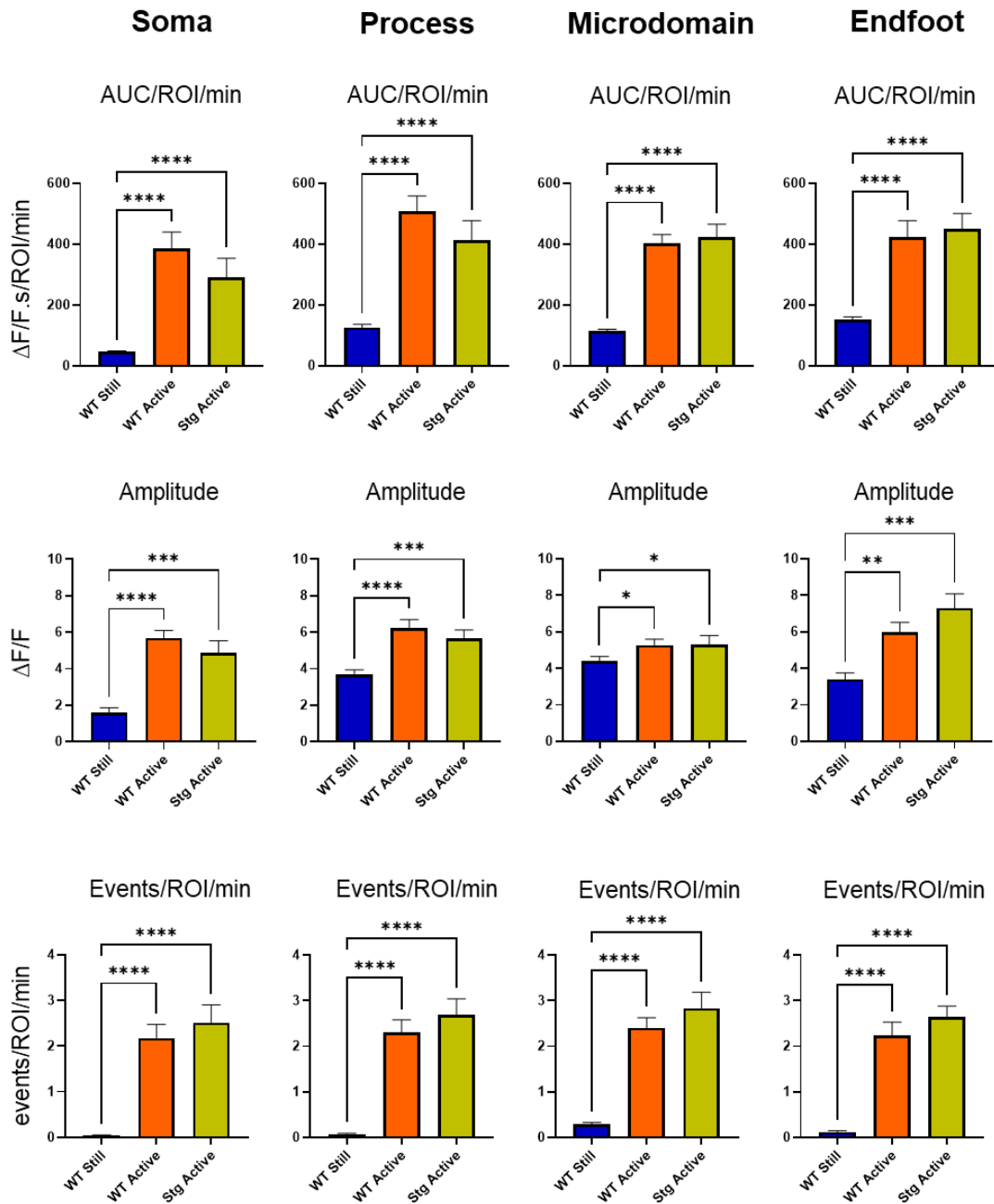


Figure 3-13: Calcium event properties of astrocyte sub-compartments in wild-types and Stargazers during locomotion.

WT Still: wild-type animals during periods of no movement; WT Active: wild-type mice during periods of movement; Stg Active: Stargazer mice during periods of movement. Active periods were characterised by more intense astrocyte calcium activity in wild-types (WT Active) and Stargazers (Stg Active), compared to periods of inactivity (WT Still). Stargazer mice show increased microdomain and endfeet activation. No differences were detected between active periods of wild-types and Stargazers. Kruskal Wallis Test followed by Dunn's post-hoc comparisons, * $p < 0.05$, ** $p < 0.01$, *** $p < 0.001$, **** $p < 0.0001$. WT Still $N = 6$ animals, 49 minutes of behavioural state data; WT active $N = 6$ animals, 39 minutes of behavioural state data; Stg active $N = 4$ animals, 27 minutes of behavioural state data.

The semi-automated calcium peak-detection algorithm did not effectively pick up differences in the duration between calcium events, since it divided large calcium events into multiple events due to fluctuations in the peak, making calcium events seem briefer. As an alternate approach, a manual analysis was performed, using the averaged calcium fluorescence traces calculated from all ROIs and sub-cellular compartments. This revealed that locomotion events in wild-types were associated with more prolonged calcium increase (28.3 ± 1.7 s vs 18.3 ± 1.3 s, mean \pm SEM, unpaired t-test, $t(138) = 4.025$, $p < 0.0001$; WT N = 3 animals, n = 82 locomotion events, Stargazer N = 3 animals, n = 58 locomotion events) and a larger AUC (44.6 ± 4.5 $\Delta F/F.s$ vs 23.3 ± 2.9 $\Delta F/F.s$, mean \pm SEM, unpaired t-test, $t(138) = 3.249$, $p < 0.005$; WT N = 3 animals, n = 82 locomotion events, Stargazer N = 3 animals, n = 58 locomotion events), but a similar amplitude (3.0 ± 0.2 $\Delta F/F$ vs 3.2 ± 0.3 $\Delta F/F$, mean \pm SEM, unpaired t-test, $t(138) = 0.4819$, $p = 0.6306$; WT n = 82 locomotion events, Stargazer n = 58 locomotion events). Since Stargazers ran for shorter durations, events associated with locomotion durations of less than 17 s (the maximum locomotion duration of Stargazers), were compared. The duration, peak amplitude and AUC of these events were similar in Stargazers and wild-types, which further indicated the strong positive correlation between the duration of the locomotion event and calcium fluorescence. However, the rise tau in Stargazers was shorter than in wild-types (11.7 ± 2.0 s vs 6.3 ± 0.8 s, mean \pm SEM, unpaired t-test, $t(130) = 2.524$, $p < 0.05$; WT N = 3 animals, n = 78 locomotion events, Stargazer N = 3 animals, n = 54 locomotion events) (Figure 3-14), indicating a more rapid response. Investigating this further revealed that Stargazer microdomains responded quickest compared to other cellular compartments (Figure 3-15), similar to the pattern observed in wild-types, and that all Stargazer sub-compartments exhibited a shorter delay to an initial calcium rise when compared to wild-types (for example in microdomains: Stargazer 1.6 ± 0.4 s, mean \pm SEM vs WT 3.0 ± 0.3 s, mean \pm SEM; unpaired t-test, $t(33) = 2.760$, $p = 0.0094$). This evidence indicated that Stargazers maintained a strong astrocyte response to locomotion, in spite of their ataxic phenotype, and indeed astrocytes may react more rapidly possibly due to chronically overactive astrocyte microdomains. In fact, Stargazer cortical neurons, especially layer V neurons, are hyperexcitable: they exhibit shorter action potential rise and decay times, a higher mean firing rate, and spontaneous bursts of activity (Di Pasquale et al. 1997). This is expected to increase astrocyte calcium transients in astrocyte microdomains and processes, in response to increased synaptic activity.

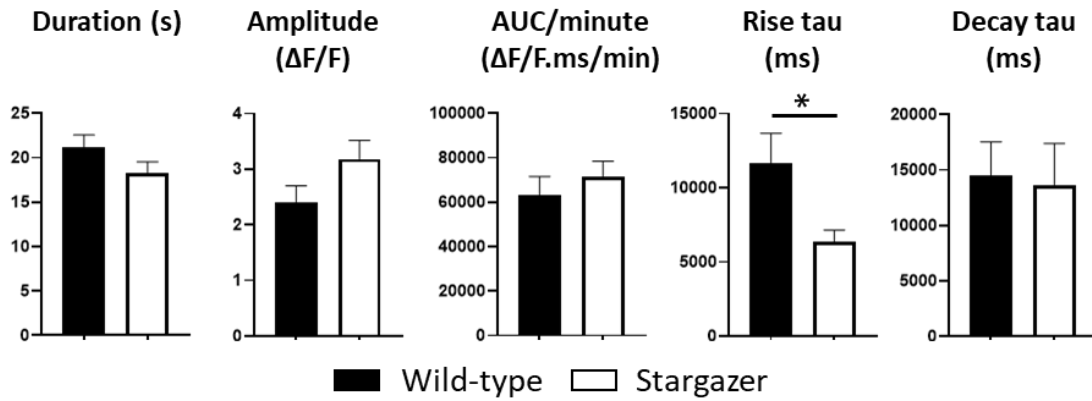


Figure 3-14: Differences in locomotion-induced averaged calcium transients between Stargazers and wild-types.

Manual analysis of calcium transients associated with locomotion periods of less than 17 s, revealed a similar astrocyte response in wild-types ($N = 3$) and Stargazers ($N = 3$), with the difference of a shorter rise time in Stargazer mice (* unpaired t-test, $t(130) = 2.524$, $p < 0.05$).

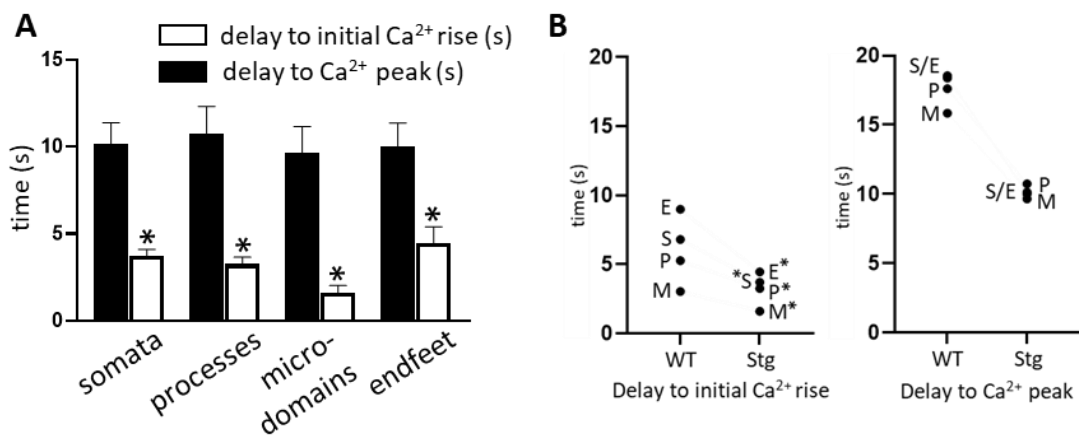


Figure 3-15: Individual compartment timing with respect to locomotion onset in Stargazer mice.

(A) The delay from onset of locomotion to the initial calcium rise was shortest in microdomains and longest in endfeet. The delay to the calcium peak following locomotion onset was similar in all sub-compartments. (*one-way ANOVA comparing the delay to initial calcium rise in the four sub-compartments: $F(3, 44) = 9.853$, $p < 0.0001$; $N = 3$ mice, $n = 11$ locomotion events). (B) Differences in the calcium delays in somata (S), processes (P), microdomains (M) and endfeet (E) of wild-types (WT) vs Stargazers (Stg). (*unpaired t-test, WT vs Stg, $p < 0.05$).

3.4 Astrocyte calcium activity following PMCA pump expression in S1 cortical astrocytes

A pilot study in wild-type mice was carried out to determine the feasibility of hPMCA2w/b pump co-expression with GCaMP6f in cortical astrocytes, and to determine its effect on astrocyte calcium activity. Co-injection of AAV5 gfaABC1D-cyto-GCaMP6f and AAV5 gfaABC1D-mCherry-hPMCA2w/b in layers 2/3 of the barrel field cortex, successfully resulted in co-expression of hPMCA2w/b and GCaMP6f selectively in astrocytes (mCherry and GFAP: N = 3 animals, n = 4 slices per animal, 200 μm x 200 μm ROI per slice, 88% colocalization of mCherry and GFAP from 80 GFAP-positive cells), with no neuronal expression (N = 3 animals, n = 5 slices per animal, 100 μm x 100 μm ROI per slice, 0% colocalization of mCherry and NeuN from 234 NeuN-positive cells) (Figure 3-16, 3-17, 3-18). Since the pump is membrane-bound, as expected labelling was extended to the finer processes and microdomains. It was also noted that certain regions that showed GCaMP6f expression lacked hPMCA2w/b expression (N = 3 animals, n = 7 slices per animal, 200 μm x 200 μm ROI per slice, 86% colocalization of mCherry and GFP from 139 GFP-positive cells).

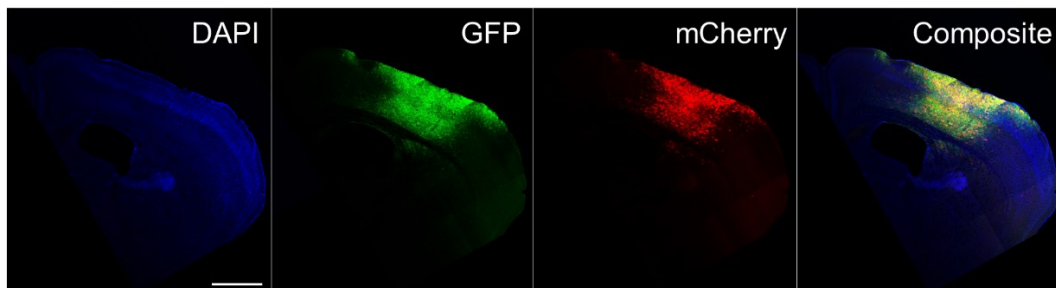


Figure 3-16: hPMCA2w/b pump expression in mouse S1BF. Immunohistochemistry with DAPI, anti-GFP and anti-mCherry revealing the spread and overlap of GCaMP6f and hPMCA2w/b pump, respectively, in S1BF. Scale bar: 1000 μm .

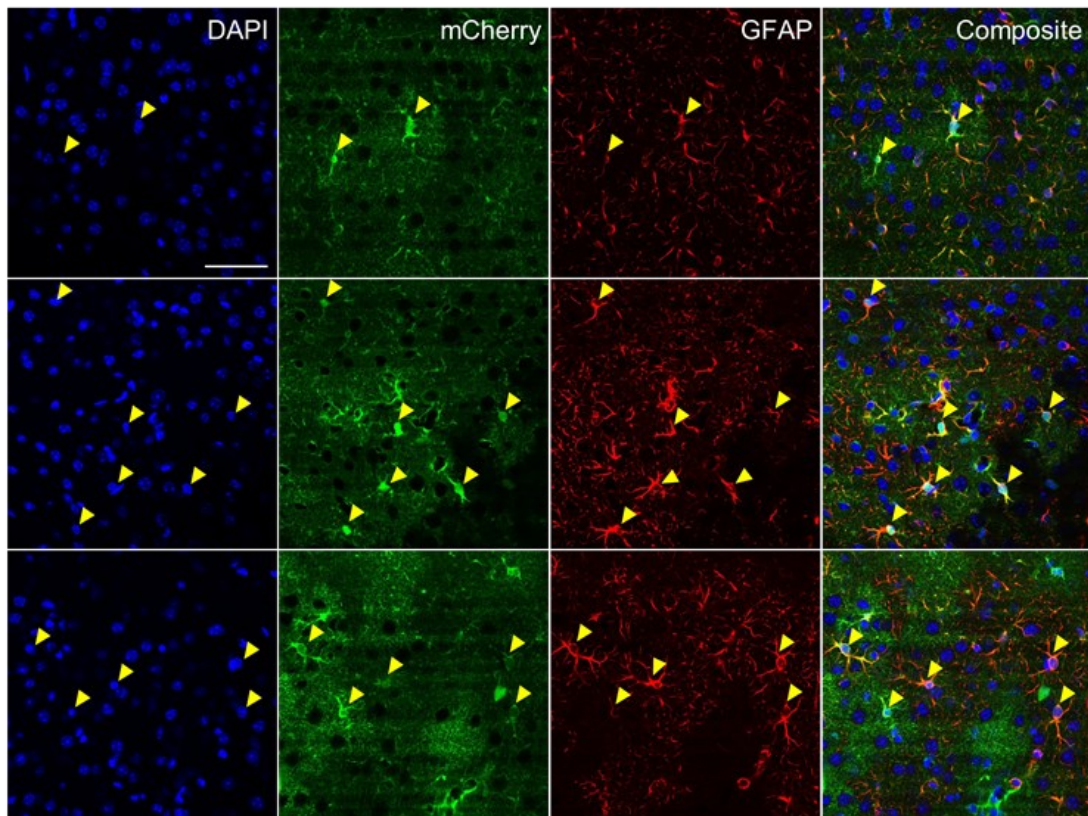


Figure 3-17: Astrocyte expression of hPMCA2w/b pump in mouse S1BF. Immunohistochemistry with DAPI, anti-mCherry and anti-GFAP. The pump's mCherry tag overlapped with anti-GFAP staining, which indicated that the pump was expressed in astrocytes. Arrows indicate astrocyte somata overlapped with DAPI, mCherry and GFAP labelling. Scale bar: 50 μ m.

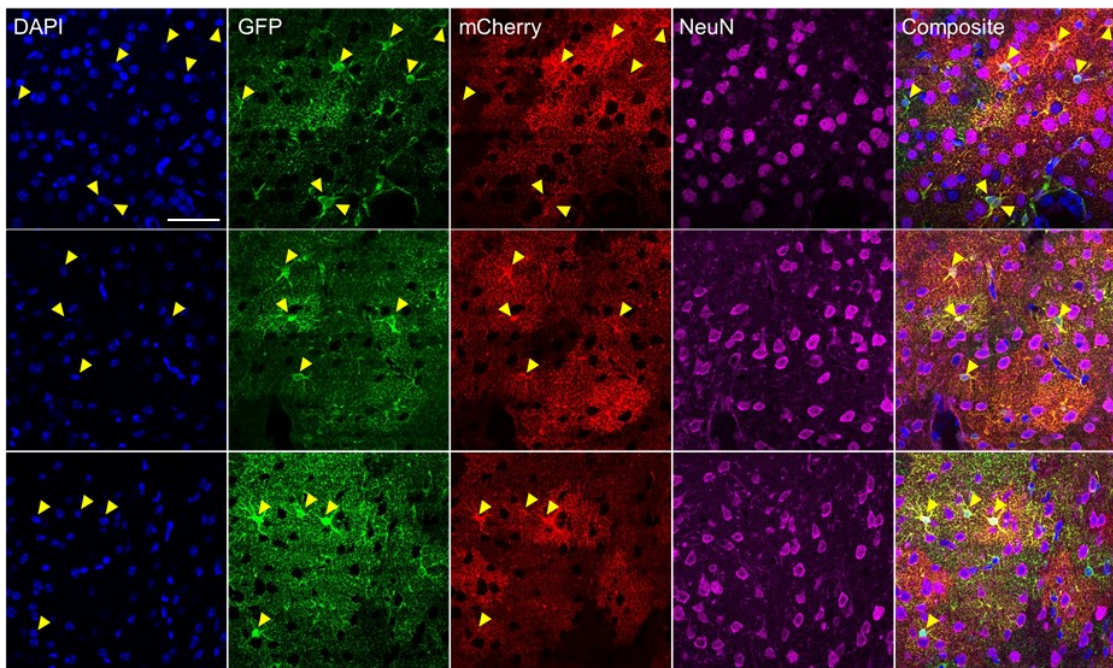


Figure 3-18: Astrocyte-selective expression of hPMCA2w/b pump in mouse S1BF. Immunohistochemistry with DAPI, anti-GFP, anti-mCherry and anti-NeuN. Composite images of the four channels revealed that GCaMP6f and hPMCA2w/b were co-

expressed in the same astrocytes, and spanned most of the field of view taken up by the finer astrocyte processes and microdomains. No overlap with NeuN was observed, which indicated that the pump was not expressed in neurons. Arrows indicate astrocyte somata overlapped with DAPI, GFP and mCherry labelling. Scale bar: 50 μ m.

Two-photon calcium imaging of head-restrained animals was performed to confirm the efficacy of hPMCA2w/b pump expression in S1 astrocytes to reduce astrocyte calcium signalling, as originally reported in striatal astrocytes (Yu et al. 2018). Overall, intracellular calcium changes in astrocytes were below detection limits or largely reduced (Figure 3-19). The duration and amplitude of the detected events following locomotion were reduced, but not totally abolished, by 74% and 62% respectively (N = 2 mice, n = 21 locomotion events), similar to that reported in the striatum (Yu et al. 2018), and as expected due to areas void of hPMCA2w/b expression observed in the immunohistochemistry.

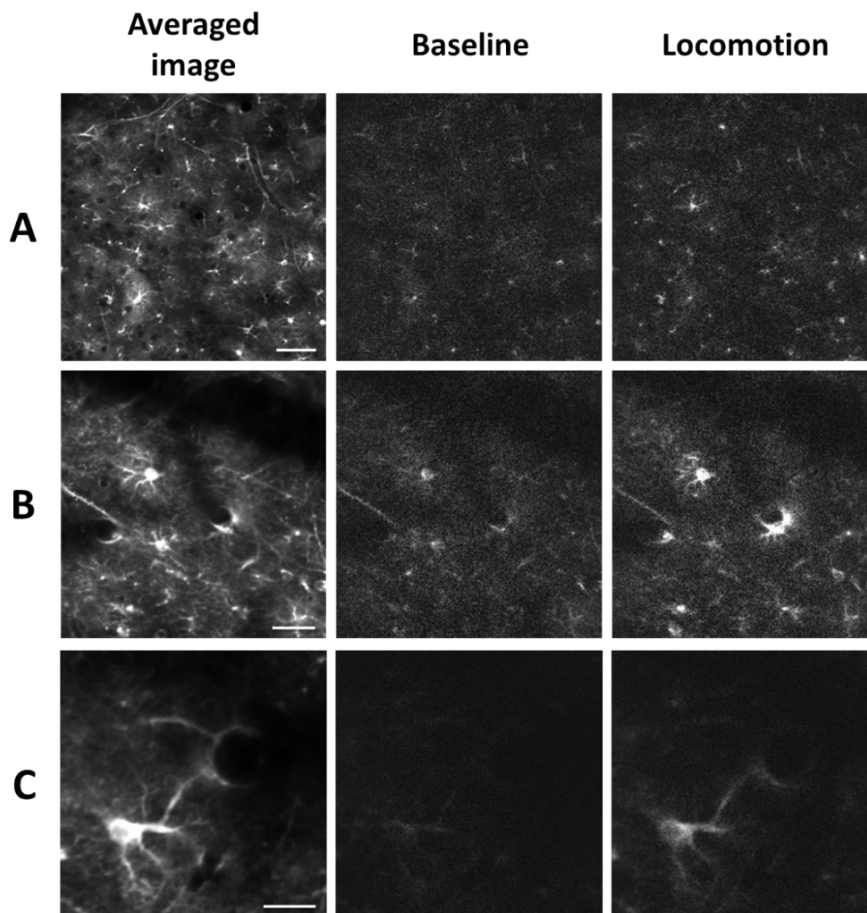


Figure 3-19. Calcium activity following hPMCA2w/b expression in S1 astrocytes. (A-C) Three different fields of view before locomotion (Baseline images) and at the peak of calcium fluorescence following locomotion (Locomotion images). ‘Averaged images’ were used to identify astrocyte morphologies and ROI selection. Scale bar in A: 60 μ m, B: 30 μ m, C: 20 μ m.

3.5 Discussion and further work

By combining head-restrained two-photon calcium imaging and ECoG recording, we documented the astrocyte calcium response to voluntary locomotion in the S1BF. We confirm previous findings of synchronous astrocyte activation and detail novel findings of microdomain-specific activation and a robust, rapid astrocyte response in the Stargazer model of ataxia. This study highlights the reliable and at times variable astrocyte-response during voluntary locomotion, investigates the flow of calcium signalling through the different cellular compartments, and hints towards astrocyte sensory summation.

3.5.1 Synchronous full-cell astrocyte activation with sub-cellular independence

We observed synchronous widespread activation of S1 astrocytes during voluntary locomotion, which is consistent with previous studies that identified a predominantly α 1-adrenergic receptor-mediated response to locomotion, due to noradrenaline release from locus coeruleus inputs and direct binding to astrocyte receptors (Ding et al. 2013; Oe et al. 2020; Paukert et al. 2014). The modulatory dominance of the noradrenergic system on calcium activation in the cortex has been recently reinforced with respect to startle-induced responses and fear conditioning responses, not only on astrocyte calcium signalling but also on cAMP astrocyte release during prolonged vigilance states, indicating that different astrocyte signalling mechanisms are modulated by noradrenergic input from the locus coeruleus (Oe et al. 2020). Other signalling mechanisms are however clearly involved in S1BF astrocyte response to sensory stimulation, including monoamines and acetylcholine (Stobart et al. 2018a), as well as the involvement of metabotropic glutamate receptors (Wang et al. 2006; Lind et al. 2013). This suggests that the subtle responses which we observed in response to locomotion, such as those specific to microdomain activation, may be mediated by such alternate signalling mechanisms, which become apparent only in the absence of widespread noradrenaline release, possibly during low vigilance states. This is backed up by the observations that AMPA and NMDA receptors act synergistically with noradrenaline signalling during locomotion in Bergmann glia (Paukert et al. 2014), and that the onset latency of fast microdomain activation was not influenced by blockade of major neuromodulators (Stobart et al. 2018a).

During population-wide astrocyte activation, it was noted that the pattern of calcium fluctuations closely followed dips and peaks in locomotory patterns, which was indicative of the ability of astrocytes to distinguish movement patterns. Astrocytes are thus actively and continuously monitoring sensory information and react accordingly to rapid ongoing cortical input. Moreover, it was noted that ECoG changes in the low frequency bands

were correlated with different phases of astrocyte activation, further indicative that astrocytes are sensitive to altered cortical states as previously reported (Poskanzer and Yuste 2016; Poskanzer and Yuste 2011; Bojarskaite et al. 2019; Ingiosi et al. 2020; Lines et al. 2020).

3.5.2 Microdomains initiate the astrocytic response to locomotory input and may engage in summation of input

Astrocyte calcium fluctuations occur with a delay to locomotory input and peak a few seconds after onset of movement, as previously described in various studies during locomotion or sensory stimulation, in various cortical regions as well as in S1 (Nimmerjahn et al. 2009; Ding et al. 2013; Lines et al. 2020; Srinivasan et al. 2015; Slezak et al. 2019; Bekar et al. 2008; Zhao et al. 2012). Our data however indicated that while the overall astrocyte response occurs with a few seconds delay, subcellular calcium events, especially those in the cell periphery, respond almost instantly, as noted in response to visual stimuli (Slezak et al. 2019) and whisker stimulation (Stobart et al. 2018a; Lind et al. 2013; Lind et al. 2018). The astrocyte response is expected to rapidly follow neuronal activation, which in the visual cortex occurs 50 ms following locomotion onset (Slezak et al. 2019), and in S1BF layer 2 occurs 10-12 ms following whisker deflections (Wang et al. 2006). Given that we imaged from S1BF layers 2/3, it is expected that deeper astrocytes in layer 4 closer to or those enwrapping sensory thalamo-cortical projections, will respond even more rapidly to ascending sensory input. Moreover, neuronal activation in S1, modulated by projections originating in the primary motor or premotor cortical areas (as observed in monkeys (Umeda et al. 2019; Soso and Fetz 1980) and in humans (Sun et al. 2015; Christensen et al. 2007; Cui et al. 2014), may occur up to 400 ms in anticipation of voluntary movements (Sun et al. 2015). This may be potentially translated into astrocyte microdomain activation in response to increased synaptic activity in the area. Nonetheless, the sub-second responses of astrocyte microdomains to the onset of locomotion serves as further evidence of the physiological importance of fine astrocyte processes in the integration of sensory and motor information.

Another important finding, was the implied ability of astrocytes to summate inputs. This has been previously evidenced, such as in hippocampal slices (Perea and Araque 2005), thalamic slices (Parri et al. 2010), and in vivo under anaesthesia in S1 in response to hind-limb stimulation (Lines et al. 2020). Our findings further evidence that the astrocyte response depends on the strength of different inputs, indicating an ability to efficiently process synaptic information. We show that weak locomotory input resulted in microdomain-specific activation, which greatly contrasted with full astrocyte activation

observed during extended periods of locomotion. Lines et al. (2020) applied different hindlimb stimulation protocols by varying the time and frequency of the stimulus, while maintaining the animal under anaesthesia. They determine that the sensory-evoked calcium response is dependent on the duration and frequency of the stimulus, both following a sigmoidal function. We add further to this evidence in our awake mice, and show that the duration of locomotion (longer duration presumably involving stronger and more prolonged sensory stimulation), and not speed, has the greatest influence on calcium signalling. This also confirms previous evidence in Bergmann glia that speed of locomotion only weakly modulates astrocyte calcium activation (Paukert et al. 2014). We did however observe cases of strong, full astrocyte activation during brief periods of locomotion, which can be explained in a number of ways. The mouse might have engaged in motor activity not detectable by the linear rotation of the wheel, or increased noradrenergic input or an accidental startle stimulus could have potentially enhanced the astrocyte response,, as outlined in section 3.5.1..

Mice with an ataxic phenotype, not only maintained a strong astrocyte response to locomotion, but also exhibited a more rapid response to locomotory input, as evidenced by the shorter delay to calcium event onset and to the calcium peak. This possibly arises from a reduced summation threshold that sparks full-cell activation more rapidly compared to wild-type animals. This may possibly be an adjustment of astrocyte function to make up for reduced AMPA receptor expression in Stargazer S1 (Adotevi and Leitch 2017) or in response to increased cortical excitability in Stargazer S1 (Di Pasquale et al. 1997), and serves as further evidence of altered astrocyte function in Stargazer mice, which have altered GAT-1 expression in thalamic astrocytes (Pirttimaki et al. 2010; Pirttimaki et al. 2013).

3.5.3 Further work

The astrocyte response to locomotion is highly complex. Indeed, we observed instances of prolonged movement with a weak or a delayed astrocyte response, and conversely, brief movements accompanied by widespread astrocyte population activation. An exhaustive study to understand astrocyte behaviour in an awake active animal would require the measurement of additional signals, most significantly, the monitoring of pupil size, whisking detection and neck EMG measurements, based on previous evidence that: (i) spontaneous calcium events in Bergmann glia have been overwhelmingly linked to an increase in EMG power (Paukert et al. 2014); (ii) spontaneous whisking has been linked to elevated calcium fluctuations in S1BF astrocytes (Bojarskaite et al. 2020), which is highly relevant since mice engage in whisking during locomotion, and a fifth of the time spent not moving involves whisking (Ayaz et al. 2019); and (iii) pupil dilation

has been positively correlated with locomotion, an increase in cholinergic and noradrenergic input to the cortex, and also with increased astrocyte calcium signalling (Zuend et al. 2020; Reimer et al. 2016; Slezak et al. 2019). Considering these extra factors would be essential for a full explanation of the complex calcium signalling in astrocytes during awake behaviours.

It has similarly been shown that the neuronal response to locomotion is highly variable. Neurons exhibit a highly integrative response to sensory stimulation by responding strongest during concurrent motor and sensory inputs, only 32% of the neuronal population in S1BF layers 2/3 activate during running, and distinct neuronal populations reliably activate specific to the running speed (Ayaz et al. 2019). This necessitates a similar study in astrocytes, whereby astrocytes neighbouring neuronal-speed-responders are investigated for a similar sensitivity or selectivity to speed. Local monitoring of neuronal populations by means of dual wavelength imaging for concomitant astrocyte and neuronal calcium imaging, will thus be critical to monitor local neuron-astrocyte signalling. This evidence would further highlight the anatomical-specific variability of astrocyte function and their role in information processing.

3.6 Conclusions

Our results confirm previous work on locomotion-induced astrocyte calcium activity. We show that astrocytes engage in spontaneous calcium signalling during periods of inactivity and undergo an efficient population response to locomotion, which is at times variable and must be dependent on a number of factors, possibly on state of arousal and on neuromodulator release. We also confirm that astrocyte population activity is tuned to neuronal network activity, as evidenced by changes in the low frequency ECoG bands during changes in astrocyte calcium activity.

We also reveal previously undescribed locomotion-related calcium activity. Astrocyte calcium patterns closely follow locomotion patterns. Multipeak calcium events are characteristic of prolonged or intermittent locomotion, and brief bursts of running activity are mirrored by multiple calcium peaks. Locomotion duration, not speed, positively modulates the calcium response. Microdomains are more receptive to locomotion-related input, because they respond most rapidly following locomotion onset and activate in instances when the other cellular compartments do not. Our findings also hint towards input summation since a microdomain-specific response accompanies brief movements, which would be perceived as weak input, whereas a full cell and population response accompanies a prolonged period of locomotion, perceived as a strong

stimulus. Ataxic mice show a similarly robust response to locomotion, indicating that the astrocyte response is not compromised by ataxia. Indeed, the response is triggered more rapidly than in wild-type counterparts, indicating an astrocytic accommodation to altered neuronal function.

Chapter 4: Cortical astrocyte calcium activity in rodent models of absence seizures

Building on the methodology that was developed in Chapter 3, here we investigate astrocyte calcium activity in rodent models of absence seizures. This part of the project addresses the current lack of knowledge about astrocyte calcium activity in genetic models of epilepsy and in models of non-convulsive epilepsies. We hypothesise that astrocyte calcium activity during non-convulsive absence seizures is vastly different to what has been previously described using convulsive and chemical models.

We explored if astrocyte calcium events were reflective or predictive of cortico-thalamo-cortical synchrony, in the form of SWDs, and we used astrocyte manipulation tools to determine the impact of modified astrocyte calcium activity on seizure occurrence. Three models were investigated, two genetic models - the Stargazer mouse and GAERS rat, and one pharmacological model - the GHB model. Several techniques were employed: (i) two-photon calcium imaging of GEC1-expressing astrocytes in the S1BF of adult epileptic mice with concurrent ECoG recording; (ii) ECoG recording of IP3R2 KO mice and WT littermates after pharmacological induction of absence seizures; (iii) ECoG recording of Stargazers and GAERS after astrocyte-specific DREADD activation in the S1BF.

4.1 S1 layers 2/3 astrocyte calcium activity in Stargazer mice

Adult, male Stargazer mice were used to investigate cortical astrocyte activity during periods of absence seizures. Similar to the two-photon calcium imaging experiments described in Chapter 3, AAV-cyto-GCaMP6f was injected in the right cortical hemisphere to express GCaMP6f in layers 2/3 S1BF astrocytes, and fronto-parietal ECoG electrodes were implanted in the left hemisphere. Awake, active mice were head-restrained on a freely rotating wheel under the two-photon microscope and monitored with video recording. Calcium imaging was performed at a wavelength of 980 nm at 30 Hz, averaged to 5 Hz, with concurrent ECoG monitoring for seizure detection. Linear voluntary locomotion was quantified with a rotary encoder. Calcium changes were detected and quantified as explained in section 2.6.4 above. Ictal events were detected as outlined in section 2.5 above.

Cortical astrocyte calcium activity was quantified during periods of ictal activity. Ictal events in Stargazers were short lasting, observed as ~7 Hz SWD oscillations that lasted 8.4 ± 0.6 s (mean \pm SEM, N = 5 animals, n = 112 seizures) (Figure 4-1), similar to what

was previously reported (Meyer et al. 2018; Aizawa et al. 1997). Due to the relatively brief absence seizure duration in the Stargazer mouse, astrocyte calcium changes were quantified during a prolonged period of mostly uninterrupted ictal events, defined here as an 'Ictal State'. An ictal state was included in the analysis only if it met specific criteria, defined as follows: (i) an ictal state was a period dominated by recurrent SWDs detected on the ECoG, (ii) accompanied by behavioural arrest during SWDs, (iii) not accompanied or preceded by locomotion events that exceeded a speed of 1.5 cm/s and/or 5 seconds duration, (iv) and of least 30 seconds duration.

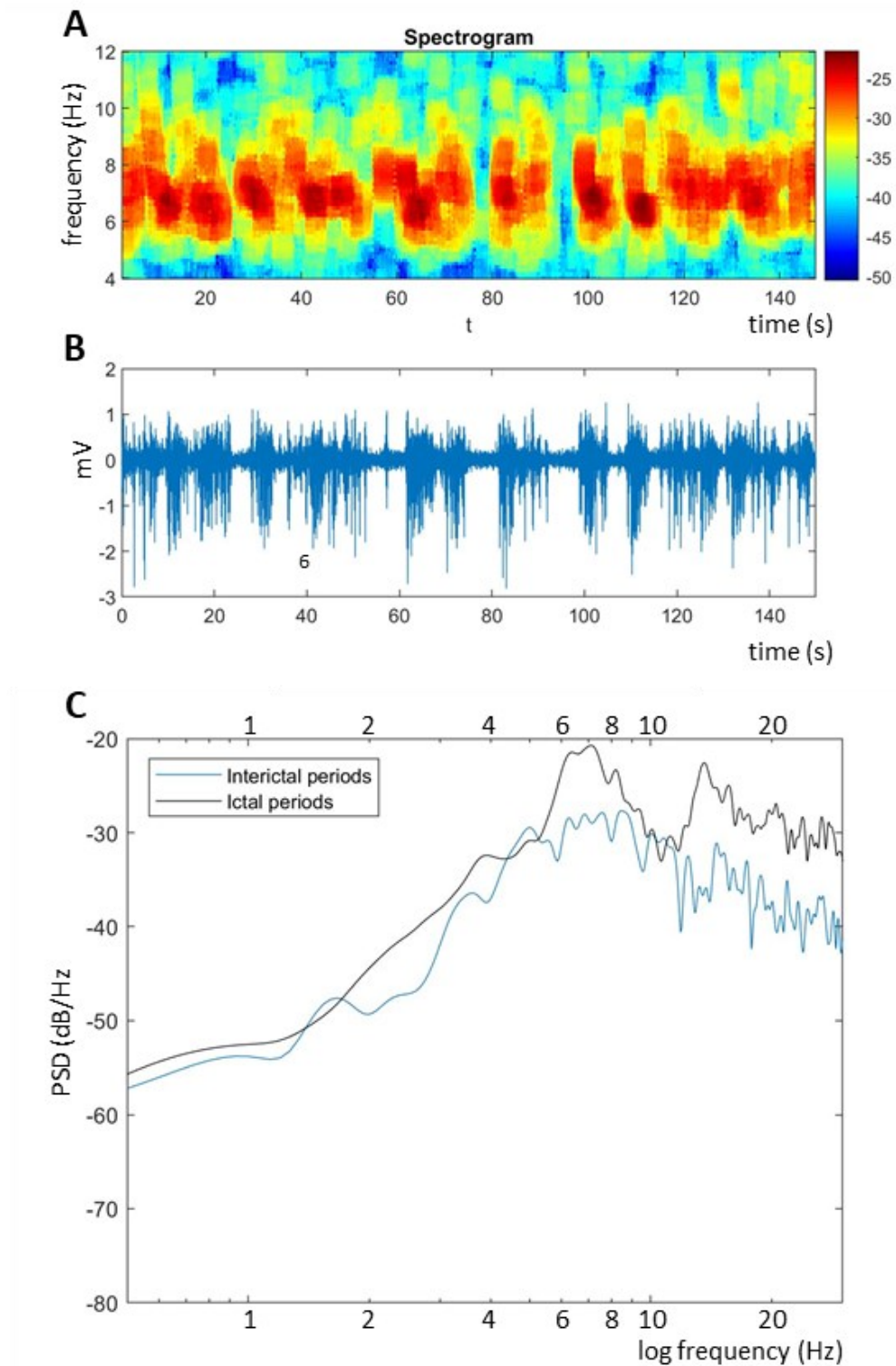


Figure 4-1: Stargazer ECoG ictal activity.

(A) ECoG multitaper spectrogram (1 second windows spaced at 50 ms intervals): 5-9 Hz oscillations coincided with periods of SWDs in the raw ECoG (shown in (B), processed with DC remove, time constant 0.1 s). (C) Welch's power spectral density estimate (L-Chebyshev window of 4 seconds, with 50% overlap) shown in a logarithmic scale: ictal periods were characterised by a peak at around 7 Hz, due to SWDs oscillating at this frequency.

Here we test the hypothesis of whether astrocyte activation in the form of increased calcium activity, is reflective or predictive of absence seizures. Ictal states were not accompanied by global calcium changes in the S1BF astrocyte population, nor were they accompanied by localised and coordinated calcium changes confined to specific astrocyte sub-compartments, i.e., somata, processes, microdomains, or endfeet (Figure 4-2). As observed in Chapter 3, global synchronised calcium changes were predominantly related to locomotor activity. Numerous calcium events were detected during ictal periods in individual ROIs within all sub-compartments (Figure 4-2 D1-4); however, their occurrence did not correspond to ictal onset. An ictal onset trigger average of the change in calcium did not reveal clear calcium changes immediately preceding or following ictal onset (Figure 4-3), as was the case for ictal offset (data not shown). A repeated measure one-way ANOVA performed on the different time-points did not reveal any significant changes in the ictal onset/offset trigger average of any astrocyte sub-compartment. Ictal onset was defined as the time of the first spike in a series of SWD cycles that lasted at least 1 second, and was not preceded or followed by locomotion with a speed greater than 2.5 cm/s, for a period of 10 seconds, or other ictal events for a period of 5 seconds. Similarly, ictal offset was defined as the time of the last spike in the SWD train.

Ictal periods were accompanied by a rise in the power of theta and alpha bands (4 – 12 Hz, refer to Figure 4-1 C), which efficiently fluctuated along with the pattern of SWD periods (Figure 4-4). As a further attempt to correlate calcium changes with ictal events, changes in the theta and alpha bands were cross-correlated against calcium transients in the different astrocyte sub-compartments (Figure 4-4). The lack of a clear correlation peak reinforced our observations that astrocyte calcium was not oscillating in harmony, in anticipation or in response to periods of SWDs.

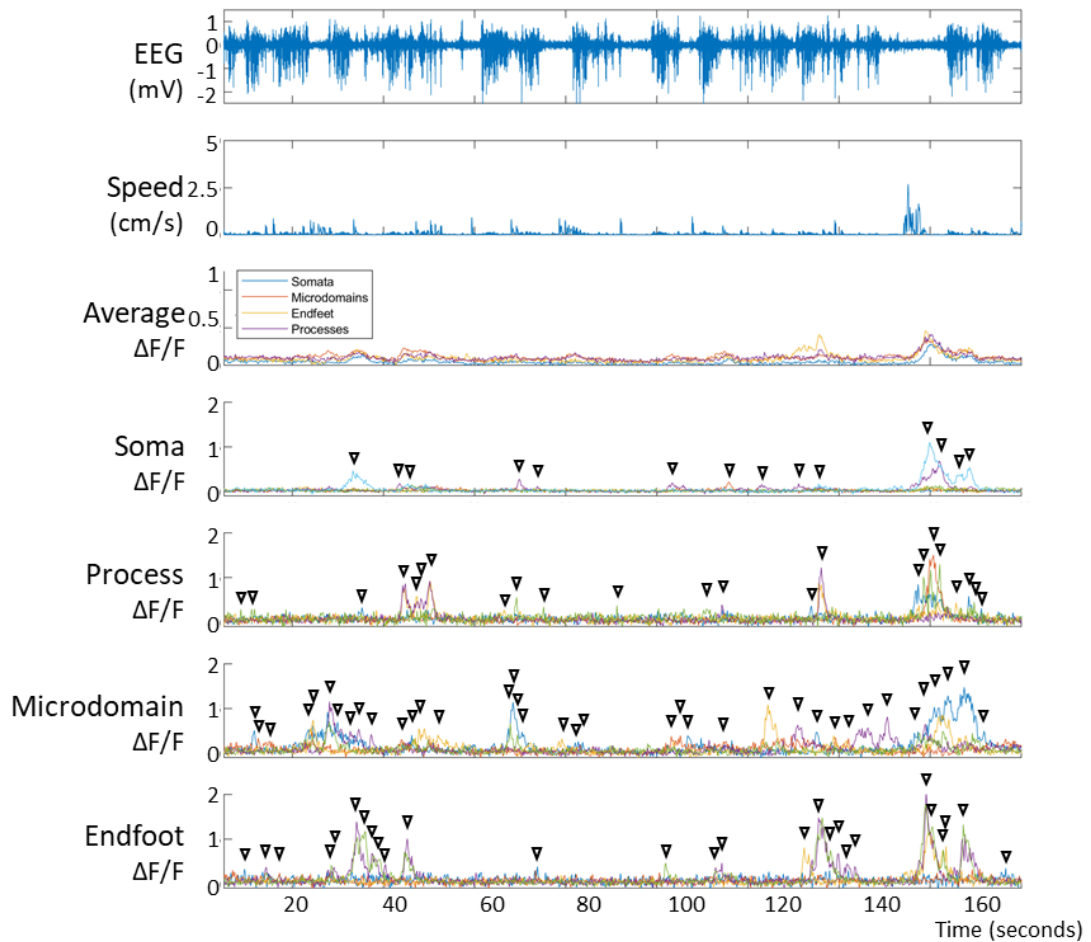


Figure 4-2: Cortical astrocyte calcium activity during ictal states. Ictal states, consisting of mostly uninterrupted periods of SWDs, were accompanied by astrocyte calcium events in all astrocyte sub-compartments, but lacked synchronous activation of full astrocyte territories or astrocyte populations. In the calcium traces, at approximately 150 seconds, a clear break in ictal activity and a brief period of locomotion gave rise to widespread and synchronous astrocyte calcium transients in all sub-compartments. Such concerted activity was absent during ictal periods. Ictal periods were instead characterised by independent events in isolated astrocyte sub-compartments.

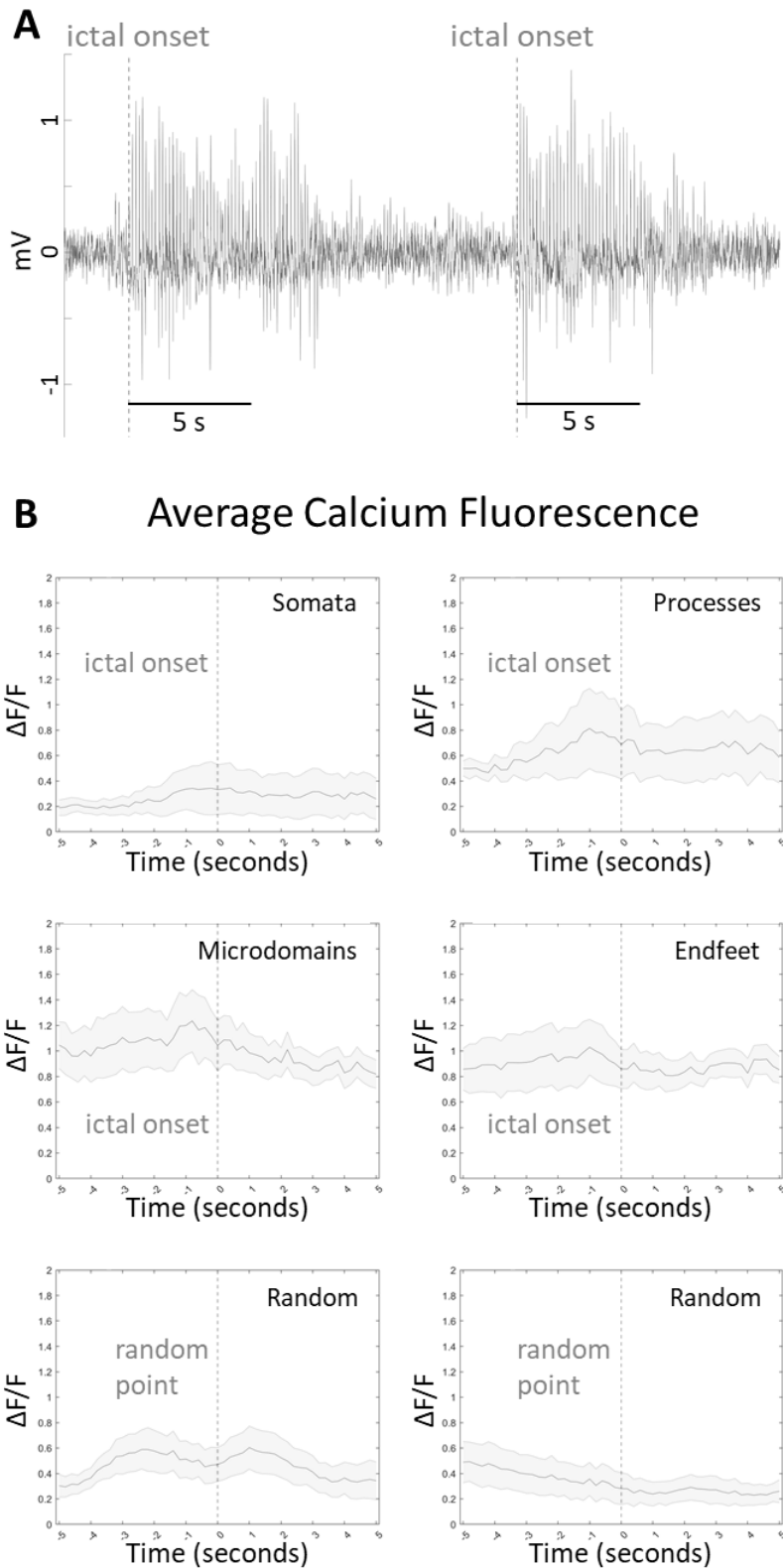


Figure 4-3: Ictal onset trigger average of calcium transients.
 (A) Ictal onset was taken as the time of the first spike detected in the SWD train. (B) Ictal onset did not coincide with significant calcium fluctuations preceding or following ictal onset. Plots created from random time points revealed similarly minor calcium changes. $N = 3$ animals, $n = 15$ seizures or random points for each plot.

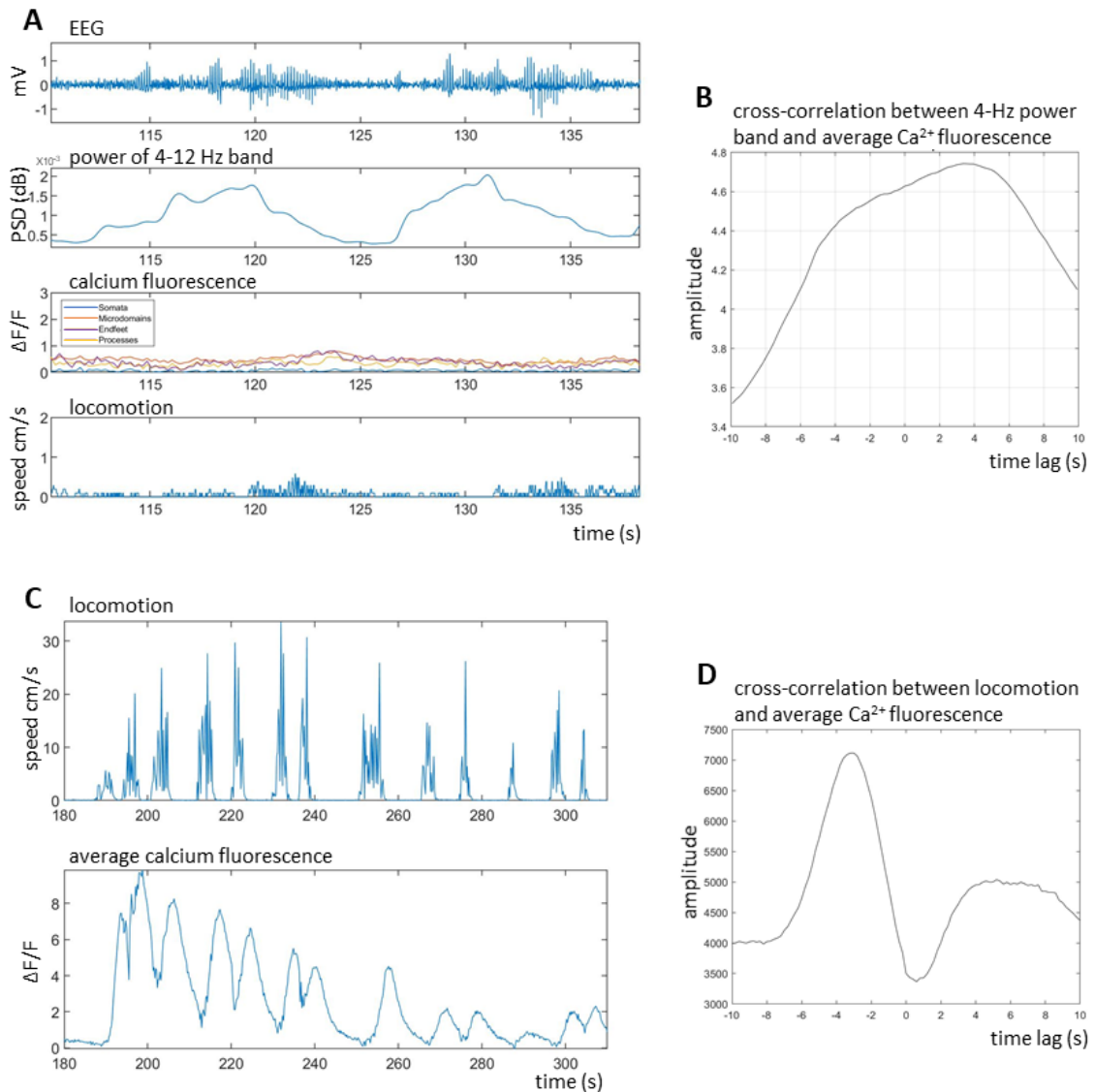


Figure 4-4: Changes in calcium fluorescence during seizure-related increase in theta and alpha activity, in comparison with changes in calcium fluorescence during locomotion.

(A) Starting from the top: raw ECoG signal (processed with DC Remove, time constant 0.1s), power spectral density (PSD) of the theta and alpha bands (4-12 Hz), averaged calcium changes in the different sub-compartments, and locomotion of the animal on the rotating wheel. (B) Cross-correlation (performed using the `xcorr` function on MATLAB) between the average calcium fluorescence of a single astrocyte and the power of the theta and alpha bands during the two consecutive absence seizures shown in A. The correlation did not reveal any sharp peaks - this indicates a lack of synchrony between the two signals. (C) and (D) serve as an example of a clear correlation between two signals, unrelated to seizure activity. (C) Top: locomotion of the animal; bottom: averaged calcium changes from a single astrocyte. (D) Cross-correlation between the speed of locomotion and the average calcium fluorescence shown in C. The correlation reveals a clear peak at about -4 seconds. This indicates that the two signals follow each other with a delay of about 4 seconds, led by the locomotion signal.

4.2 S1 layers 2/3 cortical astrocyte calcium activity in GHB-injected wild-type mice

An alternative pharmacological model of absence seizures was next used to test if similar astrocyte calcium changes are present in different models. The GHB pharmacological model was chosen since, as outlined in section 1.7.3, (i) it has been used extensively in rodents, (ii) reproduces the increase in tonic GABA_A inhibition observed in other animal models and in humans, (iii) astrocytes possess a putative GHB receptor and (iv) astrocytes in thalamic slices respond to GHB administration by an increase in intracellular calcium.

4.2.1 Suitability of the GHB-model in rats and mice

GBL administration induced long periods of absence-like seizures which suited our experimental setup and hypothesis since we required a model that induced long periods of ictal activity that was accompanied by immobility. Since rats have been used more successfully in replicating well-defined and isolated absence seizures after GHB-administration (Aizawa et al. 1997; Venzi et al. 2015), for a full review), we first characterised the GHB-model in WT Wistar rats to confirm the suitability of the model in replicating absence seizures.

Wistar rats (N = 5) were chronically implanted with bilateral fronto-parietal ECoG screws to detect ictal events, and two electromyography (EMG) wires were embedded in the right nuchal muscle to monitor changes in muscle tension. The rats were given a week to recover and were recorded in a plexi-glass arena in which they were free to move around while attached to the ECoG/EMG amplifiers. 4-6 Hz absence seizures were induced with 150 mg/kg GBL (i.p.) (hydrolysed by lactonase to GHB in the liver (Roth and Giarman 1966). As expected, shortly after GBL administration, individual and well-spaced absence seizures were detected, which became more frequent and eventually coalesced into a constant state of slow hypersynchronous oscillatory activity (3 – 5 Hz) that was eventually followed by a deep state of hypnosis and a burst-suppression ECoG pattern (Figure 4-5 A). The rat was motionless during absence seizures, and during the subsequent phases. The EMG power captured the differences in the neck muscle tension during the various phases, which was highest during locomotory activity and decreased as the animal went into interrupted absence seizures, and reduced further during the constant, synchronous slow-wave activity and the final sedated state with a burst-suppression ECoG pattern (Figure 4-5 B). Our data confirmed previous findings that described ECoG changes after GHB administration, which described the following stages occurring in succession: (i) clear isolated SWD events – absence seizures, (ii)

continuous hypersynchronous slow-wave absence-like activity, and (iii) burst-suppression ECoG pattern together with strong sedation (Venzi et al. 2015).

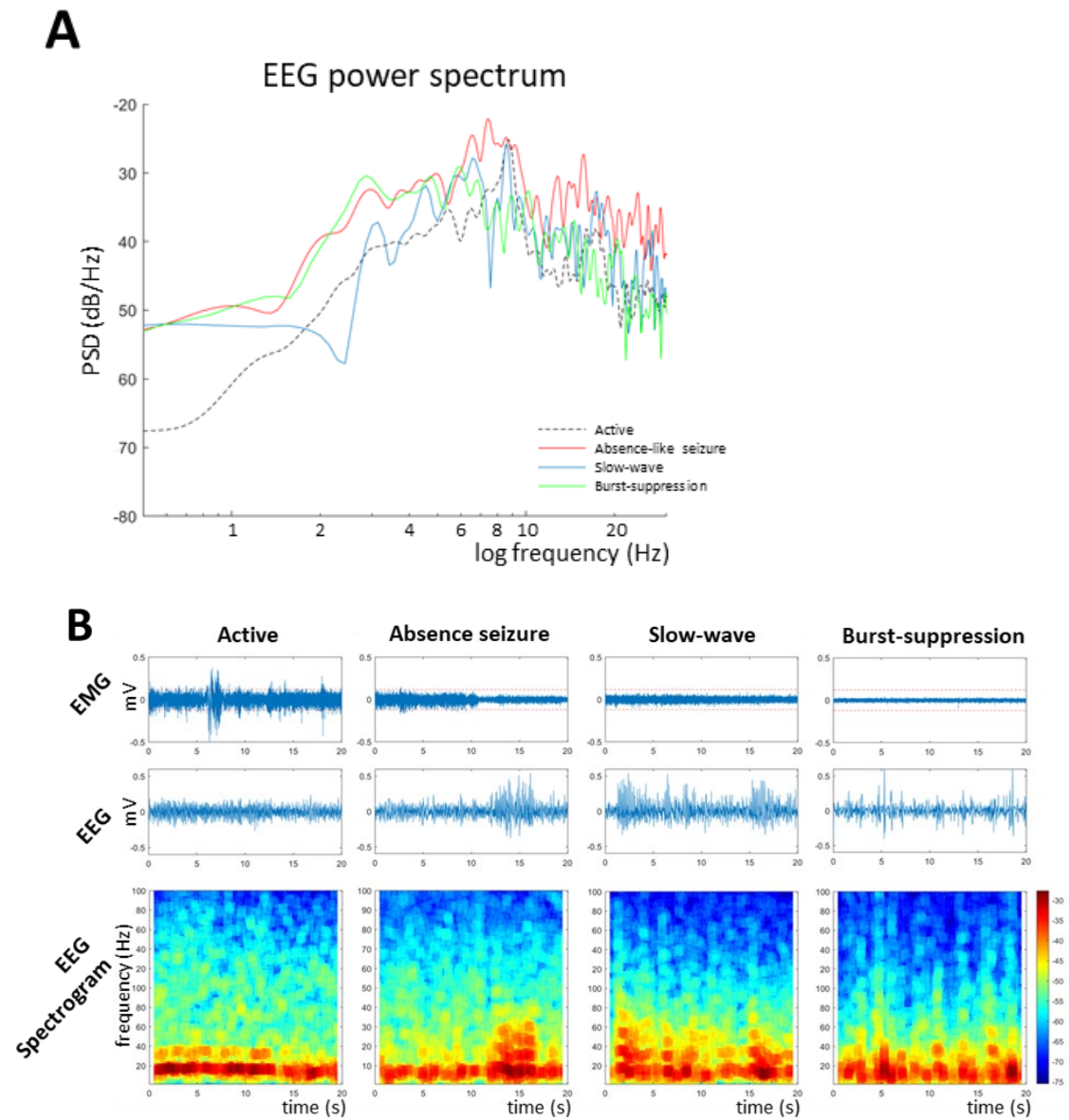


Figure 4-5: Distinct ECoG stages following GBL (150 mg/kg, i.p.) administration in Wistar rats.

(A) Power spectra (L-Chebyshev window of 4 seconds, with 50% overlap) for the different GBL stages including an Active period before the GBL effect is first observed. (B) EMG (top), raw ECoG (middle) (DC remove, time constant, 0.1 s) and ECoG multitaper spectrogram (bottom) (1 second windows spaced at 50 ms intervals) during a representative period of each GBL stage. The EMG amplitude served as a measure of tension in the neck, which was largest during periods of activity, reduced during periods of absence-like seizures (isolated periods of SWDs) and slow-wave activity (constant, uninterrupted SWD pattern), and was lowest during burst-suppression activity in the ECoG (periods of firing followed by reduced brain activity) that indicated a state of sedation/hypnosis.

Next, we attempted to replicate GHB-induced absence seizures in mice, without the use of EMG implants, due to eventual spatial limitations on the skull of the animal when implanted with a cranial window and a headplate for two-photon calcium imaging experiments. Adult, male C57Bl6/J mice (N = 5 animals) were implanted with fronto-parietal ECoG electrodes, allowed to recover and injected with 75 mg/kg GBL (i.p.) while freely moving in a plexi-glass arena. Individual absence-like seizures were rare and hard to detect; however, a long, persistent period of synchronous slow wave, absence-like, activity (3 - 5 Hz) became evident a few minutes after injection, followed by a highly sedated state defined by a burst-suppression ECoG pattern (Figure 4-6).

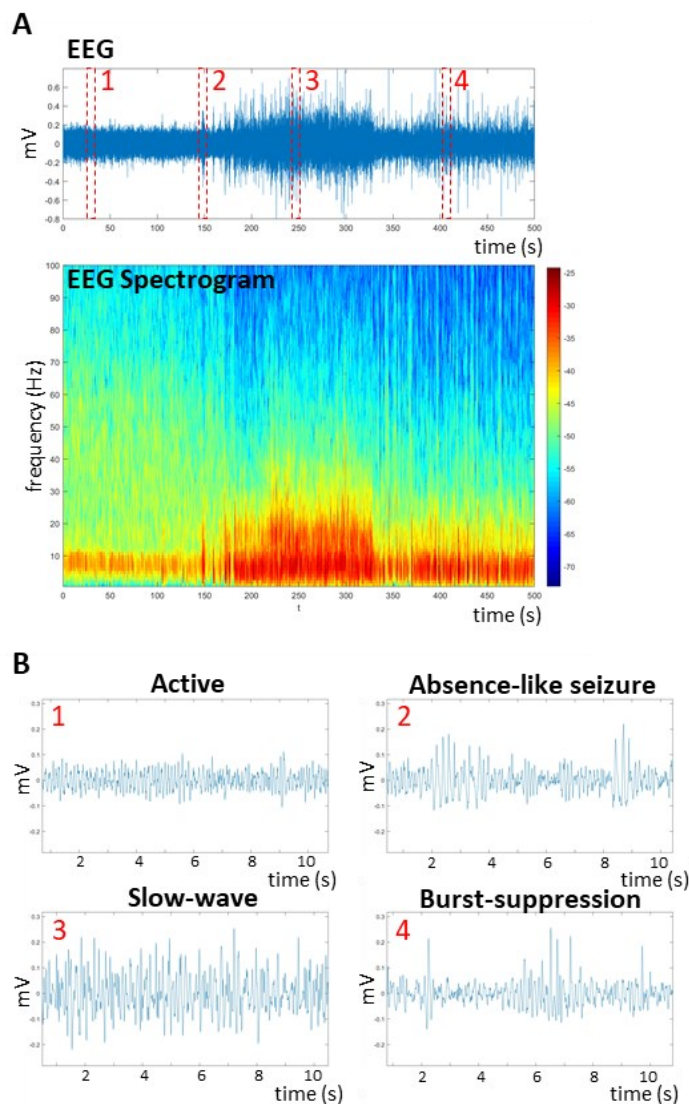


Figure 4-6: GBL-induced (75 mg/kg, i.p.) ECoG changes in C57Bl6/J mice. (A) Four different ECoG states shown in the raw ECoG (top) (DC remove, time constant, 0.1s) and the corresponding ECoG multitaper spectrogram (bottom) (1 second windows spaced at 50 ms intervals). The numbered regions in the ECoG (A) are enlarged in (B) to reveal the ECoG pattern belonging to the different stages following GBL administration.

4.2.2 Calcium imaging from S1 cortical astrocytes during GHB-induced absence-like seizures

Following these observations in freely moving animals, 2P calcium imaging experiments were carried out in head-restrained animals, to complement the Stargazer imaging experiments. C57Bl6/J mice expressing GCaMP6f in layer 2/3 S1BF astrocytes were imaged during the period of constant absence seizure-like activity that was accompanied by behavioural arrest. The mice were injected with 75 mg/kg GBL (i.p.) and recorded within 5-30 minutes of drug administration, only during periods of constant slow wave activity (Figure 4-7). Due to practical limitations and to minimise distress to the mouse, the mouse was detached from the setup during injection. It is important to note that experiments were performed on only 2 animals, which must be considered during the interpretation of the data.

Similarly to the analysis performed with Stargazer mice, ictal states were defined for GHB-induced seizures, and consisted of periods of uninterrupted slow-wave, absence-like activity in the ECoG, accompanied by behavioural arrest. No correlation was obtained between 4-12 Hz ECoG power fluctuations and calcium traces from the different sub-compartments (data not shown). Calcium oscillations were still evident during periods of movement, reinforcing the widespread belief that locomotion and global neurotransmitter release was the major driving force behind global astrocyte activation.

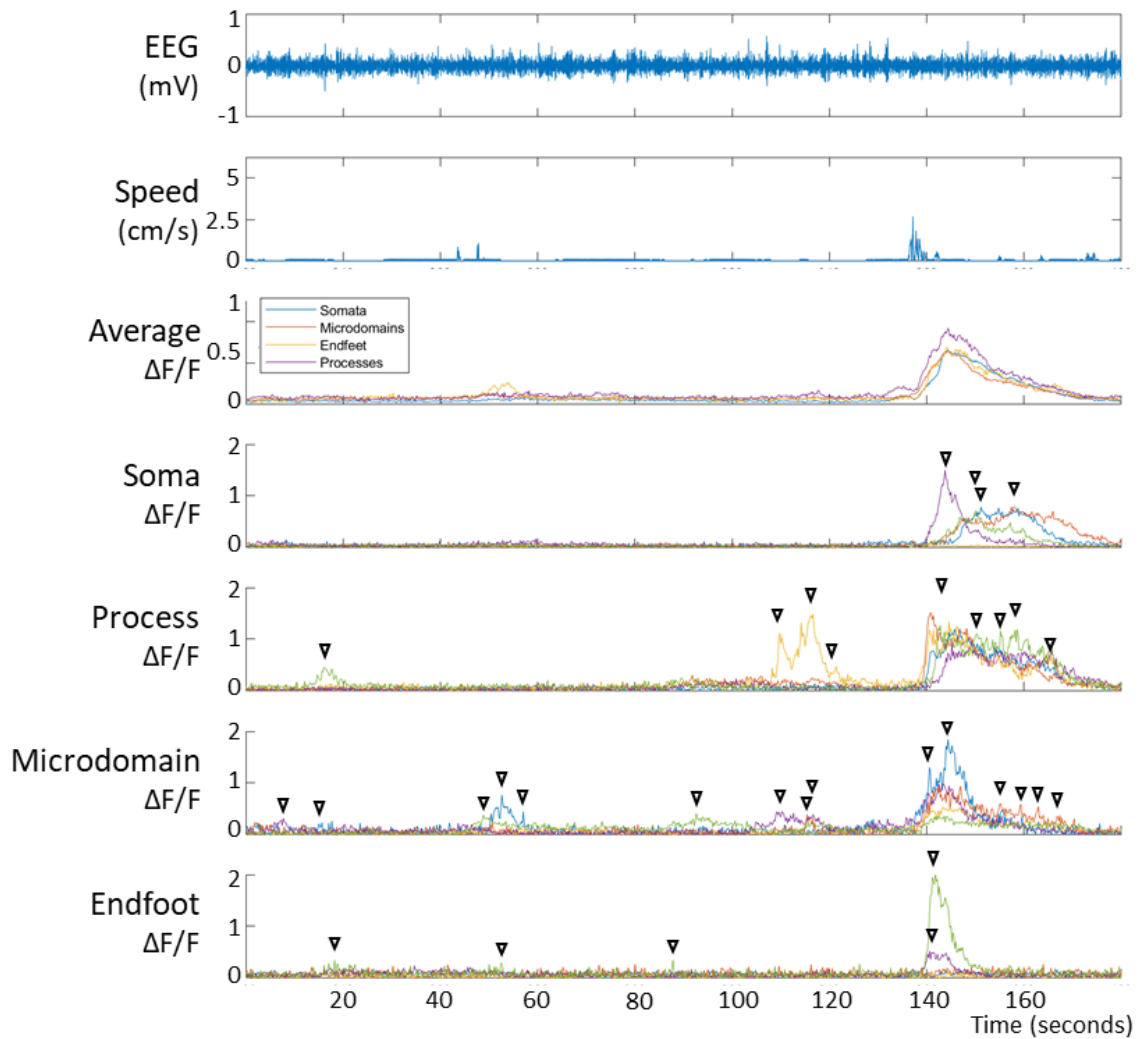


Figure 4-7: Cortical astrocyte calcium activity during GBL-induced ictal states. Ictal states, consisting of mostly uninterrupted periods of slow-wave, absence-like activity, were accompanied by isolated astrocyte calcium events in astrocyte sub-compartments. Synchronous events during ictal periods were never observed. At approximately 140 s, a clear break in ictal activity and a brief period of locomotion gave rise to widespread and synchronous astrocyte calcium transients in all sub-compartments.

4.3 Quantification of astrocyte calcium events during ictal periods

To determine if more subtle differences could be detected in astrocyte activity during ictal states, calcium event properties in wild-types during periods of inactivity (referred to from here on as WT Still) were compared with calcium events during ictal states in Stargazers and wild-types after GBL administration (referred to from here on as Stg Ictal and WT GHB respectively) (Figure 4-8). Periods of inactivity in the Stargazer mouse (Stg Still) were too infrequent to be included in the analysis, since the vast majority of the recordings included either ictal activity or locomotion. Subtle significant differences within the different cellular compartments were noted. Stg Ictal somata and proximal

processes showed a decreased calcium event duration (Kruskal Wallis Test: WT Still vs Stg Ictal vs WT GHB, Soma: $H(3) = 35.03$, $p < 0.0001$; Processes: $H(3) = 16.00$, $p = 0.0003$; with Dunn's post-hoc test: WT Still vs Stg, Soma: $p < 0.0001$, Processes: $p = 0.0260$). Stg Ictal microdomains showed an overall increase in calcium activity, observed by a significant increase in the AUC (Kruskal Wallis Test: WT Still vs Stg vs WT GHB, $H(3) = 25.20$, $p < 0.0001$; with Dunn's post-hoc test: WT Still vs Stg, $p = 0.0046$) and event frequency (Kruskal Wallis Test: WT Still vs Stg vs WT GHB, $H(3) = 13.67$, $p = 0.0011$; with Dunn's post-hoc test: WT Still vs Stg, $p = 0.0325$), as well as a higher amplitude, even though not significant (WT Still: $4.4 \pm 0.3 \Delta F/F$ (mean \pm SEM), max. $8.6 \Delta F/F$; Stg: $5.0 \pm 0.5 \Delta F/F$ (mean \pm SEM), max. $18.2 \Delta F/F$). It is worth noting that the duration of microdomain events dipped slightly, similar to what was observed in somata and proximal processes, but to a lesser extent (Kruskal Wallis Test: WT Still vs Stg vs WT GHB, $H(3) = 6.42$, $p = 0.0404$; with Dunn's post-hoc test: WT Still vs Stg, $p = 0.0355$). Stg Ictal endfeet followed a similar pattern to microdomains, with a significantly higher frequency of events (Kruskal Wallis Test: WT Still vs Stg vs WT GHB, $H(3) = 15.78$, $p = 0.0004$; with Dunn's post-hoc test: WT Still vs Stg, $p = 0.0007$) and amplitude (Kruskal Wallis Test: WT Still vs Stg vs WT GHB, $H(3) = 17.28$, $p = 0.0002$; with Dunn's post-hoc test: WT Still vs Stg, $p = 0.0296$), as well as a larger AUC, even though not significant (WT Still: $152.1 \pm 8.7 \Delta F/F.s/ROI/min$ (mean \pm SEM), max. $225.1 \Delta F/F.s/ROI/min$; Stg: $218.7 \pm 24.0 \Delta F/F.s/ROI/min$ (mean \pm SEM), max. $635.1 \Delta F/F.s/ROI/min$).

WT GHB also revealed subtle differences in the separate sub-compartments. No differences were observed in somata and processes compared to WTs, while in microdomains and endfeet a general tendency for lower calcium activity was observed. The AUCs (Microdomains WT Still: $114.1 \pm 5.9 \Delta F/F.s/ROI/min$ (mean \pm SEM), max. $238.0 \Delta F/F.s/ROI/min$; WT GHB: $92.8 \pm 5.0 \Delta F/F.s/ROI/min$ (mean \pm SEM), max. $140.2 \Delta F/F.s/ROI/min$; Endfeet WT Still: $152.1 \pm 8.7 \Delta F/F.s/ROI/min$ (mean \pm SEM), max. $225.1 \Delta F/F.s/ROI/min$; WT GHB: $98.7 \pm 3.5 \Delta F/F.s/ROI/min$ (mean \pm SEM), max. $169.3 \Delta F/F.s/ROI/min$), amplitudes (Microdomains WT Still: $4.4 \pm 0.3 \Delta F/F$ (mean \pm SEM), max. $8.6 \Delta F/F$; WT GHB: $2.3 \pm 0.1 \Delta F/F$ (mean \pm SEM), max. $3.7 \Delta F/F$; Endfeet WT Still: $3.4 \pm 0.3 \Delta F/F$ (mean \pm SEM), max. $5.7 \Delta F/F$; WT GHB: $2.7 \pm 0.2 \Delta F/F$ (mean \pm SEM), max. $4.0 \Delta F/F$), and frequency of events (Microdomains WT Still: 0.29 ± 0.04 events/ROI/min (mean \pm SEM), max. 0.85 events/ROI/min; WT GHB: 0.25 ± 0.03 events/ROI/min (mean \pm SEM), max. 0.71 events/ROI/min; Endfeet WT Still: 0.12 ± 0.03 events/ROI/min (mean \pm SEM), max. 0.77 events/ROI/min; WT GHB: 0.08 ± 0.01 events/ROI/min (mean \pm SEM), max. 0.20 events/ROI/min), were lower than in WTs during stillness, however did not reach statistical significance, except for the AUC in

endfeet which was significantly lower (Kruskal Wallis Test: WT Still vs Stg vs WT GHB, Soma: $H(3) = 28.69$, $p < 0.0001$; with Dunn's post-hoc test: WT Still vs WT GHB: $p = 0.0008$).

Differences were also observed between WT GHB and Stg Ictal (Figure 4-8). GHB had an opposite effect to Stg Ictal on calcium event properties, resulting in a dampening of calcium activity rather than an increase in calcium activity, as was observed in Stargazers, especially in microdomains and endfeet.

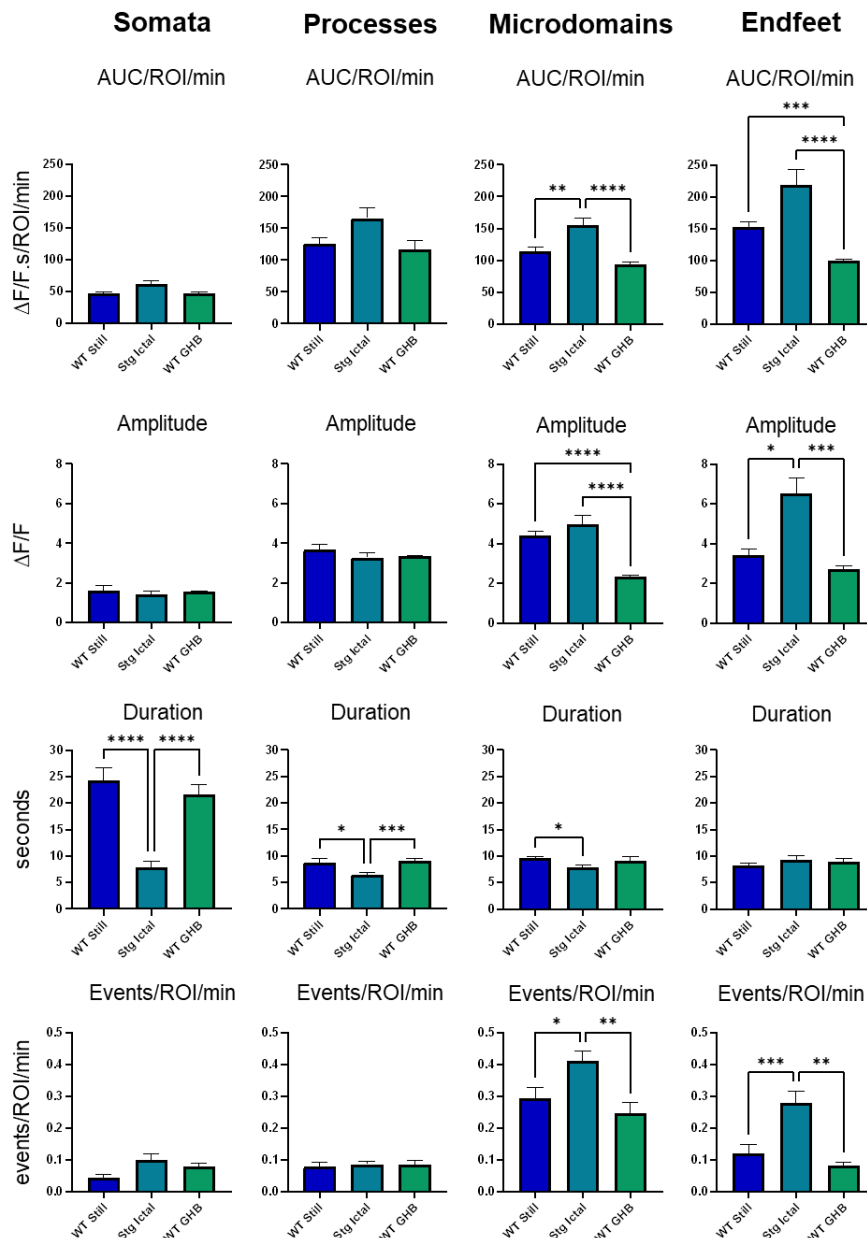


Figure 4-8: Calcium changes in astrocyte sub-compartments during spontaneous and GHB-induced absence seizures.

WT Still: wild-type animals during periods of no movement; Stg Ictal: Stargazer mice during uninterrupted periods of ictal ECoG activity; WT GHB: wild-type mice following GHB administration during periods of absence-like ECoG activity. Stargazer mice show increased microdomain and endfeet activation. GHB induces a general tendency

towards dampening of calcium activity. Kruskal Wallis Test followed by Dunn's post-hoc comparisons, * $p < 0.05$, ** $p < 0.01$, *** $p < 0.001$, **** $p < 0.0001$. WT Still N = 6 animals, 49 minutes of behavioural state data; Stg Ictal N = 5 animals, 38 minutes of behavioural state data; WT GHB N = 2 animals, 18 minutes of behavioural state data.

4.4 IP3R2 KO mice show similar susceptibility to GHB-induced absence-like seizures

To determine if astrocytes were involved in the GHB-induced effect on mice, we tested if GHB-administration had a similar effect in IP3R2 KO mice vs their WT littermates. Mice were implanted with bilateral ECoG electrodes and their ECoG was recorded while they were free to move around in a plexi-glass arena. It was determined that at 75 mg/kg (i.p.), when considering the continuous slow-wave activity phase alone, GHB had a similar impact on the ECoG of KO (N = 8, one recording per animal) and WT animals (N = 4, two recordings per animal) (**Error! Reference source not found.**). GHB significantly increased the ECoG power in the delta (WT baseline vs post-GHB: paired sample t-test, $t(10) = -18.499$, $p < 0.0001$; KO baseline vs post-GHB: paired sample t-test, $t(10) = -11.508$, $p < 0.0001$), theta (WT baseline vs post-GHB: paired sample t-test, $t(10) = -4.898$, $p = 0.0001$; KO baseline vs post-GHB: paired sample t-test, $t(10) = -5.227$, $p < 0.0001$) and gamma bands (WT baseline vs post-GHB: paired sample t-test, $t(10) = 4.159$, $p = 0.004$; KO baseline vs post-GHB: paired sample t-test, $t(10) = 5.421$, $p < 0.0001$), but had no effect on alpha and beta bands, in WTs and KOs. The ECoG power of all bands was similar in WT and KO animals following GHB administration (delta: unpaired sample t-test, $t(14) = 0.5433$, $p = 0.5955$; theta: unpaired sample t-test, $t(14) = 0.9375$, $p = 0.3644$; alpha: unpaired sample t-test, $t(14) = 1.340$, $p = 0.2015$; beta: unpaired sample t-test, $t(14) = 0.4346$, $p = 0.6705$; gamma: unpaired sample t-test, $t(14) = 0.0924$, $p = 0.9277$).

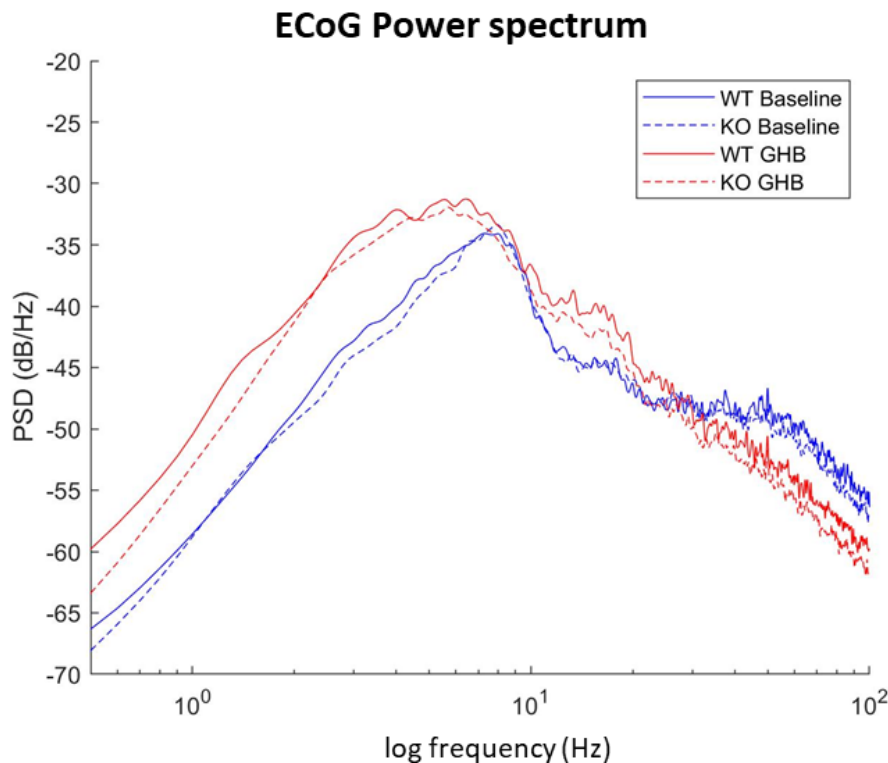


Figure 4-9: GHB-induced ECoG changes in IP3R2 knockout mice and wild-type littermates.

Power spectra (L-Chebyshev window of 4 seconds, with 50% overlap) of WT mice ($N = 4$) during baseline ECoG activity (WT Baseline) and following GHB-induced seizure-like activity (WT GHB), and of IP3R2 KO mice ($N = 8$) during baseline ECoG activity (KO Baseline) and following GHB-induced seizure-like activity (KO GHB). KO and WT mice similarly responded with a shift in ECoG power towards the lower frequency bands following GBL-administration.

4.5 Effect of Gq-DREADD cortical astrocyte activation on absence seizure properties

4.5.1 Gq-DREADD activation does not alter absence seizures in Stargazer mice and GAERS rats

As a further step to investigate if modified astrocyte functioning might influence absence seizures, Stargazer mice and their WT litter mates were injected bilaterally with a Gq-DREADD (AAV5 GFAP-HA-hM3D(Gq)-IRES-mCitrine) in the S1BF that specifically targeted astrocytes. Mice were implanted with bilateral front-parietal ECoG electrodes to monitor ongoing cortical activity and seizure events. DREADDs were selectively activated with DREADD agonists, which bind the Gq-coupled receptor that has been newly expressed on the plasma membrane of astrocytes, inducing IP3-mediated intracellular calcium release. The ECoG of freely moving Stargazers was recorded for a 1-hour baseline period and 3 hours post-DREADD activation. Each mouse was given either saline, clozapine N-oxide (CNO) DREADD agonist or Agonist 21 DREADD agonist (Ag 21) in a randomised incomplete crossover design, with at least 3 days

between recording sessions (N = 4 animals, n = 3 recordings per mouse – saline, CNO and Ag 21). Gq-DREADD activation with CNO or Agonist 21 did not alter the number or duration of SWDs or total time spent in seizure in Stargazer mice, which implied that reduced astrocyte activity in the S1BF did not influence absence seizures in a significant way (two-way ANOVA, effect of time-point and treatment on total time spent in seizure, $F(22, 99) = 1.287$, $p = 0.1992$, or average seizure duration, $F(22, 99) = 1.296$, $p = 0.1935$, or number of seizures, $F(22, 99) = 0.8983$, $p = 0.5970$) (Figure 4-10). This protocol was repeated in GAERS rats (N = 2 animals, n = 6 recordings per animal – two of saline, two of CNO and two of Ag 21) in which the S1BF is known to be the cortical initiation site of absence seizures and the driver of SWDs (Depaulis et al. 2016). Following Gq-DREADD activation in GAERS, there was no significant alteration in number or duration of seizures, or the total time spent in seizure (two-way ANOVA, effect of time-point and treatment on total time spent in seizure, $F(16, 72) = 1.178$, $p = 0.3064$, or average seizure duration, $F(16, 72) = 0.7795$, $p = 0.7028$, or number of seizures, $F(16, 72) = 0.6415$, $p = 0.8392$); however, the final 20 minutes showed a decrease in average seizure duration (Saline: 120.6 ± 15.0 %, mean \pm SEM vs CNO: 68.9 ± 7.4 %, mean \pm SEM vs Agonist 21: 55.5 ± 11.3 %, mean \pm SEM) and total time spent in seizure (Saline: 83.2 ± 19.3 %, mean \pm SEM vs CNO: 31.5 ± 9.0 %, mean \pm SEM vs Agonist 21: 22.6 ± 6.0 %, mean \pm SEM), which however did not reach statistical significance (Figure 4-11). Given the lack of effect observed during the first 100 minutes, further replicates and a recording protocol that accommodates longer recordings should be used to better investigate the effect of Gq-DREADD activation in GAERS S1BF. Overall, the GAERS data lacked a clear effect, and this suggested that astrocytes within the S1BF did not play an influential role in SWD initiation and spread.

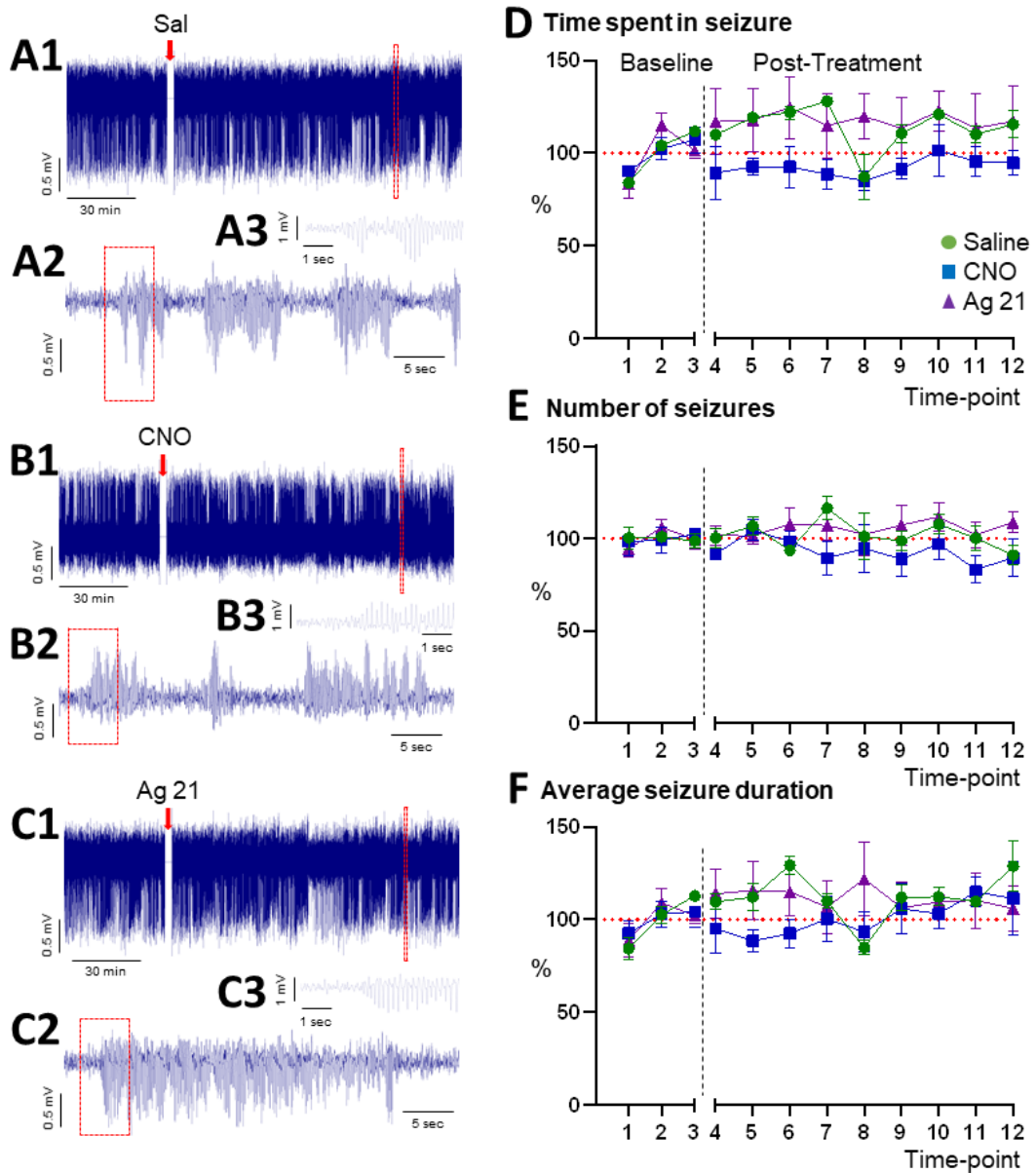


Figure 4-10: Effect of S1 cortical astrocyte DREADD activation on absence seizure properties in Stargazer mice. (A1/B1/C1) 60-minute ECoG baseline period followed by saline or CNO or Ag 21 (i.p.) injection and 180 minutes of post-injection recording. The gap in the recording is due to cable detachment to administer the intraperitoneal injection. (A2/B2/C2) Enlargement of a post-injection period, indicated in A1/B1/C1. (A3) A further enlargement of SWDs shown in A2/C2/B2. (D) The total time spent in seizure, (E) number of seizures and (F) average seizure duration, calculated in 20-minute periods and normalised to the average of the baseline period, taken as 100% and indicated by the dotted red line. N = 4 mice; Saline group n = 4 recordings, CNO group n = 4 recordings, Ag 21 group n = 4 recordings. Sal, saline; CNO, clozapine N-oxide DREADD agonist; Ag 21, Agonist 21 DREADD agonist.

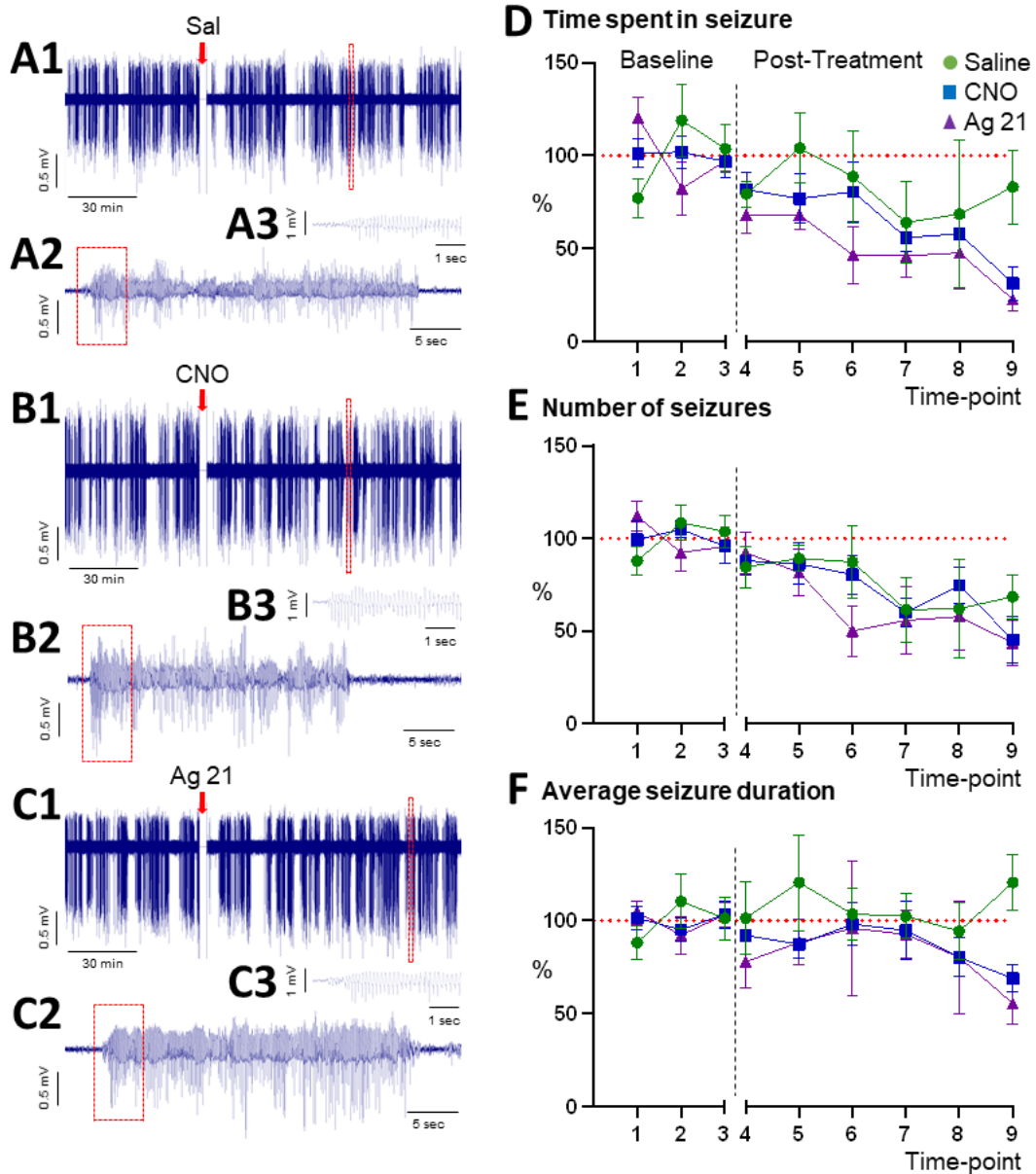


Figure 4-11: Effect of S1 cortical astrocyte DREADD activation on absence seizure properties in GAERS.

(A1/B1/C1) 60-minute ECoG baseline period followed by saline or CNO or Ag 21 (i.p.) injection and 180 minutes of post-injection recording. The gap in the recording is due to cable detachment to administer the intraperitoneal injection. (A2/B2/C2) Enlargement of a post-injection period, indicated in A1/B1/C1. (A3) A further enlargement of SWDs shown in A2/C2/B2. (D) The total time spent in seizure, (E) number of seizures and (F) average seizure duration, calculated in 20-minute periods and normalised to the average of the baseline period, taken as 100% and indicated by the dotted red line. N = 2 rats; Saline group n = 4 recordings, CNO group n = 4 recordings, Ag 21 group n = 4 recordings. Sal, saline; CNO, clozapine N-oxide DREADD agonist; Ag 21, Agonist 21 DREADD agonist.

4.5.2 Immunohistochemical confirmation of DREADD expression in cortical astrocytes

Immunohistochemical analysis was performed 6 weeks after AAV-injection to confirm that the DREADD was efficiently expressed in astrocytes and was absent from neurons. Mouse intra-cortical injection of AAV5 GFAP-HA-hM3D(Gq)-IRES-mCitrine specifically expressed the DREADD in astrocytes, as was confirmed by the co-localization of GFP and GFAP labelling (N = 3 animals, n = 5 slices per animal, 200 μm x 200 μm ROI per slice, 94% colocalization of GFP and GFAP from 98 GFAP-positive cells) and the absence of GFP and NeuN co-localization (N = 3 animals, n = 5 slices per animal, 100 μm x 100 μm ROI per slice, 0% colocalization of GFP and NeuN from 266 NeuN-positive cells) (Figure 4-12 and Figure 4-13). Controls confirmed that DREADD was only detected at the site of injection. Through visual inspection of consecutive slices labelled with GFP-antibody, it was determined that the DREADD was successfully targeted inside S1BF.

Immunohistochemical analysis of DREADD injections in GAERS were inconclusive. Under a widefield light microscope, DREADD fluorescence was weak and sparse. GFP labelling targeting the DREADD, revealed areas of fluorescence resembling what appeared to be astrocyte territories, which occasionally overlapped with GFAP labelling. However, it was clear that non-astrocyte cells were also labelled, which appeared to be neuronal cells (Figure 4-14). Unfortunately, further investigation with a confocal microscope and NeuN labelling (as was done with the Stargazer mice) was not possible due to the COVID-19 pandemic and subsequent lab-closures (the brain slices prepared for confocal imaging were lost). Consequently, further experiments to determine if astrocyte-specific labelling with DREADD was successful in GAERS were not followed through. Given the poor preliminary results obtained with the immunohistochemistry and ECoG recordings, and the time-constraints imposed by pandemic, the DREADD experiments with GAERS were discontinued.

Considering the latter, our data in Stargazers strongly indicated that Gq-DREADD astrocyte activation within S1, a vital part of the network involved in absence seizures, was not enough to alter absence seizure properties; while our preliminary data in GAERS, which is missing crucial immunohistochemical confirmation of DREADD expression, suggested that activating Gq-DREADD in the cortical initiation site of SWD had a similarly lack of effect on seizure properties. Further investigation would be required to confirm these observations, including the direct effect of Gq-DREADD activation on astrocyte calcium activity in the S1BF, as well as our missing immunohistochemical analysis of DREADD expression in rats.

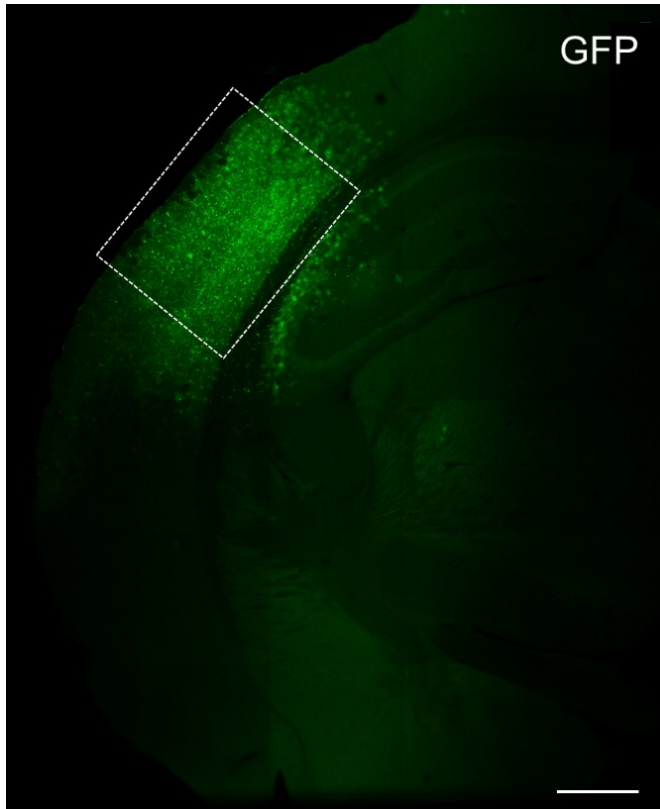


Figure 4-12: DREADD expression in Stargazer S1 astrocytes. Immunohistochemical analysis using anti-GFP antibodies was used to reveal the spread of DREADD expression in astrocytes. The DREADD spread across all the cortical layers and more than 1 μm laterally. Scale bar: 500 μm : dashed box indicates the approximate location of S1BF.

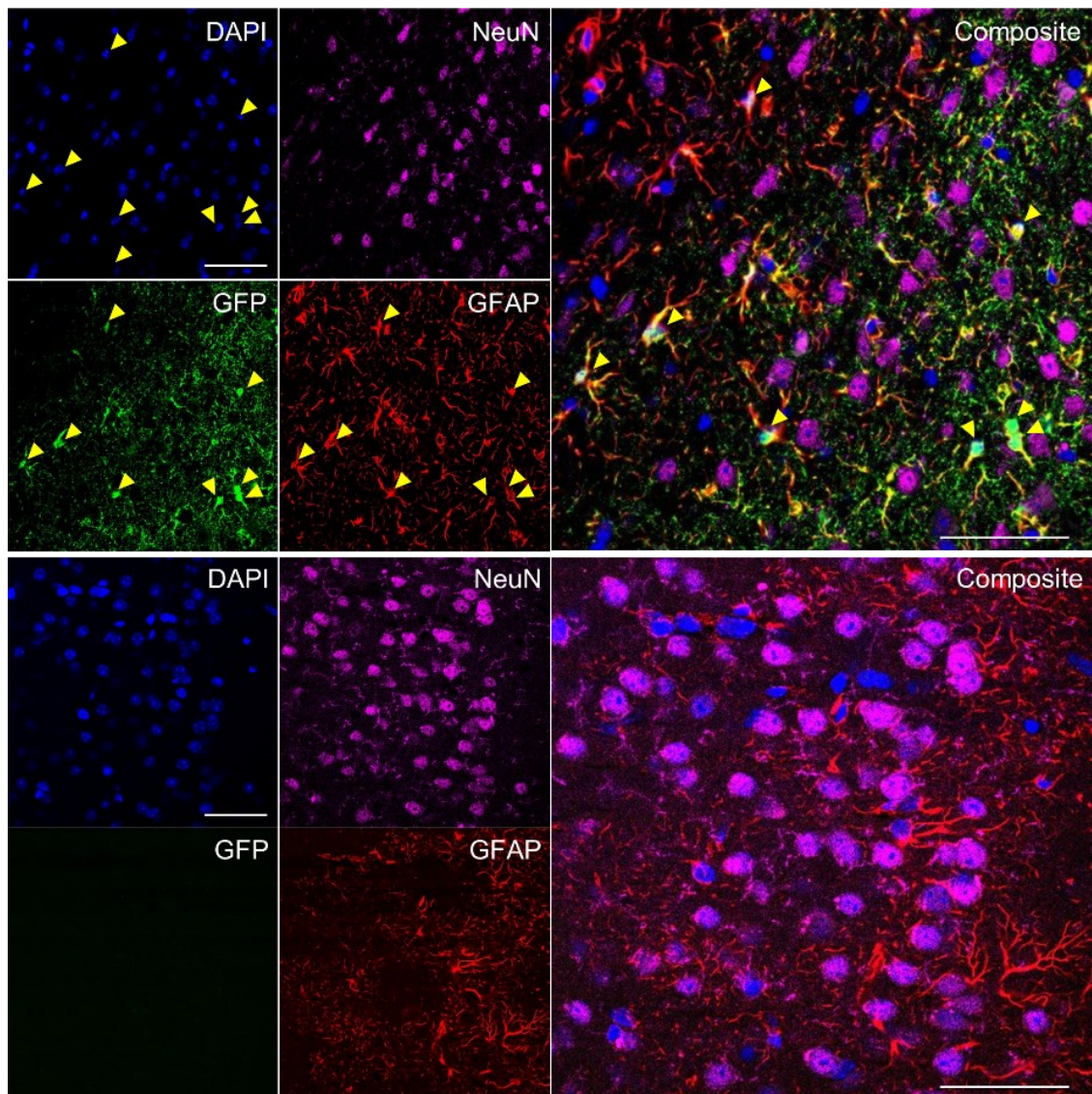


Figure 4-13: Astrocyte-specific DREADD expression in S1BF of Stargazer mice. Top: AAV-injected area. Immunohistochemistry analysis using DAPI, anti-NeuN, anti-GFP and anti-GFAP. DREADD expression was astrocyte-specific due to co-labelling of GFAP and GFP, while no co-expression of NeuN and GFP was observed. Arrows highlight regions of overlap of DAPI, GFP and GFAP, indicating DREADD expression in astrocytes. Scale bars: 50 μ m. Bottom: contralateral controls showed no GFP fluorescence. Scale bars: 50 μ m.

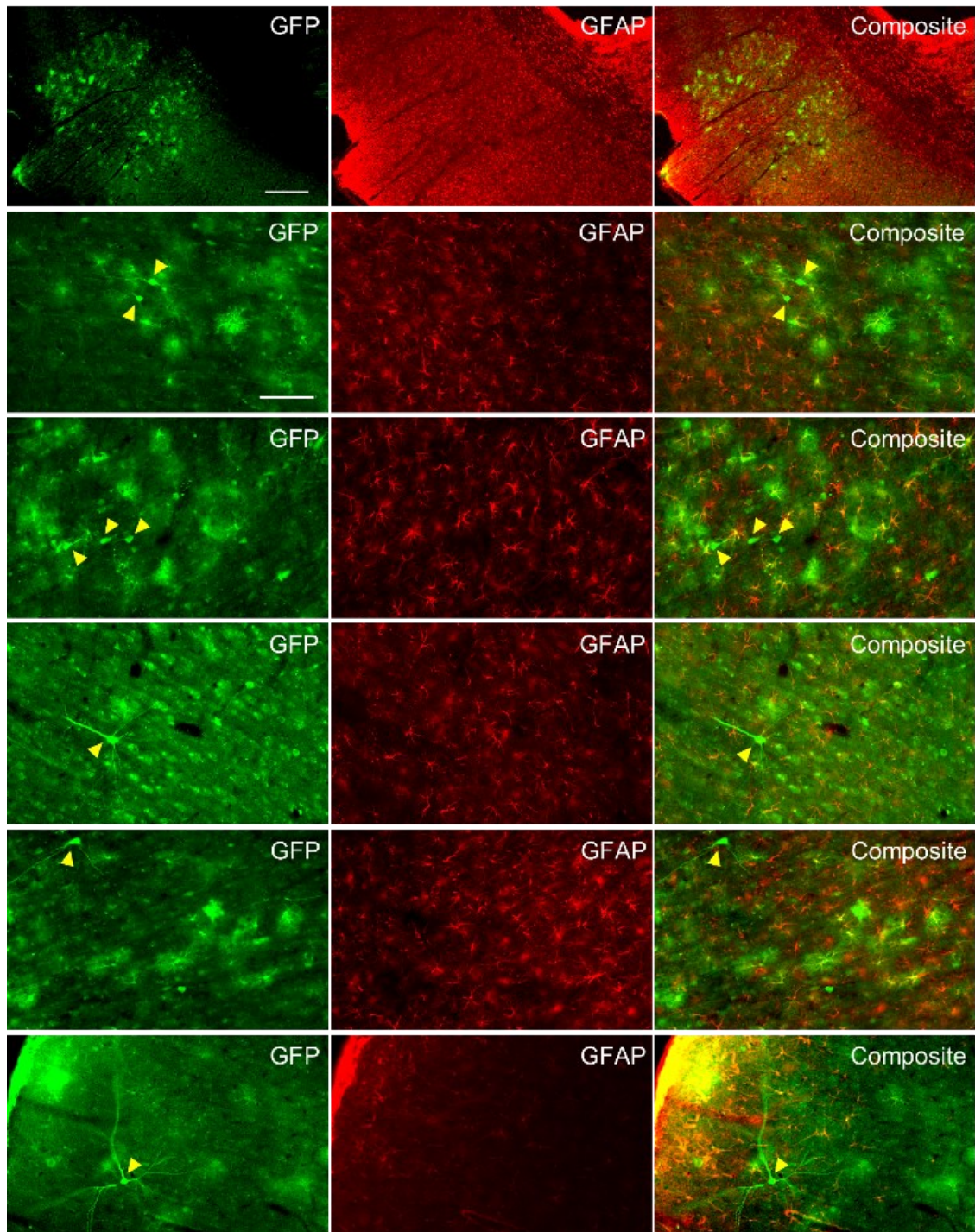


Figure 4-14. DREADD expression in S1BF of GAERS.

Top row: Immunohistochemistry with anti-GFP and anti-GFAP showing the spread of DREADD in S1BF of GAERS. The composite image clearly shows that DREADD expression was weak and sparse. Scale bar: 100 μ m. Rows 2 till 6: GFP labelling revealed DREADD expression in cells other than astrocytes. While astrocyte territories seem to have been labelled, astrocyte morphology was not clear, especially when overlaid with GFAP labelling. Yellow arrows indicate non-GFAP positive cells, that resemble neurons. Scale bar: 25 μ m.

4.6 Discussion and further work

4.6.1 Astrocytes are moderately active during periods of ictal activity.

Astrocyte calcium activity was detected during ictal periods in Stargazer mice as well as in the GHB model, however, no synchronous, population wide activation was observed at any point during ongoing seizure activity or at seizure onset or offset. This indicates that astrocytes do not undergo major perturbations in activity during absence seizures in these two mouse models. This is to some extent expected in the Stargazer model, since SWDs are the result of a chronic change in network connectivity and not an acute event that would be more likely to elicit a strong response. In fact, previous studies investigating calcium transients in astrocytes use pharmacological agents to induce prolonged epileptiform activity that persists from minutes to tens of minutes. Studies performed on genetic models with spontaneous seizures are lacking.

Various in vitro models of epileptiform activity and paroxysmal depolarisations in brain slices have shown that epileptiform activity is accompanied by clear intracellular calcium increases in astrocytes. Calcium increases in hippocampal slices were observed with low Mg^{2+} , however only under specific conditions with 0 mM Mg^{2+} and the application of picrotoxin to block inhibitory GABAergic transmission and induce hyperexcitability (Hirase et al. 2004). Using the same model, calcium increases were observed in the entorhinal cortex occurring about 2 seconds after ictal discharge (Gómez-Gonzalo et al. 2010). Astrocyte calcium changes were also observed in other models, such as the addition of bicuculline, also a GABAergic antagonist, (Hirase et al. 2004; Gómez-Gonzalo et al. 2010) or 4-AP, a potassium channel blocker (Kang et al. 2005). Using a milder convulsant model, consisting of a lower dose of 4-AP, 0.5 mM Mg^{2+} and a single NMDA pulse, paroxysmal depolarisation shifts were elicited, however intracellular astrocyte calcium increases were only observed when an extra NMDA pulse was used (Gómez-Gonzalo et al. 2010).

Astrocyte calcium changes were further evidenced using in vivo models of epileptiform activity. Pilocarpine-induced status epilepticus (a serious medical emergency with grave consequences to neuronal health, potentially resulting in death (Cherian and Thomas 2009) increased astrocyte calcium signalling in synchronised fashion for three days before going back to baseline levels (Ding et al. 2007). The kainate model of temporal lobe epilepsy induced widespread, synchronous intracellular astrocyte calcium increases (Heuser et al. 2018). 4-AP-induced seizures in the somatosensory cortex, performed under anaesthesia, elicited a glial calcium wave 2.6 seconds after ictal onset, mediated by gap-junctions (Baird-Daniel et al. 2017).

A direct comparison between my study and the aforementioned studies is difficult to make due to major methodological differences. The models employed by these studies made use of a chemical convulsant or a crucially altered extracellular composition to induce epileptiform activity and associated widespread intracellular calcium increase in astrocytes. Moreover, the induced neuronal ictal discharge and seizure activity was intense and prolonged, lasting minutes to tens of minutes. This was a vastly different and more invasive approach to the one employed in our study since the Stargazer model suffers from spontaneous seizures due to a chronic alteration in its cortico-thalamic network, so abrupt changes in astrocytic network activity is not expected. The aforementioned studies all involve the unnatural addition of a potent chemical convulsant, which does not compare to the genetic Stargazer model characterised by non-convulsive seizures that are modulated by many factors, including the state of vigilance and sensory input (Crunelli and Leresche 2002; Grosso et al. 2005). It is also important to remember that absence seizures are not treatable with typical anticonvulsants (Kessler, Sudha Kilaru and McGinnis 2019; Bouwman et al. 2007; Manning et al. 2003; Coenen et al. 1995), so an underlying mechanism different to acute convulsive models is expected.

4.6.2 Stargazers show enhanced microdomain and endfoot activation during ictal periods

Microdomains and endfeet were more active in Stargazer mice compared to their wild-type littermates during periods of no movement. This most probably reflects an increase in metabolic demand due to ongoing network activity within the cortico-thalamic loop, increased cortical output to the thalamus and an increase in synaptic activity, which would involve increased astrocyte activation and associated calcium increases (Boison and Steinhäuser 2018; Agarwal et al. 2017; Lia et al. 2021; Straub and Nelson 2007). It has been extensively shown that astrocytes are involved in neurovascular coupling and respond to synaptic activity. Astrocyte calcium increases were observed in response to neurotransmitter release during 4-AP induced epileptiform activity (Gómez-Gonzalo et al. 2010). Moreover, elevated calcium transients were observed in endfeet associated to neurovascular coupling, following AP-induced seizures in the somatosensory cortex, which made up for increased metabolic demand from ongoing epileptic activity (Zhang et al. 2019). Also, following Kainate-injection a day earlier, all astrocyte sub-compartments respond stronger to Schaffer collateral-commissural fibre stimulation in acute hippocampal slices, especially endfeet, in which activation outlasted other astrocyte sub-compartments, indicating that endfeet were hyperexcitable in epileptic tissue (Szokol et al. 2015).

Our results thus similarly show (i) a significant increase in calcium activity in the finer processes/microdomains associated with local synaptic transmission and increased neuronal excitability, (ii) a tendency for the somata to be more active as indicated by the higher, but not significant, frequency of events, and (iii) an increase in endfoot activation possibly related to increased metabolic demand and neurovascular coupling. This subtle increase in astrocyte activity may be reinforcing ongoing epileptiform activity, possibly by gliotransmitter release, that may promote the continuation of neuronal ictal activity and reduce seizure threshold, as previously suggested in different models (Gómez-Gonzalo et al. 2010).

It would be interesting to confirm if ethosuximide, the treatment of choice for childhood absence epilepsy, is able to dampen astrocyte calcium activity in microdomains and endfeet, especially since valproate, the second treatment of choice for childhood absence epilepsy, has been shown to (i) reduce calcium activity by ~70% in neurons and astrocytes in response to 4-AP seizure induction in vivo, and (ii) similarly, reduce ATP-induced calcium activity in astrocytes by ~70% (Tian et al. 2005). However, whatever the effect, it would still leave many questions unanswered. If calcium activity is dampened, are astrocytes simply reacting to a decrease in neuronal synchrony due to SWD blockade? If calcium activity remains unaltered, are astrocytes simply not contributing to ongoing SWD activity, or would this mean that ethosuximide's effect on neurons is temporarily overcoming the negative consequences of increased astrocyte activity?

4.6.3 GHB-induced absence-like activity induces a general dampening of astrocyte calcium activity

It has recently been shown that the GHB model in mice has to be interpreted with caution since the GHB-induced sedative and hypnotic effects are likely to overwhelm any observations related with absence-like events (Venzi et al. 2015). The GHB model was however still an attractive model for this project, since GHB has been shown to act directly on putative GHB receptors on thalamic and VTA astrocytes (Gould et al. 2014) and its effect on cortical astrocytes has not been investigated.

Previous reports on mouse GHB studies obtained different ECoG signatures following GHB administration, with mixed success at replicating individual well-defined SWD events. The differences were not dose-related, but possibly strain related, some observing isolated absence seizures after the first 5-20 minutes of GBL-administration (Snead et al. 2000; Aizawa et al. 1997) while others only reporting a continuous synchronous slow oscillating state (Meerlo et al. 2004; Vienne et al. 2010). A more recent study had a degree of success by using high-density EEG arrays to detect EEG

changes from different superficial brain areas, together with local field potential electrodes that detected SWDs directly from the thalamus (Lee et al. 2019). However, the seizures detected were of very short duration (1.5 ± 0.6 s) and far too infrequent (2.5 ± 2.6 per minute), shedding doubt on the successful replication of absence seizures. This highlighted the variability in the GHB-mouse model and necessitated confirmation that we could use the model to accurately replicate absence seizures in wild type mice.

In fact, while we successfully recorded SWDs using the GHB model in Wistar rats, clear SWDs were hard to detect in wild-type mice, and any observations hereafter will be related to absence-like ECoG activity, characterised by slow-wave oscillations, with little spiking activity. Modified ECoG patterns were accompanied by a reduction in muscle tone and general inactivity, as was typical in previous work with mice (Venzi et al. 2015). Also, it was not possible to reliably determine onset and offset of seizures which is why we could not use this model to investigate changes in astrocyte calcium activity during seizure onset. The failure to induce well-defined SWDs was not dose-dependent, since alternate doses were tested (data not shown), and it was previously reported that a low dose of 50 mg/kg is not sufficient to induce SWDs, whereas a slightly higher dose of 75 mg/kg induces an EEG shift to lower frequency bands with hypersynchronous neuronal activity (Venzi et al. 2015).

A few minutes after GBL administration, during ongoing absence-like activity detected in the ECoG, astrocyte calcium was dampened when compared to pre-GBL periods of inactivity in WTs and in Stargazers during ictal periods. This indicates that the animals were in a sedated state, and since GHB induces a prolonged state of hypersynchronous ECoG, similar to anaesthetising agents, and since anaesthetic is known to reduce astrocyte calcium activity (Hirase et al. 2004), a reduction in intracellular calcium activity would be expected. This would imply that the GHB model utilised in this study does not accurately represent absence seizures. A second possibility is that GHB has a dual effect on astrocyte calcium activity *in vivo*, as observed in the 4-AP and Kainate models of epileptogenesis, which I described previously. As observed in slice experiments performed on VB and VTA astrocytes (Gould et al. 2014), hypothetically, GHB might induce an initial bout of calcium increase in S1 astrocytes (which we would have been unable to image since the mouse was detached from the setup to be injected intraperitoneally) and after prolonged activation, as observed in VTA astrocytes also in slice (Gould et al. 2014), a general reduction in astrocyte calcium activity would ensue, together with reduced glutamate release (Gould et al. 2014), a reflection of dampening of brain activity. This hypothesis requires evidence from *in vitro* experiments using S1 slices and should be repeated in *in vivo* genetic models with clear SWDs, which would

be more accurate models of absence seizures. Moreover, considering that it has recently been shown that GHB-induced seizures initiate mostly in the frontal cortex, it would be worth investigating this area, however, it is worth mentioning that the location of initiation loci were not consistent between seizures (Lee et al. 2019).

4.6.4 Concerted intracellular calcium transients do not precede or follow seizure onset in Stargazer mice

No clear increase in calcium fluorescence was observed at seizure onset, or preceding seizure onset in the Stargazer model. Given that we are recording in S1 layers 2/3, and not in the deeper cortical layers where a putative initiation site would be expected, as evidence in the GAERS and WAG/Rij rats (Depaulis et al. 2016; Sarkisova and van Luijckelaar 2011), astrocyte calcium activation would not be expected to precede seizure onset, unless it occurred much earlier and a calcium wave spreading from the deeper layers reached the superficial layers and the imaging plane. Since absence seizures occur frequently in Stargazer mice (> 100 seizures per hour while awake (Noebels et al. 1990)), preceding ictal onset with each train of SWDs would be highly unlikely. An initial bout of calcium increase preceding an absence seizure after a prolonged interictal period, would be feasible, but was not observable in our data. To some extent, the lack of widespread calcium increase in S1 is corroborated by previous studies' failure to localise an initiation site in the Stargazer model. This thus fits well with our findings that no major calcium activity was observed in anticipation to seizure onset in the Stargazer S1, since we are likely not recording within close proximity to the cortical initiation site.

In contrast to our findings, previous studies describe astrocyte calcium changes that precede ictal onset. Astrocyte calcium signalling alone was sufficient to induce paroxysmal depolarising shifts in hippocampal slices, which were TTX-insensitive (Tian et al. 2005). 4-AP injection in the somatosensory cortex in awake animals induced propagating glial waves which commonly preceded epileptic neuronal discharge. However, in the initial bout of epileptiform activity, calcium changes occurred together with epileptiform activity and did not precede it (Tian et al. 2005). Intra-cranial administration in awake animals of the convulsant agent kainate, induced strong astrocyte IP3R2-mediated calcium activation that preceded the initial bout of kainate-induced seizures in the CA1 by 8 seconds, and astrocytes and neurons were synchronously active in subsequent bouts of ictal activity, this time only partially mediated by IP3R2 (Heuser et al. 2018).

The evidence discussed so far strongly suggests that astrocyte calcium activity occurs as a consequence of ictal discharge, despite its potential to induce paroxysmal depolarising shifts. The studies showing that astrocyte calcium precedes ictal discharge,

are in some way contradictory, however one must take into account the different brain regions and chemical convulsant used: (i) the kainate-model induces an initial bout of astrocyte calcium increase that precedes ictal discharge, while calcium increases occur in synchrony with ictal periods thereafter; (ii) 4-AP induced seizures elicit an initial calcium wave that occurs after ictal onset, however subsequent calcium waves generally preceded ictal discharge. All-in-all, we are faced with a complex picture of the temporal timing of astrocyte calcium activity with respect to epileptiform activity, however it is clear that astrocytes do respond with widespread intracellular calcium changes to strong convulsive agents. Direct comparison with our models would not be entirely appropriate, since the direct application of a chemical agent into the brain or in slices, is vastly different from our approach.

4.6.5 Manipulating astrocyte calcium activity does not alter seizure occurrence

Next, we tried to manipulate astrocyte calcium activity to determine if this would ameliorate or worsen absence seizures. The IP3R2 KO mouse, a mouse model with attenuated intracellular calcium release but with healthy neuronal function (Srinivasan et al. 2015; Petravicz et al. 2008), was administered GBL to determine its susceptibility to absence seizure. GHB-induced absence-like seizures were successfully induced in KO mice, with a similar ECoG shift to lower frequency bands as that observed in their WT littermates. This suggested that astrocyte IP3R2-receptor mediated mechanisms were not involved in GHB-induced ECoG changes. It would be worth confirming this observation using alternate models, such as the PTZ model, which would be suitable for an epileptogenesis study since the PTZ kindling model (Ugale et al. 2004; Itoh and Watanabe 2009; Zienowicz et al. 2005; Watanabe et al. 2013; Itoh et al. 2004) could be applied to investigate if the seizure threshold, using low non-convulsive doses, is altered in IP3R2 KO mice. Other means of reducing astrocyte calcium signalling would also be useful, such as expressing the hPMCA2w/b pump (to deplete calcium reserves, see section 3.4), which would also be suitable for use in Stargazers and even possibly in GAERS.

A second approach was used to increase astrocyte calcium activity, which involved the use of a Gq-DREADD that has been shown to induce IP3R-mediated calcium release in astrocytes. The human M3 muscarinic receptor DREADD (hM3D) was selectively expressed in S1BF astrocytes of Stargazer mice. Gq G-protein coupled receptors have been shown to increase calcium activity in astrocytes, mediated, at least partly, by IP3-dependent intracellular calcium release (Petravicz et al. 2008). Similarly, Gq-DREADD activation induces intracellular calcium fluxes in astrocytes, as observed in the visual cortex of sedated animals (Bonder and McCarthy 2014), in CA1 brain slices after acute

or prolonged activation (Adamsky et al. 2018; Durkee et al. 2019), and in vivo in S1 under urethane anaesthesia, whereby astrocyte calcium activity is elevated up to one hour after DREADD activation (Durkee et al. 2019). A recent study disputed this evidence and reported an initial increase in astrocyte calcium signalling in the first 10 minutes following Gq-DREADD activation, which quickly converted into a ~97% block that lasted up to 3 hours (Vaidyanathan et al. 2021).

Activation of the Gq-DREADD in Stargazer S1BF did not alter seizure duration, number of seizures or total time spent in seizure for three hours following DREADD activation. Assuming that Gq-DREADD activation induced an increase in astrocyte intracellular calcium release, we can conclude that increased astrocyte calcium activation does not influence absence seizures. There are a few potential explanations: (i) astrocyte calcium signalling does not influence ongoing SWDs, (ii) the area expressing the DREADD was not large enough to induce network-wide changes, (iii) the S1BF in Stargazers is not crucial in SWD initiation and spread, (iv) or Gq-DREADD activation was not strong enough to induce strong and widespread astrocyte intracellular calcium release. To confirm these hypothesis, further experiments are required. The successful activation of astrocytes and subsequent increase in intracellular calcium transients must be confirmed in vivo in the same area by co-injection of a calcium indicator and the Gq-DREADD, which would allow the direct measurement of calcium signalling from astrocytes before and after Gq-DREADD activation, as was previously shown (Vaidyanathan et al. 2021). Local neuronal activity must be monitored within the same area of DREADD activation, to determine if neurons can be modulated by the activation of this particular Gq-DREADD. To achieve this, local field potential recordings in vivo can be performed alongside astrocyte calcium imaging to detect changes in field potentials directly in the area of DREADD expression; or co-injecting two GECIs, one with an astrocyte promoter, as was used in our study, and a GECI with a neuronal promoter, such the jRGECO1a, a Synapsin-driven red fluorescent protein. This would allow direct measurement and correlation of astrocytic and neuronal activity after DREADD activation. These additions would confirm if DREADD activation successfully induces calcium signalling in astrocytes, and if this is sufficient to induce changes in local neuronal behaviours. Alternate approaches, such as chronic DREADD activation could also be considered.

4.6.6 Conclusions

We show for the first time, in vivo calcium imaging from S1 astrocytes in the Stargazer and GHB models of absence seizures, alongside simultaneous ECoG recording and monitoring of locomotion. SWDs generated within the cortico-thalamo-cortical network

were not accompanied by widespread astrocyte synchrony at any point during ictal periods. We show that Stargazer mice have increased microdomain and endfoot activation, most likely in response to increased local neuronal activity and intra-cortical signalling and increased metabolic demand. The GHB model was not an accurate model of absence seizures and induced a dampening of calcium activity, most likely a reflection of its sedative effect. Investigating absence seizures following manipulation of astrocyte activity did not alter ictal events indicating that astrocytes within the S1 are not a major driving force behind absence seizure induction or generalisation. Further studies are however needed to confirm this. The contrasting results obtained with the two models highlights the importance of making use of multiple animal models and of using well-validated models that accurately represent the human condition, especially in the case of complex and polygenic diseases, such as childhood absence epilepsy. All-in-all, our data indicates that astrocyte calcium signalling cannot be used as a predictor nor an indicator of absence seizures.

Chapter 5: Cortical astrocyte calcium imaging in freely moving rodent models of absence seizures

Despite the novel techniques we have employed so far, we were still unable to address two basic questions: (1) Is astrocyte activity within the cortical initiation site of absence seizures different to that within other cortical areas and in control animals? (2) Does astrocyte activity within the cortical initiation site contribute to the initiation of SWDs? To tackle these questions, we developed a method that directly measured astrocyte activity within the cortical initiation site while also measuring cortical neuronal activity to detect ictal periods. The Inscopix, head-mounted, miniscope technology offered a complete set of tools that made use of an implantable lens to image from the deeper cortical layers, the location of the cortical initiation site, while the animal was able to freely move around. The system consisted of one-photon epifluorescence technology capable of exciting GCaMP6f with blue light, which fit well with our proposal of imaging astrocyte calcium activity using GCaMP6f in GAERS.

5.1 Immunohistochemical confirmation of GCaMP6f-expressing astrocytes

Immunohistochemistry was performed to determine if GCaMP6f can be expressed in rat astrocytes using readily-available AAV constructs. No published evidence of GCaMP6f in rat models is available at this time. Adult, 3 month-old GAERS, were injected with AAV5 gfaABC1D-cyto-GCaMP6f (the same one used in our mouse studies) in S1BF layers 4-6. Brains were extracted 3 to 4 weeks after injection, and immunohistochemical staining was performed to determine if GCaMP6f was selectively expressed in astrocytes. Analysis of GCaMP6f expression revealed that while GCaMP6f labelling was predominantly observed in astrocytes (N = 3 rats, Figure 5-1), a small portion of neurons also expressed GCaMP6f: 1.5% of neurons (8 out of 548 neurons, N = 3 rats, Figure 5-2). This contrasted with our results in mice, which did not show any neuronal expression. Importantly, our contralateral controls showed that GCaMP6f fluorescence was only detected at the site of injection.

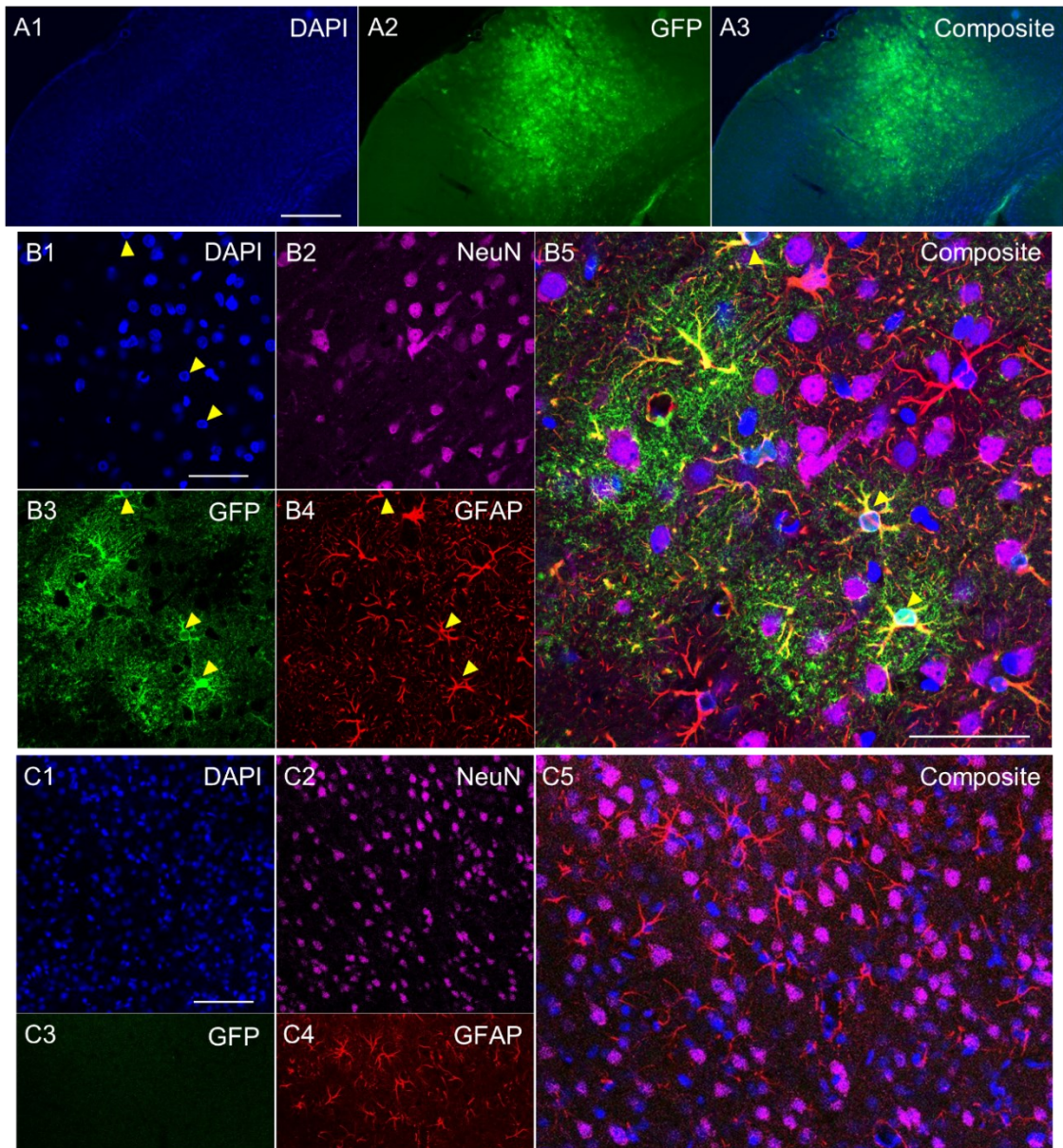


Figure 5-1: GCaMP6f expression in GAERS S1BF astrocytes.

(A) Cortical injection of AAV5 gfaABC1D-cyto-GCaMP6f in layers S1BF 5 resulted in significant spread and expression of GCaMP6f, which extended into all cortical layers. Scale bar in A1 for A1-A3: 250 μm . (B1-B4) Immunohistochemistry with DAPI, anti-NeuN, anti-GFP and anti-GFAP. Scale bar in B1 for B1-B4: 50 μm . (B5) Overlap of the four channels revealed that expression of GCaMP6f was specific to astrocytes, shown by the clear overlap of the GFP and GFAP channels, and no overlap of GFP with NeuN. Arrows indicate astrocyte somata with overlap of DAPI, GFP and GFAP. Scale bar in B5: 50 μm . (C1-C5) Contralateral control showed no GFP fluorescence. Scale bar in C1 for C1-C4: 100 μm ; scale bar in C5: 100 μm .

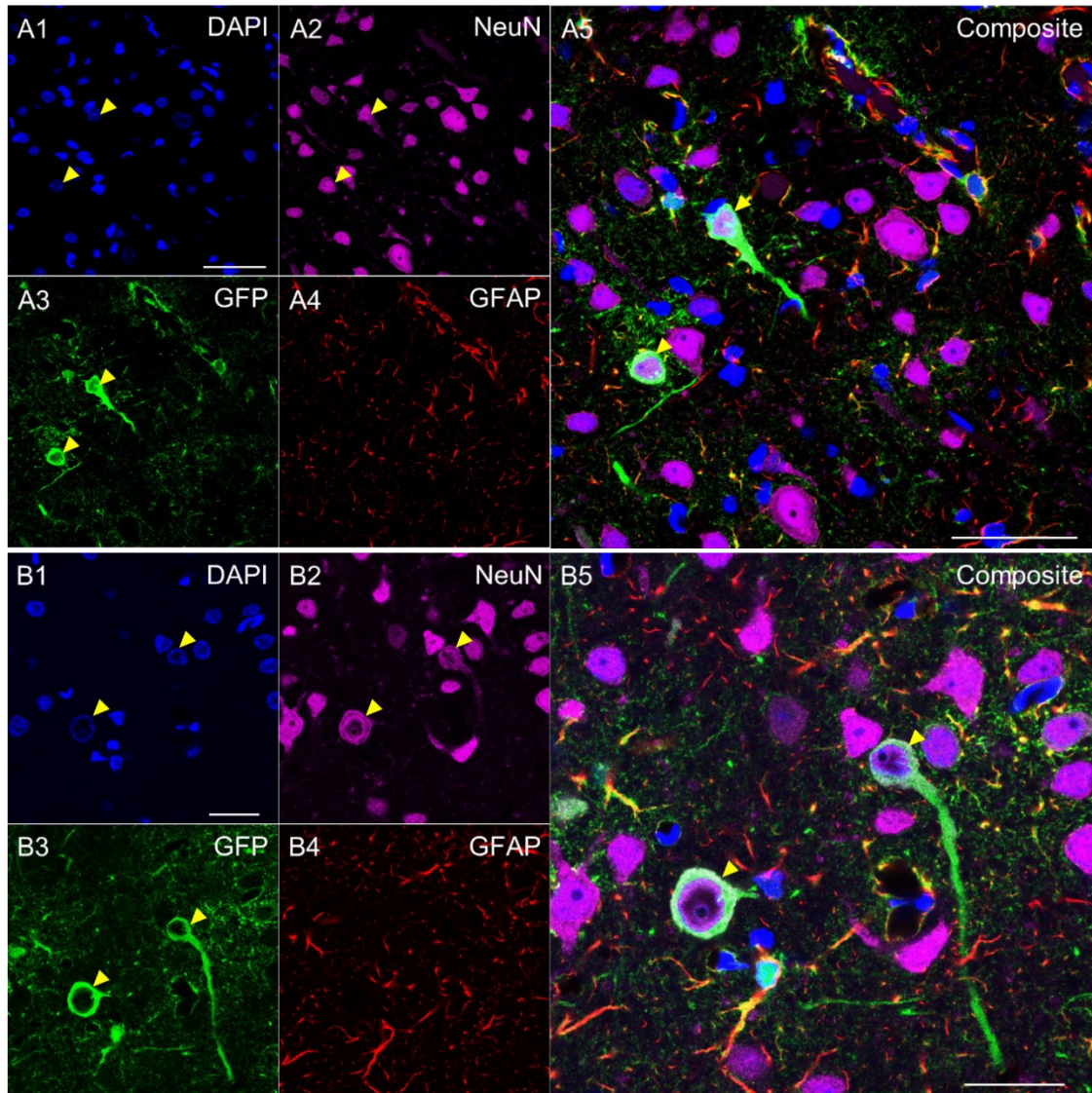


Figure 5-2: GCaMP6f expression in GAERS cortical neurons. (A1-A4 and B1-B4) Immunohistochemistry with DAPI, anti-NeuN, anti-GFP and anti-GFAP. Scale bar in A1 for A1-A4: 50 μ m; scale bar in B1 for B1-B4: 25 μ m. (A5 and B5) Overlap of the four channels revealed that expression of GCaMP6f was at times not restricted to astrocytes. This was revealed by the overlap of the GFP and NeuN channels, which indicated that GCaMP6f was also expressed in a small portion of neurons. Arrows highlight regions of overlap of DAPI, GFP and NeuN. Areas of overlap between GFAP and GFP are also evident. Scale bar in A5: 50 μ m; scale bar in B5: 25 μ m.

5.2 Pilot lens implantations in GAERS

Due to the novelty of astrocyte calcium imaging in rats with the Inscopix system, a pilot study was first carried out on three GEARS to determine the feasibility of the experiments and the imaging quality. As outlined in 2.7 above, the animals were injected with AAV5 gfaABC1D-cyto-GCaMP6f and after three weeks, they were implanted either with a cylindrical lens just above S1BF layer 5 (N = 1 animal) or with a prism lens cutting through S1BF layers 4-6 (N = 2 animals), together with ECoG electrodes. Six weeks after lens implantation, which was ample time for any tissue to have healed and bleeding cleared, and for adequate habituation to the recording cage and a dummy miniscope, the rats were imaged for the first time. All three GAERS had a clear window, and a stable FOV, a good indication that the surgery was successful and that the tissue healed well. However, calcium changes were not immediately clear, even though faint changes were observed, especially following sudden movements from the rat. Imaging was repeated a few times over the following weeks with similar disappointing results using a range of acquisition rates (from 6 Hz to 20 Hz). Faint, global network calcium transients were detectable and quantifiable using a simple manual ROI approach using the Inscopix Data Processing Suite, with no image processing since this concealed the calcium oscillations (Figure 5-3); however, cellular resolution was poor, and single astrocyte territories were not discernible. The study was halted, the rats were perfused and their brains extracted to determine whether the poor resolution was due to lack of GCaMP6f expression around the imaging site.

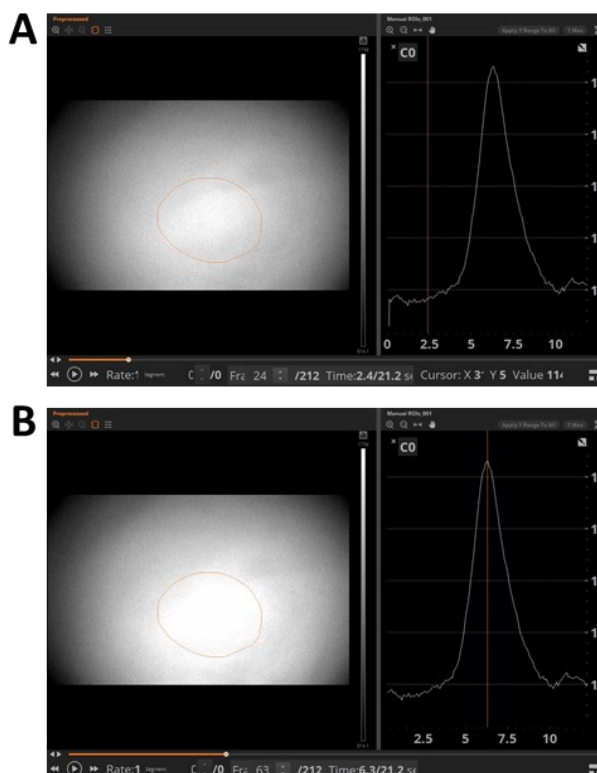


Figure 5-3: Detecting calcium fluorescence with the Inscopix Data Processing Suite.

(A) A typical 1x1 mm FOV of a prism lens during baseline activity (on the left) with the corresponding fluorescence intensity plot (on the right). A manual ROI was selected towards the centre of the FOV, and the processing suite was used to extract changes in pixel intensity using arbitrary, non-standardised, units. The time-point indicated by the vertical line in the plotted graph corresponds to the image shown on the left. (B) The image shows a global calcium event, and corresponds to the peak of the calcium transient indicated on the plotted graph. (x-axis: time in seconds, y-axis: calcium fluorescence in arbitrary units).

The GAERS animal implanted with a conventional cylindrical grin lens, showed clear GCaMP6f expression beneath the area of lens placement, displaced laterally to the lens, but nonetheless covered most of the imaging plane (Figure 5-4 A, image taken through the microscope eyepiece with a phone camera). From visual inspection of the area directly beneath the lens, astrocytes expressed GCaMP6f well within the working range of the lens. Similarly, the two GAERS animals, implanted with prism lenses, showed GCaMP6f expression adjacent to the vertical face of the prism lens, also well within the working range of the lens (Figure 5-4 B,C). In all three cases, the lenses were not implanted at the correct depth, and fell short of the desired S1BF layer 5.

It has to be noted that, as expected, lens implantation caused significant loss of cortical tissue immediately above (in case of the cylindrical lens), or adjacent to (in case of the prism lens), the imaging site (Figure 5-1).

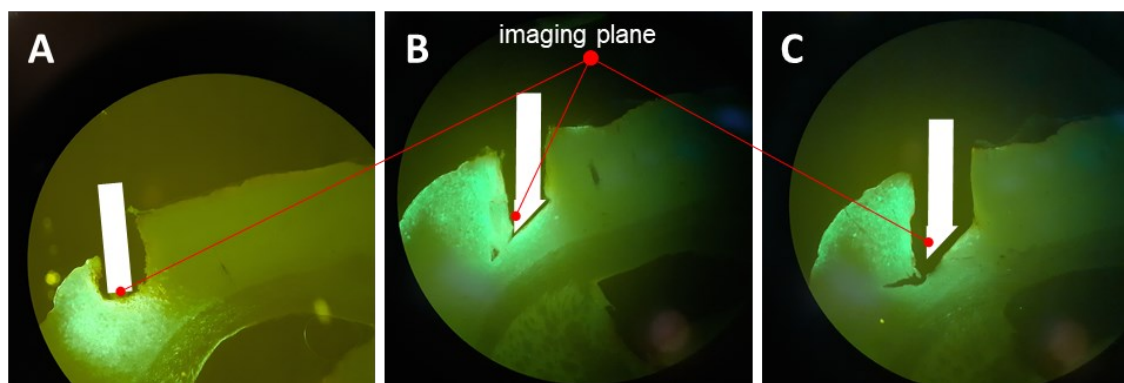


Figure 5-4: Cylindrical and prism lens placement with respect to AAV spread in S1. (A1) A 0.5 mm diameter cylindrical lens implanted in GAERS S1. The missing portion of cortical tissue represents the position of the lens, before it was detached from the rat's skull for immunohistochemical analysis. The green fluorescent region immediately beneath the lens is GCaMP6f expression. The lens is positioned too dorsal, but the expressing cells cover most of the imaging face directly beneath the lens surface. (A2,A3) A 1 mm diameter prism lens implanted in GAERS S1. In both cases, the lens was not implanted deep enough to cover S1BF layer 5; however, GCaMP6f expressing cells did cover at least part of the imaging plane of the lens, to the left of the lens. (A1-A3) Images taken with a phone camera, while imaging with the Olympus light microscope; magnification x10.

5.3 Astrocyte calcium imaging and SWD detection in a freely moving GAERS

A further GAERS was implanted with a prism lens and fronto-parietal ECoG electrodes for simultaneous calcium imaging, ECoG recording and video monitoring. Imaging was performed using new features that came along with the Inscopix DAQ software updates, with the hope that these would improve imaging quality: (1) slower acquisition rates and greater exposure times, which should improve the signal to noise ratio of global, slow

calcium transients; (2) z-plane adjustment, which allowed the user to focus on the cortical areas where calcium transients were most clear; (3) accelerometer/rotational sensors on the miniscope, which accurately monitored the animal's movement.

The animal was habituated, as described in 2.7.4 above, and imaged for a total of approximately 12 hours over eight weeks, not exceeding twelve 10 minute recordings per session, and with at least 48 hours of rest between sessions. Similarly to the GAERS implanted in the pilot study, the imaging field of view in this animal was clear, stable during imaging and even though fluorescence changes were barely discernible by eye, calcium transients were easily detected with a custom, manual ROI based analysis using ImageJ and Matlab (see section 2.7.5).

Calcium events were extracted from whole field of view ROI and correlated with neuronal ECoG oscillations and head movements or locomotion. The lack of imaging resolution limited our options for the analysis of calcium transients. ROI selection was not possible, since astrocyte territories were not discernible. Moreover, software packages available for calcium imaging, including GECIQuant, AQUA and NETCAL, were not suitable or able to pick up calcium transients, meaning that automated or semi-automated ROI detection was not suitable. For this reason, the analysis workflow was in necessity, kept simple,

Calcium events were identified and quantified based on 9 different behaviours, stimuli or ECoG state:

- (1) SPONTANEOUS calcium events, not associated with changes in ECoG activity or detectable head movements or locomotion;
- (2) SEIZURE ONSET related calcium events that occurred immediately after the start of an ictal period (such transients were only considered if they were preceded by a period of 10 seconds that was free from seizures or movement);
- (3) events that occurred DURING SEIZURE activity, i.e. during ongoing and uninterrupted SWDs, but not within the first 5 seconds of a seizure;
- (4) events that occurred at a TRANSITION, i.e. a short gap between SWDs with an altered electrophysiological signature distinct from baseline ECoG; a transition has been defined here as the time-point between the end of the transition period and the first SWD;
- (5) events that occurred DURING SLEEP; since sleep was beyond the scope of this study, sleep was only defined as putative sleep due to the absence of EMG implants to correctly identify the different sleep stages, i.e. NREM vs REM sleep; putative sleep was

defined as an increase in slow wave activity of 0.5-4 Hz, typical of NREM sleep (Yamabe et al. 2019), using power spectra, together with evidence of immobility from the video feed and accelerometer data from the miniscope;

(6) events that occurred at the END of SLEEP; defined here as the time-point when the animal shifted to a state of wakefulness from a period of putative sleep;

(7) events that occurred at the END of REST, usually accompanied by some head movement; defined here as the time-point when the animal shifted to a state of wakefulness from a period of rest, the latter consisting of a prolonged period of time when the animal was completely still;

(8) events that occurred during periods of MOVEMENT, i.e., locomotion or behaviours involving head and/or body movement;

(9) events following a STARTLE stimulus (delivered manually as an air puff).

Ictal ECoG activity was associated with numerous calcium events. Absence seizures, especially those that lasted tens of seconds, were accompanied by calcium oscillations, with few transients occurring immediately after seizure onset (20 from 74 seizures, 27%; Figure 5-5 A). Transients that occurred at seizure onset were occasionally accompanied by some form of motor activity, such as jaw contractions or face twitches, which typically accompany absence seizures in GAERS (Marescaux et al. 1992). Given that astrocytes are activated following motor activity, the transients that coincided with motor activity at the start of a seizure, are possibly in response to motor activity rather than directly related to changes in ictal ECoG.

It was noted that long trains of SWDs were occasionally interrupted by brief gaps of less than one second. During these ECoG events, which will be referred to from here on as 'transitions', large increases in calcium fluorescence were detected. The onset of calcium was identified as occurring after the brief transition period, at the start of the successive period of SWDs. Interestingly, the calcium events occurring at seizure onset and those occurring after transitions had different properties (see Table 5-1; transition vs seizure onset: AUC*: 244.9 ± 18.5 vs 80.0 ± 11.3 $\Delta F/F.s$; maximum rise slope*: 2.3 ± 0.1 vs 1.2 ± 0.1 $\% \Delta F/F.s$; amplitude*: 4.1 ± 0.2 vs 1.6 ± 0.1 $\% \Delta F/F.s$; duration*: 12.6 ± 0.6 vs 7.2 ± 0.7 s; *Mann Whitney, unpaired test, $p < 0.05$). At seizure onset, calcium events started 2.3 ± 0.1 s ($n = 20$, average \pm SEM) after the first SWD was detected, while during a transition, calcium events initiated much sooner, only 0.4 ± 0.2 s ($n = 40$, average \pm SEM) after the first SWD was detected (Mann Whitney, unpaired test, $U = 38$, $p < 0.0001$).

Calcium events were also detected at seizure offset, however since the animal typically moved once the seizure period ended, the calcium changes were highly likely in response to locomotion (Figure 5-5 B).

Calcium oscillations were occasionally detected during putative sleep, as well as during brief interruptions of sleep and at the end of a sleep period (Figure 5-5 C,D). In some cases, calcium transients predicted the end of putative sleep, and preceded it by 4.4 ± 0.8 s ($n = 12$ from 40, average \pm SEM), compared to the calcium events that were triggered 0.8 ± 0.1 s ($n = 18$ from 40, average \pm SEM) after the switch to wakefulness (Mann Whitney, unpaired test, $U = 0$, $p < 0.0001$). The end of a putative sleep period was typically accompanied by a large calcium transient, which was exacerbated when accompanied by some head or body movement (Figure 5-5 D).

As expected, movement or locomotion was generally accompanied by large calcium transients (Figure 5-5 E). Calcium transients also appeared spontaneously in the absence of any clear motor activity or ECoG changes (Figure 5-5 E). A manually applied air puff (startle stimulus) was reliably followed by a strong calcium transient (Figure 5-5 F) that was accompanied by locomotion, or at the least a head jerk. Ethosuximide (200 mg/kg, i.p.) blocked absence seizures and also any SWD-related calcium transients; however, it had no effect on other transients, such as startle-induced calcium transients (Figure 5-5 F).

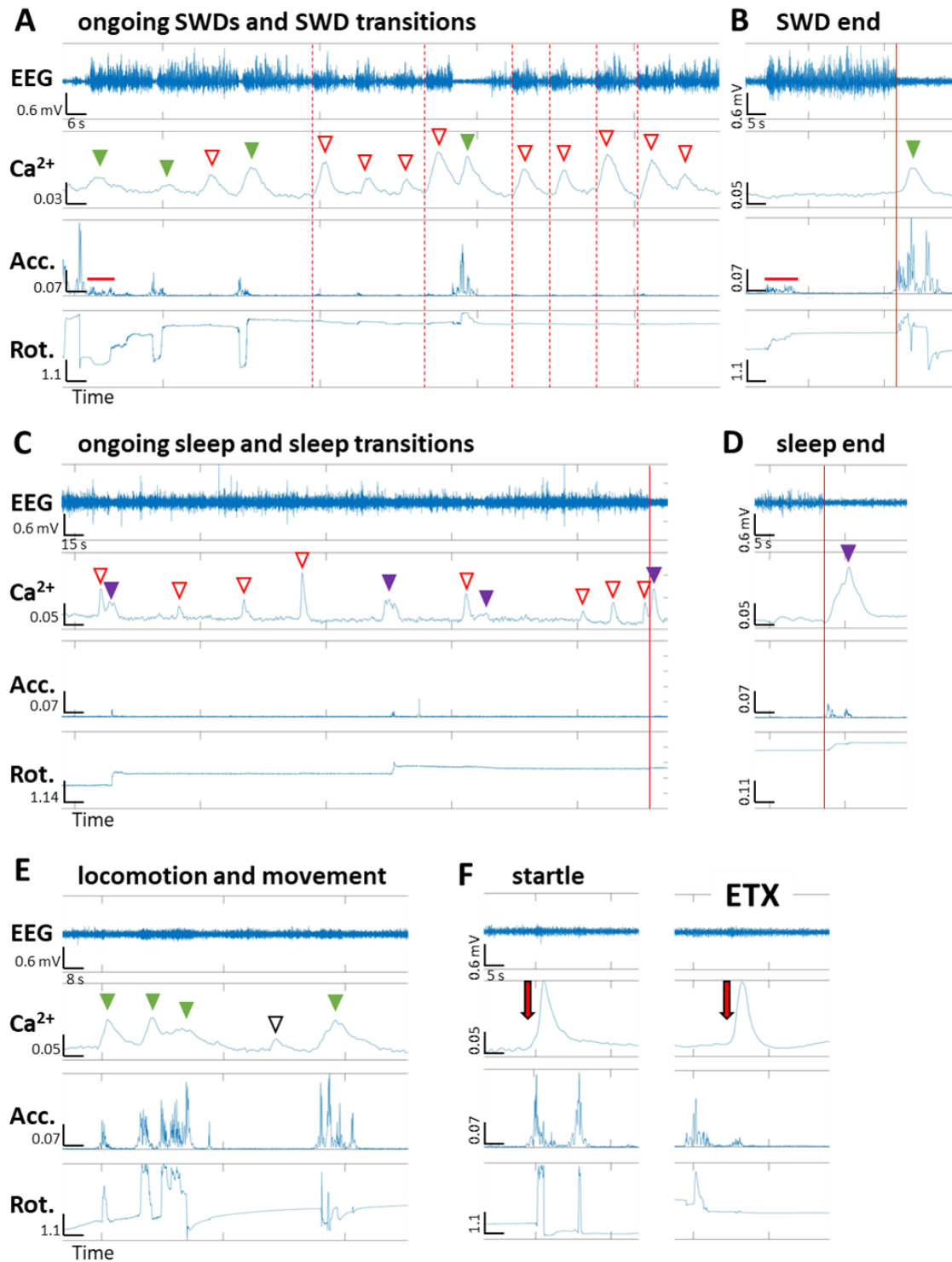


Figure 5-5. Astrocyte calcium activity in a freely moving GAERS during various behaviours. Traces in each panel, starting from top: ECoG trace (processed with DC remove, time constant 0.1 s), in mV; Calcium fluorescence, in $\Delta F/F$; Accelerometer data (x, y or z), in arbitrary unit; Rotational (yaw, roll and pitch) data, in arbitrary unit; x-axis: time, in seconds). (A) Calcium events were detected at ictal onset, during ongoing ictal periods and during switches from transition periods to SWDs. Green, solid arrows indicate calcium events during or following movement: the first three coincide with ictal onset and some movement, while the last one follows a period of locomotion. Red, hollow arrows indicate calcium events during ictal activity, at times following transition periods indicated by a red, vertical, dashed line. The red horizontal line indicated on the accelerometer trace corresponds to the onset of a seizure that was accompanied by jaw

movement, which was picked up by the miniscope motion sensors and confirmed through visual inspection of the video recording. (B) An example of an ictal period with no detected calcium changes. Note the jaw movements at seizure onset (indicated by the horizontal, red line on the accelerometer trace) but the lack of calcium response. At seizure termination (solid red, vertical line), the animal regained consciousness and this was accompanied by a period of locomotion and a calcium peak. (C) Calcium events were detected during periods of sleep (indicated by the hollow, red arrows), during brief breaks in sleep (indicated by the solid purple arrows), and during transition to wakefulness (indicated by the peaks flanking the solid vertical line). Note that an initial calcium increase is detected before the switch to wakefulness. (D) An example of a calcium event that started after the animal switched to wakefulness (solid red, vertical line). Note the large peak and the gentle movement that accompanied the change. (E) Calcium events during periods of heavy movement and locomotion. First three solid, green peaks correspond to grooming behaviour (confirmed by visual inspection of video recording) and the fourth solid, green peak corresponds to a period of locomotion. The hollow black peak, corresponds to a spontaneous event not associated with any visible or detectable movement, or any clear ECoG change. (F) A startle stimulus (time of manual stimulus roughly indicated by the red arrow) induced a strong and efficient calcium response in every case. ETX blocked SWDs and did not have an effect on a startle-induced calcium response.

Four parameters were used to describe calcium events, and a comparison was performed between those occurring during the different behaviours, stimuli or ECoG states defined above: (1) the maximum amplitude of the event peak; (2) the area under the curve; (3) the duration of the event; (4) and the maximum rise of the slope (see Table 5-1). Based on these four parameters, the startle response induced the largest calcium changes in astrocytes, which reflected the widespread recruitment of astrocyte activity (Figure 5-5, Figure 5-6). A startle response was associated with calcium events that had significantly larger amplitudes and AUC, and steeper rise slopes than calcium events occurring during the other defined behaviours or ECoG states (see Table 5-1 (one-way ANOVA for amplitudes: $F(8, 245) = 83.15, p < 0.0001$, followed by Tukey's multiple comparison test, $p < 0.0001$; one-way ANOVA for AUC: $F(8, 245) = 63.23, p < 0.0001$, followed by Tukey's multiple comparison test, $p < 0.0001$; one-way ANOVA for rise slope: $F(8, 245) = 40.87, p < 0.0001$, followed by Tukey's multiple comparison test, $p < 0.0001$). Locomotion, ECoG shifts from sleep to wakefulness, or a shift from a state of rest to wakefulness, induced large calcium events with similar durations to startle-induced calcium events (Table 5-1, Figure 5-6, one-way ANOVA for durations: $F(8, 245) = 30.16, p < 0.0001$, followed by Tukey's multiple comparison test for startle v locomotion or sleep end or rest, $p > 0.05$). Interestingly, transition events between periods of SWDs were linked with calcium events that were significantly stronger than spontaneous calcium events, events that occurred during seizures or during sleep, or calcium events that occurred at seizure onset (larger AUC, duration and amplitude; see Table 5-1 and Figure 5-6). This implied that transition events involved a unique physiological state distinct from seizure onset, ongoing seizure activity, and sensory events such as startle and locomotion.

		Area under curve ($\Delta F/F.s$)	Max slope rise ($\% \Delta F/F/s$)	Amplitude ($\% \Delta F/F$)	Duration (s)
Event Type	n	Mean \pm SEM	Mean \pm SEM	Mean \pm SEM	Mean \pm SEM
Spontaneous	30	62.0 ^d 10.0	1.2 ^e 0.1	1.6 ^d 0.1	6.1 ^b 0.4
Seizure Onset	20	80.0 ^d 11.3	1.2 ^e 0.1	1.6 ^d 0.2	7.2 ^b 0.7
During Seizure	30	102.0 ^d 12.6	1.3 ^e 0.1	1.7 ^d 0.1	6.6 ^b 0.4
Transition	40	244.9 ^c 18.5	2.3 ^e 0.1	4.1 ^c 0.2	12.6 ^a 0.6
During Sleep	30	78.3 ^d 13.2	2.0 ^e 0.3	2.3 ^d 0.4	5.5 ^b 0.3
Sleep End	40	573.2 ^b 61.5	3.4 ^d 0.3	7.0 ^b 0.6	14.2 ^a 0.8
Rest End	4	427.5 ^b 51.5	4.7 ^c 0.8	7.3 ^b 1.0	12.5 ^a 0.4
Movement	40	481.4 ^b 38.4	5.2 ^b 0.9	8.6 ^b 0.9	13.6 ^a 0.8
Startle	30	796.6 ^a 39.4	14.6 ^a 1.5	16.8 ^a 0.7	12.3 ^a 0.7

Table 5-1: Calcium event properties during different behaviours, stimuli or ECoG state. Superscripts represent significant one-way ANOVA results, in descending order of the mean, lighter shades representing larger values. Area under curve: $F(8, 245) = 63.23$, $p < 0.0001$, followed by Tukey's multiple comparison test, $a > \text{all}$; $b > c/d$ & $< a$; $c > d$ & $< a/b$; $d < a/b/c$. Maximum slope rise: $F(8, 245) = 40.87$, $p < 0.0001$, followed by Tukey's multiple comparison test, $a > \text{all}$; $b > d$ & $< a$; $c < a$; $d < a/b$. Amplitude: $F(8, 245) = 83.15$, $p < 0.0001$, followed by Tukey's multiple comparison test, $a > \text{all}$; $b > c/d$ & $< a$; $c > d$ & $< a/b$; $d < a/b/c$. Duration: $F(8, 245) = 30.16$, $p < 0.0001$, followed by Tukey's multiple comparison test, $a > b$.

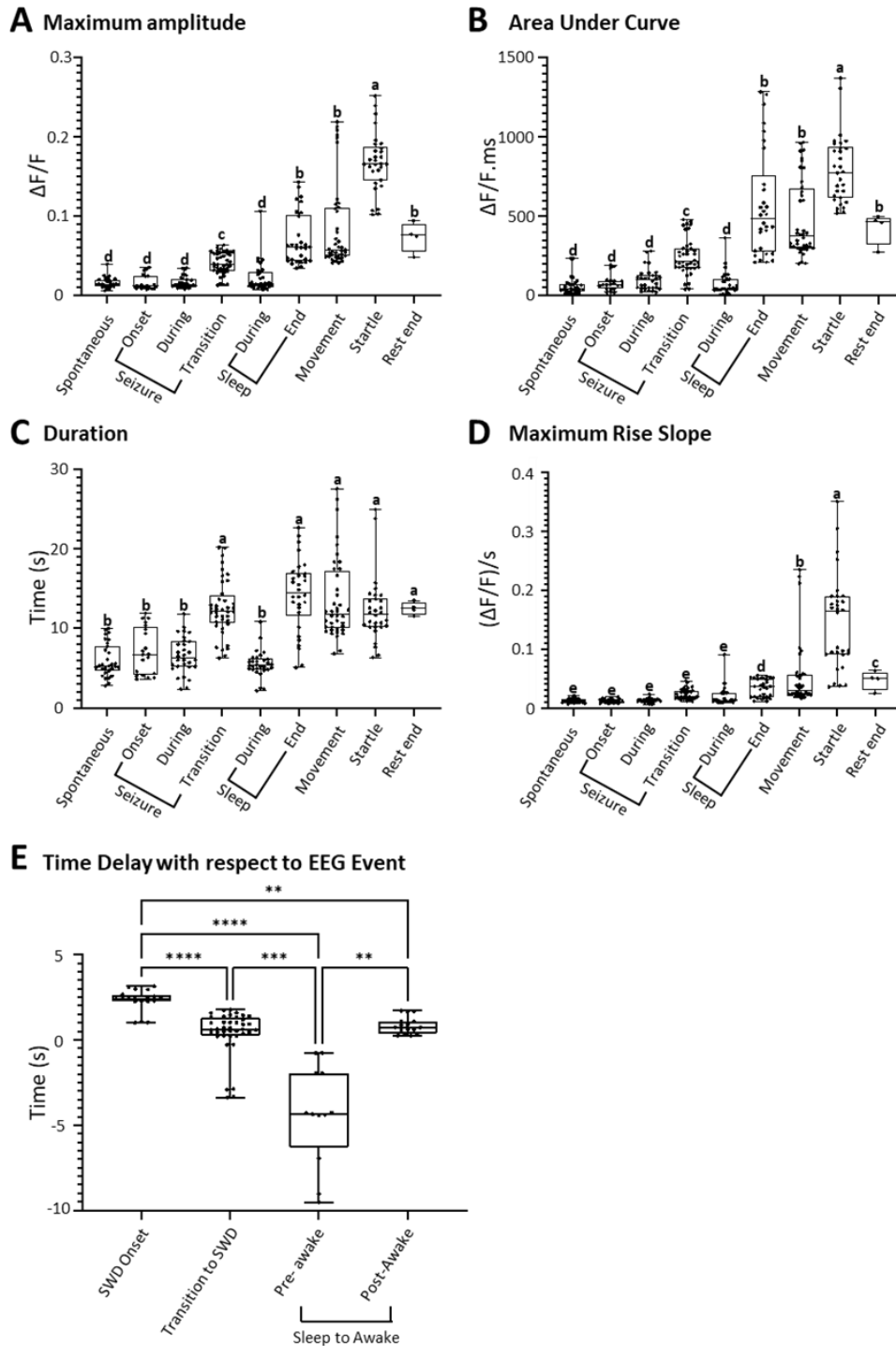


Figure 5-6: Calcium event properties associated with different behavioural events. (A-D) Differences in the maximum amplitude, area under curve, duration and maximum rise slope for the different calcium event types. See Table 5-1 for explanation of statistics. (E) The time delay from SWD onset to calcium rise, end of transition period to calcium rise, and end of sleep to calcium rise (classified as calcium events that initiate before the end of sleep, and calcium events that initiate after the end of sleep). Asterisk represent p -values for post-hoc Tukey test (**, $p < 0.01$; ***, $p < 0.001$; ****, $p < 0.0001$), after one-way ANOVA $F(3, 84) = 57.92, p < 0.0001$.

Following the observation of numerous calcium transients immediately following what was defined here as transition states between periods of SWDs, ECoG power spectra were used to confirm that transition states are different from baseline ECoG activity and from SWDs (Figure 5-7 A). These transition states (i) lacked the typical 7 Hz oscillation that define absence seizures in GAERS, (ii) showed an increase in power of lower frequency oscillations of around 5 Hz, and (iii) showed a reduction in power of higher frequencies, greater than 10 Hz (Figure 5-7 C). These calcium events were characterised by a quick calcium increase initiated only 0.4 ± 0.2 s ($n = 40$, average \pm SEM) after SWD onset (Figure 5-7 B).

ECoG changes in relation to sleep were also confirmed. Sleep activity was easily distinguishable by an increase in low frequency oscillations (0 – 10 Hz).

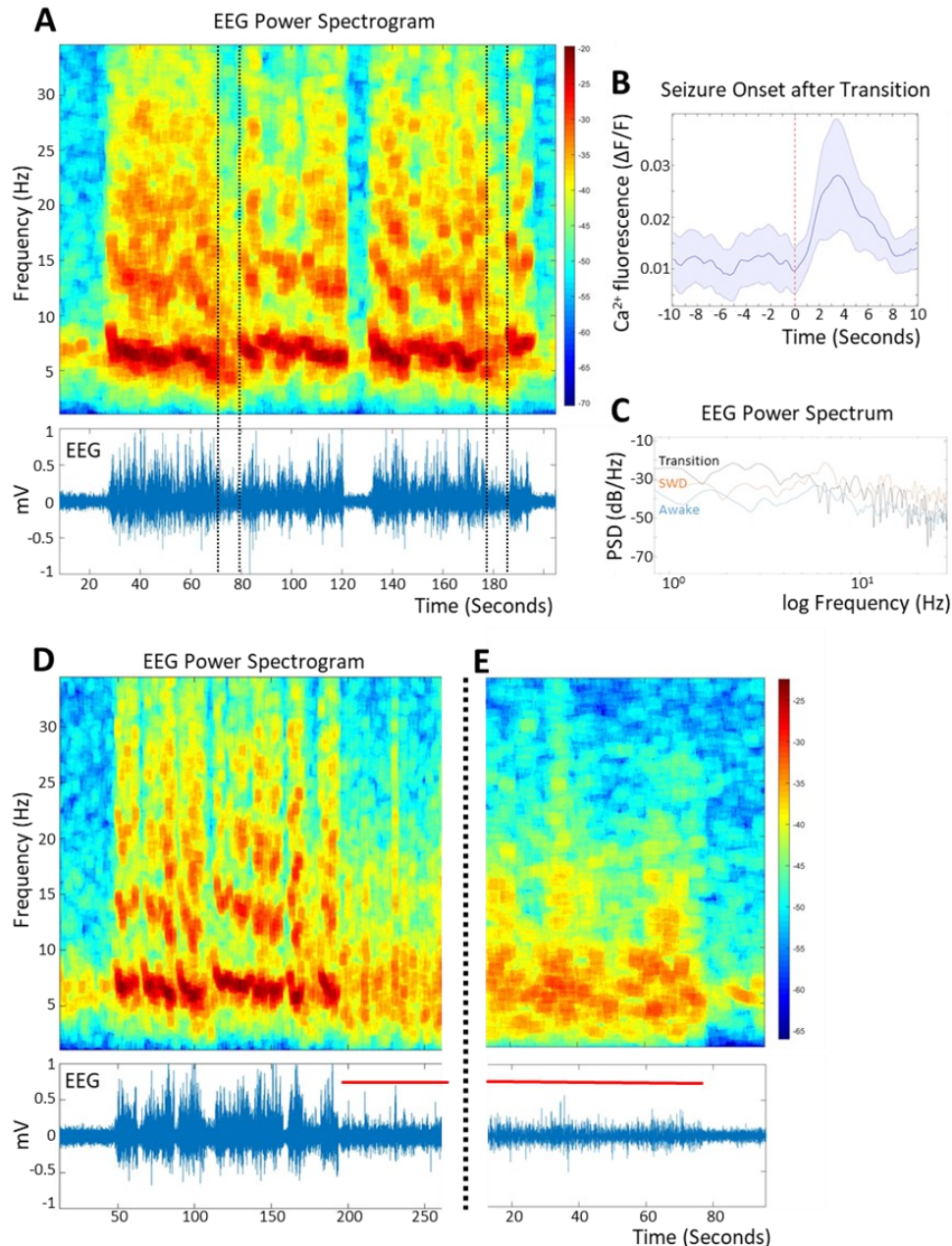


Figure 5-7: Electrophysiological confirmation of SWDs, transition states and sleep. (A) SWDs were easily identified by an increase in ECoG amplitude and the typical 7 Hz oscillations shown in the spectrogram. Transition states between periods of SWDs, were identified by the loss of the 7 Hz oscillations and an increase in 1-5 Hz oscillations. Such states were distinct from periods of SWDs and wakefulness. Top: Power spectrogram, bottom: ECoG trace (DC Remove, 0.1 s time-constant). (B) The plot shows the average calcium fluorescence during the switch from a transition state to SWDs (indicated by the vertical red line, at time = 0 s; $n = 15$ calcium events; shaded area indicates \pm SEM). (C) Power spectra showing the different ECoG signatures of SWDs, transition states, and wakefulness. Note the 7 Hz peak of the SWD trace, and the increase in power of 1 - 4 Hz of the transition trace. (D,E) Putative sleep could be distinguished from periods of wakefulness and SWDs, by the typical increase in the lower frequency bands (0 – 10 Hz). Top trace: Power spectrogram, bottom trace: ECoG trace (DC Remove, 0.1 s time-constant).

After the last recording session, the rat was perfused and its brain extracted. Immunohistochemistry confirmed GCaMP6f expression adjacent to the lens imaging plane and within S1BF layer 5 (Figure 5-8). Astrocyte expression of GCaMP6f spanned the entire vertical face of the prism lens, in terms of DV and AP, and was within the prism working distance.

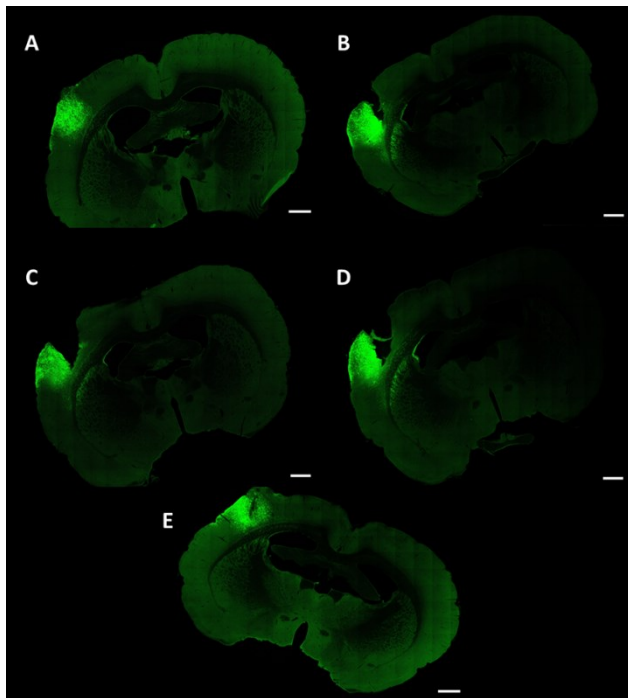


Figure 5-8: Prism lens placement with respect to AAV spread in S1BF
Prism lens placement in GAERS used for simultaneous calcium imaging and ECoG recording. (A-E) Coronal slices taken at different AP coordinates, show the spread of GCaMP6f directly in front of the lens imaging face (to the left of the prism), and visible in all AP positions, notably also anterior (A) and posterior (E) to lens placement. (A-E) Scale bars: 1000 μ m.

5.4 Astrocyte calcium imaging in a freely moving mouse

Given previous successes other labs have had with the Inscopix system when applied to neuronal calcium imaging in various mouse models, we decided to test the Inscopix system in a congenic mouse expressing GCaMP6f in astrocytes. This would determine if our inability to visualise single astrocyte territories was an issue related specifically to rats or was simply beyond the capability of the system when applied to astrocyte calcium imaging. A brief set of experiments was carried out at the Collège de France in Dr Nathalie Rouach's lab, with the help of Dr Josien Visser and Dr Jérôme Ribot. A transgenic mouse expressing GCaMP6f in astrocytes was implanted with a cylindrical 1 mm diameter grin lens, which was rested on the dura above layer 1 S1BF and cemented in place, without penetrating the brain. The animal was allowed to recover, habituated to the recording setup and imaged with the Inscopix miniscope using a 20 Hz acquisition

rate. Changes in fluorescence were immediately visible by eye, and the PCA-ICA algorithm available with the Inscopix analysis suite was able to isolate and extract calcium transients from distinct ROIs, that resembled single astrocyte territories (Figure 5-9). This was a vast improvement on the rat recordings I described above, in which local astrocyte activity was not identifiable.

Experiments were unfortunately cut short due to the COVID-19 pandemic which forced lab closures. Given that this was the first try, in only one animal, the technique showed great potential for astrocyte calcium imaging in freely moving mice, as was shown in more recent work by the Volterra lab who managed to image calcium transients and calcium wave events from dorsal CA1 astrocytes, in transgenic mice that conditionally expressed GCaMP3 (Kikuchi et al. 2020).

We thus still have unanswered questions, such as if a similar technique in rats, that avoids dura and cortical tissue penetration, would yield similarly good results. The latter would imply that tissue damage is detrimental to imaging quality from astrocytes, even though this has been successfully applied to deep brain imaging of neuronal networks (such as Hornung et al. 2020). Alternative explanations to our poor cellular resolution would be: (i) more time was required for better GCaMP6f expression prior to lens implantation and for complete tissue healing, which would have impaired imaging quality; or (ii) the miniscope was not focussed well on GCaMP6f-labelled cells. The latter explanation is plausible since we were unable to focus the lens on GCaMP-expressing astrocytes during the lens implantation. A crucial step during the Inscopix lens implantation is using real-time imaging to place the lens at the correct location in an area of GCaMP6f-expressing cells, correctly focussed on the cells of interest. We could not perform this step correctly during lens implantation since we could not identify any GCaMP6f-expressing cells, possibly due to reduced astrocyte calcium activity under anaesthesia, as previously observed (Thrane et al. 2012), or due to GCaMP6f's low baseline fluorescence (Gee et al. 2015; Ye et al. 2017). These reservations need to be addressed before any further work with the Inscopix system is performed on rats.

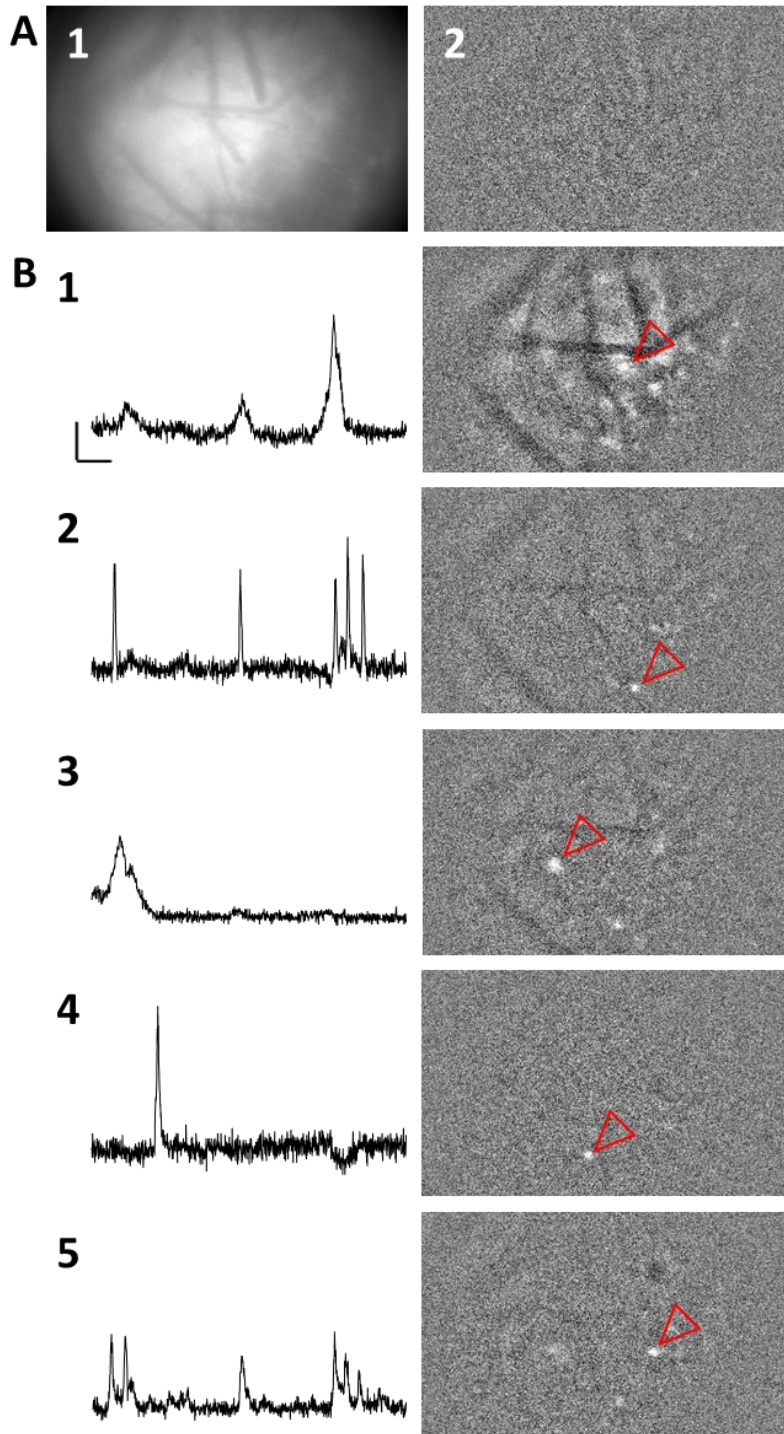


Figure 5-9: Astrocyte calcium imaging in a freely moving mouse with the Inscopix system.

(A1) A typical 1 mm diameter FOV of mouse S1 during baseline activity, and (A2) the corresponding image after PCA-ICA processing. (B1-5) Single astrocyte territories were isolated using PCA-ICA to create ROIs. Calcium transients were extracted from each ROI (calcium plots on the left correspond to the active ROI indicated in the images on the right). B1 depicts a global calcium response, typically following mouse locomotion. B2-5 highlight calcium events that are more local and may represent independent local astrocyte activity in response to sensory input from whisking or otherwise.

5.5 Discussion and further work

When we first devised these experiments, the combination of the GAERS model with the Inscopix system offered a highly attractive and an ideal approach to image astrocytes deep within the cortical initiation site. The GAERS model offered several advantages over the Stargazer model due to its well-described cortical initiation site and well-defined absence seizures (Polack et al. 2007; Studer et al. 2019; Depaulis et al. 2016), and the Inscopix system had been previously used to image deep brain tissue in freely moving animals (over 100 publications). Our proposal was however entirely novel at the time, due to the lack of studies performed in rat models or astrocytes. In fact, since then, only a handful of works have been published, which investigated rat neuronal populations (Hornung et al. 2020; Anner et al. 2020; Cameron et al. 2019; Genzel et al. 2019) or mouse astrocyte networks (Ingiosi et al. 2020), but never rat astrocytes, which further highlights the novelty and challenges of our study.

Nonetheless, we determined that GCaMP6f can be expressed in rat astrocytes using commercially available viral constructs and we successfully imaged astrocyte calcium activity from the cortical initiation site of absence seizures. This study thus provided us with promising and consistent within animal preliminary data that for the first time describes astrocyte calcium activity within critical cortico-thalamic circuitry involved in AS generation.

5.5.1 Astrocyte calcium activity patterns are modified during SWDs

The most striking and novel aspect of our study lies in our observations with respect to the timing between cortico-thalamic-generated SWDs and astrocyte calcium changes. We have shown that (1) astrocytes are active during periods of uninterrupted SWDs, (2) astrocytes are active 27% of the time at seizure onset and (3) astrocytes are especially active during periods of alternating transition states and SWDs.

Astrocytes in the cortical initiation site alter their pattern of activity during bouts of SWDs, which might be causative or simply a manifestation of the ongoing aberrant neuronal activity. It is not surprising that astrocytes change their activity pattern during these large ECoG state changes, given the evidence that astrocytes respond to shifts in EEG states (Poskanzer and Yuste 2016; Poskanzer and Yuste 2011), but it was surprising that astrocytes were not reliably responding to seizure onset.

The transition states we define here are likely what was described decades ago by the Marescaux/Pinault group who found that 5 - 9 Hz oscillations precede SWDs and are involved in the recurrence of SWDs (Pinault et al. 2001). Transition states were associated with a pattern of calcium changes distinct from calcium events that occurred

at seizure onset or during SWDs, and also different from other calcium event types unrelated to absence seizures, which we described. One interpretation would be that during transition states astrocytes are receiving subcortical ascending neuromodulator input, possibly noradrenergic, which is a major source of astrocyte calcium signalling activation and has been shown to modulate absence seizures (Sitnikova and van Luijtelaar 2005; Snead 1987). In fact, partial depletion of noradrenaline in the cortex ameliorates GBL-induced absence seizures in rat models (Snead 1987) and lesions of locus coeruleus noradrenergic axons during developmental stages of the tottering mouse, which suffers from spontaneous seizures, completely blocks the occurrence of SWDs (Noebels 1984), possibly since noradrenaline increases NRT firing that would worsen tonic inhibition of TC neurons (Hirata et al. 2006). It would be important to determine if the timing of astrocyte calcium increase in the cortical initiation site corresponds to local neuronal paroxysmal events, since astrocytes are known to exacerbate initial paroxysmal depolarisations that facilitate seizure generalisation (Gómez-Gonzalo et al. 2010), which may well be the case within the cortical initiation site of absence seizures. Alternatively, astrocytes might be unreceptive to local neuronal activity and simply respond to the altered state of the cortico-thalamic network that is actively engaged in the generalisation of SWDs.

Besides the need for more data from multiple GAERS and control animals that lack the epileptic phenotype (non-epileptic controls, NEC), it would be important to measure astrocyte activity patterns in other areas, namely S1BF layers 2-4 and the thalamic nuclei. This will determine if this behaviour is peculiar to astrocytes within the cortical initiation site or if it is common to astrocytes in the cortico-thalamic network. This would lead to the question of whether disrupting astrocyte activity in part (or all) of the network would alter absence seizure properties, or possibly block them entirely.

It has been shown that neurons in layers 5/6 of the cortical initiation site of GAERS have an elevated firing rate, ictally and inter-ictally, due to a more depolarised membrane potential when compared to the upper cortical layers (Polack et al. 2007). However, there is no knowledge of what effect this aberrant activity is having on neighbouring astrocytes. It has been shown that layer 5 astrocytes are less spontaneously active than layer 2/3 astrocytes in wild type animals (Schipke et al. 2008), but this might not be the case in GAERS due to the elevated neuronal firing rate in layer 5, which might be accompanied by similarly overactive astrocytes, for various reasons: (i) increased synaptic activity will induce increased neurotransmitter uptake and subsequent gliotransmitter release from astrocytes (Araque et al. 2014); (ii) increased neuronal discharge during seizures results in elevated K^+ levels (Wang et al. 2020) which will in

turn result in increased astrocyte K⁺ clearance (Seifert and Steinhäuser 2013); (iii) increased endocannabinoid release from pyramidal cells during seizures has been shown to induce increased CB1 receptor activation on astrocytes with subsequent intracellular calcium release and potential gliotransmitter release, which sustains neuronal epileptiform activity (Coiret et al. 2012). This hyperactive astrocyte network, might thus result in feed-forward excitation of neurons (as I mentioned previously) that will maintain the recurrence of SWDs.

It has also been shown that neuronal firing patterns in the somatosensory cortex reliably follow the spike and wave components of absence seizures (Polack et al. 2007) and so it would be interesting to apply this to astrocyte activity, and determine if astrocytes are reliably responding to local neuronal activation in S1BF, or indeed precede it. Higher resolution imaging using 2-photon laser scanning microscopy would reveal crucial ongoing activity in the cell periphery that are more likely to reflect local synaptic activity and possibly seizure initiation.

Another important observation would be to determine if subcellular astrocyte activity is in fact different in the initiation site compared to other cortical areas and the thalamus, which each have their own neuronal firing patterns and role in SWD generation. It would also be interesting to determine if astrocytes in the cortical initiation site show altered responses to sensory stimuli, since neuronal responses to whisking stimulation in GAERS are less selective and less synchronised compared to control animals (Studer et al. 2019). Given that layer 4 S1BF astrocytes respond to barrel stimulation with a contained response within individual barrels and which then spreads to layers 2/3 and 5 beyond the barrel column (Schipke et al. 2008), it would be relevant to determine if this property is maintained in the GAERS model. GAERS show a decrease in phasic GABA_A inhibition in the cortex (Crunelli et al. 2012) and blocking GABAergic inhibition has been shown to result in stronger astrocyte responses to barrel field stimulation (Schipke et al. 2008), which might be the case under normal physiological conditions in GAERS that would therefore indicate an altered response to sensory stimulation.

5.5.2 Comparison with established in vivo astrocyte calcium activity in mouse models

Apart from absence-seizure related events, we also picked up astrocyte activity that has been previously described in in vivo mouse models, including spontaneous events, locomotion-induced events, startle-induced responses and sleep-related events (Ingiosi et al. 2020; Vaidyanathan et al. 2021; Srinivasan et al. 2015; Paukert et al. 2014; Stobart et al. 2018a; Slezak et al. 2019; Nimmerjahn et al. 2009; Shigetomi et al. 2013a). Direct comparisons are hard to make, due to major differences in imaging techniques, rodent

species and viral constructs used in previous studies. Spontaneous and startle-induced calcium events were comparable to those previously reported in astrocyte somata in mouse visual cortex using the same viral construct (Srinivasan et al. 2015). The authors reported: (1) spontaneous calcium events with a half width of approximately 2.2 s, similar to our 3.4 ± 0.3 s (average \pm SEM); and (2) startle-induced calcium events that lasted approximately 14 ± 1 s (average \pm SEM), similar to our 12.3 ± 0.7 s (average \pm SEM). Differences between our studies were expected since their experiments were performed on head-restrained mice, not freely moving rats, using two-photon calcium imaging with superior resolution and focussing capabilities, and a better signal to noise ratio for fluorescence detection. We also reported similar calcium event durations with respect to voluntary locomotion events. We observed an event peak half-width of 7.1 ± 0.5 s (average \pm SEM), similar to what was reported in Bergmann glia (8.3 ± 1.2 s, average \pm SEM) and visual cortex (Paukert et al. 2014). Differences were once again expected, due to the different species (mouse), imaging technique (head-restrained two-photon imaging) and brain areas studied. A crucial observation highlighted by Paukert et al. (2014) was that what appeared to be spontaneous events were in fact motor-related, since most were accompanied by an increase in neck muscle tension measured through EMG detection, an output which we lacked in our study. We also confirmed that spontaneous calcium events were weaker than locomotion or startle-induced calcium transients (Nimmerjahn et al. 2009; Stobart et al. 2018a; Slezak et al. 2019; Srinivasan et al. 2015; Shigetomi et al. 2013a).

Recently, the role of astrocytes in sleep has been re-appraised and their role in regulating slow wave sleep has been described with two-photon calcium imaging studies in head-restrained mice (Bojarskaite et al. 2020) and in freely moving mice using the Inscopix system (Ingiosi et al. 2020). The latter study also included a more detailed two-photon study, which confirmed the widely accepted fact that two-photon resolution is required to fully appreciate the complexity of astrocyte calcium signalling (Bazargani and Attwell 2016; Bindocci et al. 2017). We confirmed that astrocytes were active during sleep and that astrocytes were even more strongly activated during the switch from sleep to awake, as shown in previous studies (Ingiosi et al. 2020; Bojarskaite et al. 2020). We also provided evidence that astrocytes might have a role in predicting the neuronal switch from a state of sleep to awake, as shown in Bojarskaite et al. (2020), during a switch from NREM sleep to wakefulness. Bojarskaite et al. (2020) also demonstrated that astrocyte did not predict a switch from REM sleep to wakefulness and responded to this shift after approximately one second. This corroborated our observation that in certain cases astrocyte calcium transients preceded a switch to awake. In spite of our

useful observations, our data set is incomplete and more experiments are required to replicate our findings in more animals and, very importantly, in naïve non-epileptic animals, using EMG to characterise the different sleep stages accurately and not putatively as was done in our study.

5.5.3 Considerations and further work

Our results show that the Inscopix system has a lot of potential, but clearly requires practice and expertise to obtain clear FOVs with a good resolution, due to the many invasive steps involved and the unavoidable cortical damage during grin lens insertion. Different labs have success rates that vary from less than 50% to over 90% in the hands of experienced users (informal discussions at the Inscopix European meet In Paris, 2019). In fact, a 50% success rate has been reported using the system in rats (Hornung et al. 2020). With the Rouach lab, we were able to obtain good results relatively quickly, mainly because we used a validated, transgenic mouse line that conditionally expressed GCaMP6f, and since we avoided damage to cortical tissue by simply resting the grin lens on the dura mater, similar to what was done by Ingiosi et al. (2020). The latter study made use of a viral construct to selectively express GCaMP6f in cortical astrocytes, AAV5.GfaABC1D.cytoGCaMP6f.SV40, a custom preparation from the Penn Vector Core (Cat# AV-5-52925), and replaced the grin lens with a cover slip that rested on the dura mater. It would be worth investigating if alternate viral constructs similar to the one used from the Penn Vector Core, would have given us better results.

While we were able to pick up novel astrocyte calcium patterns, we were unable to make a complete assessment of astrocyte calcium signalling in the cortical initiation of absence seizures, mainly due to a lack of cellular and sub-cellular resolution. Astrocytes show predominant activity within processes and microdomains during sensory input and other physiological processes, which is why it seems counterintuitive to move away from a high resolution system, since subcellular resolution is a must to delve into mechanistic details of astrocyte function. While population studies are highly useful to determine global calcium event patterns, subtler changes in astrocyte activity such as those related to synaptic input as observed in microdomains, require subcellular resolution which can only be achieved by 2-photon calcium imaging. The contribution of subtler signalling that affects astrocytes during sensory input, such as mGluR activation, would not be detectable in comparison to the overwhelming activation induced by widespread noradrenergic activation, which astrocytes respond strongly to. For this reason, a miniature implantable two-photon microscope would be desirable. The technology has been described; however, it is unfortunately not widely available for purchase (Zong et al. 2021; Ozbay et al. 2018). Other alternatives that require further technical

developments might also be considered, such as head-restrained calcium imaging using three-photon microscopy (Wang et al. 2018), or two-photon microscopy coupled with red-shifted calcium indicators (Tischbirek et al. 2015), both of which would allow deeper tissue penetration and avoid the use of grin lenses and cortical damage. Having attained sub-cellular resolution, one could then go a step further and couple astrocyte calcium imaging with manipulation of astrocyte function, such as DREADD or optogenetic activation, or silencing by expressing the hPMCA2w/b pump (to deplete calcium reserves). This would directly address whether astrocytes are able to influence local neuronal activity related to SWD initiation, and also, more generally, if modifying their activity can ameliorate or worsen absence seizures. Coupling DREADD or optogenetic activation of astrocytes with local neuronal recordings, such as LFP recordings or imaging with neuronal GECIs, would be highly informative, since it would demonstrate if an increase in astrocyte intracellular calcium is sufficient to induce changes in local neuronal activity within the cortical initiation site. Astrocyte activation could potentially release gliotransmitters and induce neuronal paroxysmal depolarisation shifts (such as those observed in the cortical initiation site prior to SWD generalisation (Polack et al. 2007) by recruitment of a wider population of nearby neurons (as previously shown; Gómez-Gonzalo et al. 2010; Tian et al. 2005). The already depolarised and excitable ictogenic cells within the cortical initiation site (Polack et al. 2007; Studer et al. 2019) are highly likely to engage in increased firing and potentially initiate absence seizures following further depolarisation induced by astrocyte gliotransmitter release, or at the very least worsen the absence seizure pathology with respect to the number of seizures initiated and/or seizure duration. This can be performed using acute or chronic activation to ascertain if more sustained astrocyte activation is required to alter neuronal excitability sufficiently to induce SWDs. Also, if performed in control animals, NEC, one could determine if acute or chronic astrocyte activation within the cortical initiation site is sufficient to induce an absence seizure phenotype. Moreover, inhibiting astrocyte calcium activity, might also have a similarly negative effect due to, for instance, impaired neurotransmitter uptake or potassium buffering, which may just as well worsen the absence seizure phenotype.

5.6 Conclusion

Here we show, for the first time, concurrent SWD detection and population astrocyte calcium imaging directly from the cortical initiation site of an absence seizure model. We show a clear correlation between the occurrence of long bouts of SWDs and intracellular astrocyte calcium changes, especially during the presence of brief transitions between

SWDs. The latter observation implies a potential role of astrocyte activity in the maintenance of SWDs.

Further studies using a similar approach and with better cellular and subcellular resolution, will reveal the accurate timing of calcium activity within different cellular sub-compartments with respect to seizure onset or ongoing SWDs. Moreover, manipulation of astrocyte calcium activity will reveal if astrocytes have a causative role in the generation of ictal discharges in this model.

Chapter 6: Concluding discussion

6.1 Summary of main findings

This study investigates astrocyte calcium signalling in S1 of rodent models during locomotion or seizures. Intracellular calcium changes were detected using an AAV-delivered GECl, GCaMP6f, specifically expressed in astrocytes. A two-photon laser scanner was used to image calcium fluorescence through a chronic cranial window in head-restrained mice. The Inscopix implantable miniscope was used to image freely moving rats implanted with a prism lens. In addition to astrocyte calcium changes, neuronal activity was detected with chronically implanted ECoG electrodes to correlate astrocyte calcium changes with neuronal activity.

We first wanted to investigate astrocyte calcium signalling during a normal physiological function, locomotion, to enable understanding of astrocyte calcium signalling in a diseased state, epilepsy. To determine layer 2/3 astrocyte calcium activity during locomotion, mice were head-restrained under a two-photon laser scanning microscope and allowed to move freely on a rotating wheel from which we extracted the speed of movement. Using a semi-automated static ROI detection method, we picked up spontaneous calcium activity in the somata, processes, microdomains and endfeet, unrelated to locomotion or global ECoG changes. Synchronous astrocyte population activation followed locomotion with a few seconds of delay. This confirmed previous published findings that describe the α 1-noradrenergic-mediated astrocyte response to locomotion (Ding et al. 2013; Paukert et al. 2014; Srinivasan et al. 2015; Slezak et al. 2019). We add interesting findings to this already described phenomenon, and show that calcium fluctuations closely follow locomotion patterns, and that locomotion duration, but not speed, is positively correlated with calcium increases. Moreover, widespread microdomain activation was consistent with periods of locomotion, occurred even in the absence of soma activation, and rapidly followed locomotion onset within less than a second. This indicated the ability of astrocytes to synchronously respond at a sub-cellular level, presumably following neuronal activation. The astrocyte response was initiated in the cell periphery, with events in the microdomains occurring instantly with locomotion onset, and quickly spread to the soma and peaked synchronously in all compartments ~15-20 seconds later. We also provide evidence of altered astrocyte function in Stargazer mice, with an ataxic phenotype, which show a more rapid response to locomotion, especially in the microdomains that on a population level activate on average ~1.5 seconds before WT microdomains. We also show a tight association

between astrocytes and global neuronal oscillations, since changes in low frequency ECoG bands accompany locomotion-induced astrocyte calcium signalling. These findings provide further evidence that astrocytes may engage in rapid signalling and that astrocytes are capable of information processing.

Next, we wanted to investigate astrocyte calcium signalling in a diseased state. We chose to investigate childhood absence epilepsy because of previously published evidence of astrocyte dysfunction in animal models of absence seizures (Pirttimaki et al. 2010; Pirttimaki et al. 2013; Sitnikova 2009) and because of a lack of studies that investigate genetic models of spontaneous generalised seizures. To determine the contribution of astrocyte calcium signalling to absence seizure generation, we performed a series of experiments. We imaged layer 2/3 astrocyte calcium activity in awake, head-restrained Stargazer mice during ongoing seizure activity picked up by ECoG electrodes. Astrocytes were active during periods of ongoing ictal events, and showed more frequent microdomain and endfoot calcium increases, possibly indicative of increased metabolic demand and synaptic activity owing to ongoing SWDs. We failed to replicate this data with the GHB pharmacological model used on WT animals, which conversely showed a tendency towards reduced calcium signalling, possibly due to increased sedation and a failure of the pharmacological model to accurately replicate SWDs. We next wanted to determine the influence of reduced or increased astrocyte calcium signalling on seizure activity. Applying the GHB model to the IP3R2 KO mouse with impaired calcium signalling, while monitoring ECoG activity, resulted in similar ECoG changes in KO and WT mice, and indicated that the GHB-induced ECoG changes were not modulated by astrocyte IP3R2-mediated mechanisms. Moreover, inducing intracellular astrocyte calcium release using an astrocyte-specific DREADD expressed in the S1BF deeper layers, did not reveal changes in seizure properties as assessed by ECoG seizure detection and quantification. This was performed in Stargazers and GAERS, the latter having a well-defined initiation site, and suggested that SWDs were not mediated by astrocyte-calcium-dependent mechanisms. However, the findings with the GAERS must be interpreted with caution due to insufficient evidence of immunohistochemical expression of the DREADD.

Finally, we wanted to investigate the timing of astrocyte calcium changes within the GAERS cortical initiation site with respect to seizure onset and ongoing SWDs, to determine if astrocytes may be implicated in seizure initiation and/or maintenance. To image astrocyte calcium activity directly from the cortical initiation site, we implanted GCaMP6f-expressing GAERS with a prism lens that allowed us to image vertically through the deeper cortical layers of the S1BF. The implantable Inscopix miniscope

allowed us to image freely moving and seizing GAERS, seizures picked up with contralaterally implanted ECoG electrodes. Astrocytes showed altered calcium signalling patterns during long trains of SWDs, and keeping in mind the limited cellular resolution, there was no evidence of calcium events that preceded SWD initiation. Astrocytes were active a quarter of the time following seizure onset, and strong calcium increases occurred during brief transitions in SWDs, which indicated a possible role of astrocytes in the maintenance of SWDs but not in absence seizure initiation. These findings contrast with well-documented observations of astrocyte activation preceding seizure onset in chemical models that relied on the direct intracranial application of a convulsant or in slice (Gómez-Gonzalo et al. 2010; Tian et al. 2005; Zhang et al. 2019; Szokol et al. 2015; Heuser et al. 2018). This highlights the importance of supplementing such findings using genetic models of epilepsy that accurately or at least partly replicate the human condition.

6.2 The astrocyte calcium response to locomotion vs SWDs

This study investigates the activity of astrocytes in the S1BF of rodents during two different behavioural states: (i) during voluntary locomotion and presumed ongoing sensory input from whiskers, and (ii) during absence seizures characterised by SWDs. I have so far discussed the two astrocyte responses separately, however, it is important to note the similarities between the two behavioural states involved. Absence seizures might seem entirely distinct from sensory input to the S1BF, because while whisking and locomotion involve an active sensory task and exploration, absence seizures induce immobility and a loss of sensory awareness. However, sensory input during whisking/locomotion and SWDs are related, for various reasons: (i) sensory input to the S1BF, and the initiation and spread of SWDs make use of common circuitry involving the trigeminal system (van Luijtelaar and Sitnikova 2006); (ii) during SWDs, whisker tremors are commonly induced (Willoughby and Mackenzie 1992; Buzsáki et al. 1990); (iii) the development of the S1BF has a direct influence on SWD occurrence in adulthood (Sitnikova et al. 2020); (iv) 7 – 12 Hz oscillations in the vibrissal areas of S1, thalamus and brainstem are triggered during whisking activity (Nicolelis and Fanselow 2002; Nicolelis et al. 1995), and oscillations of a similar frequency are also initiated in S1 that leads to the generalisation of SWDs (Depaulis et al. 2016; Bosnyakova et al. 2006; Polack et al. 2007; Meeren et al. 2002); (v) sensory- or SWD-related 7 – 12 Hz oscillations more easily arise during states of idleness, and can be interrupted by whisker stimulation (van Luijtelaar and Sitnikova 2006, for review). These highlight the involvement of the S1BF in sensory input and also SWDs, and the similar pathways

involved. A major difference is however the NRT's involvement in the two processes. While the NRT contributes to sensory input under normal physiological conditions, since it is reciprocally connected to the VB that forms part of the vibrissae sensorimotor system (see section 1.5.1) and is intricately involved in maintaining thalamo-cortical rhythms by modulating inhibitory tone on various thalamic structures (Halassa and Acsády 2016; Clemente-Perez et al. 2017), SWDs are characterised by abnormal NRT hyperactivity. Indeed, blocking NRT-TC inhibition induces a SWD block (McCafferty et al. 2018; Huguenard 2019), since the excitatory cortical input to the NRT is enhanced in a network susceptible to SWDs, and stimulates stronger NRT-TC inhibition which drives SWD maintenance. The CT and TC projections then utilise the trigeminal network system to further generalise SWDs, with a significant role identified in the basal ganglia that receive enhanced excitatory cortical input and project this to TC neurons in the form of enhanced inhibitory input. This complements and exacerbates the inhibitory influence from the NRT (see section 1.7.4.2). So, while the two processes, i.e. whisker sensory input during locomotion and SWDs, involve common circuitry, differences do exist. This implies that while astrocytes will be similarly involved in both scenarios, the astrocyte response will be different, also considering the different involvement of major neuromodulators.

Astrocytes respond more strongly to sensory stimuli during a state of arousal or a heightened state of vigilance, in the presence of widespread neuromodulator release (Paukert et al. 2014; Wahis and Holt 2021). This is consistent with our data in which we observe an increase in S1BF astrocyte calcium activity as the mouse goes from no movement during stillness (during which some ongoing whisking is expected (Ayaz et al. 2019)) or seizures (during which whisker tremors accompany SWDs) to locomotion (during which active whisking is expected (Ayaz et al. 2019)). During locomotion in mice, noradrenergic and cholinergic axons that project to the cortex are active (Reimer et al. 2016) and this is expected to induce intracellular calcium increases in cortical astrocytes, since stimulation of the locus coeruleus or nucleus basalis of Meynert, both of which project to the cortex, induce astrocyte calcium increases in cortical astrocytes (Takata et al. 2011; Bekar et al. 2008). Moreover, Reimer et al. (2016) observed different patterns of cholinergic and noradrenergic activation during locomotion. Cholinergic activation was maintained throughout locomotion whereas noradrenergic activation peaked at the beginning of the locomotion period and was maintained at a lower level throughout the movement. This likely explains why our data shows that calcium fluorescence patterns followed closely the pattern of locomotion, since neuromodulator activation closely followed locomotor activity. This implies that a gap in movement would

result in a fresh burst of noradrenergic input upon the next bout of movement, creating a fresh activation of astrocytes and a corresponding calcium peak, as observed in our data. The influence of neuromodulator release on astrocyte activation is further evidenced in the astrocyte calcium response to startle stimuli which is consistently evoked following each stimulus trial (Srinivasan et al. 2015), which we also observed in our pilot experiments with the GAERS, and which is mediated by astrocyte α 1-noradrenergic receptor activation (Srinivasan et al. 2015).

During absence seizures, widespread neuromodulator release is not expected, so in spite of S1BF activation due to whisker movements, a global astrocyte calcium response is unlikely. Stargazer mice did not show synchronous astrocyte population activation during ongoing SWDs, however, we did observe increased calcium activity in microdomains and endfeet. This is likely in response to increased metabolic demand and synaptic activity due to the ongoing cortico-thalamo-cortical network activity, and in response to local neuronal activation from sensory input to the S1BF due to whisker tremors. Indeed, in awake head-restrained mice, it was shown that whisking during immobility is accompanied by increased astrocyte calcium activity compared to immobility without whisking (Bojarskaite et al. 2020). Since Stargazers suffer from frequent absence seizures, a chronic increase in astrocyte calcium signalling might be expected in the periphery of Stargazer astrocytes, which might explain the more rapid astrocyte calcium response to locomotion observed compared to WT animals. It may be argued that the already active astrocyte microdomains will require a lower increase in synaptic or sensory input to induce a full cell response. So, the threshold from peripheral activation to full cell activation will be achieved more easily resulting in a more rapid astrocyte response to locomotion. This interpretation is based on observations in slices that show that the strength of the astrocyte response depends on the frequency and duration of synaptic stimulation (Parri et al. 2010; Perea and Araque 2005), and on in vivo observations that show that increased synaptic input results in a stronger and full cell calcium response (Lines et al. 2020; Bindocci et al. 2017).

While in the Stargazers there was no clear correlation between the timing of astrocyte calcium signalling and SWD occurrence, in the pilot study we performed on the GAERS, we did occasionally observe gentle population-wide S1BF astrocyte activation following seizure onset and during ongoing SWDs. This is consistent with observations of astrocyte calcium signalling during another well-established thalamocortical rhythm, sleep. During periods of REM and NREM sleep, Bojarskaite et al. (2020) reported subtle S1BF astrocyte calcium activity, mostly restricted to the cell periphery. Such activity was less frequent than during awake periods of stillness, whisking or locomotion. We

similarly observed gentle calcium increases during periods of putative sleep in our GAERS recordings. In contrast, we observed strong calcium increases during brief transitions in SWDs that were accompanied by a change in ECoG power bands, with a shift towards stronger 1 – 5 Hz oscillations. This increase in calcium fluorescence resembled astrocyte calcium activation associated with brain state shifts, observed in numerous studies. We observed a strong calcium increase during a shift from putative sleep to wakefulness, as shown by Bojarskaite et al. (2020) during the shift from NREM sleep to wakefulness, which coincides with norepinephrine release from the locus coeruleus (Takahashi, Kayama, Lin, & Sakai, 2010). Similarly strong calcium activation was evoked during shifts in cortical UP/DOWN states (Poskanzer and Yuste 2011) and shifts to slow oscillation states characteristic of a resting state (Poskanzer and Yuste 2016). It is this clear that changes in thalamocortical rhythms are strongly associated with an astrocyte calcium response, during which astrocytes are more receptive to the wider network rhythms rather than to local neuronal activity (Bojarskaite et al. 2020).

6.3 The contribution of S1 astrocyte calcium signalling to seizure initiation

The involvement of astrocyte calcium signalling in absence seizure initiation has not been previously investigated. The existence of a cortical initiation site has been confirmed in various animal models, namely S1BF layer V in GAERS (Polack et al. 2007), peri-oral subregion of S1 in WAG/Rij (Meeren et al. 2002), and S1 in the GHB pharmacological model (Choi et al. 2010). This was an important finding since it showed that SWDs first formed in these regions, and preceded generalisation to other cortical areas and the thalamus, and shifted the focus of research to cortico-thalamic interactions. Similarly, in humans, a predominant initiation in the frontal cortex has been well described (Tenney et al. 2013), with some variability between and within patients, but most commonly in the orbitofrontal cortex (Holmes et al. 2004), corroborating data obtained in animal models. However, interesting evidence emerged of potential brain activity that preceded SWD onset. A simultaneous EEG-fMRI study in human patients revealed local increases in the BOLD fMRI signal in the orbital/medial frontal and medial/lateral parietal cortex, eight to fourteen seconds prior to seizure onset, together with a decrease in the BOLD fMRI signal that lasted more than twenty seconds after seizure termination (Bai et al. 2010). Bai et al. (2010) argued that such changes cannot be attributed to local electrical events since these occur over a shorter timescale than fMRI signals, and could not be correlated with changes in the EEG signal acquired simultaneously. This potentially implicated the involvement of cell types other than

neurons, such as astrocytes, which modulate the haemodynamic response that contributes to the BOLD fMRI signal (Drew 2019). Moreover, optogenetic astrocyte-specific activation is sufficient to trigger an increase in the BOLD fMRI signal, independently of neuronal activity (Takata et al. 2018). This led us to hypothesise that astrocytes may be active prior to seizure onset in animal models of absence seizures and are possibly evoking SWD onset. We were unable to identify clear increases in S1BF astrocyte calcium signalling prior to seizure onset in the Stargazer model. However, since a cortical initiation site has not been identified in the Stargazer model, this finding was inconclusive, since the increase in BOLD fMRI signal prior to seizure onset was localised within or close to the cortical initiation site. To obtain more conclusive evidence, we therefore imaged directly from the initiation site of the GAERS model, S1BF layer V. Once again we failed to detect global increases in astrocyte calcium fluorescence prior to seizure onset, and we found no evidence of widespread astrocyte activation in the seconds before seizure onset. However, we were severely limited with respect to cellular and subcellular resolution, and it may have well been the case that global changes limited to astrocyte microdomains occurred prior to seizure onset. Given our use of a one-photon system with the GAERS and the poor cellular resolution, we may have easily missed calcium activity restricted to the cell periphery. Therefore, based on our findings with the Stargazer and GAERS models, we cannot confirm an astrocyte-contribution to SWD onset in the cortex, and the role of astrocytes is more likely to be limited to the generalisation and/or maintenance of SWDs.

6.4 Conclusion

In conclusion, our results further highlight the complexity of astrocyte calcium signalling during awake states in relation locomotion and seizure activity. We confirmed the reliable astrocyte calcium response to locomotion and showed that astrocyte calcium signalling closely followed locomotion patterns, possibly reflecting neuromodulator stimulation of the sensory cortex. Furthermore, our data demonstrated that microdomains were more receptive to locomotion-related information, activated in instances when the other cellular compartments did not, and responded most rapidly. This highlighted the ability of microdomains to rapidly respond to local synaptic activity or weak input, and in possibly coordinating a more substantial cellular or population response.

While it is clear that astrocytes are involved in local neuronal activity in the S1BF and in cortical and thalamic rhythms, we were unable to decisively determine the role of astrocytes in the initiation and maintenance of SWDs related to absence seizures. Our

data suggested that modifying S1BF astrocyte function did not influence the occurrence of absence seizures, and we did not identify astrocyte calcium activity that preceded SWD onset. We did however identify novel astrocyte calcium patterns in the cortical initiation site of GAERS during ongoing SWDs, that may be critical in the maintenance of SWDs. We also observed increased activation of the astrocyte periphery in Stargazer mice that possibly contributed to their altered response to locomotion. Further work is required to fully appreciate the significance of astrocyte calcium signalling during absence seizures, to conclusively determine the role of astrocytes in SWD initiation and spread.

Chapter 7: References

- Adotevi, N.K. and Leitch, B. 2017. Synaptic changes in AMPA receptor subunit expression in cortical parvalbumin interneurons in the stargazer model of absence epilepsy. *Frontiers in Molecular Neuroscience* 10, p. 434.
- Agarwal, A., Wu, P.-H., Hughes, E.G., Fukaya, M., Tischfield, M.A., Langseth, A.J., Wirtz, D. and Bergles, D.E. 2017. Transient opening of the mitochondrial permeability transition pore induces microdomain calcium transients in astrocyte processes. *Neuron* 93(3), pp. 587–605.
- Agulhon, C., Boyt, K.M., Xie, A.X., Friocourt, F., Roth, B.L. and McCarthy, K.D. 2013. Modulation of the autonomic nervous system and behaviour by acute glial cell Gq protein-coupled receptor activation in vivo. *The Journal of Physiology* 591(22), pp. 5599–5609.
- Agulhon, C., Fiacco, T.A. and McCarthy, K.D. 2010. Hippocampal short- and long-term plasticity are not modulated by astrocyte Ca²⁺ signaling. *Science* 327(5970), pp. 1250–1254.
- Aizawa, M., Ito, Y. and Fukuda, H. 1997. Pharmacological profiles of generalized absence seizures in lethargic, stargazer and γ -hydroxybutyrate-treated model mice. *Neuroscience Research* 29(1), pp. 17–25.
- Akerboom, J., Chen, T.-W., Wardill, T.J., Tian, L., Marvin, J.S., Mutlu, S., Calderón, N.C., Esposti, F., Borghuis, B.G., Sun, X.R., Gordus, A., Orger, M.B., Portugues, R., Engert, F., Macklin, J.J., Filosa, A., Aggarwal, A., Kerr, R.A., Takagi, R., Kracun, S., Shigetomi, E., Khakh, B.S., Baier, H., Lagnado, L., Wang, S.S.-H., Bargmann, C.I., Kimmel, B.E., Jayaraman, V., Svoboda, K., Kim, D.S., Schreiter, E.R. and Looger, L.L. 2012. Optimization of a GCaMP calcium indicator for neural activity imaging. *The Journal of Neuroscience* 32(40), pp. 13819–13840.
- Akin, D., Ravizza, T., Maroso, M., Carcak, N., Eryigit, T., Vanzulli, I., Aker, R.G., Vezzani, A. and Onat, F.Y. 2011. IL-1 β is induced in reactive astrocytes in the somatosensory cortex of rats with genetic absence epilepsy at the onset of spike-and-wave discharges, and contributes to their occurrence. *Neurobiology of Disease* 44(3), pp. 259–269.
- Angyán, L. and Czopf, J. 1998. Exercise-induced slow waves in the EEG of cats. *Physiology & Behavior* 64(3), pp. 267–272.
- Anner, P., Passecker, J., Klausberger, T. and Dorffner, G. 2020. Ca²⁺ imaging of neurons in freely moving rats with automatic post hoc histological identification. *Journal of Neuroscience Methods* 341, p. 108765.
- Araque, A. 2008. Astrocytes process synaptic information. *Neuron Glia Biology* 4(1), pp. 3–10.
- Araque, A., Carmignoto, G., Haydon, P.G., Oliet, S.H.R., Robitaille, R. and Volterra, A. 2014. Gliotransmitters travel in time and space. *Neuron* 81(4), pp. 728–739.
- Araque, A., Martín, E.D., Perea, G., Arellano, J.I. and Buño, W. 2002. Synaptically released acetylcholine evokes Ca²⁺ elevations in astrocytes in hippocampal slices. *The Journal of Neuroscience* 22(7), pp. 2443–2450.
- Araque, A., Parpura, V., Sanzgiri, R.P. and Haydon, P.G. 1998. Glutamate-dependent astrocyte modulation of synaptic transmission between cultured hippocampal neurons. *The European Journal of Neuroscience* 10(6), pp. 2129–2142.

- Araque, A., Parpura, V., Sanzgiri, R.P. and Haydon, P.G. 1999. Tripartite synapses: glia, the unacknowledged partner. *Trends in Neurosciences* 22(5), pp. 208–215.
- Araque, A., Sanzgiri, R.P., Parpura, V. and Haydon, P.G. 1998. Calcium elevation in astrocytes causes an NMDA receptor-dependent increase in the frequency of miniature synaptic currents in cultured hippocampal neurons. *The Journal of Neuroscience* 18(17), pp. 6822–6829.
- Armbruster, B.N., Li, X., Pausch, M.H., Herlitze, S. and Roth, B.L. 2007. Evolving the lock to fit the key to create a family of G protein-coupled receptors potentially activated by an inert ligand. *Proceedings of the National Academy of Sciences of the United States of America* 104(12), pp. 5163–5168.
- Aronica, E., van Vliet, E.A., Mayboroda, O.A., Troost, D., da Silva, F.H. and Gorter, J.A. 2000. Upregulation of metabotropic glutamate receptor subtype mGluR3 and mGluR5 in reactive astrocytes in a rat model of mesial temporal lobe epilepsy. *The European Journal of Neuroscience* 12(7), pp. 2333–2344.
- Asada, A., Ujita, S., Nakayama, R., Oba, S., Ishii, S., Matsuki, N. and Ikegaya, Y. 2015. Subtle modulation of ongoing calcium dynamics in astrocytic microdomains by sensory inputs. *Physiological reports* 3(10), e12454.
- Atkin, S.D., Patel, S., Kocharyan, A., Holtzclaw, L.A., Weerth, S.H., Schram, V., Pickel, J. and Russell, J.T. 2009. Transgenic mice expressing aameleon fluorescent Ca²⁺ indicator in astrocytes and Schwann cells allow study of glial cell Ca²⁺ signals in situ and in vivo. *Journal of Neuroscience Methods* 181(2), pp. 212–226.
- Avoli, M. 2012. A brief history on the oscillating roles of thalamus and cortex in absence seizures. *Epilepsia* 53(5), pp. 779–789.
- Ayaz, A., Stäuble, A., Hamada, M., Wulf, M.-A., Saleem, A.B. and Helmchen, F. 2019. Layer-specific integration of locomotion and sensory information in mouse barrel cortex. *Nature Communications* 10(1), e2585.
- Babiloni, C., Babiloni, F., Carducci, F., Cincotti, F., Coccozza, G., Del Percio, C., Moretti, D.V. and Rossini, P.M. 2002. Human cortical electroencephalography (EEG) rhythms during the observation of simple aimless movements: a high-resolution EEG study. *Neuroimage* 17(2), pp. 559–572.
- Bai, X., Vestal, M., Berman, R., Negishi, M., Spann, M., Vega, C., Desalvo, M., Novotny, E.J., Constable, R.T. and Blumenfeld, H. 2010. Dynamic time course of typical childhood absence seizures: EEG, behavior, and functional magnetic resonance imaging. *The Journal of Neuroscience* 30(17), pp. 5884–5893.
- Baird-Daniel, E., Daniel, A.G.S., Wenzel, M., Li, D., Liou, J.-Y., Laffont, P., Zhao, M., Yuste, R., Ma, H. and Schwartz, T.H. 2017. Glial calcium waves are triggered by seizure activity and not essential for initiating ictal onset or neurovascular coupling. *Cerebral Cortex* 27(6), pp. 3318–3330.
- Barrett, M.J.P., Ferrari, K.D., Stobart, J.L., Holub, M. and Weber, B. 2018. CHIPS: an Extensible Toolbox for Cellular and Hemodynamic Two-Photon Image Analysis. *Neuroinformatics* 16(1), pp. 145–147.
- Bazargani, N. and Attwell, D. 2017. Amines, astrocytes, and arousal. *Neuron* 94(2), pp. 228–231.
- Bazargani, N. and Attwell, D. 2016. Astrocyte calcium signaling: the third wave. *Nature Neuroscience* 19(2), pp. 182–189.
- Bedner, P., Dupper, A., Hüttmann, K., Müller, J., Herde, M.K., Dublin, P., Deshpande, T., Schramm, J., Häussler, U., Haas, C.A., Henneberger, C., Theis, M. and

- Steinhäuser, C. 2015. Astrocyte uncoupling as a cause of human temporal lobe epilepsy. *Brain: A Journal of Neurology* 138(Pt 5), pp. 1208–1222.
- Beenhakker, M.P. and Huguenard, J.R. 2010. Astrocytes as gatekeepers of GABAB receptor function. *The Journal of Neuroscience* 30(45), pp. 15262–15276.
- Beghi, E. 2020. The epidemiology of epilepsy. *Neuroepidemiology* 54(2), pp. 185–191.
- Bekar, L.K., He, W. and Nedergaard, M. 2008. Locus coeruleus alpha-adrenergic-mediated activation of cortical astrocytes in vivo. *Cerebral Cortex* 18(12), pp. 2789–2795.
- Ben Haim, L. and Rowitch, D.H. 2017. Functional diversity of astrocytes in neural circuit regulation. *Nature Reviews. Neuroscience* 18(1), pp. 31–41.
- Berg, A.T., Levy, S.R., Testa, F.M. and Blumenfeld, H. 2014. Long-term seizure remission in childhood absence epilepsy: might initial treatment matter? *Epilepsia* 55(4), pp. 551–557.
- Bezzi, P. and Volterra, A. 2001. A neuron-glia signalling network in the active brain. *Current Opinion in Neurobiology* 11(3), pp. 387–394.
- Bignami, A., Eng, L.F., Dahl, D. and Uyeda, C.T. 1972. Localization of the glial fibrillary acidic protein in astrocytes by immunofluorescence. *Brain Research* 43(2), pp. 429–435.
- Binder, D.K. and Carson, M.J. 2013. Glial cells as primary therapeutic targets for epilepsy. *Neurochemistry International* 63(7), pp. 635–637.
- Binder, D.K. and Steinhäuser, C. 2021. Astrocytes and Epilepsy. *Neurochemical Research* 46:2687–2695.
- Bindocci, E., Savtchouk, I., Liaudet, N., Becker, D., Carriero, G. and Volterra, A. 2017. Three-dimensional Ca²⁺ imaging advances understanding of astrocyte biology. *Science* 356(6339).
- Bjørnstad, D.M., Åbjørsbråten, K.S., Hennestad, E., Cunen, C., Hermansen, G.H., Bojarskaite, L., Pettersen, K.H., Vervaeke, K. and Enger, R. 2021. Begonia-A Two-Photon Imaging Analysis Pipeline for Astrocytic Ca²⁺ Signals. *Frontiers in Cellular Neuroscience* 15.
- Blumenfeld, H. 2005. Cellular and network mechanisms of spike-wave seizures. *Epilepsia* 46 Suppl 9, pp. 21–33.
- Boison, D. 2005. Adenosine and epilepsy: from therapeutic rationale to new therapeutic strategies. *The Neuroscientist* 11(1), pp. 25–36.
- Boison, D. and Steinhäuser, C. 2018. Epilepsy and astrocyte energy metabolism. *Glia* 66(6), pp. 1235–1243.
- Bojarskaite, L., Bjørnstad, D.M., Pettersen, K.H., Cunen, C., Hermansen, G.H., Åbjørsbråten, K.S., Chambers, A.R., Sprengel, R., Vervaeke, K., Tang, W., Enger, R. and Nagelhus, E.A. 2020. Astrocytic Ca²⁺ signaling is reduced during sleep and is involved in the regulation of slow wave sleep. *Nature Communications* 11(1), e3240.
- Bojarskaite, L., Bjørnstad, D.M., Pettersen, K.H., Cunen, C., Hermansen, G.H., Åbjørsbråten, K.S., Sprengel, R., Vervaeke, K., Tang, W., Enger, R. and Nagelhus, E.A. 2019. Ca²⁺ signaling in astrocytes is sleep-wake state specific and modulates sleep. *BioRxiv*.
- Bonder, D.E. and McCarthy, K.D. 2014. Astrocytic Gq-PCR-linked IP3R-dependent Ca²⁺ signaling does not mediate neurovascular coupling in mouse visual cortex in vivo. *The Journal of Neuroscience* 34(39), pp. 13139–13150.

- Borden, L.A. 1996. GABA transporter heterogeneity: pharmacology and cellular localization. *Neurochemistry International* 29(4), pp. 335–356.
- Bosnyakova, D., Gabova, A., Kuznetsova, G., Obukhov, Y., Midzyanovskaya, I., Salonin, D., van Rijn, C., Coenen, A., Tuomisto, L. and van Luijtelaaar, G. 2006. Time-frequency analysis of spike-wave discharges using a modified wavelet transform. *Journal of Neuroscience Methods* 154(1-2), pp. 80–88.
- Bourassa, J., Pinault, D. and Deschênes, M. 1995. Corticothalamic projections from the cortical barrel field to the somatosensory thalamus in rats: a single-fibre study using biocytin as an anterograde tracer. *The European Journal of Neuroscience* 7(1), pp. 19–30.
- Bouwman, B.M., Suffczynski, P., Midzyanovskaya, I.S., Maris, E., van den Broek, P.L.C. and van Rijn, C.M. 2007. The effects of vigabatrin on spike and wave discharges in WAG/Rij rats. *Epilepsy Research* 76(1), pp. 34–40.
- Bowser, D.N. and Khakh, B.S. 2004. ATP excites interneurons and astrocytes to increase synaptic inhibition in neuronal networks. *The Journal of Neuroscience* 24(39), pp. 8606–8620.
- Brigo, F., Igwe, S.C. and Lattanzi, S. 2021. Ethosuximide, sodium valproate or lamotrigine for absence seizures in children and adolescents. *Cochrane Database of Systematic Reviews* 1, CD003032.
- Broussard, G.J., Liang, R. and Tian, L. 2014. Monitoring activity in neural circuits with genetically encoded indicators. *Frontiers in Molecular Neuroscience* 7.
- Bushong, E.A., Martone, M.E., Jones, Y.Z. and Ellisman, M.H. 2002. Protoplasmic astrocytes in CA1 stratum radiatum occupy separate anatomical domains. *The Journal of Neuroscience* 22(1), pp. 183–192.
- Buzsáki, G. and Draguhn, A. 2004. Neuronal oscillations in cortical networks. *Science* 304(5679), pp. 1926–1929.
- Buzsáki, G., Laszlovszky, I., Lajtha, A. and Vadász, C. 1990. Spike-and-wave neocortical patterns in rats: genetic and aminergic control. *Neuroscience* 38(2), pp. 323–333.
- Cahoy, J.D., Emery, B., Kaushal, A., Foo, L.C., Zamanian, J.L., Christopherson, K.S., Xing, Y., Lubischer, J.L., Krieg, P.A., Krupenko, S.A., Thompson, W.J. and Barres, B.A. 2008. A transcriptome database for astrocytes, neurons, and oligodendrocytes: a new resource for understanding brain development and function. *The Journal of Neuroscience* 28(1), pp. 264–278.
- Cameron, C.M., Murugan, M., Choi, J.Y., Engel, E.A. and Witten, I.B. 2019. Increased Cocaine Motivation Is Associated with Degraded Spatial and Temporal Representations in IL-NAc Neurons. *Neuron* 103(1), pp. 80–91.e7.
- Caplan, R., Siddarth, P., Stahl, L., Lanphier, E., Vona, P., Gurbani, S., Koh, S., Sankar, R. and Shields, W.D. 2008. Childhood absence epilepsy: behavioral, cognitive, and linguistic comorbidities. *Epilepsia* 49(11), pp. 1838–1846.
- Carmignoto, G. 2000. Reciprocal communication systems between astrocytes and neurones. *Progress in Neurobiology* 62(6), pp. 561–581.
- Carmignoto, G. and Fellin, T. 2006. Glutamate release from astrocytes as a non-synaptic mechanism for neuronal synchronization in the hippocampus. *Journal of physiology, Paris* 99(2-3), pp. 98–102.
- Carmignoto, G. and Haydon, P.G. 2012. Astrocyte calcium signaling and epilepsy. *Glia* 60(8), pp. 1227–1233.

- Carter, L.P., Richards, B.D., Mintzer, M.Z. and Griffiths, R.R. 2006. Relative abuse liability of GHB in humans: A comparison of psychomotor, subjective, and cognitive effects of supratherapeutic doses of triazolam, pentobarbital, and GHB. *Neuropsychopharmacology* 31(11), pp. 2537–2551.
- Cavdar, S., Köse, B., Sur, İ. and Özkan, M. 2021. Comparing Astrocytic Gap Junction of Genetic Absence Epileptic Rats with Control Rats: An Experimental Study. *Brain Struct Funct* 226(7), pp. 2113–2123.
- Cebolla, A.M. and Cheron, G. 2019. Understanding neural oscillations in the human brain: from movement to consciousness and vice versa. *Frontiers in Psychology* 10, p. 1930.
- Chen, T.-W., Wardill, T.J., Sun, Y., Pulver, S.R., Renninger, S.L., Baohan, A., Schreiter, E.R., Kerr, R.A., Orger, M.B., Jayaraman, V., Looger, L.L., Svoboda, K. and Kim, D.S. 2013. Ultrasensitive fluorescent proteins for imaging neuronal activity. *Nature* 499(7458), pp. 295–300.
- Chen, X., Choo, H., Huang, X.-P., Yang, X., Stone, O., Roth, B.L. and Jin, J. 2015. The first structure-activity relationship studies for designer receptors exclusively activated by designer drugs. *ACS Chemical Neuroscience* 6(3), pp. 476–484.
- Chen, Y., Lu, J., Pan, H., Zhang, Y., Wu, H., Xu, K., Liu, X., Jiang, Y., Bao, X., Yao, Z., Ding, K., Lo, W.H.Y., Qiang, B., Chan, P., Shen, Y. and Wu, X. 2003. Association between genetic variation of CACNA1H and childhood absence epilepsy. *Annals of Neurology* 54(2), pp. 239–243.
- Cherian, A. and Thomas, S.V. 2009. Status epilepticus. *Annals of Indian Academy of Neurology* 12(3), pp. 140–153.
- Choi, J.H., Koch, K.P., Poppendieck, W., Lee, M. and Shin, H.-S. 2010. High resolution electroencephalography in freely moving mice. *Journal of Neurophysiology* 104(3), pp. 1825–1834.
- Christensen, M.S., Lundbye-Jensen, J., Geertsen, S.S., Petersen, T.H., Paulson, O.B. and Nielsen, J.B. 2007. Premotor cortex modulates somatosensory cortex during voluntary movements without proprioceptive feedback. *Nature Neuroscience* 10(4), pp. 417–419.
- Claus, L., Philippot, C., Griemsmann, S., Timmermann, A., Jabs, R., Henneberger, C., Kettenmann, H. and Steinhäuser, C. 2018. Barreloid Borders and Neuronal Activity Shape Panglial Gap Junction-Coupled Networks in the Mouse Thalamus. *Cerebral Cortex* 28(1), pp. 213–222.
- Clemente-Perez, A., Makinson, S.R., Higashikubo, B., Brovarney, S., Cho, F.S., Urry, A., Holden, S.S., Wimer, M., Dávid, C., Fenno, L.E., Acsády, L., Deisseroth, K. and Paz, J.T. 2017. Distinct thalamic reticular cell types differentially modulate normal and pathological cortical rhythms. *Cell reports* 19(10), pp. 2130–2142.
- Coenen, A.M., Blezer, E.H. and van Lujtelaar, E.L. 1995. Effects of the GABA-uptake inhibitor tiagabine on electroencephalogram, spike-wave discharges and behaviour of rats. *Epilepsy Research* 21(2), pp. 89–94.
- Coggeshall, R.E. 1986. Nonclassical features of dorsal root ganglion cell organization. *Spinal afferent processing*.
- Coiret, G., Ster, J., Grewe, B., Wendling, F., Helmchen, F., Gerber, U. and Benquet, P. 2012. Neuron to astrocyte communication via cannabinoid receptors is necessary for sustained epileptiform activity in rat hippocampus. *Plos One* 7(5), p. e37320.

- Cope, D.W., Di Giovanni, G., Fyson, S.J., Orbán, G., Errington, A.C., Lorincz, M.L., Gould, T.M., Carter, D.A. and Crunelli, V. 2009. Enhanced tonic GABAA inhibition in typical absence epilepsy. *Nature Medicine* 15(12), pp. 1392–1398.
- Cornell-Bell, A.H., Finkbeiner, S.M., Cooper, M.S. and Smith, S.J. 1990. Glutamate induces calcium waves in cultured astrocytes: long-range glial signaling. *Science* 247(4941), pp. 470–473.
- Coulter, D.A., Huguenard, J.R. and Prince, D.A. 1989. Characterization of ethosuximide reduction of low-threshold calcium current in thalamic neurons. *Annals of Neurology* 25(6), pp. 582–593.
- Crunelli, V. and Carmignoto, G. 2013. New vistas on astroglia in convulsive and non-convulsive epilepsy highlight novel astrocytic targets for treatment. *The Journal of Physiology* 591(4), pp. 775–785.
- Crunelli, V., Emri, Z. and Leresche, N. 2006. Unravelling the brain targets of γ -hydroxybutyric acid. *Current opinion in pharmacology* 6(1): 44–52.
- Crunelli, V. and Leresche, N. 2002. Childhood absence epilepsy: genes, channels, neurons and networks. *Nature Reviews. Neuroscience* 3(5), pp. 371–382.
- Crunelli, V., Leresche, N. and Cope, D.W. 2012. GABA-A Receptor Function in Typical Absence Seizures. In: Noebels, J. L., Avoli, M., Rogawski, M. A., Olsen, R. W., and Delgado-Escueta, A. V. eds. *Jasper's basic mechanisms of the epilepsies*. 4th ed. Bethesda (MD): National Center for Biotechnology Information (US).
- Crunelli, V., Lőrincz, M.L., McCafferty, C., Lambert, R.C., Leresche, N., Di Giovanni, G. and David, F. 2020. Clinical and experimental insight into pathophysiology, comorbidity and therapy of absence seizures. *Brain: A Journal of Neurology* 143(8), pp. 2341–2368.
- Cui, F., Arnstein, D., Thomas, R.M., Maurits, N.M., Keysers, C. and Gazzola, V. 2014. Functional magnetic resonance imaging connectivity analyses reveal efference-copy to primary somatosensory area, BA2. *Plos One* 9(1), p. e84367.
- Dani, J.W., Chernjavsky, A. and Smith, S.J. 1992. Neuronal activity triggers calcium waves in hippocampal astrocyte networks. *Neuron* 8(3), pp. 429–440.
- Danover, L., Deransart, C., Depaulis, A., Vergnes, M. and Marescaux, C. 1998. Pathophysiological mechanisms of genetic absence epilepsy in the rat. *Progress in Neurobiology* 55(1), pp. 27–57.
- Darian-Smith, I. 1969. Somatic sensation. *Annual Review of Physiology* 31, pp. 417–450.
- De Biasi, S., Vitellaro-Zuccarello, L. and Brecha, N.C. 1998. Immunoreactivity for the GABA transporter-1 and GABA transporter-3 is restricted to astrocytes in the rat thalamus. A light and electron-microscopic immunolocalization. *Neuroscience* 83(3), pp. 815–828.
- Degenhardt, L., Copeland, J. and Dillon, P. 2005. Recent trends in the use of “club drugs”: an Australian review. *Substance Use & Misuse* 40(9-10), pp. 1241–1256.
- Dennis, M.J. and Gerschenfeld, H.M. 1969. Some physiological properties of identified mammalian neuroglial cells. *The Journal of Physiology* 203(1), pp. 211–222.
- Depaulis, A. and Charpier, S. 2018. Pathophysiology of absence epilepsy: Insights from genetic models. *Neuroscience Letters* 667, pp. 53–65.
- Depaulis, A., David, O. and Charpier, S. 2016. The genetic absence epilepsy rat from Strasbourg as a model to decipher the neuronal and network mechanisms of

- generalized idiopathic epilepsies. *Journal of Neuroscience Methods* 260, pp. 159–174.
- Depaulis, A., Snead, O.C., Marescaux, C. and Vergnes, M. 1989. Suppressive effects of intranigral injection of muscimol in three models of generalized non-convulsive epilepsy induced by chemical agents. *Brain Research* 498(1), pp. 64–72.
- Deransart, C., Hellwig, B., Heupel-Reuter, M., Léger, J.-F., Heck, D. and Lücking, C.H. 2003. Single-unit analysis of substantia nigra pars reticulata neurons in freely behaving rats with genetic absence epilepsy. *Epilepsia* 44(12), pp. 1513–1520.
- Deransart, C., Riban, V., Lê, B., Marescaux, C. and Depaulis, A. 2000. Dopamine in the striatum modulates seizures in a genetic model of absence epilepsy in the rat. *Neuroscience* 100(2), pp. 335–344.
- Dermietzel, R. and Spray, D.C. 1993. Gap junctions in the brain: where, what type, how many and why? *Trends in Neurosciences* 16(5), pp. 186–192.
- Di Pasquale, E., Keegan, K.D. and Noebels, J.L. 1997. Increased excitability and inward rectification in layer V cortical pyramidal neurons in the epileptic mutant mouse Stargazer. *Journal of Neurophysiology* 77(2), pp. 621–631.
- Ding, F., O'Donnell, J., Thrane, A.S., Zeppenfeld, D., Kang, H., Xie, L., Wang, F. and Nedergaard, M. 2013. α 1-Adrenergic receptors mediate coordinated Ca^{2+} signaling of cortical astrocytes in awake, behaving mice. *Cell Calcium* 54(6), pp. 387–394.
- Ding, S., Fellin, T., Zhu, Y., Lee, S.-Y., Auberson, Y.P., Meaney, D.F., Coulter, D.A., Carmignoto, G. and Haydon, P.G. 2007. Enhanced astrocytic Ca^{2+} signals contribute to neuronal excitotoxicity after status epilepticus. *The Journal of Neuroscience* 27(40), pp. 10674–10684.
- Dombeck, D.A., Khabbaz, A.N., Collman, F., Adelman, T.L. and Tank, D.W. 2007. Imaging large-scale neural activity with cellular resolution in awake, mobile mice. *Neuron* 56(1), pp. 43–57.
- Drew, P.J. 2019. Vascular and neural basis of the BOLD signal. *Current Opinion in Neurobiology* 58, pp. 61–69.
- Dube, C., Vezzani, A., Behrens, M., Bartfai, T. and Baram, T.Z. 2005. Interleukin-1beta contributes to the generation of experimental febrile seizures [comment]. *Ann Neurol.* 57(1), pp.152–155.
- Durkee, C.A., Covelo, A., Lines, J., Kofuji, P., Aguilar, J. and Araque, A. 2019. Gi/o protein-coupled receptors inhibit neurons but activate astrocytes and stimulate gliotransmission. *Glia* 67(6), pp. 1076–1093.
- Dutuit, M., Didier-Bazès, M., Vergnes, M., Mutin, M., Conjard, A., Akaoka, H., Belin, M.F. and Touret, M. 2000. Specific alteration in the expression of glial fibrillary acidic protein, glutamate dehydrogenase, and glutamine synthetase in rats with genetic absence epilepsy. *Glia* 32(1), pp. 15–24.
- Dutuit, M., Touret, M., Szymocha, R., Nehlig, A., Belin, M.-F. and Didier-Bazès, M. 2002. Decreased expression of glutamate transporters in genetic absence epilepsy rats before seizure occurrence. *Journal of Neurochemistry* 80(6), pp. 1029–1038.
- EPICURE Consortium, EMINet Consortium, Steffens, M., Leu, C., Ruppert, A.-K., et al. 2012. Genome-wide association analysis of genetic generalized epilepsies implicates susceptibility loci at 1q43, 2p16.1, 2q22.3 and 17q21.32. *Human Molecular Genetics* 21(24), pp. 5359–5372.
- Falco-Walter, J.J., Scheffer, I.E. and Fisher, R.S. 2018. The new definition and classification of seizures and epilepsy. *Epilepsy Research* 139, pp. 73–79.

- Felix, R. 2002. Insights from mouse models of absence epilepsy into Ca²⁺ channel physiology and disease etiology. *Cellular and Molecular Neurobiology* 22(2), pp. 103–120.
- Fellin, T. and Carmignoto, G. 2004. Neurone-to-astrocyte signalling in the brain represents a distinct multifunctional unit. *The Journal of Physiology* 559(Pt 1), pp. 3–15.
- Fellin, T., Gomez-Gonzalo, M., Gobbo, S., Carmignoto, G. and Haydon, P.G. 2006. Astrocytic glutamate is not necessary for the generation of epileptiform neuronal activity in hippocampal slices. *The Journal of Neuroscience* 26(36), pp. 9312–9322.
- Fellin, T., Halassa, M.M., Terunuma, M., Succol, F., Takano, H., Frank, M., Moss, S.J. and Haydon, P.G. 2009. Endogenous nonneuronal modulators of synaptic transmission control cortical slow oscillations in vivo. *Proceedings of the National Academy of Sciences of the United States of America* 106(35), pp. 15037–15042.
- Fellin, T., Pascual, O., Gobbo, S., Pozzan, T., Haydon, P.G. and Carmignoto, G. 2004. Neuronal synchrony mediated by astrocytic glutamate through activation of extrasynaptic NMDA receptors. *Neuron* 43(5), pp. 729–743.
- Finkbeiner, S. 1992. Calcium waves in astrocytes-filling in the gaps. *Neuron* 8(6), pp. 1101–1108.
- Fisher, R.S., van Emde Boas, W., Blume, W., Elger, C., Genton, P., Lee, P. and Engel, J. 2005. Epileptic seizures and epilepsy: definitions proposed by the International League Against Epilepsy (ILAE) and the International Bureau for Epilepsy (IBE). *Epilepsia* 46(4), pp. 470–472.
- Fonseca, C.G., Green, C.R. and Nicholson, L.F.B. 2002. Upregulation in astrocytic connexin 43 gap junction levels may exacerbate generalized seizures in mesial temporal lobe epilepsy. *Brain Research* 929(1), pp. 105–116.
- Gee, J.M., Gibbons, M.B., Taheri, M., Palumbos, S., Morris, S.C., Smeal, R.M., Flynn, K.F., Economo, M.N., Cizek, C.G., Capecchi, M.R., Tvrdik, P., Wilcox, K.S. and White, J.A. 2015. Imaging activity in astrocytes and neurons with genetically encoded calcium indicators following in utero electroporation. *Frontiers in Molecular Neuroscience* 8, p. 10.
- Genzel, L., Schut, E., Schröder, T., Eichler, R., Khamassi, M., Gomez, A., Navarro Lobato, I. and Battaglia, F. 2019. The object space task shows cumulative memory expression in both mice and rats. *PLoS Biology* 17(6), p. e3000322.
- Giovannucci, A., Friedrich, J., Gunn, P., Kalfon, J., Brown, B.L., Koay, S.A., Taxidis, J., Najafi, F., Gauthier, J.L., Zhou, P., Khakh, B.S., Tank, D.W., Chklovskii, D.B. and Pnevmatikakis, E.A. 2019. CalmAn an open source tool for scalable calcium imaging data analysis. *eLife* 8.
- Glauser, T.A., Cnaan, A., Shinnar, S., Hirtz, D.G., Dlugos, D., Masur, D., Clark, P.O., Adamson, P.C. and Childhood Absence Epilepsy Study Team 2013. Ethosuximide, valproic acid, and lamotrigine in childhood absence epilepsy: initial monotherapy outcomes at 12 months. *Epilepsia* 54(1), pp. 141–155.
- Glauser, T.A., Holland, K., O'Brien, V.P., Keddache, M., Martin, L.J., Clark, P.O., Cnaan, A., Dlugos, D., Hirtz, D.G., Shinnar, S., Grabowski, G. and Childhood Absence Epilepsy Study Group 2017. Pharmacogenetics of antiepileptic drug efficacy in childhood absence epilepsy. *Annals of Neurology* 81(3), pp. 444–453.
- Goldey, G.J., Roumis, D.K., Glickfeld, L.L., Kerlin, A.M., Reid, R.C., Bonin, V., Schafer, D.P. and Andermann, M.L. 2014. Removable cranial windows for long-term imaging in awake mice. *Nature Protocols* 9(11), pp. 2515–2538.

- Gómez-Gonzalo, M., Losi, G., Chiavegato, A., Zonta, M., Cammarota, M., Brondi, M., Vetri, F., Uva, L., Pozzan, T., de Curtis, M., Ratto, G.M. and Carmignoto, G. 2010. An excitatory loop with astrocytes contributes to drive neurons to seizure threshold. *PLoS Biology* 8(4), e1000352.
- Gómez-Gonzalo, M., Navarrete, M., Perea, G., Covelo, A., Martín-Fernández, M., Shigemoto, R., Luján, R. and Araque, A. 2015. Endocannabinoids Induce Lateral Long-Term Potentiation of Transmitter Release by Stimulation of Gliotransmission. *Cerebral Cortex* 25(10), pp. 3699–3712.
- Gould, Timothy, Chen, L., Emri, Z., Pirttimaki, T., Errington, A.C., Crunelli, V. and Parri, H.R. 2014. GABA(B) receptor-mediated activation of astrocytes by gamma-hydroxybutyric acid. *Philosophical Transactions of the Royal Society of London. Series B, Biological Sciences* 369(1654), p. 20130607.
- Griemsmann, S., Höft, S.P., Bedner, P., Zhang, J., von Staden, E., Beinhauer, A., Degen, J., Dublin, P., Cope, D.W., Richter, N., Crunelli, V., Jabs, R., Willecke, K., Theis, M., Seifert, G., Kettenmann, H. and Steinhäuser, C. 2015. Characterization of pial gap junction networks in the thalamus, neocortex, and hippocampus reveals a unique population of glial cells. *Cerebral Cortex* 25(10), pp. 3420–3433.
- Grosso, S., Galimberti, D., Vezzosi, P., Farnetani, M., Di Bartolo, R.M., Bazzotti, S., Morgese, G. and Balestri, P. 2005. Childhood absence epilepsy: evolution and prognostic factors. *Epilepsia* 46(11), pp. 1796–1801.
- Guerra-Gomes, S., Sousa, N., Pinto, L. and Oliveira, J.F. 2017. Functional roles of astrocyte calcium elevations: from synapses to behavior. *Frontiers in Cellular Neuroscience* 11, p. 427.
- Guizar-Sicairos, M., Thurman, S.T. and Fienup, J.R. 2008. Efficient subpixel image registration algorithms. *Optics Letters* 33(2), pp. 156–158.
- Guthrie, P.B., Knappenberger, J., Segal, M., Bennett, M.V., Charles, A.C. and Kater, S.B. 1999. ATP released from astrocytes mediates glial calcium waves. *The Journal of Neuroscience* 19(2), pp. 520–528.
- Haas, B., Schipke, C.G., Peters, O., Söhl, G., Willecke, K. and Kettenmann, H. 2006. Activity-dependent ATP-waves in the mouse neocortex are independent from astrocytic calcium waves. *Cerebral Cortex* 16(2), pp. 237–246.
- Halassa, M.M. and Acsády, L. 2016. Thalamic inhibition: diverse sources, diverse scales. *Trends in Neurosciences* 39(10), pp. 680–693.
- Halassa, M.M., Fellin, T. and Haydon, P.G. 2009a. Tripartite synapses: roles for astrocytic purines in the control of synaptic physiology and behavior. *Neuropharmacology* 57(4), pp. 343–346.
- Halassa, M.M., Fellin, T., Takano, H., Dong, J.-H. and Haydon, P.G. 2007. Synaptic islands defined by the territory of a single astrocyte. *The Journal of Neuroscience* 27(24), pp. 6473–6477.
- Halassa, M.M., Florian, C., Fellin, T., Munoz, J.R., Lee, S.-Y., Abel, T., Haydon, P.G. and Frank, M.G. 2009b. Astrocytic modulation of sleep homeostasis and cognitive consequences of sleep loss. *Neuron* 61(2), pp. 213–219.
- Haustein, M.D., Kracun, S., Lu, X.-H., Shih, T., Jackson-Weaver, O., Tong, X., Xu, J., Yang, X.W., O'Dell, T.J., Marvin, J.S., Ellisman, M.H., Bushong, E.A., Looger, L.L. and Khakh, B.S. 2014. Conditions and constraints for astrocyte calcium signaling in the hippocampal mossy fiber pathway. *Neuron* 82(2), pp. 413–429.

- Herculano-Houzel, S. 2014. The glia/neuron ratio: how it varies uniformly across brain structures and species and what that means for brain physiology and evolution. *Glia* 62(9), pp. 1377–1391.
- Heuser, K., Nome, C.G., Pettersen, K.H., Åbjørsbråten, K.S., Jensen, V., Tang, W., Sprengel, R., Taubøll, E., Nagelhus, E.A. and Enger, R. 2018. Ca²⁺ signals in astrocytes facilitate spread of epileptiform activity. *Cerebral Cortex* 28(11), pp. 4036–4048.
- Hirase, H., Qian, L., Barthó, P. and Buzsáki, G. 2004. Calcium dynamics of cortical astrocytic networks in vivo. *PLoS Biology* 2(4), E96.
- Hirata, A., Aguilar, J. and Castro-Alamancos, M.A. 2006. Noradrenergic activation amplifies bottom-up and top-down signal-to-noise ratios in sensory thalamus. *The Journal of Neuroscience* 26(16), pp. 4426–4436.
- Hodge, R.D., Bakken, T.E., Miller, J.A., Smith, K.A., Barkan, E.R., et al. 2019. Conserved cell types with divergent features in human versus mouse cortex. *Nature* 573(7772), pp. 61–68.
- Holmes, M.D., Brown, M. and Tucker, D.M. 2004. Are “generalized” seizures truly generalized? Evidence of localized mesial frontal and frontopolar discharges in absence. *Epilepsia* 45(12), pp. 1568–1579.
- Horikawa, K., Yamada, Y., Matsuda, T., Kobayashi, K., Hashimoto, M., Matsu-ura, T., Miyawaki, A., Michikawa, T., Mikoshiba, K. and Nagai, T. 2010. Spontaneous network activity visualized by ultrasensitive Ca(2+) indicators, yellow Cameleon-Nano. *Nature Methods* 7(9), pp. 729–732.
- Hornung, R., Pritchard, A., Kinchington, P.R. and Kramer, P.R. 2020. Reduced activity of GAD67 expressing cells in the reticular thalamus enhance thalamic excitatory activity and varicella zoster virus associated pain. *Neuroscience Letters* 736, p. 135287.
- Houades, V., Koulakoff, A., Ezan, P., Seif, I. and Giaume, C. 2008. Gap junction-mediated astrocytic networks in the mouse barrel cortex. *The Journal of Neuroscience* 28(20), pp. 5207–5217.
- Houades, V., Rouach, N., Ezan, P., Kirchhoff, F., Koulakoff, A. and Giaume, C. 2006. Shapes of astrocyte networks in the juvenile brain. *Neuron Glia Biology* 2(1), pp. 3–14.
- Hughes, S.W., Cope, D.W., Blethyn, K.L. and Crunelli, V. 2002. Cellular mechanisms of the slow (<1 Hz) oscillation in thalamocortical neurons in vitro. *Neuron* 33(6), pp. 947–958.
- Hughes, S.W., Lőrincz, M.L., Blethyn, K., Kékesi, K.A., Juhász, G., Turmaine, M., Parnavelas, J.G. and Crunelli, V. 2011. Thalamic Gap Junctions Control Local Neuronal Synchrony and Influence Macroscopic Oscillation Amplitude during EEG Alpha Rhythms. *Frontiers in Psychology* 2, p. 193.
- Huguenard, J. 2019. Current controversy: spikes, bursts, and synchrony in generalized absence epilepsy: unresolved questions regarding thalamocortical synchrony in absence epilepsy. *Epilepsy Currents* 19(2), pp. 105–111.
- Ingiosi, A.M., Hayworth, C.R., Harvey, D.O., Singletary, K.G., Rempe, M.J., Wisor, J.P. and Frank, M.G. 2020. A role for astroglial calcium in mammalian sleep and sleep regulation. *Current Biology* 30(22), pp. 4373–4383.e7.
- International League Against Epilepsy Consortium on Complex Epilepsies 2018. Genome-wide mega-analysis identifies 16 loci and highlights diverse biological mechanisms in the common epilepsies. *Nature Communications* 9(1), p. 5269.

- Ishige, K., Aizawa, M., Ito, Y. and Fukuda, H. 1996. γ -Butyrolactone-induced absence-like seizures increase nuclear CRE- and AP-1 DNA-binding activities in mouse brain. *Neuropharmacology* 35(1), pp. 45–55.
- Itoh, K. and Watanabe, M. 2009. Paradoxical facilitation of pentylenetetrazole-induced convulsion susceptibility in mice lacking neuronal nitric oxide synthase. *Neuroscience* 159(2), pp. 735–743.
- Itoh, K., Watanabe, M., Yoshikawa, K., Kanaho, Y., Berliner, L.J. and Fujii, H. 2004. Magnetic resonance and biochemical studies during pentylenetetrazole-kindling development: the relationship between nitric oxide, neuronal nitric oxide synthase and seizures. *Neuroscience* 129(3), pp. 757–766.
- Jafarian, M., Esmaeil Alipour, M. and Karimzadeh, F. 2020. Experimental models of absence epilepsy. *Basic and clinical neuroscience* 11(6), pp. 715–726.
- Jones, E.G. and Friedman, D.P. 1982. Thalamic basis of place- and modality-specific columns in monkey somatosensory cortex: a correlative anatomical and physiological study. *Journal of Neurophysiology* 48(2), pp. 545–68.
- Jouveneau, A., Eunson, L.H., Spauschus, A., Ramesh, V., Zuberi, S.M., Kullmann, D.M. and Hanna, M.G. 2001. Human epilepsy associated with dysfunction of the brain P/Q-type calcium channel. *The Lancet* 358(9284), pp. 801–807.
- Kang, N., Xu, J., Xu, Q., Nedergaard, M. and Kang, J. 2005. Astrocytic glutamate release-induced transient depolarization and epileptiform discharges in hippocampal CA1 pyramidal neurons. *Journal of Neurophysiology* 94(6), pp. 4121–4130.
- Keller, D., Erö, C. and Markram, H. 2018. Cell densities in the mouse brain: A systematic review. *Frontiers in Neuroanatomy* 12, p. 83.
- Kessler, Sudha Kilaru and McGinnis, E. 2019. A practical guide to treatment of childhood absence epilepsy. *Paediatric drugs* 21(1), pp. 15–24.
- Kettenmann, H. and Verkhratsky, A. 2011. [Neuroglia--living nerve glue]. *Fortschritte der Neurologie-Psychiatrie* 79(10), pp. 588–597.
- Khakh, B.S. and McCarthy, K.D. 2015. Astrocyte calcium signaling: from observations to functions and the challenges therein. *Cold Spring Harbor Perspectives in Biology* 7(4), p. a020404.
- Khakh, B.S. and Sofroniew, M.V. 2015. Diversity of astrocyte functions and phenotypes in neural circuits. *Nature Neuroscience* 18(7), pp. 942–952.
- Kofuji, P. and Newman, E.A. 2004. Potassium buffering in the central nervous system. *Neuroscience* 129(4), pp. 1045–1056.
- Koralek, K.A., Olavarria, J. and Killackey, H.P. 1990. Areal and laminar organization of corticocortical projections in the rat somatosensory cortex. *The Journal of Comparative Neurology* 299(2), pp. 133–150.
- Kustikova, V., Krivonosov, M. and Pimashkin, A. 2018. CalciumCV: Computer vision software for calcium signaling in astrocytes. In: van der Aalst W. et al. (eds) *Analysis of Images, Social Networks and Texts. AIST 2018. Lecture Notes in Computer Science*, vol 11179. Springer, Cham.
- Lannes, B., Micheletti, G., Vergnes, M., Marescaux, C., Depaulis, A. and Warter, J.M. 1988. Relationship between spike-wave discharges and vigilance levels in rats with spontaneous petit mal-like epilepsy. *Neuroscience Letters* 94(1-2), pp. 187–191.

- Lapato, A.S. and Tiwari-Woodruff, S.K. 2018. Connexins and pannexins: At the junction of neuro-glial homeostasis & disease. *Journal of Neuroscience Research* 96(1), pp. 31–44.
- Leal, A., Vieira, J.P., Lopes, R., Nunes, R.G., Gonçalves, S.I., Lopes da Silva, F. and Figueiredo, P. 2016. Dynamics of epileptic activity in a peculiar case of childhood absence epilepsy and correlation with thalamic levels of GABA. *Epilepsy & behavior case reports* 5, pp. 57–65.
- Lee, H.S., Ghetti, A., Pinto-Duarte, A., Wang, X., Dziewczapolski, G., Galimi, F., Huitron-Resendiz, S., Piña-Crespo, J.C., Roberts, A.J., Verma, I.M., Sejnowski, T.J. and Heinemann, S.F. 2014. Astrocytes contribute to gamma oscillations and recognition memory. *Proceedings of the National Academy of Sciences of the United States of America* 111(32), pp. E3343–52.
- Lee, S., Hwang, E., Lee, M. and Choi, J.H. 2019. Distinct Topographical Patterns of Spike-Wave Discharge in Transgenic and Pharmacologically Induced Absence Seizure Models. *Experimental neurobiology* 28(4), pp. 474–484.
- Lee, S.H., Magge, S., Spencer, D.D., Sontheimer, H. and Cornell-Bell, A.H. 1995. Human epileptic astrocytes exhibit increased gap junction coupling. *Glia* 15(2), pp. 195–202.
- Letts, V.A. 2005. Stargazer—a mouse to seize! *Epilepsy currents* 5(5), pp. 161–165.
- Li, Q., Luo, C., Yang, T., Yao, Z., He, L., Liu, L., Xu, H., Gong, Q., Yao, D. and Zhou, D. 2009. EEG-fMRI study on the interictal and ictal generalized spike-wave discharges in patients with childhood absence epilepsy. *Epilepsy Research* 87(2-3), pp. 160–168.
- Lia, A., Henriques, V.J., Zonta, M., Chiavegato, A., Carmignoto, G., Gómez-Gonzalo, M. and Losi, G. 2021. Calcium signals in astrocyte microdomains, a decade of great advances. *Frontiers in Cellular Neuroscience* 15, p. 673433.
- Liang, J., Zhang, Y., Wang, J., Pan, H., Wu, H., Xu, K., Liu, X., Jiang, Y., Shen, Y. and Wu, X. 2006. New variants in the CACNA1H gene identified in childhood absence epilepsy. *Neuroscience Letters* 406(1-2), pp. 27–32.
- Lind, B.L., Brazhe, A.R., Jessen, S.B., Tan, F.C.C. and Lauritzen, M.J. 2013. Rapid stimulus-evoked astrocyte Ca²⁺ elevations and hemodynamic responses in mouse somatosensory cortex in vivo. *Proceedings of the National Academy of Sciences of the United States of America* 110(48), pp. E4678–87.
- Lind, B.L., Jessen, S.B., Lønstrup, M., Joséphine, C., Bonvento, G. and Lauritzen, M. 2018. Fast Ca²⁺ responses in astrocyte end-feet and neurovascular coupling in mice. *Glia* 66(2), pp. 348–358.
- Lines, J., Martin, E.D., Kofuji, P., Aguilar, J. and Araque, A. 2020. Astrocytes modulate sensory-evoked neuronal network activity. *Nature Communications* 11(1), p. 3689.
- Lingenhoehl, K., Brom, R., Heid, J., Beck, P. and Froestl, W. 1999. γ -Hydroxybutyrate is a weak agonist at recombinant GABAB receptors. *Neuropharmacology* 38(11), pp. 1667–73.
- Lohr, C., Beiersdorfer, A., Fischer, T., Hirnet, D., Rotermund, N., Sauer, J., Schulz, K. and Gee, C.E. 2021. Using genetically encoded calcium indicators to study astrocyte physiology: A field guide. *Frontiers in Cellular Neuroscience* 15, p. 690147.
- Lübke, J., Roth, A., Feldmeyer, D. and Sakmann, B. 2003. Morphometric analysis of the columnar innervation domain of neurons connecting layer 4 and layer 2/3 of juvenile rat barrel cortex. *Cerebral Cortex* 13(10), pp. 1051–1063.

- Ludwin, S.K., Kosek, J.C. and Eng, L.F. 1976. The topographical distribution of S-100 and GFA proteins in the adult rat brain: an immunohistochemical study using horseradish peroxidase-labelled antibodies. *The Journal of Comparative Neurology* 165(2), pp. 197–207.
- Luo, C., Xia, Y., Li, Q., Xue, K., Lai, Y., Gong, Q., Zhou, D. and Yao, D. 2011. Diffusion and volumetry abnormalities in subcortical nuclei of patients with absence seizures. *Epilepsia* 52(6), pp. 1092–1099.
- Maheshwari, A. and Noebels, J.L. 2014. Monogenic models of absence epilepsy: windows into the complex balance between inhibition and excitation in thalamocortical microcircuits. *Progress in Brain Research* 213, pp. 223–252.
- Maitre, M. 1997. The γ -hydroxybutyrate signalling system in brain: organization and functional implications. *Progress in neurobiology* 51(3), pp. 337–61.
- Malarkey, E.B. and Parpura, V. 2008. Mechanisms of glutamate release from astrocytes. *Neurochemistry International* 52(1-2), pp. 142–154.
- Manning, J.-P.A., Richards, D.A. and Bowery, N.G. 2003. Pharmacology of absence epilepsy. *Trends in Pharmacological Sciences* 24(10), pp. 542–549.
- Manning, J.P.A., Richards, D.A., Leresche, N., Crunelli, V. and Bowery, N.G. 2004. Cortical-area specific block of genetically determined absence seizures by ethosuximide. *Neuroscience* 123(1), pp. 5–9.
- Marescaux, C., Vergnes, M. and Depaulis, A. 1992. Genetic absence epilepsy in rats from Strasbourg--a review. *Journal of Neural Transmission. Supplementum* 35, pp. 37–69.
- Mariotti, L., Losi, G., Lia, A., Melone, M., Chiavegato, A., Gómez-Gonzalo, M., Sessolo, M., Bovetti, S., Forli, A., Zonta, M., Requeie, L.M., Marcon, I., Pugliese, A., Viollet, C., Bettler, B., Fellin, T., Conti, F. and Carmignoto, G. 2018. Interneuron-specific signaling evokes distinctive somatostatin-mediated responses in adult cortical astrocytes. *Nature Communications* 9(1), p. 82.
- Mariotti, L., Losi, G., Sessolo, M., Marcon, I. and Carmignoto, G. 2016. The inhibitory neurotransmitter GABA evokes long-lasting Ca(2+) oscillations in cortical astrocytes. *Glia* 64(3), pp. 363–373.
- Masur, D., Shinnar, S., Cnaan, A., Shinnar, R.C., Clark, P., Wang, J., Weiss, E.F., Hirtz, D.G., Glauser, T.A. and Childhood Absence Epilepsy Study Group 2013. Pretreatment cognitive deficits and treatment effects on attention in childhood absence epilepsy. *Neurology* 81(18), pp. 1572–1580.
- Mathivet, P., Bernasconi, R., Barry, J.D., Marescaux, C. and Bittiger, H. 1997. Binding characteristics of γ -hydroxybutyric acid as a weak but selective GABAB receptor agonist. *European Journal of Pharmacology* 321(1), pp. 67–75.
- Matricardi, S., Verrotti, A., Chiarelli, F., Cerminara, C. and Curatolo, P. 2014. Current advances in childhood absence epilepsy. *Pediatric Neurology* 50(3), pp. 205–212.
- Matyash, V. and Kettenmann, H. 2010. Heterogeneity in astrocyte morphology and physiology. *Brain Research Reviews* 63(1-2), pp. 2–10.
- Mauleon, G., Lo, J.F., Peterson, B.L., Fall, C.P. and Eddington, D.T. 2013. Enhanced loading of Fura-2/AM calcium indicator dye in adult rodent brain slices via a microfluidic oxygenator. *Journal of Neuroscience Methods* 216(2), pp. 110–117.
- McCafferty, C., David, F., Venzi, M., Lőrincz, M.L., Delicata, F., Atherton, Z., Recchia, G., Orban, G., Lambert, R.C., Di Giovanni, G., Leresche, N. and Crunelli, V. 2018. Cortical drive and thalamic feed-forward inhibition control thalamic output synchrony during absence seizures. *Nature Neuroscience* 21(5), pp. 744–756.

- Meeren, H.K.M., Pijn, J.P.M., Van Luijtelaar, E.L.J.M., Coenen, A.M.L. and Lopes da Silva, F.H. 2002. Cortical focus drives widespread corticothalamic networks during spontaneous absence seizures in rats. *The Journal of Neuroscience* 22(4), pp. 1480–1495.
- Meerlo, P., Westerveld, P., Turek, F.W. and Koehl, M. 2004. Effects of gamma-hydroxybutyrate (GHB) on vigilance states and EEG in mice. *Sleep* 27(5), pp. 899–904.
- Meyer, J., Maheshwari, A., Noebels, J. and Smirnakis, S. 2018. Asynchronous suppression of visual cortex during absence seizures in stargazer mice. *Nature Communications* 9(1), p. 1938.
- Min, R. and Nevian, T. 2012. Astrocyte signaling controls spike timing-dependent depression at neocortical synapses. *Nature Neuroscience* 15(5), pp. 746–753.
- Miotto, K., Darakjian, J. and Basch, J. 2001. Gamma-hydroxybutyric acid: patterns of use, effects and withdrawal. *American Journal on Addictions* 10(3), pp. 232–41.
- Miyamoto, H., Tatsukawa, T., Shimohata, A., Yamagata, T., Suzuki, T., Amano, K., Mazaki, E., Raveau, M., Ogiwara, I., Oba-Asaka, A., Hensch, T.K., Itohara, S., Sakimura, K., Kobayashi, Kenta, Kobayashi, Kazuto and Yamakawa, K. 2019. Impaired cortico-striatal excitatory transmission triggers epilepsy. *Nature Communications* 10(1), p. 1917.
- Mukamel, E.A., Nimmerjahn, A. and Schnitzer, M.J. 2009. Automated analysis of cellular signals from large-scale calcium imaging data. *Neuron* 63(6), pp. 747–760.
- Nagelhus, E.A. and Ottersen, O.P. 2013. Physiological roles of aquaporin-4 in brain. *Physiological Reviews* 93(4), pp. 1543–1562.
- Nagy, J.I., Dudek, F.E. and Rash, J.E. 2004. Update on connexins and gap junctions in neurons and glia in the mammalian nervous system. *Brain Research. Brain Research Reviews* 47(1-3), pp. 191–215.
- Navarrete, M., Perea, G., Maglio, L., Pastor, J., García de Sola, R. and Araque, A. 2013. Astrocyte calcium signal and gliotransmission in human brain tissue. *Cerebral Cortex* 23(5), pp. 1240–1246.
- Nedergaard, M. 1994. Direct signaling from astrocytes to neurons in cultures of mammalian brain cells. *Science* 263(5154), pp. 1768–1771.
- Nedergaard, M., Ransom, B. and Goldman, S.A. 2003. New roles for astrocytes: redefining the functional architecture of the brain. *Trends in Neurosciences* 26(10), pp. 523–530.
- Nett, W.J., Oloff, S.H. and McCarthy, K.D. 2002. Hippocampal astrocytes in situ exhibit calcium oscillations that occur independent of neuronal activity. *Journal of Neurophysiology* 87(1), pp. 528–537.
- Nicolelis, M.A., Baccala, L.A., Lin, R.C. and Chapin, J.K. 1995. Sensorimotor encoding by synchronous neural ensemble activity at multiple levels of the somatosensory system. *Science* 268(5215), pp. 1353–1358.
- Nicolelis, M.A.L. and Fanselow, E.E. 2002. Thalamocortical optimization of tactile processing according to behavioral state. *Nature neuroscience*.
- Nimmerjahn, A. 2009. Astrocytes going live: advances and challenges. *The Journal of Physiology* 587(Pt 8), pp. 1639–1647.
- Nimmerjahn, A., Mukamel, E.A. and Schnitzer, M.J. 2009. Motor behavior activates Bergmann glial networks. *Neuron* 62(3), pp. 400–412.

- Noebels, J.L. 1984. A single gene error of noradrenergic axon growth synchronizes central neurones. *Nature* 310(5976), pp. 409–411.
- Noebels, J.L., Qiao, X., Bronson, R.T., Spencer, C. and Davisson, M.T. 1990. Stargazer: a new neurological mutant on chromosome 15 in the mouse with prolonged cortical seizures. *Epilepsy Research* 7(2), pp. 129–135.
- Snead, O.C. 1987. Noradrenergic mechanisms in γ -hydroxybutyrate-induced seizure activity. *European journal of pharmacology*.
- Oe, Y., Wang, X., Patriarchi, T., Konno, A., Ozawa, K., Yahagi, K., Hirai, H., Tsuboi, T., Kitaguchi, T., Tian, L., McHugh, T.J. and Hirase, H. 2020. Distinct temporal integration of noradrenaline signaling by astrocytic second messengers during vigilance. *Nature Communications* 11(1), p. 471.
- Oliveira, J.F., Sardinha, V.M., Guerra-Gomes, S., Araque, A. and Sousa, N. 2015. Do stars govern our actions? Astrocyte involvement in rodent behavior. *Trends in Neurosciences* 38(9), pp. 535–549.
- Orlandi, J.G., Comella-Bolla, A. and Masana, M. 2017. NETCAL: an interactive platform for large-scale, NETWORK and population dynamics analysis of CALcium imaging recordings. *Neuroscience*.
- Ortinski, P.I., Dong, J., Mungenast, A., Yue, C., Takano, H., Watson, D.J., Haydon, P.G. and Coulter, D.A. 2010. Selective induction of astrocytic gliosis generates deficits in neuronal inhibition. *Nature Neuroscience* 13(5), pp. 584–591.
- Otsu, N. 1979. A Threshold Selection Method from Gray-Level Histograms. *IEEE transactions on systems, man, and cybernetics* 9(1), pp. 62–66.
- Ozbay, B.N., Futia, G.L., Ma, M., Bright, V.M., Gopinath, J.T., Hughes, E.G., Restrepo, D. and Gibson, E.A. 2018. Three dimensional two-photon brain imaging in freely moving mice using a miniature fiber coupled microscope with active axial-scanning. *Scientific Reports* 8(1), p. 8108.
- Pachitariu, M., Stringer, C., Schröder, S., Dipoppa, M., Rossi, L.F., Carandini, M. and Harris, K.D. 2016. Suite2p: beyond 10,000 neurons with standard two-photon microscopy. *BioRxiv*.
- Panatier, A., Vallée, J., Haber, M., Murai, K.K., Lacaille, J.-C. and Robitaille, R. 2011. Astrocytes are endogenous regulators of basal transmission at central synapses. *Cell* 146(5), pp. 785–798.
- Panayiotopoulos, C.P. 2001. Treatment of typical absence seizures and related epileptic syndromes. *Paediatric drugs* 3(5), pp. 379–403.
- Pannasch, U., Vargová, L., Reingruber, J., Ezan, P., Holcman, D., Giaume, C., Syková, E. and Rouach, N. 2011. Astroglial networks scale synaptic activity and plasticity. *Proceedings of the National Academy of Sciences of the United States of America* 108(20), pp. 8467–8472.
- Park, K. and Lee, S.J. 2020. Deciphering the star codings: astrocyte manipulation alters mouse behavior. *Experimental & Molecular Medicine* 52, pp. 1028–1038.
- Parpura, V., Basarsky, T.A., Liu, F., Jęftinija, K., Jęftinija, S. and Haydon, P.G. 1994. Glutamate-mediated astrocyte-neuron signalling. *Nature* 369(6483), pp. 744–747.
- Parri, H.R. and Crunelli, V. 2001. Pacemaker calcium oscillations in thalamic astrocytes in situ. *Neuroreport* 12(18), pp. 3897–3900.
- Parri, H.R. and Crunelli, V. 2003. The role of Ca²⁺ in the generation of spontaneous astrocytic Ca²⁺ oscillations. *Neuroscience* 120(4), pp. 979–992.

- Parri, H.R., Gould, T.M. and Crunelli, V. 2010. Sensory and cortical activation of distinct glial cell subtypes in the somatosensory thalamus of young rats. *The European Journal of Neuroscience* 32(1), pp. 29–40.
- Parri, H.R., Gould, T.M. and Crunelli, V. 2001. Spontaneous astrocytic Ca²⁺ oscillations in situ drive NMDAR-mediated neuronal excitation. *Nature Neuroscience* 4(8), pp. 803–812.
- Pasti, L., Volterra, A., Pozzan, T. and Carmignoto, G. 1997. Intracellular calcium oscillations in astrocytes: a highly plastic, bidirectional form of communication between neurons and astrocytes in situ. *The Journal of Neuroscience* 17(20), pp. 7817–7830.
- Paukert, M., Agarwal, A., Cha, J., Doze, V.A., Kang, J.U. and Bergles, D.E. 2014. Norepinephrine controls astroglial responsiveness to local circuit activity. *Neuron* 82(6), pp. 1263–1270.
- Paxinos, G. and Franklin, K.B.J. 2001. The mouse brain in stereotaxic coordinates. 2001 Academic Press. *San Diego*.
- Paz, J.T., Deniau, J.-M. and Charpier, S. 2005. Rhythmic bursting in the cortico-subthalamo-pallidal network during spontaneous genetically determined spike and wave discharges. *The Journal of Neuroscience* 25(8), pp. 2092–2101.
- Pelvig, D.P., Pakkenberg, H., Stark, A.K. and Pakkenberg, B. 2008. Neocortical glial cell numbers in human brains. *Neurobiology of Aging* 29(11), pp. 1754–1762.
- Perea, G. and Araque, A. 2005. Properties of synaptically evoked astrocyte calcium signal reveal synaptic information processing by astrocytes. *The Journal of Neuroscience* 25(9), pp. 2192–2203.
- Perea, G., Gómez, R., Mederos, S., Covelos, A., Ballesteros, J.J., Schlosser, L., Hernández-Vivanco, A., Martín-Fernández, M., Quintana, R., Rayan, A., Díez, A., Fuenzalida, M., Agarwal, A., Bergles, D.E., Bettler, B., Manahan-Vaughan, D., Martín, E.D., Kirchhoff, F. and Araque, A. 2016. Activity-dependent switch of GABAergic inhibition into glutamatergic excitation in astrocyte-neuron networks. *eLife* 5.
- Perea, G., Navarrete, M. and Araque, A. 2009. Tripartite synapses: astrocytes process and control synaptic information. *Trends in Neurosciences* 32(8), pp. 421–431.
- Perez-Reyes, E. 2003. Molecular physiology of low-voltage-activated t-type calcium channels. *Physiological Reviews* 83(1), pp. 117–161.
- Petersen, C.C. and Sakmann, B. 2001. Functionally independent columns of rat somatosensory barrel cortex revealed with voltage-sensitive dye imaging. *The Journal of Neuroscience* 21(21), pp. 8435–8446.
- Petersen, C.C.H. 2007. The functional organization of the barrel cortex. *Neuron* 56(2), pp. 339–355.
- Petravicz, J., Fiacco, T.A. and McCarthy, K.D. 2008. Loss of IP3 receptor-dependent Ca²⁺ increases in hippocampal astrocytes does not affect baseline CA1 pyramidal neuron synaptic activity. *The Journal of Neuroscience* 28(19), pp. 4967–4973.
- Pinault, D., Vergnes, M. and Marescaux, C. 2001. Medium-voltage 5-9-Hz oscillations give rise to spike-and-wave discharges in a genetic model of absence epilepsy: in vivo dual extracellular recording of thalamic relay and reticular neurons. *Neuroscience* 105(1), pp. 181–201.
- Pirttimaki, T., Parri, H.R. and Crunelli, V. 2013. Astrocytic GABA transporter GAT-1 dysfunction in experimental absence seizures. *The Journal of Physiology* 591(4), pp. 823–833.

- Pirttimaki, T.M., Cope, D.W., Parri, H.R. and Crunelli, V. 2010. Glial signalling in the ventrobasal thalamus of rats with absence seizures. *Soc Neurosci Abstr*.
- Pirttimaki, T.M., Hall, S.D. and Parri, H.R. 2011. Sustained neuronal activity generated by glial plasticity. *The Journal of Neuroscience* 31(21), pp. 7637–7647.
- Pirttimaki, T.M. and Parri, H.R. 2013. Astrocyte plasticity: implications for synaptic and neuronal activity. *The Neuroscientist* 19(6), pp. 604–615.
- Pirttimaki, T.M., Sims, R.E., Saunders, G., Antonio, S.A., Codadu, N.K. and Parri, H.R. 2017. Astrocyte-Mediated Neuronal Synchronization Properties Revealed by False Gliotransmitter Release. *The Journal of Neuroscience* 37(41), pp. 9859–9870.
- Pistis, M., Muntoni, A.L., Pillolla, G., Perra, S. and Cignarella, G. 2005. γ -Hydroxybutyric acid (GHB) and the mesoaccumbens reward circuit: Evidence for GABAB receptor-mediated effects. *Neuroscience* 131(2), pp. 465–74.
- Polack, P.-O. and Charpier, S. 2009. Ethosuximide converts ictogenic neurons initiating absence seizures into normal neurons in a genetic model. *Epilepsia* 50(7), pp. 1816–1820.
- Polack, P.-O., Guillemain, I., Hu, E., Deransart, C., Depaulis, A. and Charpier, S. 2007. Deep layer somatosensory cortical neurons initiate spike-and-wave discharges in a genetic model of absence seizures. *The Journal of Neuroscience* 27(24), pp. 6590–6599.
- Polack, P.-O., Mahon, S., Chavez, M. and Charpier, S. 2009. Inactivation of the somatosensory cortex prevents paroxysmal oscillations in cortical and related thalamic neurons in a genetic model of absence epilepsy. *Cerebral Cortex* 19(9), pp. 2078–2091.
- Porter, J.T. and McCarthy, K.D. 1996. Hippocampal astrocytes in situ respond to glutamate released from synaptic terminals. *The Journal of Neuroscience* 16(16), pp. 5073–5081.
- Poskanzer, K.E. and Yuste, R. 2016. Astrocytes regulate cortical state switching in vivo. *Proceedings of the National Academy of Sciences of the United States of America* 113(19), pp. E2675–84.
- Poskanzer, K.E. and Yuste, R. 2011. Astrocytic regulation of cortical UP states. *Proceedings of the National Academy of Sciences of the United States of America* 108(45), pp. 18453–18458.
- Pow, D.V., Sullivan, R.K.P., Williams, S.M., Scott, H.L., Dodd, P.R. and Finkelstein, D. 2005. Differential expression of the GABA transporters GAT-1 and GAT-3 in brains of rats, cats, monkeys and humans. *Cell and Tissue Research* 320(3), pp. 379–392.
- Ransom, B., Behar, T. and Nedergaard, M. 2003. New roles for astrocytes (stars at last). *Trends in Neurosciences* 26(10), pp. 520–522.
- Ravizza, T., Gagliardi, B., Noé, F., Boer, K., Aronica, E. and Vezzani, A. 2008. Innate and adaptive immunity during epileptogenesis and spontaneous seizures: evidence from experimental models and human temporal lobe epilepsy. *Neurobiology of Disease* 29(1), pp. 142–160.
- Reeves, A.M.B., Shigetomi, E. and Khakh, B.S. 2011. Bulk loading of calcium indicator dyes to study astrocyte physiology: key limitations and improvements using morphological maps. *The Journal of Neuroscience* 31(25), pp. 9353–9358.

- Reimer, J., McGinley, M.J., Liu, Y., Rodenkirch, C., Wang, Q., McCormick, D.A. and Tolias, A.S. 2016. Pupil fluctuations track rapid changes in adrenergic and cholinergic activity in cortex. *Nature Communications* 7, p. 13289.
- Resendez, S.L., Jennings, J.H., Ung, R.L., Namboodiri, V.M.K., Zhou, Z.C., Otis, J.M., Nomura, H., McHenry, J.A., Kosyk, O. and Stuber, G.D. 2016. Visualization of cortical, subcortical and deep brain neural circuit dynamics during naturalistic mammalian behavior with head-mounted microscopes and chronically implanted lenses. *Nature Protocols* 11(3), pp. 566–597.
- Robbins, M., Christensen, C.N. and Kaminski, C.F. 2021. Calcium imaging analysis—how far have we come? *F1000Research* 10(258).
- Rosenfalck, A. 1969. Somatic sensation: transfer and processing of information. Peripheral nerve. *Electroencephalography and Clinical Neurophysiology* 27(7), p. 654.
- Roth, R.H. and Giarman, N.J. 1966. Butyrolactone and gamma hydroxybutyric acid. Distribution and metabolism. *Biochem Pharmacol.*
- Russell, J.T. 2011. Imaging calcium signals in vivo: a powerful tool in physiology and pharmacology. *British Journal of Pharmacology* 163(8), pp. 1605–1625.
- Sanchez Panchuelo, R.M., Besle, J., Schluppeck, D., Humberstone, M. and Francis, S. 2018. Somatotopy in the human somatosensory system. *Frontiers in Human Neuroscience* 12, p. 235.
- Sarkisova, Karine and van Luijtelaar, G. 2011. The WAG/Rij strain: a genetic animal model of absence epilepsy with comorbidity of depression [corrected]. *Progress in Neuro-Psychopharmacology & Biological Psychiatry* 35(4), pp. 854–876.
- Scheffer, I.E., Berkovic, S., Capovilla, G., Connolly, M.B., French, J., Guilhoto, L., Hirsch, E., Jain, S., Mathern, G.W., Moshé, S.L., Nordli, D.R., Perucca, E., Tomson, T., Wiebe, S., Zhang, Y.-H. and Zuberi, S.M. 2017. ILAE classification of the epilepsies: Position paper of the ILAE Commission for Classification and Terminology. *Epilepsia* 58(4), pp. 512–521.
- Schipke, C.G., Haas, B. and Kettenmann, H. 2008. Astrocytes discriminate and selectively respond to the activity of a subpopulation of neurons within the barrel cortex. *Cerebral Cortex* 18(10), pp. 2450–2459.
- Seifert, G. and Steinhäuser, C. 2013. Neuron-astrocyte signaling and epilepsy. *Experimental Neurology* 244, pp. 4–10.
- Shao, Y. and McCarthy, K.D. 1995. Receptor-mediated calcium signals in astroglia: multiple receptors, common stores and all-or-nothing responses. *Cell Calcium* 17(3), pp. 187–196.
- Shepherd, G.M.G., Yamawaki, N. 2021. Untangling the cortico-thalamo-cortical loop: cellular pieces of a knotty circuit puzzle. *Nature Reviews Neuroscience* 22, pp. 389–406.
- Shigetomi, E., Bushong, E.A., Hausteiner, M.D., Tong, X., Jackson-Weaver, O., Kracun, S., Xu, J., Sofroniew, M.V., Ellisman, M.H. and Khakh, B.S. 2013a. Imaging calcium microdomains within entire astrocyte territories and endfeet with GCaMPs expressed using adeno-associated viruses. *The Journal of General Physiology* 141(5), pp. 633–647.
- Shigetomi, E., Jackson-Weaver, O., Huckstepp, R.T., O'Dell, T.J. and Khakh, B.S. 2013b. TRPA1 channels are regulators of astrocyte basal calcium levels and long-term potentiation via constitutive D-serine release. *The Journal of Neuroscience* 33(24), pp. 10143–10153.

- Shigetomi, E., Patel, S. and Khakh, B.S. 2016. Probing the complexities of astrocyte calcium signaling. *Trends in Cell Biology* 26(4), pp. 300–312.
- Shinnar, R.C., Shinnar, S., Cnaan, A., Clark, P., Dlugos, D., Hirtz, D.G., Hu, F., Liu, C., Masur, D., Weiss, E.F., Glauser, T.A. and Childhood Absence Epilepsy Study Group 2017. Pretreatment behavior and subsequent medication effects in childhood absence epilepsy. *Neurology* 89(16), pp. 1698–1706.
- Sitnikova, E. 2009. The role of somatosensory cortex in absence epilepsy (studies in genetic rat model). *Brain Research* 2(5).
- Sitnikova, E., Smirnov, K. and Raevsky, V.V. 2020. Sensory Inflow from Whiskers Modulates Development of Absence Epilepsy in WAG/Rij Rats. *International Conference on Cognitive Sciences*, pp 510–519.
- Sitnikova, E. and van Luijtelaar, G. 2005. Reduction of adrenergic neurotransmission with clonidine aggravates spike-wave seizures and alters activity in the cortex and the thalamus in WAG/Rij rats. *Brain research bulletin* 64(6), pp. 533–40.
- Slezak, M., Kandler, S., Van Veldhoven, P.P., Van den Haute, C., Bonin, V. and Holt, M.G. 2019. Distinct Mechanisms for Visual and Motor-Related Astrocyte Responses in Mouse Visual Cortex. *Current Biology* 29(18), pp. 3120–3127.e5.
- Snead, O.C., Banerjee, P.K., Burnham, M. and Hampson, D. 2000. Modulation of absence seizures by the GABA(A) receptor: a critical role for metabotropic glutamate receptor 4 (mGluR4). *The Journal of Neuroscience* 20(16), pp. 6218–6224.
- Sofroniew, M.V. and Vinters, H.V. 2010. Astrocytes: biology and pathology. *Acta Neuropathologica* 119(1), pp. 7–35.
- Sonoda, K., Matsui, T., Bito, H. and Ohki, K. 2018. Astrocytes in the mouse visual cortex reliably respond to visual stimulation. *Biochemical and Biophysical Research Communications* 505(4), pp. 1216–1222.
- Soso, M.J. and Fetz, E.E. 1980. Responses of identified cells in postcentral cortex of awake monkeys during comparable active and passive joint movements. *Journal of Neurophysiology* 43(4), pp. 1090–1110.
- Srinivasan, R., Huang, B.S., Venugopal, S., Johnston, A.D., Chai, H., Zeng, H., Golshani, P. and Khakh, B.S. 2015. Ca(2+) signaling in astrocytes from *Ip3r2(-/-)* mice in brain slices and during startle responses in vivo. *Nature Neuroscience* 18(5), pp. 708–717.
- Steriade, M., Nuñez, A. and Amzica, F. 1993. A novel slow (< 1 Hz) oscillation of neocortical neurons in vivo: depolarizing and hyperpolarizing components. *The Journal of Neuroscience* 13(8), pp. 3252–3265.
- Stobart, J.L., Ferrari, K.D., Barrett, M.J.P., Glück, C., Stobart, M.J., Zuend, M. and Weber, B. 2018a. Cortical circuit activity evokes rapid astrocyte calcium signals on a similar timescale to neurons. *Neuron* 98(4), pp. 726–735.e4.
- Stobart, J.L., Ferrari, K.D., Barrett, M.J.P. and Stobart, M.J. 2018b. Long-term in vivo calcium imaging of astrocytes reveals distinct cellular compartment responses to sensory stimulation. *Cerebral cortex* 28(1), pp. 184–198.
- Straub, S.V. and Nelson, M.T. 2007. Astrocytic calcium signaling: the information currency coupling neuronal activity to the cerebral microcirculation. *Trends in cardiovascular medicine* 17(6), pp. 183–190.
- Studer, F., Laghouati, E., Jarre, G., David, O., Pouyatos, B. and Depaulis, A. 2019. Sensory coding is impaired in rat absence epilepsy. *The Journal of Physiology* 597(3), pp. 951–966.

- Sun, H., Blakely, T.M., Darvas, F., Wander, J.D., Johnson, L.A., Su, D.K., Miller, K.J., Fetz, E.E. and Ojemann, J.G. 2015. Sequential activation of premotor, primary somatosensory and primary motor areas in humans during cued finger movements. *Clinical Neurophysiology* 126(11), pp. 2150–2161.
- Szokol, K., Heuser, K., Tang, W., Jensen, V., Enger, R., Bedner, P., Steinhäuser, C., Taubøll, E., Ottersen, O.P. and Nagelhus, E.A. 2015. Augmentation of Ca²⁺ signaling in astrocytic endfeet in the latent phase of temporal lobe epilepsy. *Frontiers in Cellular Neuroscience* 9, p. 49.
- Takata, N., Mishima, T., Hisatsune, C., Nagai, T., Ebisui, E., Mikoshiba, K. and Hirase, H. 2011. Astrocyte calcium signaling transforms cholinergic modulation to cortical plasticity in vivo. *The Journal of Neuroscience* 31(49), pp. 18155–18165.
- Takata, N., Sugiura, Y., Yoshida, K., Koizumi, M., Hiroshi, N., Honda, K., Yano, R., Komaki, Y., Matsui, K., Suematsu, M., Mimura, M., Okano, H. and Tanaka, K.F. 2018. Optogenetic astrocyte activation evokes BOLD fMRI response with oxygen consumption without neuronal activity modulation. *Glia* 66(9), pp. 2013–2023.
- Tan, L.L., Oswald, M.J., Heintz, C., Retana Romero, O.A., Kaushalya, S.K., Monyer, H. and Kuner, R. 2019. Gamma oscillations in somatosensory cortex recruit prefrontal and descending serotonergic pathways in aversion and nociception. *Nature Communications* 10(1), p. 983.
- Tangwiriyasakul, C., Perani, S., Centeno, M., Yaakub, S.N., Abela, E., Carmichael, D.W. and Richardson, M.P. 2018. Dynamic brain network states in human generalized spike-wave discharges. *Brain: A Journal of Neurology* 141(10), pp. 2981–2994.
- Tashiro, A., Goldberg, J. and Yuste, R. 2002. Calcium oscillations in neocortical astrocytes under epileptiform conditions. *Journal of Neurobiology* 50(1), pp. 45–55.
- Tenney, J.R., Fujiwara, H., Horn, P.S., Jacobson, S.E., Glauser, T.A. and Rose, D.F. 2013. Focal corticothalamic sources during generalized absence seizures: a MEG study. *Epilepsy Research* 106(1-2), pp. 113–122.
- Thompson, K.J., Khajehali, E., Bradley, S.J., Navarrete, J.S., Huang, X.P., Slocum, S., Jin, J., Liu, J., Xiong, Y., Olsen, R.H.J., Diberto, J.F., Boyt, K.M., Pina, M.M., Pati, D., Molloy, C., Bundgaard, C., Sexton, P.M., Kash, T.L., Krashes, M.J., Christopoulos, A., Roth, B.L. and Tobin, A.B. 2018. DREADD Agonist 21 Is an Effective Agonist for Muscarinic-Based DREADDs in Vitro and in Vivo. *ACS pharmacology & translational science* 1(1), pp. 61–72.
- Thrane, A.S., Rangroo Thrane, V., Zeppenfeld, D., Lou, N., Xu, Q., Nagelhus, E.A. and Nedergaard, M. 2012. General anesthesia selectively disrupts astrocyte calcium signaling in the awake mouse cortex. *Proceedings of the National Academy of Sciences of the United States of America* 109(46), pp. 18974–18979.
- Tian, G.-F., Azmi, H., Takano, T., Xu, Q., Peng, W., Lin, J., Oberheim, N., Lou, N., Wang, X., Zielke, H.R., Kang, J. and Nedergaard, M. 2005. An astrocytic basis of epilepsy. *Nature Medicine* 11(9), pp. 973–981.
- Tischbirek, C., Birkner, A., Jia, H., Sakmann, B. and Konnerth, A. 2015. Deep two-photon brain imaging with a red-shifted fluorometric Ca²⁺ indicator. *Proceedings of the National Academy of Sciences of the United States of America* 112(36), pp. 11377–11382.
- Torres, A., Wang, F., Xu, Q. and Fujita, T. 2012. Extracellular Ca²⁺ acts as a mediator of communication from neurons to glia. *Science Signal* 5(208).

- Touret, M., Parrot, S., Denoroy, L., Belin, M.-F. and Didier-Bazes, M. 2007. Glutamatergic alterations in the cortex of genetic absence epilepsy rats. *BMC Neuroscience* 8, p. 69.
- Ugale, R.R., Mittal, N., Hirani, K. and Chopde, C.T. 2004. Essentiality of central GABAergic neuroactive steroid allopregnanolone for anticonvulsant action of fluoxetine against pentylenetetrazole-induced seizures in mice. *Brain Research* 1023(1), pp. 102–111.
- Uhlhaas, P.J., Haenschel, C., Nikolić, D. and Singer, W. 2008. The role of oscillations and synchrony in cortical networks and their putative relevance for the pathophysiology of schizophrenia. *Schizophrenia Bulletin* 34(5), pp. 927–943.
- Umeda, T., Isa, T. and Nishimura, Y. 2019. The somatosensory cortex receives information about motor output. *Sci. Adv.* 5,.
- Vaidyanathan, T.V., Collard, M., Yokoyama, S., Reitman, M.E. and Poskanzer, K.E. 2021. Cortical astrocytes independently regulate sleep depth and duration via separate GPCR pathways. *eLife* 10.
- Van Der Loos, H. 1976. Barreloids in mouse somatosensory thalamus. *Neuroscience Letters* 2(1), pp. 1–6.
- van Lujtelaar, G. and Sitnikova, E. 2006. Global and focal aspects of absence epilepsy: the contribution of genetic models. *Neuroscience and Biobehavioral Reviews* 30(7), pp. 983–1003.
- Velazquez, J.L.P., Huo, J.Z., Dominguez, L.G., Leshchenko, Y. and Snead, O.C. 2007. Typical versus atypical absence seizures: network mechanisms of the spread of paroxysms. *Epilepsia* 48(8), pp. 1585–1593.
- Venugopal, S., Srinivasan, R. and Khakh, B.S. 2019. GECIquant: Semi-automated Detection and Quantification of Astrocyte Intracellular Ca²⁺ Signals Monitored with GCaMP6f. *Computational Glioscience*, pp. 455–470.
- Venzi, M., David, F., Bellet, J., Cavaccini, A., Bombardi, C., Crunelli, V. and Di Giovanni, G. 2016. Role for serotonin_{2A} (5-HT_{2A}) and 2C (5-HT_{2C}) receptors in experimental absence seizures. *Neuropharmacology* 108, pp. 292–304.
- Venzi, M., Di Giovanni, G. and Crunelli, V. 2015. A critical evaluation of the gamma-hydroxybutyrate (GHB) model of absence seizures. *CNS Neuroscience & Therapeutics* 21(2), pp. 123–140.
- Verkhatsky, A. and Nedergaard, M. 2018. Physiology of Astroglia. *Physiological Reviews* 98(1), pp. 239–389.
- Verkhatsky, A. and Toescu, E.C. 2006. Neuronal-glia networks as substrate for CNS integration. *Journal of Cellular and Molecular Medicine* 10(4), pp. 826–836.
- Vezzani, A., Moneta, D., Conti, M., Richichi, C., Ravizza, T., De Luigi, A., De Simoni, M.G., Sperk, G., Andell-Jonsson, S., Lundkvist, J., Iverfeldt, K. and Bartfai, T. 2000. Powerful anticonvulsant action of IL-1 receptor antagonist on intracerebral injection and astrocytic overexpression in mice. *Proceedings of the National Academy of Sciences of the United States of America* 97(21), pp. 11534–11539.
- Vienne, J., Bettler, B., Franken, P. and Tafti, M. 2010. Differential effects of GABAB receptor subtypes, γ -hydroxybutyric acid, and baclofen on EEG activity and sleep regulation. *Journal of Neuroscience* 30(42), pp. 14194–14204.
- Vincze, R., Péter, M., Szabó, Z., Kardos, J., Héja, L. and Kovács, Z. 2019. Connexin 43 Differentially Regulates Epileptiform Activity in Models of Convulsive and Non-convulsive Epilepsies. *Frontiers in Cellular Neuroscience* 13, p. 173.

- Wahis, J. and Holt, M.G. 2021. Astrocytes, Noradrenaline, α 1-Adrenoreceptors, and Neuromodulation: Evidence and Unanswered Questions. *Frontiers in Cellular Neuroscience* 15, p. 645691.
- Wallace, R.H., Marini, C., Petrou, S., Harkin, L.A., Bowser, D.N., Panchal, R.G., Williams, D.A., Sutherland, G.R., Mulley, J.C., Scheffer, I.E. and Berkovic, S.F. 2001. Mutant GABA(A) receptor gamma2-subunit in childhood absence epilepsy and febrile seizures. *Nature Genetics* 28(1), pp. 49–52.
- Wang, F., Qi, X., Zhang, J. and Huang, J.H. 2020. Astrocytic modulation of potassium under seizures. *Neural regeneration research* 15(6), pp. 980–987.
- Wang, T., Ouzounov, D.G., Wu, C., Horton, N.G., Zhang, B., Wu, C.-H., Zhang, Y., Schnitzer, M.J. and Xu, C. 2018. Three-photon imaging of mouse brain structure and function through the intact skull. *Nature Methods* 15(10), pp. 789–792.
- Wang, X., Lou, N., Xu, Q., Tian, G.-F., Peng, W.G., Han, X., Kang, J., Takano, T. and Nedergaard, M. 2006. Astrocytic Ca^{2+} signaling evoked by sensory stimulation in vivo. *Nature Neuroscience* 9(6), pp. 816–823.
- Wang, Y., DelRosso, N.V., Vaidyanathan, T.V., Cahill, M.K., Reitman, M.E., Pittolo, S., Mi, X., Yu, G. and Poskanzer, K.E. 2019. Accurate quantification of astrocyte and neurotransmitter fluorescence dynamics for single-cell and population-level physiology. *Nature Neuroscience* 22(11), pp. 1936–1944.
- Watanabe, M., Miyai, A., Danjo, S., Nakamura, Y. and Itoh, K. 2013. The threshold of pentylenetetrazole-induced convulsive seizures, but not that of nonconvulsive seizures, is controlled by the nitric oxide levels in murine brains. *Experimental Neurology* 247, pp. 645–652.
- Willoughby, J.O. and Mackenzie, L. 1992. Nonconvulsive electrocorticographic paroxysms (absence epilepsy) in rat strains. *Laboratory animal science*.
- Wong, C.G.T., Gibson, K.M. and Snead O.C., 2004. From the street to the brain: neurobiology of the recreational drug γ -hydroxybutyric acid. *Trends in pharmacological sciences*.
- Yamabe, M., Horie, K., Shiokawa, H., Funato, H., Yanagisawa, M. and Kitagawa, H. 2019. MC-SleepNet: Large-scale Sleep Stage Scoring in Mice by Deep Neural Networks. *Scientific Reports* 9(1), p. 15793.
- Ye, L., Haroon, M.A., Salinas, A. and Paukert, M. 2017. Comparison of GCaMP3 and GCaMP6f for studying astrocyte Ca^{2+} dynamics in the awake mouse brain. *Plos One* 12(7), p. e0181113.
- Yu, X., Taylor, A.M.W., Nagai, J., Golshani, P., Evans, C.J., Coppola, G. and Khakh, B.S. 2018. Reducing astrocyte calcium signaling in vivo alters striatal microcircuits and causes repetitive behavior. *Neuron* 99(6), pp. 1170–1187.e9.
- Yuste, R. and Katz, L.C. 1991. Control of postsynaptic Ca^{2+} influx in developing neocortex by excitatory and inhibitory neurotransmitters. *Neuron* 6(3), pp. 333–344.
- Zariwala, H.A., Borghuis, B.G., Hoogland, T.M., Madisen, L., Tian, L., De Zeeuw, C.I., Zeng, H., Looger, L.L., Svoboda, K. and Chen, T.-W. 2012. A Cre-dependent GCaMP3 reporter mouse for neuronal imaging in vivo. *The Journal of Neuroscience* 32(9), pp. 3131–3141.
- Zhang, C., Tabatabaei, M., Bélanger, S., Girouard, H., Moeini, M., Lu, X. and Lesage, F. 2019. Astrocytic endfoot Ca^{2+} correlates with parenchymal vessel responses during 4-AP induced epilepsy: An in vivo two-photon lifetime microscopy study. *Journal of Cerebral Blood Flow and Metabolism* 39(2), pp. 260–271.

- Zhao, J., Wang, D. and Wang, J.-H. 2012. Barrel cortical neurons and astrocytes coordinately respond to an increased whisker stimulus frequency. *Molecular Brain* 5, p. 12.
- Zienowicz, M., Wisłowska, A., Lehner, M., Taracha, E., Skórzewska, A., Maciejak, P. and Płaźnik, A. 2005. The effect of fluoxetine in a model of chemically induced seizures--behavioral and immunocytochemical study. *Neuroscience Letters* 373(3), pp. 226–231.
- Zong, W., Wu, R., Chen, S., Wu, J., Wang, H., Zhao, Z., Chen, G., Tu, R., Wu, D., Hu, Y., Xu, Y., Wang, Y., Duan, Z., Wu, H., Zhang, Y., Zhang, J., Wang, A., Chen, L. and Cheng, H. 2021. Miniature two-photon microscopy for enlarged field-of-view, multi-plane and long-term brain imaging. *Nature Methods* 18(1), pp. 46–49.
- Zuend, M., Saab, A.S., Wyss, M.T., Ferrari, K.D., Hösli, L., Looser, Z.J., Stobart, J.L., Duran, J., Guinovart, J.J., Barros, L.F. and Weber, B. 2020. Arousal-induced cortical activity triggers lactate release from astrocytes. *Nature Metabolism* 2(2), pp. 179–191.